

Draft
Compendium of In-Situ
Radiological Methods
and Applications
at Rocky Flats Plant
April 2, 1993

ADMIN RECORD

A-SW-000582

U NU

REVIEWED FOR CLASSIFICATION/UCNI
BY <u>G. T. Ostdiek</u> <i>GT</i>
DATE <u>4-12-93</u>

Table of Contents

Introduction	1
Background.	4
Atomic Structure.	4
Ions and Ionization	6
Radiation and Radioactivity	7
Radiation Quantities and Units	10
Radiation Detection Instrumentation	10
Gas Filled Detectors	13
Ionization Chambers-Operation and Application	19
Proportional Counters-Operation and Application	19
Geiger-Muller Counters—Operation and Application	20
Scintillation Detectors	22
Semiconductor Detectors	24
Comparison of NaI and HPGe Sensors	27
In-Situ Detector Characteristics	29
The Theory of In-Situ Measurement	44

APPENDICES

I. Beck, DeCampo and Gogolak; 1972 *In-Situ Ge(Li) and NaI(Tl) Gamma-Ray Spectrometry*
Health and Safety Laboratory (HASL-258)

II. Miller and Shebell; *In Situ Gamma-Ray Spectrometry; Lecture Notes—A Short Course for
Environmental Radiation Researchers* U.S. Department of Energy, Environmental
Measurements Laboratory

Introduction

In recent years there have been many advances in radiation detection equipment and methods. A comparison of these methods and applications is needed so the project manager or regulator can compare the pros, cons, and limitations of each of the methods to ensure that the chosen method meets the data quality objectives of the project. The choice of methods and hardware has, and will have, an impact on remedial investigations at the Rocky Flats Plant.

Remedial Program Managers are primarily interested in characterizing radiological contamination at Rocky Flats that may have occurred via four main release mechanisms:

- Release to the surface in a concentrated spill
- Release to the subsurface from either a leak in a process waste line or from buried materials.
- Dispersion of contaminated soils from an area contaminated by a surface spill, or:
- releases from documented industrial fires

Each remedial project has its own model for release and a set of specific data quality objectives (DQOs) outlined in the work plan for that particular Operable Unit (OU) or project. Together these parameters define or dictate the end use of the data.

To define the radiological character of an area one needs to:

- Measure the radionuclides,
- Identify the radionuclides,
- Quantify each radionuclide, and
- Define the spatial extent of the radionuclides that may be present.

Prior to performing these tasks it is prudent to consider:

- The size of the area of interest,
- The degree of spatial resolution required,
- The possible complexity of the radionuclide content,
- The resources available, and
- The end use of the data.

For example, the data could either be used for screening the presence or absence of contaminants, or for complete characterization with subsequent transport and fate modelling. There may be different DQOs for early stages of an investigation than for subsequent stages or phases. The first stage of an investigation may only be interested in answering whether there is radioactive contamination present. Subsequent investigations will want to specifically identify which type of contaminant is present at the lowest limits of detection. This type of data would be used to infer the nature and extent of contamination from the results of the sampling program.

Either objective can be met by using the proper equipment and method. There are two primary methods employed to accomplish characterization. The first is to bring part of the site into the laboratory by way of classical soil sampling. The other is to bring the laboratory to the site and perform in situ radiometric measurements. Both methods have been used for sometime throughout the industry.

Screening level data is typically collected by conducting a survey of the area with hand held detectors. A detailed sampling plan traditionally would require that soil samples be sent to a laboratory to gather the more detailed information to make inferences about the nature and extent of contamination. Such sampling is based on a statistically valid method from which data gathered at specific points is used to construct a model. This model should correctly predict the occurrence of the contamination. However, even with a large number of samples, there is always a chance of missing an anomalous area when using a representative sampling technique.

Both methods, soil sampling with analyses and in situ measurements, should be utilized in concert to accomplish radiological characterization of a site. Soil sampling with analyses has proven to be very expensive and time consuming. In situ measurements can be made fairly inexpensive and can yield results in 'near real time'.

In the past, simple counting systems moved from the laboratory to the field and today there are countless models of 'health physics' instrumentation. In 1972 Harold Beck with his colleagues, J. DeCampo and C. Gogolak at the United States Atomic Energy Commission, Health and Safety Laboratory now called the United States Department of Energy, Environmental Measurements Laboratory, published a paper entitled In situ Ge(Li) and NaI(Tl) Gamma-Ray Spectrometry, HASL 258 (see Appendix I). This document has become the 'bible' to the in situ gamma-ray spectroscopist. HASL 258 shows that the in situ measurement integrates the activity over a large volume and the results can be presented as activity per unit mass averaged over the measured volume. The spatial variability of the activity is smoothed and a more representative value for the activity in a given plot of land could be obtained. This methodology does not pre-empt the requirement for soil samples but rather enables the investigator to develop a more meaningful sample strategy.

At Rocky Flats, the areas that need to be surveyed are large. Many Individual Hazardous Substance Sites (IHSSs) cover several acres. Sampling on a grid basis becomes prohibitively expensive. In the course of developing the various work plans at Rocky Flats, it became clear that alternatives needed to be developed. Several methods of in-situ radiological analysis are available. These methods can reduce the number of samples taken to be sent to the laboratory for analysis resulting in lower costs.

This document is designed to give an overview of the choices available and a discussion of the limitations facing the project manager. The document presents an overview of the basic principles involved in radiation detection, a brief description of the types of radiation detectors and sensors that may be of interest to the project manager. This is followed by a discussion of the two principle types of detectors used at Rocky Flats Plant and an overview of the theory behind In-situ methods. The complete papers in the appendices present a detailed and complete discussion of the in-situ gamma-ray spectrometry.

Background

All radiation detectors use products of the ionization or excitation process to produce a measurable output that is proportional to the incident radiation intensity and/or the incident radiation energy. A brief review of elementary physics and the basis of radiation will be helpful in understanding how the various detectors work and what they measure. More information on these topics is available from numerous textbooks on chemistry and physics. Much of the information presented in this background section appears in the EG&G Reference Handbooks on Basic Radiation Safety, Nuclear Criticality, and Radiation Detection Instrumentation.

Radiation Detection and Measurement (2nd edition © 1979, 1989 John Wiley and Sons, Inc.) by Dr. Glenn Knoll is a key reference and covers the information about the types of detectors much more thoroughly and should be consulted for further information. This text was used extensively to develop much of the information presented in this section.

Atomic Structure

The atom is the smallest unit into which an element can be divided and still retain the characteristics of the element. Atoms of all elements are made up of three primary subatomic components: protons, neutrons and electrons. These components are contained in two main parts of the atom: the nucleus and the electron cloud. Figure 1 shows a representation of a helium atom.

The nucleus is the central part of the atom. The nucleus is extremely dense and compact. It contains two of the three subatomic components—the neutrons and the protons. Together these two particles account for almost all of the atom's mass. Protons are positively charged with one electrostatic unit (esu) and have a mass of about one atomic mass unit (amu). An atomic mass unit is extremely small— 1.6×10^{-24} grams. That is a decimal point followed by 23 zeros before the 16 appears—.000 000 000 000 000 000 000 001 6 grams. Neutrons don't carry an electrostatic charge and also have a mass of about 1 amu. The number of protons is equal to the element's atomic number.

The electrons surround the nucleus in the electron cloud. Electron orbits are extremely large when compared with the size of the nucleus. Electrons are negatively charged and have an atomic mass of .00055 amu. The electrons are in constant motion about the nucleus. They are grouped in levels (orbitals) and sublevels which are labeled with numbers and the letters s, p, d and f. Each orbital and sublevel has a fixed number of electrons which can reside within it. These levels are filled with electrons on the basis of increasing energy. (See Figure 2.) The levels are filled in the following order 1s, 2s, 2p, 3s, 3p, 4s, 3d, 4p, 5s, 4d, 5p, 6s, 4f, 5d, 6p, 7s, 5f, 6d, and 7p. (See Figure 3.)

There are 94 naturally occurring elements and a number of artificially created elements. Each element has a unique number of protons in its nucleus and unique chemical properties. The atomic number, mass and electron configuration of an element govern many of its important physical properties. The elements are arranged according to these properties in the periodic table. Currently the periodic table ranges from hydrogen which has an atomic number of 1 to an as of yet unnamed element which has an atomic number of 109. Atoms of different elements are identified by their chemical symbol and two numbers, its atomic number and its mass.

Figures 1-3

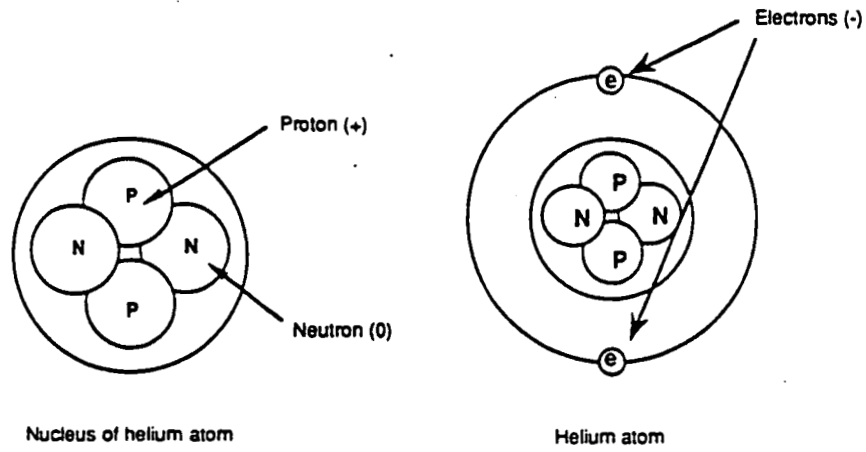


Figure 1: Atomic Particles

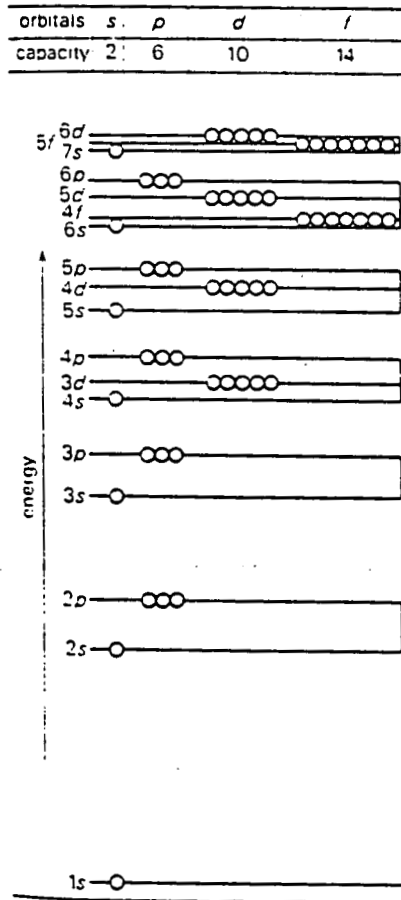


FIGURE 2 Approximate relative energy ranking of atomic orbitals for atoms with more than one electron.

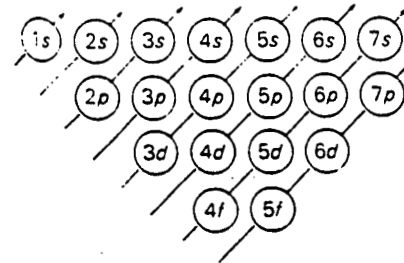


FIGURE 3 The approximate order in which sublevels are filled with increasing numbers of electrons. Follow through each slanting arrow in turn, starting with the lowest and continuing with the next higher. For example, after 3*s* is filled, there follow 3*p*, 4*s*, 3*d*, 4*p*, etc. SOURCE: Adapted from Therald Moeller, *Inorganic Chemistry*, John Wiley & Sons, Inc., New York, 1952.

Protons and neutrons are often referred to as nucleons. Atoms characterized by their atomic number and the number of their nucleons are called nuclides. Shorthand notation is sometimes used to represent the nuclides. There are two common conventions in this shorthand:



where A= the atomic mass, Z= the Atomic number and X= the chemical symbol.

The first notation is the currently preferred notation but many references use the second. The shorthand notation for plutonium is:



Other ways of designating a nuclide such as plutonium are: Plutonium-239, Pu-239, ^{239}Pu . Note that the atomic number has been dropped because the element has already been defined by its chemical symbol.

The number of protons in the nucleus of the atom determines which element it is. However the number of neutrons in the nucleus of a particular element can vary. These atoms are called isotopes.

Ions and Ionization

All of the atoms in their natural, lowest energy state have the same number of electrons as they do protons. This lowest energy state is sometimes called *stable*, *ground*, or *relaxed* state. In this state the atom does not carry an electrostatic charge. However, atoms can interact with other atoms or parts of atoms and absorb extra energy. This energy can be distributed through out the electron cloud. It may cause the outermost electrons to become more loosely bound to the atom. This process is called *excitation*. If there is enough energy absorbed, the excitation can be sufficient to eject electrons from the atom. This process is known as *ionization*. As soon as the electron is ejected, the atom becomes positively charged because the positively-charged protons now outnumber the negatively-charged electrons. Both the residual, positively charged atom and the ejected free electron are called ions.

Positive ions are produced when electrons are removed from neutral atoms or molecules.

Negative ions can be produced when electrons are added to or absorbed by neutral atoms or molecules.

Ionization is the process of producing ions. Anything with enough energy to remove electrons from neutral atoms or molecules is capable of causing ionization. This is known as an *ionizing event*. The ionizing event produces an ion pair, which consists of the removed electron and the residual positively-charged atom or molecule.

Ionization is important because two oppositely charged ions can come together to form an uncharged, stable compound. This is the process which allows elements to join together to form chemical compounds. It also allows the radioactive decay process to be detected and measured.

Radiation and Radioactivity

The number of protons in an atom's nucleus determines the element to which the atom belongs. For example, any atom with a single proton is a hydrogen atom, any atom with two protons is a helium atom, and any atom with 92 protons is a uranium atom. The number of neutrons in the nucleus can vary between atoms of the same element, but the number of protons remains constant. Atoms of one element with different numbers of neutrons are called *isotopes* or *nuclides* of that element. For example, U-238 (uranium-238) and U-239 are both isotopes of uranium because they both have 92 protons, but different numbers of neutrons (146 and 147, respectively). Isotopes of the same element are generally distinguishable physically. For example, U-238 and U-239 have different atomic masses because of the different numbers of protons in their nuclei. However, such isotopes are not distinguishable chemically, because chemical properties depend on the number, activity, and arrangement of orbital electrons, which are determined by the number of protons, not the number of neutrons.

There are approximately 2200 known isotopes of the 109 known elements. Only about 280 of these isotopes are stable. *Stability* means that the ratio of protons to neutrons, their configurations, and the forces they exert on each other are such that no changes in the isotope will occur without adding an external energy source.

Unstable isotopes, on the other hand, exist in such a state that some type of nuclear transformation naturally occurs to allow the isotope to reach a more stable state. These unstable isotopes are said to be *radioactive* and are called *radionuclides*. *Radioactivity* is the spontaneous disintegration of the nucleus of an atom. The transformations of unstable isotopes occur through a process called *radioactive decay*. Radioactivity results in a release of *ionizing radiation*, which is radiation that has enough energy to cause ionization of surrounding atoms or molecules. Some forms of ionizing radiation are energy (X-rays or gamma rays), while other forms are energetic particles (alpha particles, beta particles, or neutrons).

Disintegration occurs when the physical makeup of an atom's nucleus changes and the atom transforms into an entirely different element. Disintegration is also called *radioactive decay*. The original atom in the transformation is called the *parent*, while the new atom is called the *daughter*. The daughter atom may then become the parent to a third, new daughter atom as the decay continues. This process of continuing radioactive decay is called a *decay chain*—one atom is transformed into another, which in turn is transformed into another, and so on, until a stable atomic configuration is reached. (See Figure 4.)

Ionizing radiation may be non-penetrating or penetrating. *Non-penetrating radiation* can travel only short distances and cannot penetrate through the skin. This type of radiation is considered harmful only when present inside the body. *Penetrating radiation*, on the other hand, can travel long distances and can penetrate the body, impart some of its energy, and then continue on at a lower energy level. It is this exchange of energy in the body cells that needs to be avoided.

At Rocky Flats, we are concerned with four types of radiation: alpha particles, beta particles, gamma rays, and neutrons. There are two basic types of non-penetrating radiation, both of which are particulate in form: alpha particles and beta particles.

Figure 4

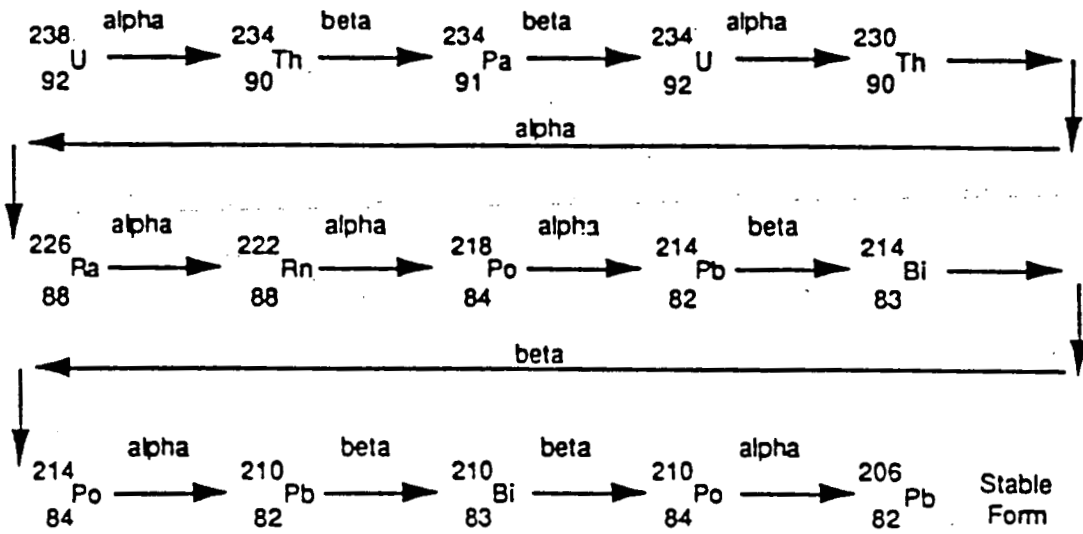


Figure 4: Radioactive Decay

Alpha particles are charged particles emitted from an atom's nucleus. An alpha particle has a mass and charge equal to that of a helium nucleus (two protons and two neutrons). Alpha particles are emitted from naturally-occurring elements such as uranium, radium, and polonium, as well as from man-made elements such as plutonium as they decay. They can also be produced when a neutron is absorbed into a nucleus of one of the lighter elements such as lithium or boron.

Alpha radiation will just barely penetrate the surface of the skin and can be stopped completely by a sheet of paper. The greatest potential danger of alpha-emitting materials is the possibility of their being taken into the body via inhalation, ingestion, or a contaminated wound, thus allowing the alpha particles to come into intimate contact with living cells and tissues in the body.

Beta particles are charged particles with a mass and charge equal to that of an electron. Beta particles are ejected from the nucleus of an atom when a neutron within the nucleus divides into a proton and an electron. The new proton remains in the nucleus, while the electron is ejected as a beta particle.

Beta particles are much more penetrating than alpha particles, but can be stopped by a thin sheet of metal such as aluminum. Although beta radiation can be a serious external exposure hazard to the skin or lens of the eye, it is relatively easy to shield and, like alpha radiation, is regarded primarily as an internal hazard.

There are three basic types of penetrating radiation; two of them, X-rays and gamma rays, are forms of energy, while the other, the neutron, is a particle.

Often after radioactive decay, the resulting nucleus is formed in an excited, unstable state. Electromagnetic radiation is released during the transition of this daughter nucleus to a more stable state. This form of radiation is pure energy and has no mass. *Gamma rays* (or *gamma photons*) and *X-rays* are the two types of electromagnetic radiation with which personnel who handle radioactive materials should be most concerned. Gamma photons, which typically have high energy and are highly penetrating, can pass completely through people and objects alike. When they do interact with other atoms, however, they do so very effectively, transferring their energy to electrons of stable atoms and causing ionization. X-rays are identical in nature to gamma photons, but they typically have lower average energies and are not quite as penetrating.

The primary differences between these two types of electromagnetic radiation are their energies, as just mentioned, and their points of origin. Gamma photons originate from the nucleus following nuclear transformations, while X-rays originate from the electron cloud as a result of interactions between electrons. The most effective shielding against gamma photons and X-rays is a heavy, dense material, such as lead or some types of concrete.

Neutrons, the third type of penetrating radiation, are particles having no electrical charge that depend on collisions with other atoms to expend their energy. Neutrons are highly penetrating and can pass through or bounce off heavy metals. In general, energy transfer is more efficient between moving bodies of similar mass. Since neutrons have about the same mass as a hydrogen atom, however, they tend to interact readily with materials containing many hydrogen atoms. Therefore, water and polyethylene are ideal shields for neutrons

because of their high hydrogen content.

Any time an atom emits alpha, beta, gamma, X-ray, or neutron radiation from the nucleus, the atom has changed by giving up a part of its structure and/or a part of its energy in the radioactive decay process. This the basis on which radiation detectors are designed.

Radiation Quantities and Units

Discussions of radioactivity use a common unit, the *Curie (Ci)*, to express the radiative activity. A Curie is the activity of that quantity of radioactive material in which 3.7×10^{10} disintegrations take place every second. It is important to understand that the Curie is not a measure of the *rate* of decay, but rather a measure of total *activity*.

Because one Curie is a relatively large quantity of activity, the following submultiples are commonly used:

milliCurie (mCi)	=	10^{-3}Ci
microCurie (μCi)	=	10^{-6}Ci
nanoCurie (nCi)	=	10^{-9}Ci
picoCurie (pCi)	=	10^{-12}Ci

The Curie's drawback for some uses is that it does not take the mass or volume of the radioactive material into account. When the relative activity of two or more radioactive materials is discussed, units of *specific activity* (or Curies per unit mass or volume) are used to define the relationship between the mass of each substance and its associated activity. A common unit is Ci/g, or Curies per gram.

For example, it takes 16.3 grams of plutonium-239 to decay at the rate of 3.7×10^{10} disintegrations per second (or 1 Curie). Therefore, the specific activity of plutonium-239 is (1 Curie)/(16.3 grams), or 0.0614 Ci/g.

Radiation Detection Instrumentation

Detection of radioactivity has always been of prime interest to researchers. All radiation detectors use products of the ionization or excitation process to produce a measurable output that is proportional to the incident radiation intensity and/or the incident radiation energy. During the early days of scientific inquiry—before the turn of the century the only way to detect X-rays and radiation from isotopes was to study the exposure of photographic films or observe the discharge of an electroscope by the ionization produced in air.

By 1905 the earliest detectors capable of detecting individual charged alpha particles were developed. The alpha particles caused minute light flashes called scintillations on the surface

of zinc sulphide foil which could be observed under a low powered microscope in a darkened room. In fact, Baron Ernest Rutherford's early experiments with radioactivity were conducted by groups of assistants peering into microscopes and using mechanical registers to count the scintillations.

In 1912 Hans Geiger discovered that an alpha particle was capable of triggering a small discharge of electric current. That current was used to switch a solenoid on a mechanical register. This new device was capable of measuring tens of pulses per second as compared with the several pulses per second detectable under the microscope by Rutherford's assistants. Improvements in the electronics and design of self-quenching detectors allowed count rates of up to 10^6 counts per second to be achieved by 1950.

Other important developments included the development of the photomultiplier tube in 1940, the discovery of bulk scintillating properties of various organic crystals such as anthracene and stilbene in the late 1940s, and the development of inorganic scintillation crystals such as sodium iodide in 1950. The 1950s saw the development of detectors in which the organic scintillators were dissolved in liquids or polymerized in plastics. This led to the feeling at the time that the scintillation counters were superior to the existing forms of the gas filled detectors in terms of pulse speed, signal amplitude, coverage, count rate and cost.

Recent (post 1960) advances in semiconductors have led to the development of new types of detectors based on the properties of materials unknown only a decade earlier. Computers, various high speed optical and electronic readouts have led to the development of the modern era detection instruments. New developments, and the application and/or rediscovery of early phenomena that were not fully understood in previous decades will shape research efforts in the future. (Adapted from Knoll, 1991)

The following types of detectors will be discussed:

- Ionization chambers
- Proportional counters
- Geiger-Muller tubes
- Scintillation detectors
- Semiconductor detectors

Detectors fall under one of the following classifications:

- Portable survey instruments
- Area radiation monitors
- Personnel monitoring devices

Radiation detectors depend on either charge collection (of ion pairs or "electron-hole" pairs produced by ionization), or light collection (of light produced by de-excitation of electrons or molecules). Detector choice depends on the type and energy of the radiation to be measured. The types of radiation and the mechanism by which they are measured are:

- **Alpha and Beta**

Charged particles such as alphas (+2) and betas (-1) ionize substances by direct interactions. The number of ion pairs produced depends on the particle's mass and charge. The much heavier alpha particle produces greater (specific) ionization over a shorter distance than the smaller beta particle. Since the alpha and beta particles lose energy with each collision, it follows that neither radiation can penetrate very far into matter; consequently, alpha and beta detection instruments have thin detection windows.

- **Gamma**

Gamma radiation interacts with matter according to the following basic mechanisms:

Photoelectric Effect at low gamma energies: the gamma energy is completely absorbed and an electron is ejected.

Compton Scattering at low to intermediate gamma energies: the electron is ejected but the gamma continues at reduced energy.

Pair Production at energies greater than 1.02 MeV¹: the gamma is completely absorbed and an electron-positron pair is created.

A gamma ray passing through the fill gas of a detection instrument has a much lower chance of causing ionization than an alpha or beta particle. Since the chances of a reaction occurring in the fill gas are so low, most of the gammas picked up by instruments are actually the result of reactions in the detector walls. These energetic electrons then travel into the fill gas to produce ion pairs. This process is referred to as indirect ionization.

- **Neutrons**

Neutrons cannot strip out electrons in the same way as charged particles (alphas and betas) or electromagnetic radiation (gammas) can. Therefore, neutron detectors operate by capturing neutrons in a suitable absorber (lithium or boron) that coats the detector walls or is part of the fill gas. The resulting nuclear reaction produces charged particles which can then

¹ MeV is the abbreviation for Megaelectron volt which is 10⁶ electron volts. An electron volt is the amount of energy acquired by a singly charged particle when it falls through a potential of one volt. This is a very small amount of energy—it would require about 2x10²² eV to melt a 10g ice cube at 0°C.

be collected and measured. A typical reaction, (employed in the Ludlum-111) is:



This equation shows an incident neutron striking a lithium atom, producing tritium (H^3) and helium (He^4). The reaction is so energetic that both tritium and helium are produced without electrons (they are positive ions). Three free electrons (negative ions) are also produced. Boron is also frequently used as a neutron detecting material.

The probability of a neutron being absorbed by a material such as boron or lithium is much greater at low energies than at intermediate or high energies. However, in production situations at Rocky Flats, neutrons which would be released during a criticality incident are "born" at very high energies. To detect these neutrons, they must be slowed down to a point where boron or lithium will absorb the neutron and release measurable ion products. The process of slowing down neutrons is called moderation and the material used to slow down neutrons is called a moderator. A good moderator, such as water or polyethylene, slows neutrons down by absorbing their energies in scattering-type collisions. Thus, neutron detectors must be surrounded with a moderating material—such as polyethylene, so the neutrons are slowed down enough to react with the boron or lithium.

Gas-Filled Detectors

The gas-filled radiation detector is one of the oldest devices used in the radiation protection field. Gas-filled radiation detectors are relatively simple, inexpensive, and reliable. They are the most common type of detector used at Rocky Flats in the health physics area.

Detector Theory

When gas is enclosed in a radiation detector chamber and a voltage (V) is applied to the chamber, a positive charge accumulates on the central wire (anode) and a negative charge accumulates on the detector chamber wall (cathode). In effect, an electric field is established throughout the detector chamber. As radiation enters the gas chamber, ion pairs are created. The negatively-charged free electrons are attracted toward the positively-charged anode and the positively charged gas ions are attracted toward the negatively-charged cathode. (See Figure 5.)

While moving toward the anode or cathode, one of three things can happen to an ion:

- 1) it can combine with an oppositely-charged ion to form a neutral atom,
- 2) it can reach the electrode to which it is attracted with no further interactions, or
- 3) if it has enough kinetic energy, it can produce further ionization.

The speed of the ion pairs depends on the applied electrical field strength and characteristics of the gas. The collection of these electrons on the central wire causes current on the wire to decrease; i.e., a lower positive charge on the wire, and thereby a voltage drop in the system.

Figures 5&6

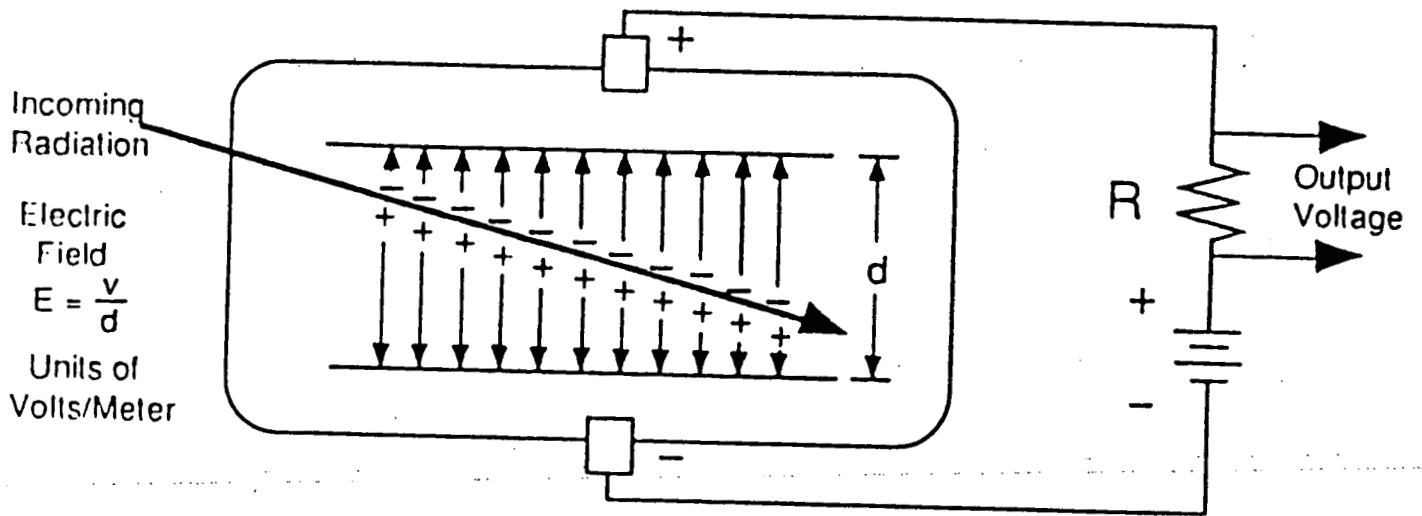


Figure 5: Basic Schematic of Gas-Filled Detector

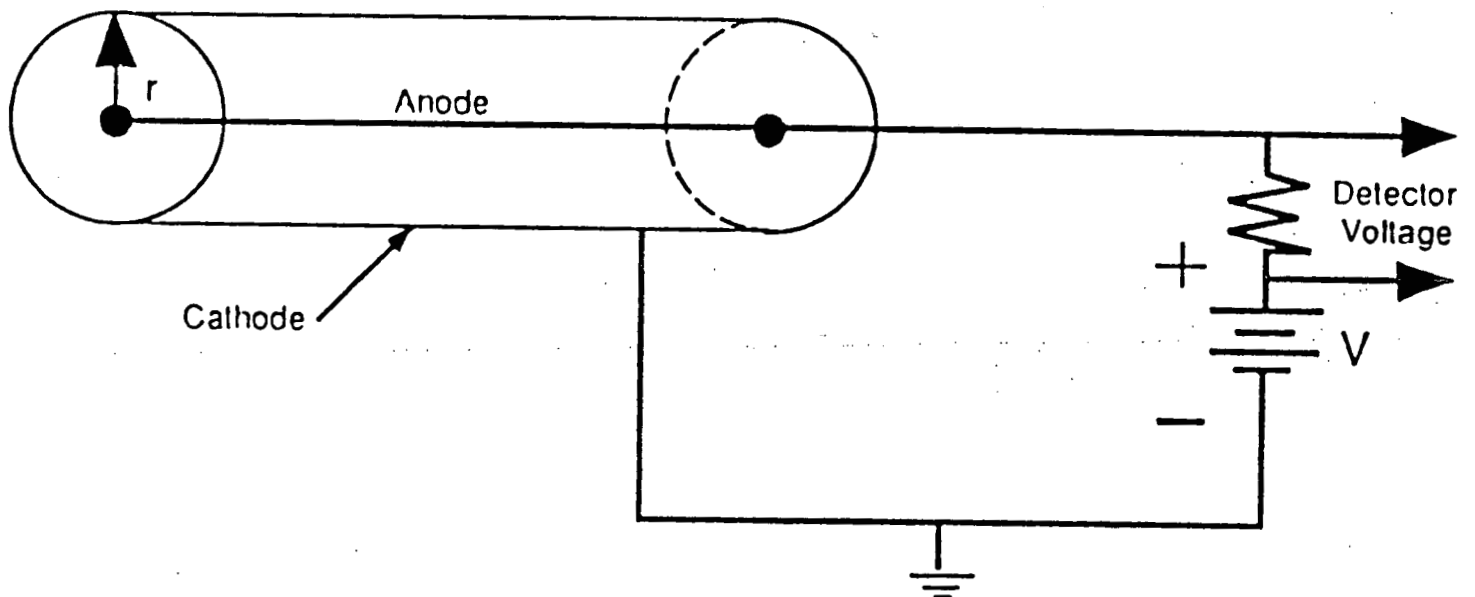


Figure 6: Cylindrical Gas-Filled Detector

This drop in voltage is commonly referred to as pulse and its size is directly related to the number of ion pairs collected. The presence of this pulse in the circuit causes current to flow, which is normally fed to an ammeter where a reading is produced.

Detector Construction

Because it is extremely versatile, the gas-filled detector is the most commonly used detection instrument. Gas-filled detectors, like the one shown in Figure 6 are capable of detecting and discerning all types of radiation over the entire energy spectrum. Most gas-filled detectors are of cylindrical geometry. The anode is the positively-charged wire in the center of the can. The can, called the cathode, is negatively charged to collect positive gas ions.

Cylindrical configurations of gas-filled detectors are the most widely used because a higher electric field strength can be attained close to the anode without using a high applied voltage.

Modes of Operation

Radiation detection instruments can be designed to operate in either a pulse mode or a current mode.

Pulse Mode

In the pulse mode, the detector counts radiation interactions by individual particle interactions. Each interaction results in a distinct pulse which produces a charge. The output pulses are then fed to the electronic circuit. This system acts on the pulse signals to produce shaped pulses which retain the size and time relationships of the original input signals. These signals are usually passed through a discriminator circuit, which eliminates all pulses below a given size. A typical application of a discriminator circuit is shown in Figure 7.

Incoming neutrons and gammas produce ionization with pulse heights proportional to the number of ion pairs collected. Recall that neutrons react with boron or lithium to produce ionization, and that the number of ion pairs produced is larger than the number produced by gamma radiation. The discriminator circuit eliminates gamma pulses and produces a pulsed output proportional to neutrons only. The resulting pulses then proceed to a scaling circuit which adds up the pulses as they arrive from the discriminator. The pulses are displayed as counts through LED or liquid crystal display counters.

Current Mode

In the current mode, the rate of radiation interactions is measured directly. In this detector, the pulses passing through the discriminator are used to charge a capacitor connected to a fairly high resistance. The pulses are so shaped that as each arrives, it supplies a constant charge to the capacitor, which produces a voltage across the capacitor proportional to the number of pulses arriving per unit of time, and thereby indicates the current count rate.

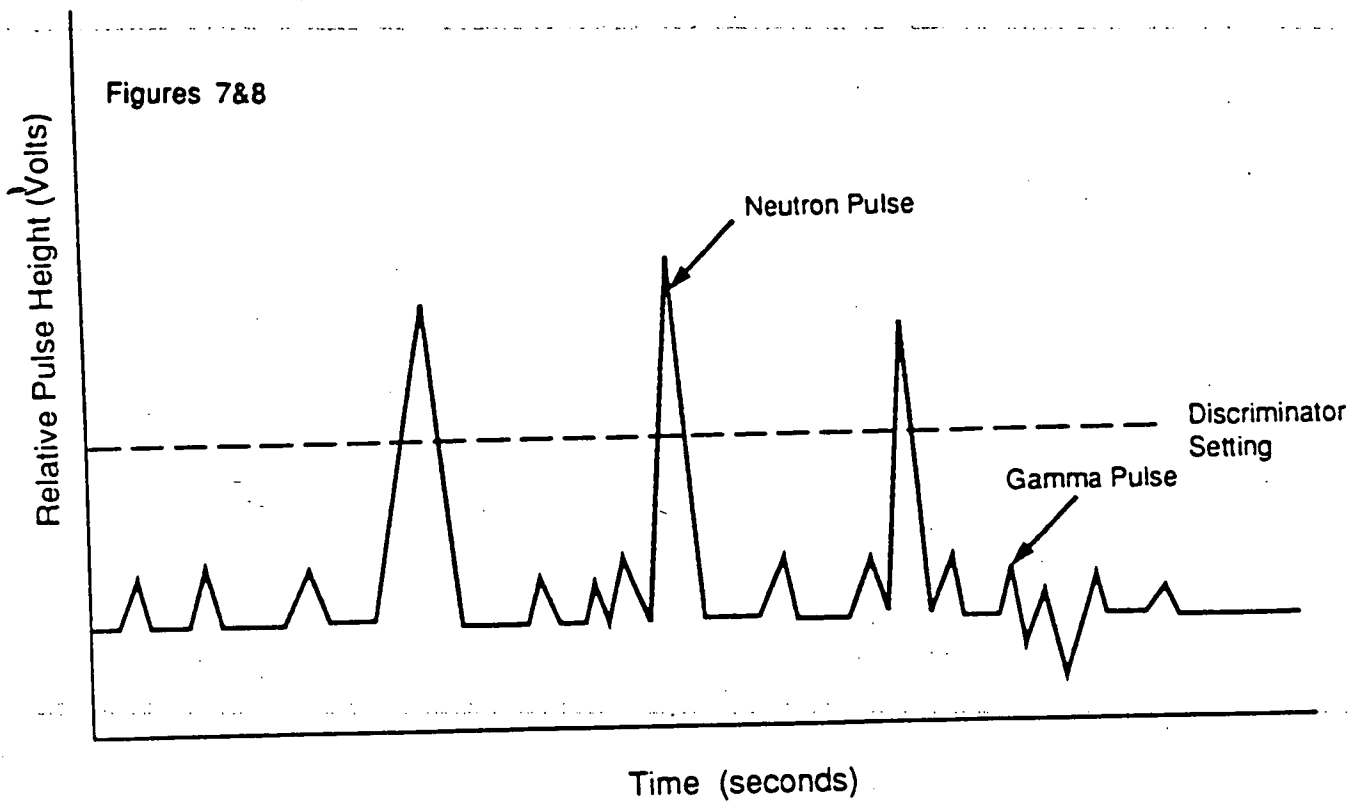


Figure 7: Discriminator Circuit Application

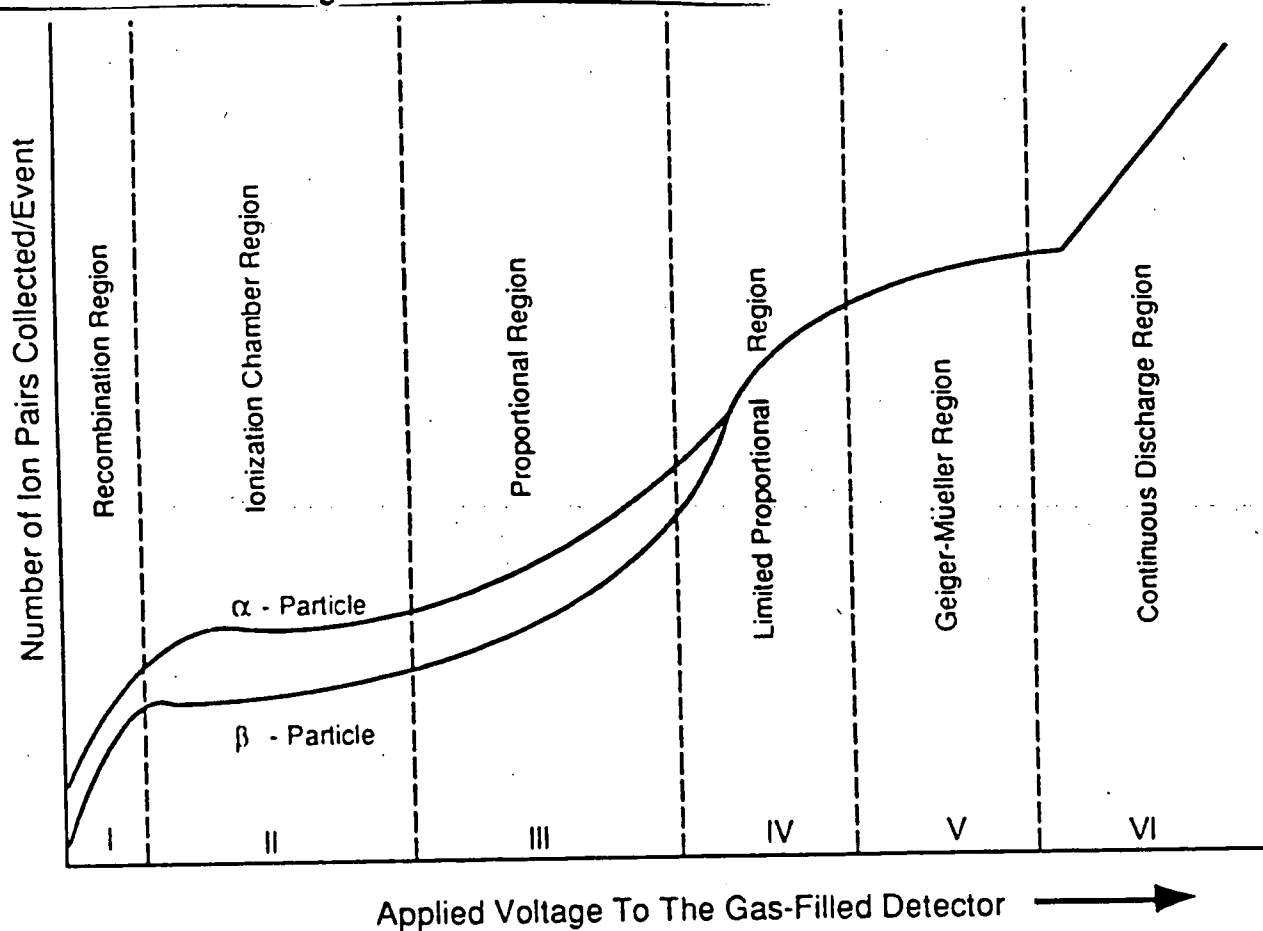


Figure 8: Gas-Filled Detector Characteristic Curve

Detector Characteristic Curve

The Gas-Filled Detector Characteristic Curve in Figure 8 illustrates the relationship between the natural logarithm of the number of ion pairs collected and the detector voltage. The curve has been divided into six regions, each with unique operating characteristics: Recombination Region, Ionization Chamber Region, Proportional Region, Limited Proportional Region, Geiger-Muller Region, and Continuous Discharge Region. The following terms are used in discussion:

Dead time: a period of time during which the detector cannot detect any subsequent events. This dead time restricts the number of radiation events that can be detected. The detector recovers after the positive ions migrate to the cathode.

Quenching: the process of inhibiting continuous or multiple ion discharge in a counter tube caused by gas multiplication or amplification. Gas amplification occurs when primary ions (created by incoming radiation) are quickly accelerated toward the detector's anode, acquiring enough added energy to produce more ions as they move through the gas. The extent of this increase in energy is a direct function of the applied voltage. This process forms an avalanche of ions.

Recombination Region

The recombination region of the curve exhibits the property of a low electric field condition. The voltage applied to the detector is low, and when a radiation event takes place, only a portion of the ion pairs are collected. The remaining ion pairs recombine within the detector. As the detector voltage is increased, ion attraction to the anode and cathode increases, less recombination occurs, and more ion pairs are collected. Operating a detector in the recombination region could be dangerous, as it would underestimate the amount of incoming radiation. No detectors at Rocky Flats operate in this region.

Ionization Chamber Region

Operating in the ionization chamber region begins as increased voltage is applied to the detector. The pulse size levels off and the applied voltage is so high that the recombination process becomes negligible. Almost all the ions formed are collected. The pulse height is dependent only on the number of ion pairs produced by the incident radiation. If the type of radiation is known, the energy determines the pulse height. Since the current reading is independent of the voltage, there is no need for a highly stable voltage supply. The ionization chamber region is the most accurate region of operation.

Summary: Gas-filled detectors operating in the ionization chamber region have the following characteristics:

- Used to detect gamma and X-rays
- Low applied voltage
- No gas multiplication
- Increase/decrease in voltage to detector not critical
- Almost 100% of ions produced are detected
- Ionization chambers respond to a wide energy range

Proportional Region

As the voltage is further increased, the pulse size again begins to increase. The voltage in the proportional region is large enough to create gas amplification. The total pulse size that results depends upon the initial number of ions produced in the gas; i.e., the two values are proportional. The ions produced after the initial ionizing event undergo secondary ionization and are referred to as secondary ions. The increase in secondary ions is generally referred to as gas amplification factor. Since the result of each ionization event is amplified by the applied voltage, detectors that operate in this region are more sensitive than those in the ionization chamber region and can measure lower radiation intensities. A potential disadvantage of proportional region detectors is that they are not as accurate as ionization chamber detectors. In the proportional region, changes in readings are proportional to changes in the incidental radiation.

Summary: Gas-filled detectors operating in the proportional region have the following characteristics:

- Slight changes in applied voltage cause large changes in output pulse size
- Primarily used to detect alpha radiation
- Gas multiplication occurs
- Has a short dead time (about 0.5 microseconds)

Limited Proportional Region

In the limited proportional region, the total charge collected becomes independent of the amount of primary ionization. For a given applied voltage, any type of incident radiation results in the same collected charge. In this region, the voltage is high enough for the secondary ions to produce more ionization. The production of further ionization from secondary ions is called a Townsend avalanche. This creates a space charge which affects the shape of the electric field in the detector. The total charge collected then loses its dependency on the initial primary ionization and therefore becomes inaccurate as a measure of the incident radiation. No detectors at Rocky Flats operate in this region.

Geiger-Muller (GM) Region

If we continue to increase voltage, we reach a value at which all pulse sizes become equal, known as the Geiger Threshold Voltage. At this point, the pulse size becomes independent of the number of primary ions formed, and even a single ionizing event produces a cascade effect; therefore, the GM region is the most sensitive region. Also, the voltage is now so high that each ion in the cascade gains enough energy to produce a new cascade, which produces a discharge along the entire length of the central wire. Because the entire wire length is involved, the pulse size is no longer dependent on the primary number of ions created. If we increase the voltage above the threshold, the counter is said to be operating in the Geiger-Muller region. However, since all pulse sizes are the same, regardless of origin, the device can no longer distinguish between types of radiation. The Geiger-Muller region is the most sensitive region of operation.

Summary: Gas-filled detectors operating in the Geiger-Muller region have the following characteristics:

- Used for beta and gamma radiation
- Avalanche conditions exist
- Saturation may occur
- Alcohol and chlorine are used as quenchers
- Has a long dead time (about 300 microseconds)

Continuous Discharge Region

The electric field strength is so intense in the continuous discharge region that no initial radiation event is required to completely ionize the gas. The strength of the electric field itself produces ionization in the gas and complete avalanching occurs. Due to the region's characteristics, no practical detection of radiation is possible. No detectors at Rocky Flats operate in this region.

Ionization Chambers

Operation and Application

The ionization chamber is normally used for radiation dose and dose rate measurements because of its high level of accuracy. The detector operates in the ionization chamber region, in the current mode, and thus produces an output current which exactly reflects the rate of ionization occurring in the detector.

Since the ionization chamber does not provide any gas amplification, the sensitivity of the detector (the minimum detectable incident radiation intensity) is limited by the minimum current that can be accurately measured.

Although an ionization chamber could be used to count pulses and measure pulse heights, its relatively low sensitivity makes use of other types of gas-filled detectors that are simpler and more effective.

Examples of Ionization Chambers Used at Rocky Flats:

- Victoreen 440: used primarily for building re-entries.
- Victoreen 450-G: the primary gamma detection instrument used at Rocky Flats.

Proportional Counters

Operation and Application

Instruments operating in the proportional region are in the pulse mode. Therefore, they are not used to determine exposure rate, but to count the number of particles or rays interacting in the detector.

Proportional counters are especially useful in applications where discrimination must be made between different types of radiation. At any given applied detector voltage, the pulse heights generated by alpha, beta, gamma, or neutron radiation will be distinctly different, so it is relatively easy to provide circuitry to discriminate against overly large or small pulses.

At Rocky Flats, proportional counters are primarily used for detecting alpha radiation. We are concerned about alpha radiation because it is the primary indicator of contamination from uranium, plutonium, or americium.

Examples of Proportional Counters Used at Rocky Flats:

- Ludlum Model 12-1A: used to survey equipment, areas, and personnel for fixed and removable alpha contamination. A mylar screen is covered by a plate on the detector; the plate is removed during use to allow alphas to penetrate the mylar.
- Combo: combination hand and foot counter; used for self-monitoring of booties, coveralls, and skin of personnel who work in radiation control areas.
- Alpha Met (Meter): installed on gloveboxes; used for self-monitoring of hands and arms as they are removed from glovebox gloves.

Geiger-Muller Counters

Operation and Application

Detectors functioning in the Geiger-Muller (GM) region are often called Geiger Counters or GM Counters. Developed early this century, these detectors are still widely used today because of their simplicity and low cost.

Recall that in the Geiger-Muller region, the applied voltage is sufficient to allow one ionizing event anywhere in the detector to propagate a series of "avalanches" of secondary ionization. This avalanche continues until the detector is completely flooded with ionization. The avalanche terminates when enough positive ions have been created to reduce the electric field strength below the point required to trigger secondary ionizations.

Since the avalanche terminates when a fixed number of positive ions have accumulated, it follows that the output pulse is the same size, regardless of the number of original ion pairs. This is the main disadvantage of the GM detector--it can be used to count events, but delivers no information about the energy spectrum of the incident radiation.

The advantage of the GM detector is that the output pulse is very large and requires only simple signal processing circuitry. The GM detector is also relatively inexpensive.

Dead Time

The minimum time between two separate pulses which are collected in a GM detector chamber is commonly referred to as the resolving time. As ionization occurs in the chamber and electrons move toward the central wire (anode), a field of positively-charged ions is generated near the anode. The negatively-charged electrons are collected quite rapidly (in about a

microsecond) by the central wire.

The positive ions are much larger and take a longer period of time (several hundred microseconds) to travel to the cylinder wall.

This delay in the transport of the positive ion field away from the central wire allows the positive ion field to effectively reduce the electron field at the central wire and stop the discharge current in the detector. These positive ions must be swept away so that the field will return to normal and another discharge can take place. If an ionizing event occurs during the time in which these positive ions are being removed, a pulse in the detector will not occur. Therefore it can be said that the GM counter has a period in which no ionizing events will be seen and no pulses will be produced. This time is referred to as the dead time.

Quenching

In order to minimize the length of the dead time associated with gas-filled detectors, a quenching gas mixture is often added to the detector chamber. This gas mixture is typically about 90 % argon and 10% alcohol. When the avalanche develops, the positive ion field contains both argon and alcohol ions. As these ions move to be collected, collisions with neutral molecules may lead to electron transfer. That is, an argon ion that collides with an alcohol molecule may produce a neutral argon atom and an ionized alcohol molecule. This occurs because the ionization potential in alcohol is less than that of argon. By the time the positive ion field reaches the counter wall, it will contain almost 100% alcohol ions.

The alcohol ions perform two important functions. First, alcohol strongly absorbs any photons that may be produced during avalanche conditions. This decreases the probability of the photoelectric effect, which could result in a continuous discharge. Second, when the alcohol ions reach the wall and become neutral, the excess energy often causes the molecule to break up or dissociate. In the dissociation process, no photons are emitted so that no new discharge occurs.

Saturation

In some older GM systems, detectors would fail low in high radiation fields--an extremely unsafe response. The detector failed low because it saturated. Saturation occurs in a GM detector when ionizing events are occurring so quickly that full-size pulses are not being developed, resulting in severe underestimation of the count rate. Current generation GM meters are designed to fail high or offscale in case of saturation.

Examples of Geiger-Muller Counters Used at Rocky Flats

The instruments following employ a Geiger-Muller (GM)-type, gas-filled probe, connected by a cable to a portable survey meter. The thin wall-type GM probe with retractable beta shield is most common, but other types such as end window and pancake probes are also available. GM instruments are used to monitor beta particles and low-level gamma and X-rays.

- CDV-700: used primarily for checking dosimeter badges following a criticality evacuation.

- Teletector: used for radiation surveys in inaccessible locations and for reducing monitor exposure when surveying high-level sources.
- Ludlum Model 31: designed for use in beta-gamma surveys; utilizes a high sensitivity pancake-type probe.

Scintillation Detectors

Basic Theory

Luminescence is the process whereby energy is absorbed by a substance, and then remitted as visible light; this principle is used to detect radiation with a scintillation detector. Incident radiation interacts with the scintillation material, causing ionization and excitation of the electrons. The de-excitation of the scintillator electrons results in a visible light pulse.

A wide variety of scintillator materials can be used. A good scintillator material is highly efficient in converting incident radiation energy to light. The scintillator must also be transparent to its own light emissions. To minimize dead time, a good scintillator has a short decay time (the time elapsed from absorption to emission). Scintillation detectors like the one shown in Figure 9 can be used to detect any type of radiation, depending on the scintillation material used.

The incident radiation interacts with the scintillator material, causing ionization and excitation of the electrons. When the electrons de-excite, they emit a visible light pulse. These light flashes are channeled by an optical coupling (light pipe) into a photomultiplier tube where the light is analyzed. The photomultiplier tube converts the light pulse to electrons, and multiplies the electrons to produce an output signal.

As the light enters the photomultiplier tube, the photocathode is encountered. The surface of the photocathode is coated with a substance that emits electrons when struck by light. A typical photocathode emits one electron for every 10 photons absorbed.

The electrons emitted from the photocathode are then multiplied by striking dynodes placed at successively high electrical potentials. The potential difference between dynodes accelerates the electrons, so as the electrons travel to each succeeding dynode, more energy is acquired (facilitating the release of an increased amount of electrons at each succeeding dynode). For every electron initially striking a dynode, a specific number of electrons is released. This provides an amplification of the initiating signal to a much larger and useful signal.

The final step in the scintillator detection process is the conversion of the detector output to usable information in the circuitry attached to the detector. This process is external to the scintillation detector and photomultiplier tube.

Operation and Application

Scintillation detectors possess a much better counting efficiency for gamma rays than do gas-filled detectors. Sodium iodide, for example, has a density of 3.7 grams/cm³, while gasses have

Figure 9

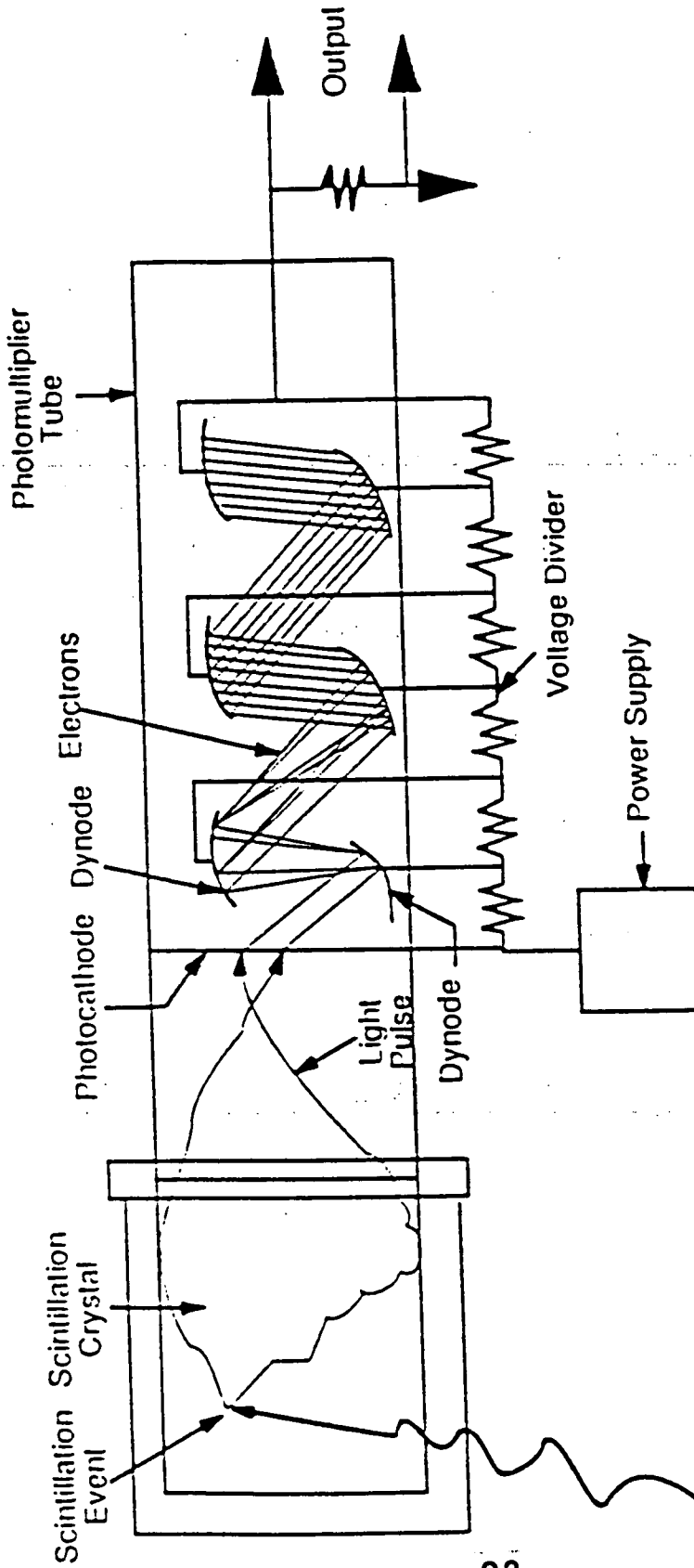


Figure 9 : Scintillation Detector

densities of around 0.001 grams/cm³. Therefore, there are many more atoms available with which gamma rays can interact.

It is possible to use the scintillation detector for gamma ray spectroscopy, since the output pulse height is proportional to the initial gamma ray energy that was deposited. In this case, the output pulses can be fed to a multichannel analyzer to determine the amplitudes of the pulses. Scintillation detectors are also used for neutron detection by using lithium or boron to produce an alpha particle. The alpha particle is then detected as previously described.

Examples of Scintillation Detectors Used at Rocky Flats

- **Alpha Smear Counter:** used to determine low levels of alpha contamination; loose contamination which is gathered by use of the smear test is determined by placing smear paper in the Alpha Smear Counter and counting for a predetermined time. The Alpha Smear Counter is more sensitive than proportional instruments and is read in counts per unit of time.
- **Victoreen 440:** used primarily for building re-entries.
- **Ludlum 111:** used for detection of neutrons; mounted on a wheeled cart for mobility. The detector is surrounded by a 10-inch diameter polyethylene ball which moderates (slows) the fast neutrons down to the instrument's detectable range.
- **Portable Neutron Counter:** a Rocky Flats-designed, portable instrument used for neutron detection by the radiation protection technologists (RPTs). The electronics case is carried on a belt, and the handle-equipped polysphere is hand-carried, thereby allowing the RPT to use the instrument in almost any location.

Semiconductor Detectors

The semiconductor detector can be thought of as the solid-state analogue of an ionization chamber, except that it measures radiation by collection of electron-hole pairs rather than ion pairs.

Basic Theory

Semiconductor detectors are devices which use solid crystals to detect the presence of radiation. In theory, the operation is much like that of a gas-filled detector. The difference lies in the fact that atoms in a solid are packed much closer together than in gasses.

A semiconductor is a material with electrical properties somewhere between those of a good conductor and a good insulator. Earlier, Figure 2 illustrated the comparative energy levels in the electron cloud of an atom. The energy for any electron is confined to those energy bands. The bands are separated by gaps or ranges of forbidden energies—levels where the electrons are not found. A simplified diagram representing these bands is shown in Figure 10. In the lower band the electrons are bound to specific sites within the crystal lattice. This lower band is called the *valence band*. The upper band is called the *conduction band*. Here electrons are free to migrate through out the crystal lattice. These are the electrons that

Figure 10

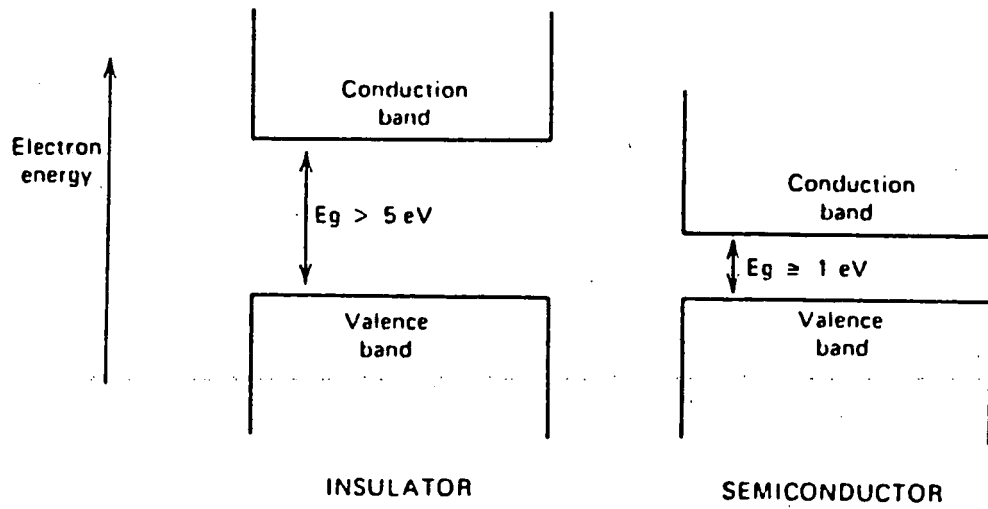


Figure 10 Band structure for electron energies in insulators and semiconductors.

contribute to the overall electrical conductivity of the material. The two bands are separated by the *bandgap*. The size of the bandgap determines whether a material is an insulator or semiconductor. In both, the number of electrons within the crystal lattice is sufficient to fill completely all of the available electron sites within the valence band. Without any thermal excitation, both insulators and semiconductors would have the same configuration—the valence band would be completely full and the conductive band would be completely empty. Neither the semiconductor or the insulator would show any electrical conductivity.

In metals, the highest occupied energy band is not completely full. Electrons can migrate with ease through out the material because they only need to achieve a small increase in energy to be above the occupied state. Metals are characterized by very high electrical conductivity because of this configuration of electrons.

Conversely, electrons in insulators or semiconductors must be able to cross the bandgap to reach the conductive band. Hence the conductivity of the material is orders of magnitude lower. The larger the bandgap, the better the insulator. The bandgap in insulators is 5eV or more, whereas in semiconductors the bandgap is approximately 1 eV.

Materials such as germanium or silicon are used since they can be ionized very easily. In these materials, the electrons that are normally part of the covalent bonds can be easily excited and freed from the specific bonding sites to drift about in the crystal lattice. When excited, not only are electrons created in the otherwise empty conduction band, but a corresponding vacancy or hole for each electron is created in the valence band. Together these are called *electron-hole pairs*. This process is similar to the formation of ion pairs in the gas detectors. Instead of moving freely through a gas toward the anode or cathode, the electrons can be made to move by the application of an electric field. The electron migrates by successive exchanges with electrons in neighboring atoms of the crystal lattice; the corresponding holes behave similarly but in a direction opposite to that of the electrons. This movement of these charges is observed as the level of conductivity in the crystal which can be measured.

Operation and Application

Because the distances traveled are much less than those in a gas-filled detector, the response time for a semiconductor detector is much lower. Also, the amount of energy required to produce one ion pair in a gas-filled detector is 10 times that required to produce an electron-hole pair in a semiconductor. Therefore, for the same level of incident radiation, the semiconductor can produce 10 times the number of charge-carrying ions as can the gas-filled detector.

Two major advantages of semiconductor detectors over scintillation detectors or gas-filled detectors are as follows: They have a very low resolving time, and a very high energy resolution, due to the large number of electron-hole pairs created and the accurate correlation between radiation energy and the number of electron-hole pairs collected.

One major disadvantage is that they are very sensitive to thermal excitation (heat). As a result, they must be kept cool.

Examples of Semiconductor Detectors Used at Rocky Flats

- HPGe (tripod and vehicle mounted models)

A Comparison of NaI and HPGe Sensors

Most of the instrumentation that has been used to perform in situ measurements fall into the category of 'health physics' instrumentation. This instrumentation has been used to screen people, equipment, and areas for signs of gross radioactivity and/or for changes in the background levels of radioactivity. The health physics instrumentation includes but is not limited to gas filled ionization tubes, plastic scintillators, and crystalline scintillators each coupled to a scalar. The scalar typically displays a count rate or an exposure rate. Some of the newer designs that provide energy discrimination can process the count rate within an energy window and yield concentration for a nuclide. These types measurements are appropriate for field screening. They do not provide sufficient information for characterization. Characterization requires the ability to identify and quantify all radionuclides that may be present. Health physics instrumentation, in general, does not have that capability. This includes the 0.0625 inch x 5 inch sodium iodide (NaI) crystal coupled to a scalar commonly referred to as the FIDLER.

The FIDLER instrument was developed to find plutonium that might be dispersed in a weapons accident. The instrument is designed to measure low energy gamma-rays and x-rays which are characteristic of americium and plutonium. The sensor of the FIDLER, 0.0625 in. x 5 in. NaI crystal, by virtue of its design follows a cosine response function to angle. This translates to a narrow field of view, about 30 cm or about 1 foot diameter when held 5cm or 2 inches above the ground. The sensor typically has a frontal active area of about 122 cm^2 and a photopeak resolution of about 25% (15 keV FWHM) for 59.5 keV photons. This means that although it has good sensitivity to low energy photons it can not discriminate between gamma-rays or x-rays that are closer than 10 keV. A sample background spectrum resulting from a FIDLER measurement is shown in Figure 11.

When a FIDLER survey is conducted the operator places the sensor approximately 5cm (2 in.) above the ground and slowly swings it from side to side as he/she moves forward. Given this methodology for a survey the minimum detectable activity (MDA) for americium-241 should be on the order of 15 pCi/g for a distributed source and 50 mCi for a point source.

MDA is that quantity of radioactivity needed to be present before the sensor can measure it with any certainty. The MDA is a function of gamma-ray energy, distribution in the media, other gamma emitting radionuclides present, the sensor and its geometry, count time, and analysis methodology; there are many factors that can affect MDA.

The NaI sensors of which the FIDLER sensor is a special case can be manufactured in a variety of shapes and sizes. These sensors can be coupled with a scalar or a multichannel analyzer. Their angular response, energy response, and resolution varies with size, shape, and photo multiplier tube mounting. For a typical 3 in. x 3 in. NaI crystal the response is nearly isotropic as a function of angle, it exhibits a frontal active area for 59.5 keV photons of about 46 cm^2 , and has a typical resolution of about 13% (7.7 keV FWHM). This sensor is sensitive to a wide range of gamma-ray and x-ray energies. The sensor when coupled to a multichannel analyzer can be used to measure and identify a number of radionuclides. A

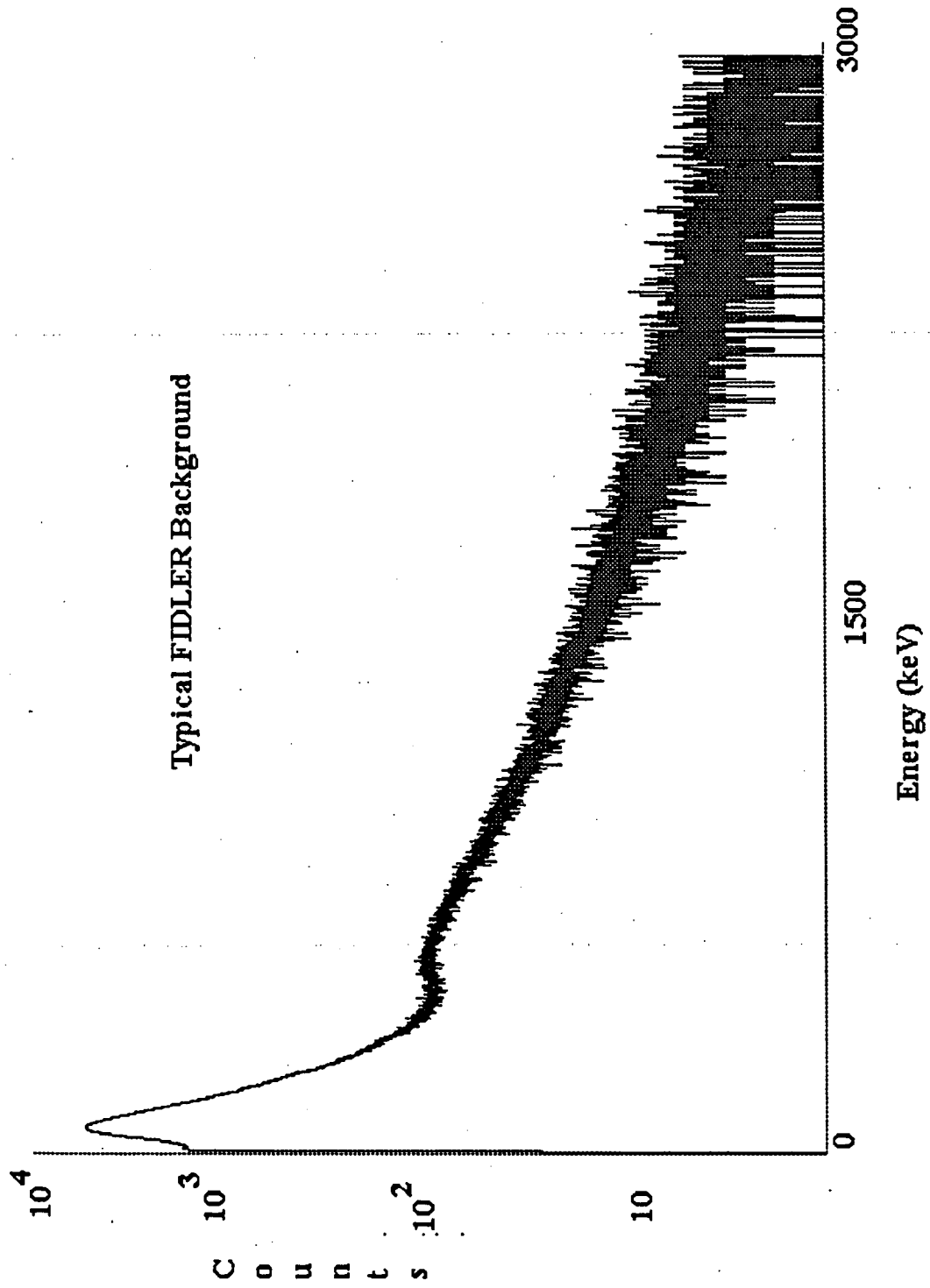


Figure 11. Sample FIDLER Background Spectrum

sample background spectrum resulting from a NaI measurement is shown in Figure 12. One of the factors limiting in its ability to perform characterization is its photopeak resolution. Sites that have low concentrations of contaminating radionuclides whose gamma-ray signatures compete with naturally occurring radionuclides would not benefit from use of NaI sensor for characterization.

High purity germanium (HPGe) sensors can, like the NaI sensor, be manufactured in a number shapes and sizes. These HPGe sensors are normally coupled to multichannel analyzers. For a typical 75% n-type coaxial HPGe sensor the response is nearly isotropic, it has a frontal active area for 59.5 keV photons of about 38 cps*cm²/gam/s, and has a typical resolution of about 1.5% (0.9 keV FWHM). These sensors are sensitive to a wide range of gamma-ray and x-ray energies. A sample background spectrum resulting from a HPGe measurement is shown in Figure 13. The MDA for americium-241 is typically 0.23 pCi/g for a distributed source and 1.8 mCi for a point source. This is correct for a single sensor suspended one meter above the ground with an acquisition time of one hour. The HPGe sensor typically exhibits high energy resolution, on the order of 1 to 3 keV FWHM of detected photopeaks. This high resolution enhances the ability to identify photopeaks and quantify their emanating isotopes making this sensor the one of choice for in situ characterization of radionuclides.

The theory behind in situ measurements applies equally to each of the above sensors. The flux at a given point in space is independent of the sensor or detector used to measure it. What a detector can measure is directly related to the material the sensor is constructed from and its size and shape. So it is critical to choose a detector that will measure the gamma-ray flux to the level of interest.

In-situ Detector Characterization

It is necessary to determine the sensor's response characteristics for the purposes of computing conversion factors and to aide in determining appropriateness of a detector to an application. The Gamma Survey Group (GSG) of Environmental Sciences and Engineering, EG&G Rocky Flats performs a complete sensor characterization prior to systems deployment. The GSG currently employs HPGe for characterization of radionuclides. The detector characterization was accomplished by measuring the detector sensitivity to a number of gamma-ray energies at angles ranging from 0 degrees to 90 degrees. The sources were certified by the United States Department of Commerce, National Institute of Standards and Technology (NIST) as to their isotopic activity. The sources used were ²⁴¹Am, ¹³⁷Cs, ⁶⁰Co, and ¹⁵²Eu. These sources emit useful gamma and/or x-rays at energies ranging from 32.1 keV to 1408.0 keV.

The sources were placed one at a time on the detector characterization fixture. The fixture allowed the sources to sweep out a solid angle at one meter from the detector face while a measurement was made. This was done to smooth out any detector asymmetries. At the completion of each measurement the source was moved 10 degrees on the fixture and another measurement was made. This was repeated until measurements had been made from 0 degrees to 90 degrees. At the completion of the 90 degree measurement the source was placed at 0 degrees and a duplicate measurement was made. This duplicate measurement was made to document any changes in the fixture's geometry relative to the detector. The

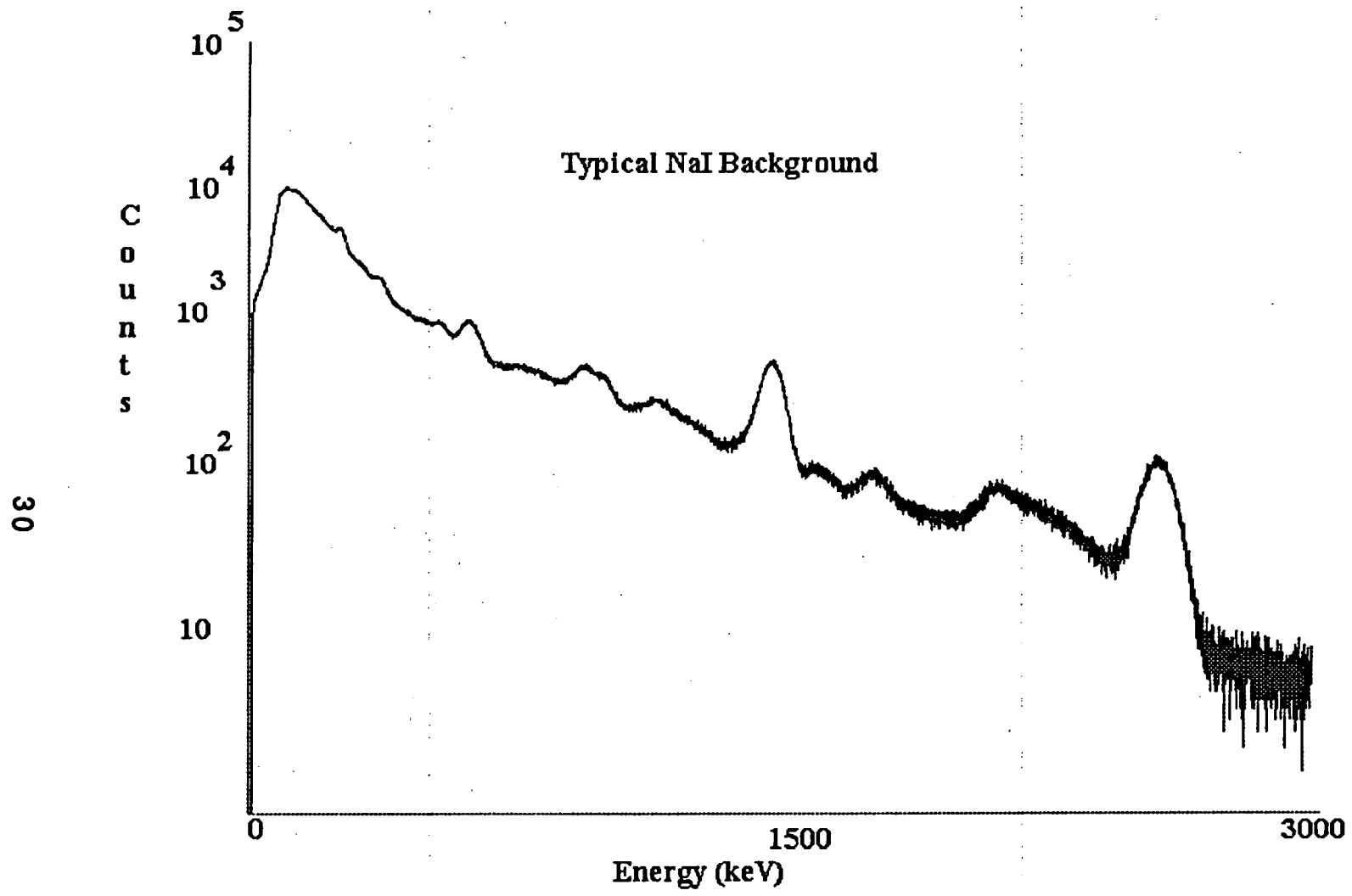


Figure 2. Sample NaI Background Spectrum

measurements at 0 degrees were used to determine the detector's effective area by solving Equation (1).

$$A_0 = \{(4\pi r^2 CR)/(S_0)\}e^{(r/\gamma)} \quad (1)$$

where:

A_0 = detector effective area at 0 degrees in units of $\text{cm}^2 \cdot \text{cps}/\text{g}/\text{s}$

r = source distance from the detector in units of cm

CR = measured photopeak count rate in units of cps

S_0 = source strength in units of g/s

γ = mean free path in air for the gamma energy in units of cm

The effective area generally varies as a function of gamma-ray energy and gamma-ray angle of incidence. Figure 14, graphically displays this for the six detector array, 1A6. Figure 15, shows the response of the center detector, 1A4, of that array. Figure 16, reflects the response of the same center detector, 40227, while it is configured in its own individual cryostat. (Detector 1A4 is detector 40227. The label 1A4 signifies the array mounting as opposed to a single cryostat.) There is a significant change in the response of 1A4 and 40227. This is a result of the other five detectors mounted around 1A4. The other five detectors exhibit a similar response when mounted on individual cryostat as detector 40227. Figure 6, is representative of the response of the other detectors when they are used individually as in a tripod configuration. This relationship for a given energy can be expressed as:

$$A = A_0 R(\theta) \quad (2)$$

where:

$R(\theta)$ = the ratio of the detector response at an angle θ to that at $\theta = 0$ degrees.

The angular response of the detector package is folded into a sensitivity calculation to determine conversion factors for the in situ measurement. (The theory of in situ measurements is provided and the sensitivity calculation formulas derived there.) It is convenient to compute conversion factors for two detector heights with a branching of unity and plot the results ($\text{pCi}/\text{g}/\text{cps}$) as a function of energy. The resulting plots are shown by Figures 17 through 24. The curves are fitted and the coefficients are loaded into analysis software. The software package can then compute the appropriate conversion factor for any isotope within its library for given detector height.

The conversion factors computed and loaded into the analysis software for the in situ detectors reflect the following assumptions:

soil density = 1.5 g/cm^3

soil moisture = 10%

vertical distribution = homogeneous

averaging depth = 3.0 cm

air density = 0.001293 g/cm^3

Detector IA6

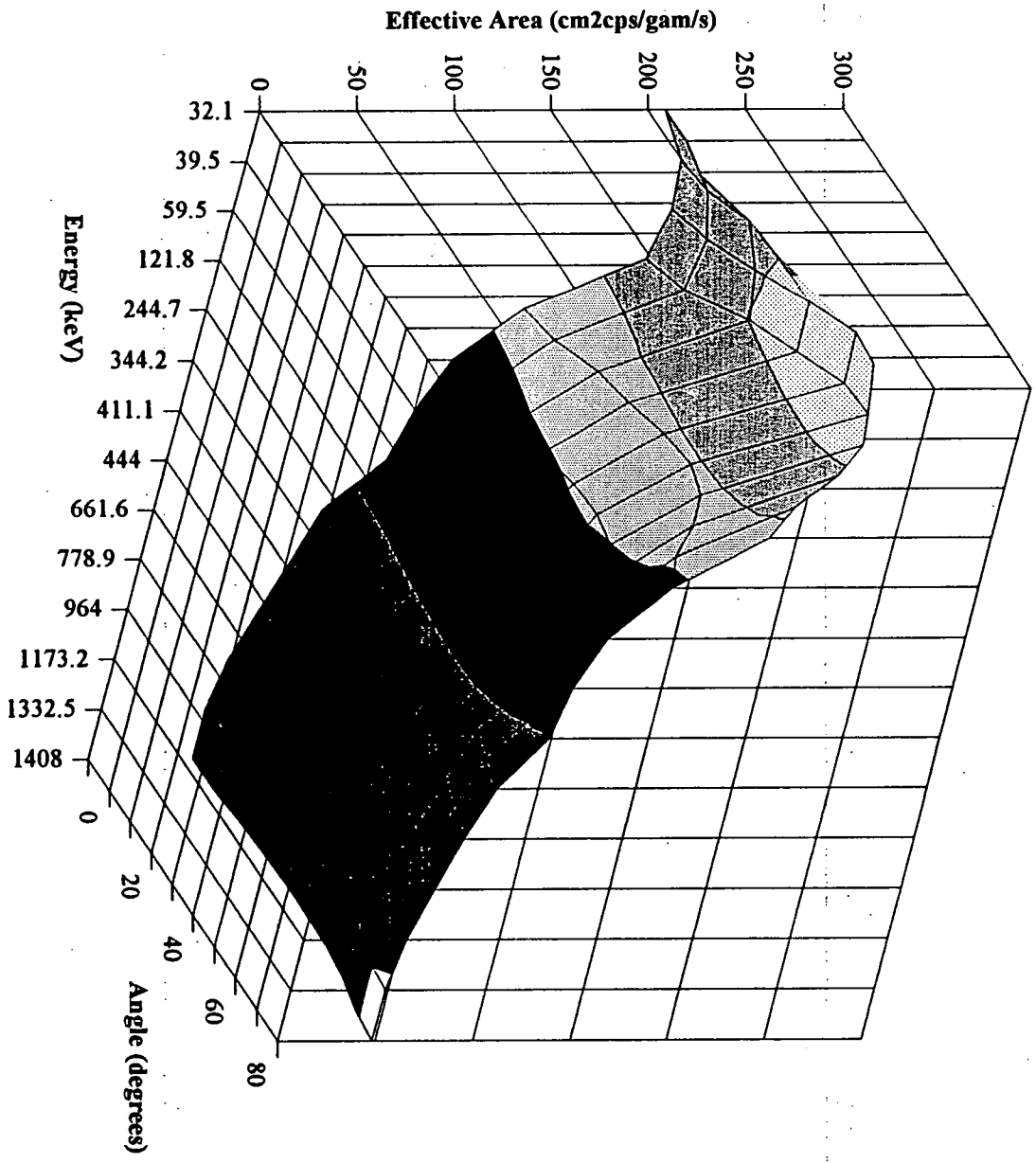


Figure 4. Detector IA6 Response.

Detector 1A4

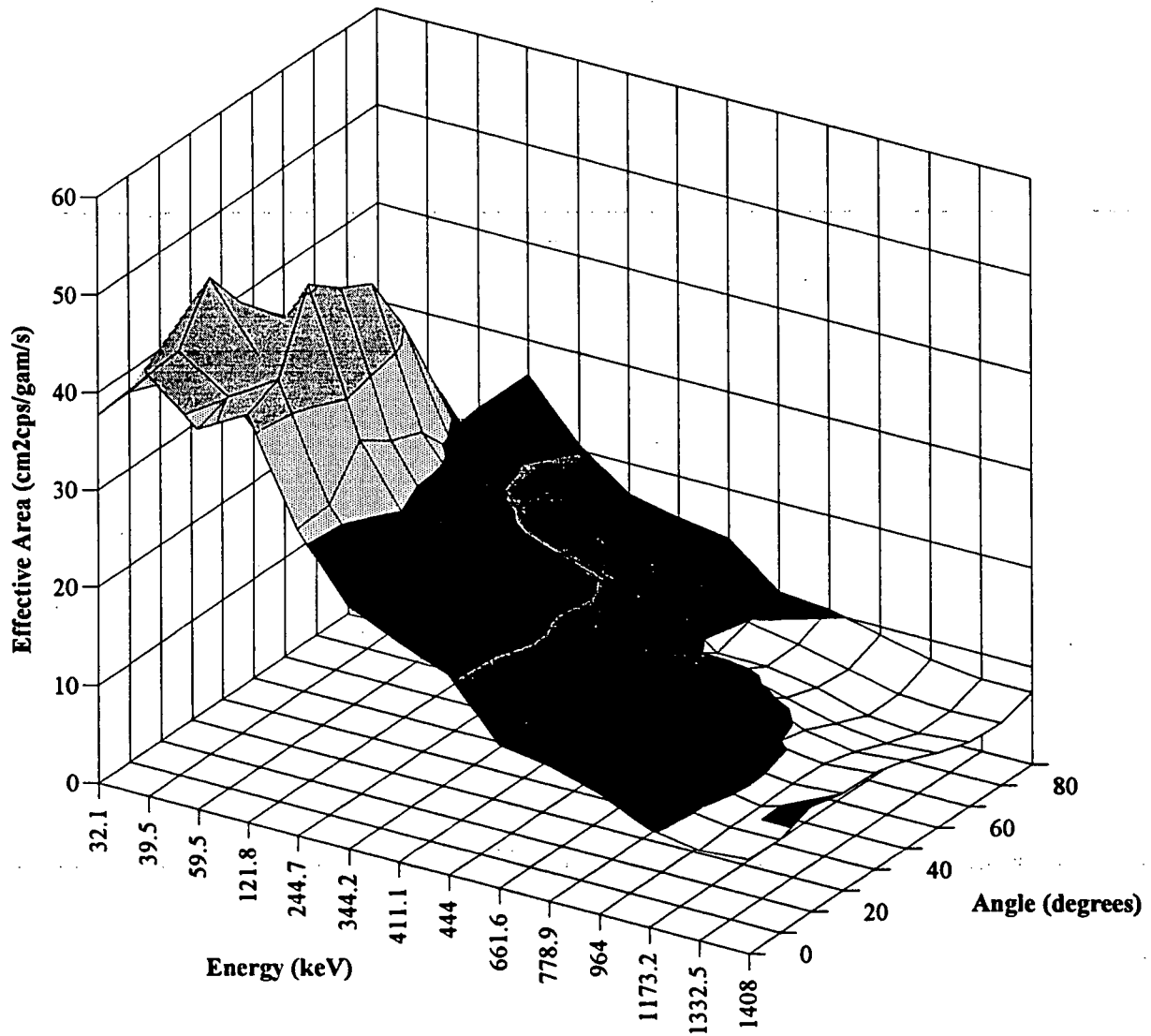


Figure 5. Detector 1A4 Response.

Detector 40227

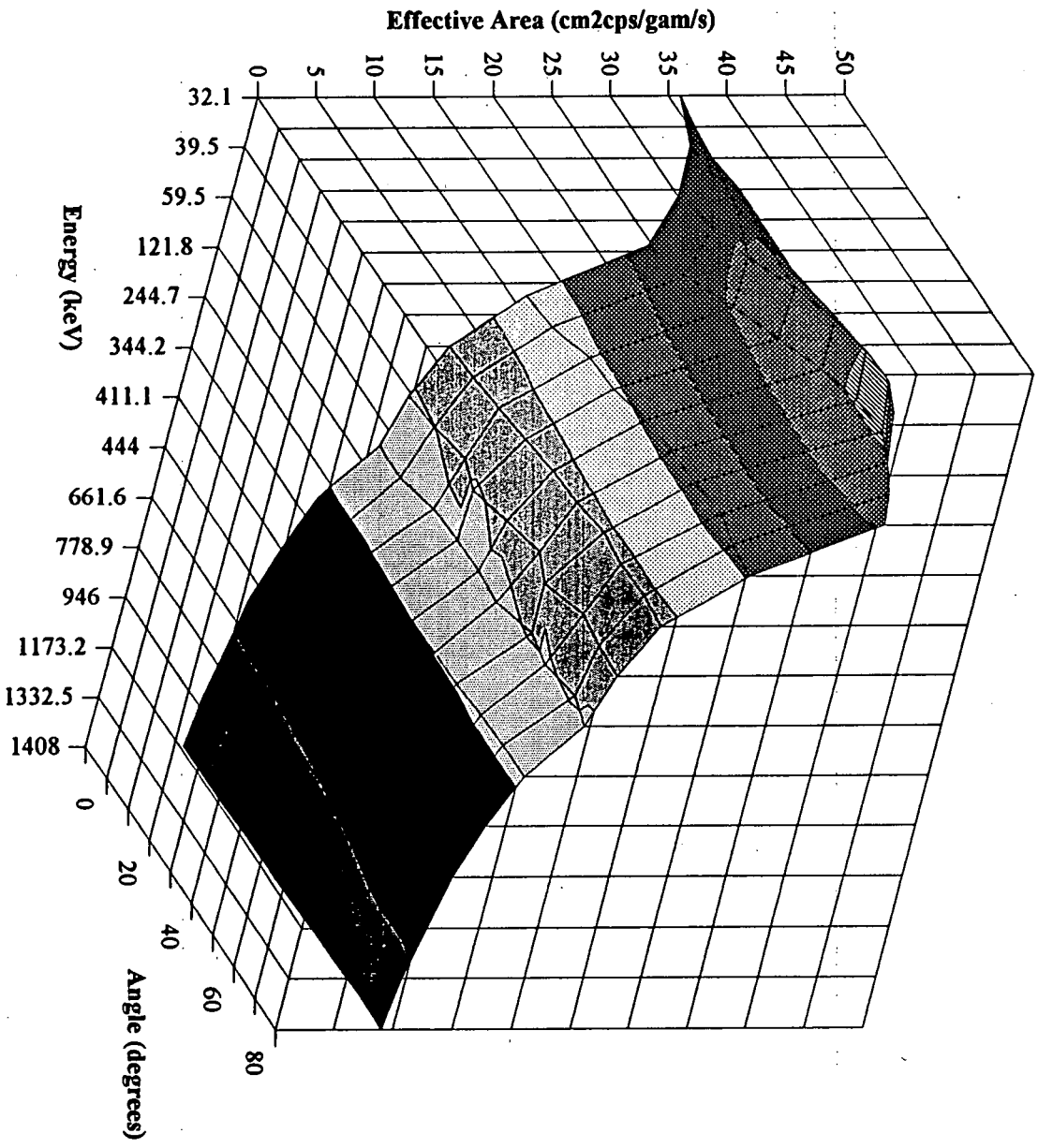


Figure 6. Detector 40227 Response.
35

Detector 1A6

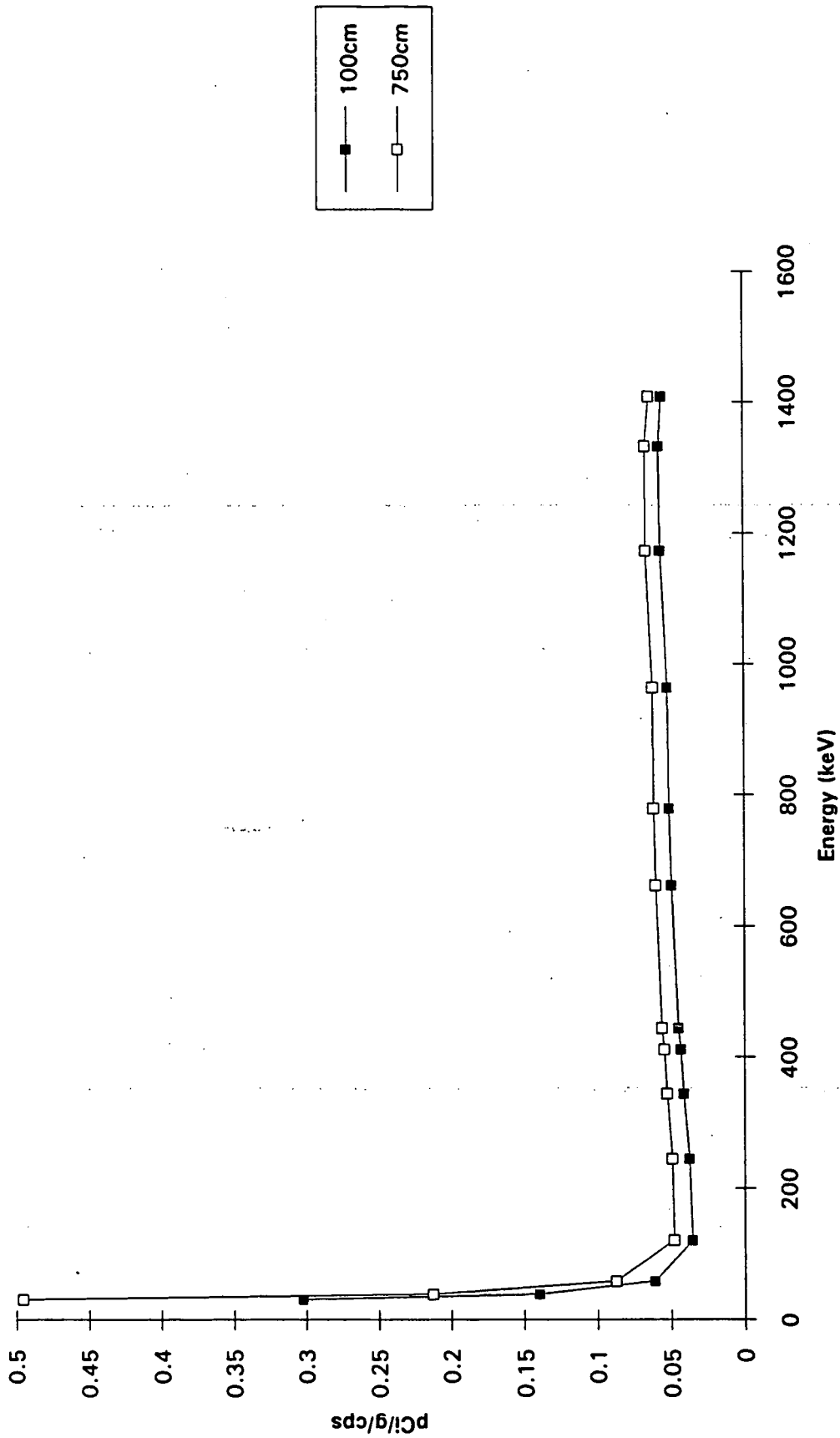


Figure 17. Detector 1A6, Conversion Factors vs Energy at 100cm and 750cm.

Detector 1A4

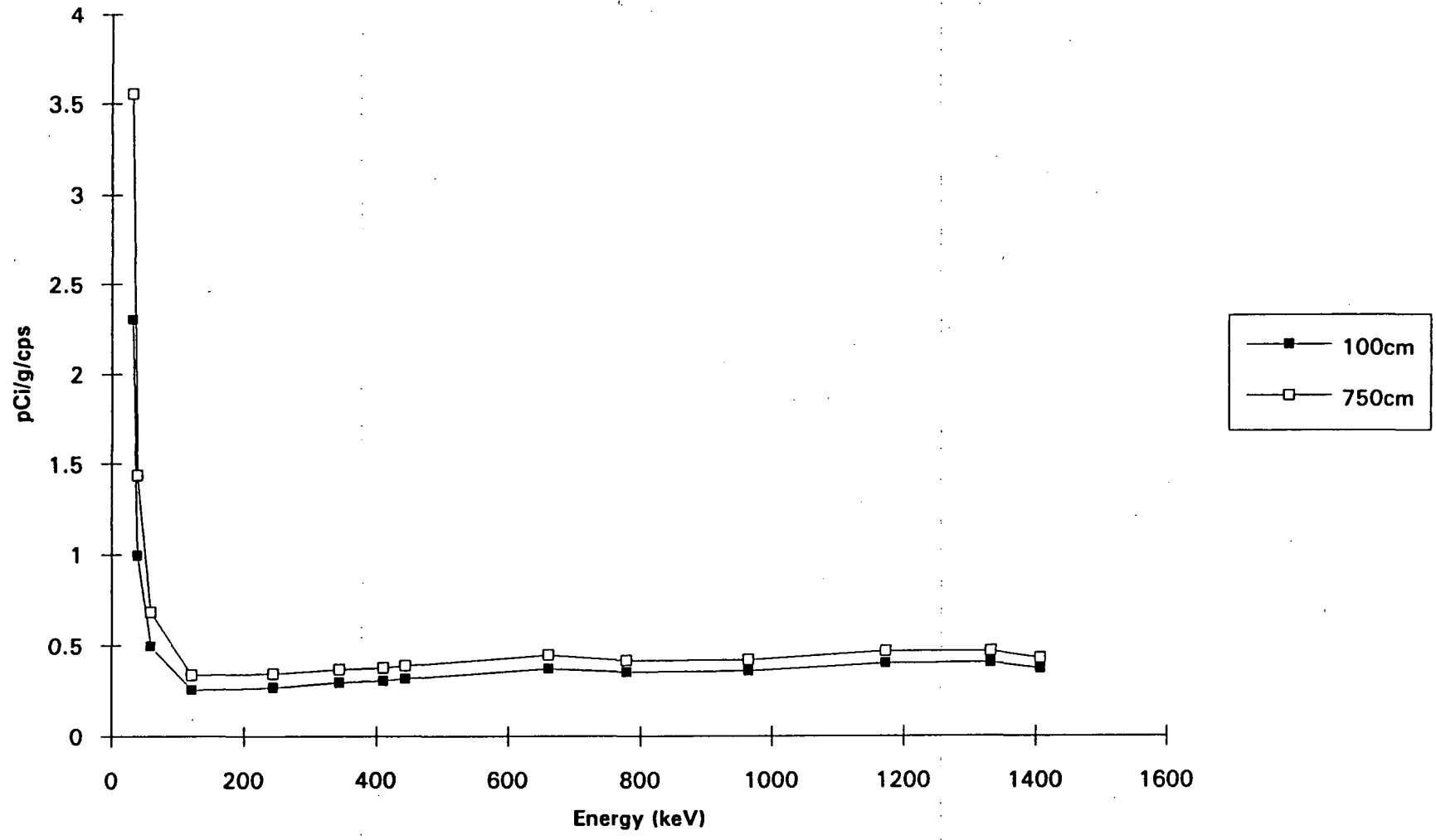


Figure 8. Detector 1A4, Conversion Factors as a Function of Energy at Detector Height of 100cm and 750cm.

Detector #30687

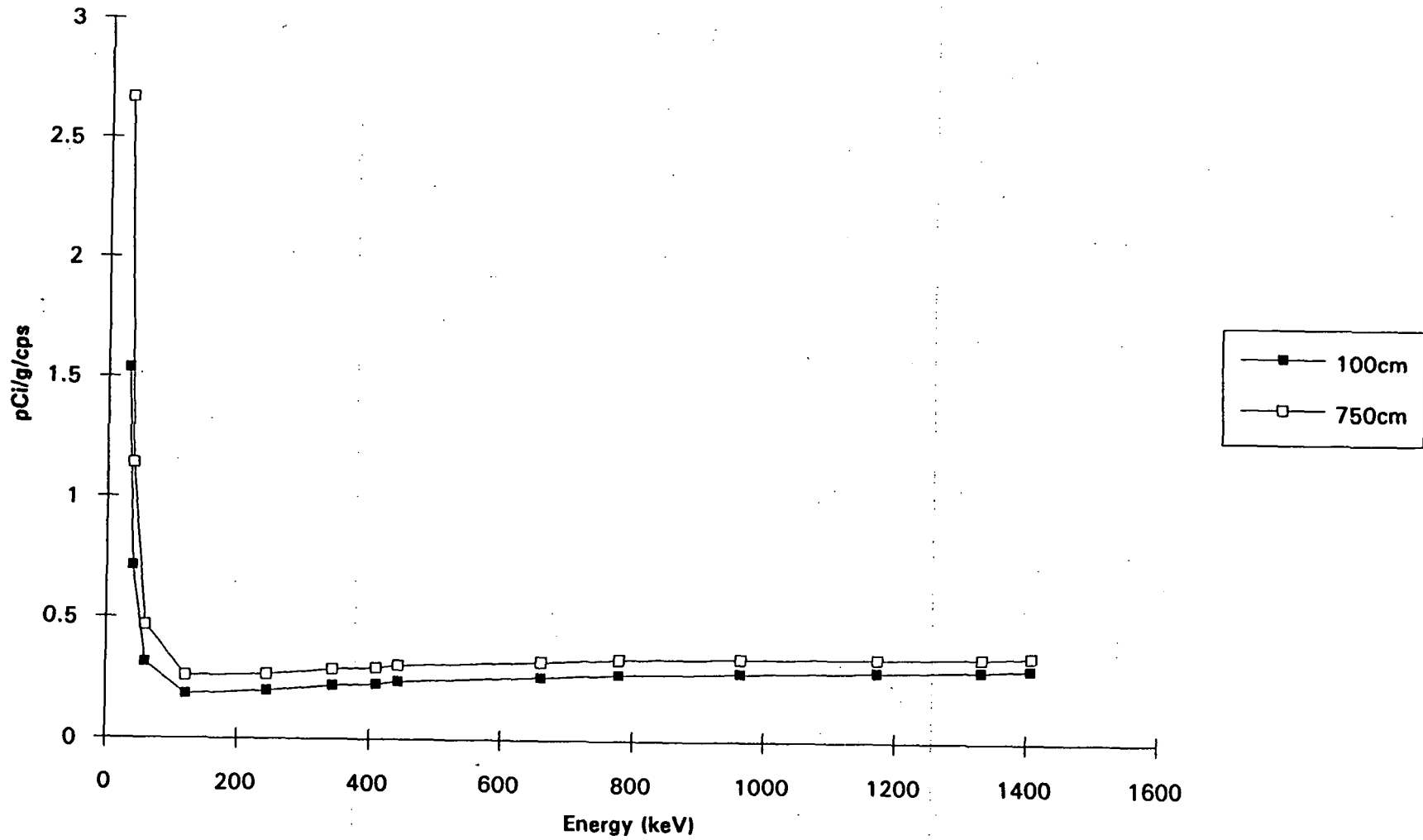


Figure 19. Detector #30687 Conversion Factors vs Energy at Detector Height of 100cm and 750cm.

Detector #30699

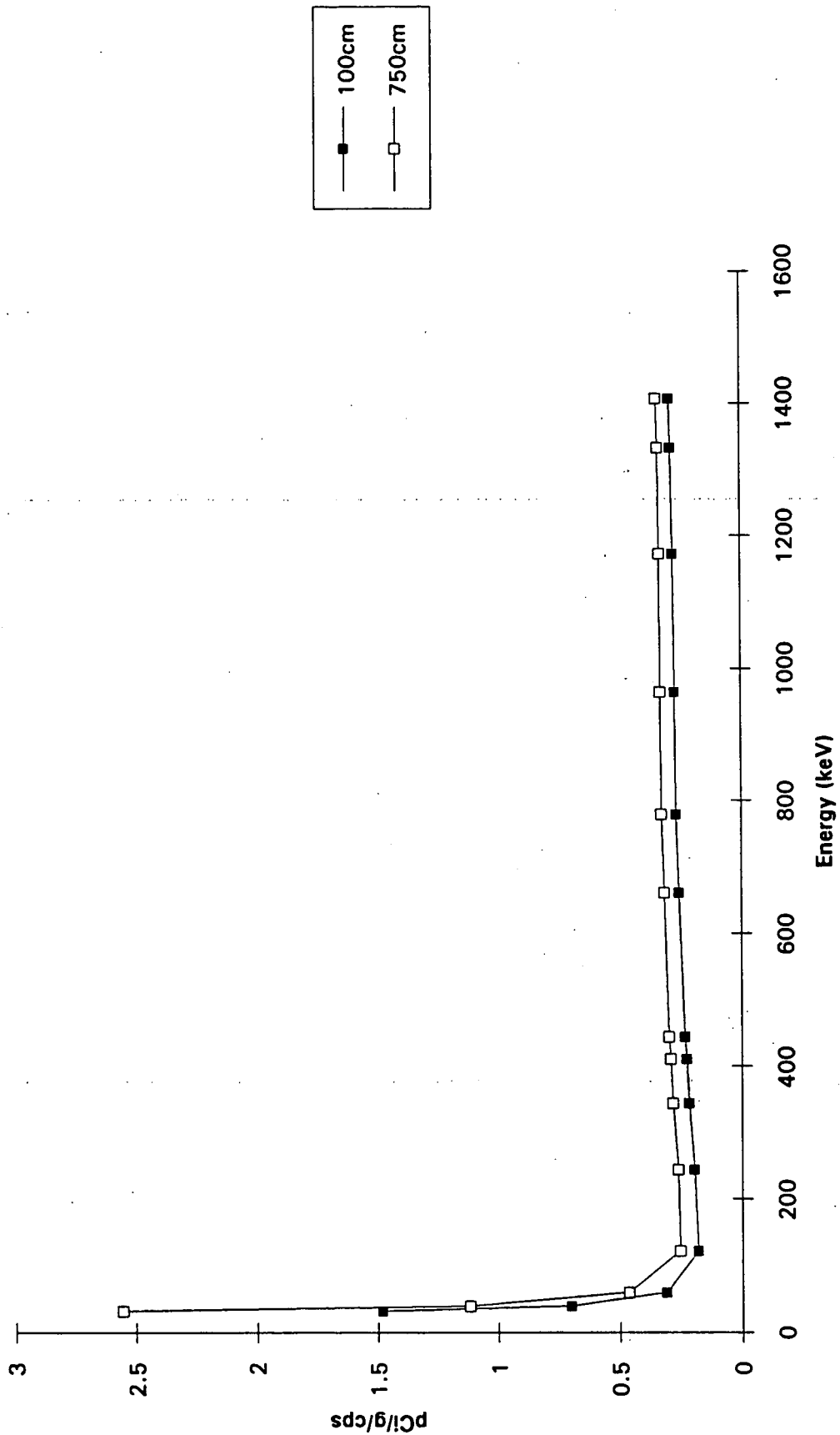


Figure 20. Detector #30699 Conversion Factors vs Energy at Detector Height of 100cm and 750 cm.

Detector #30716

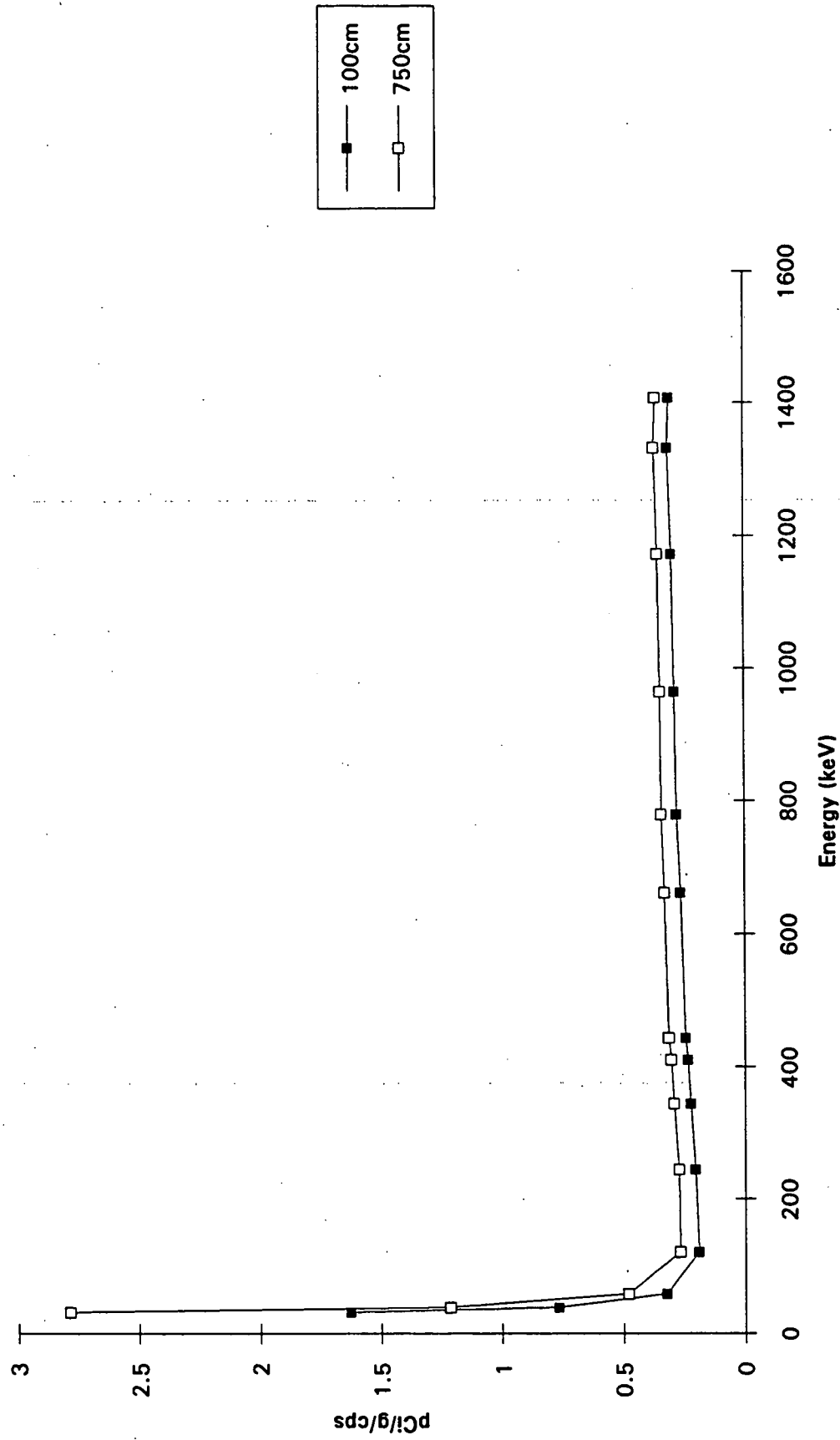


Figure 21. Detector #30716 Conversion Factors vs Energy At Detector Height of 100cm and 750cm.

Detector #40227

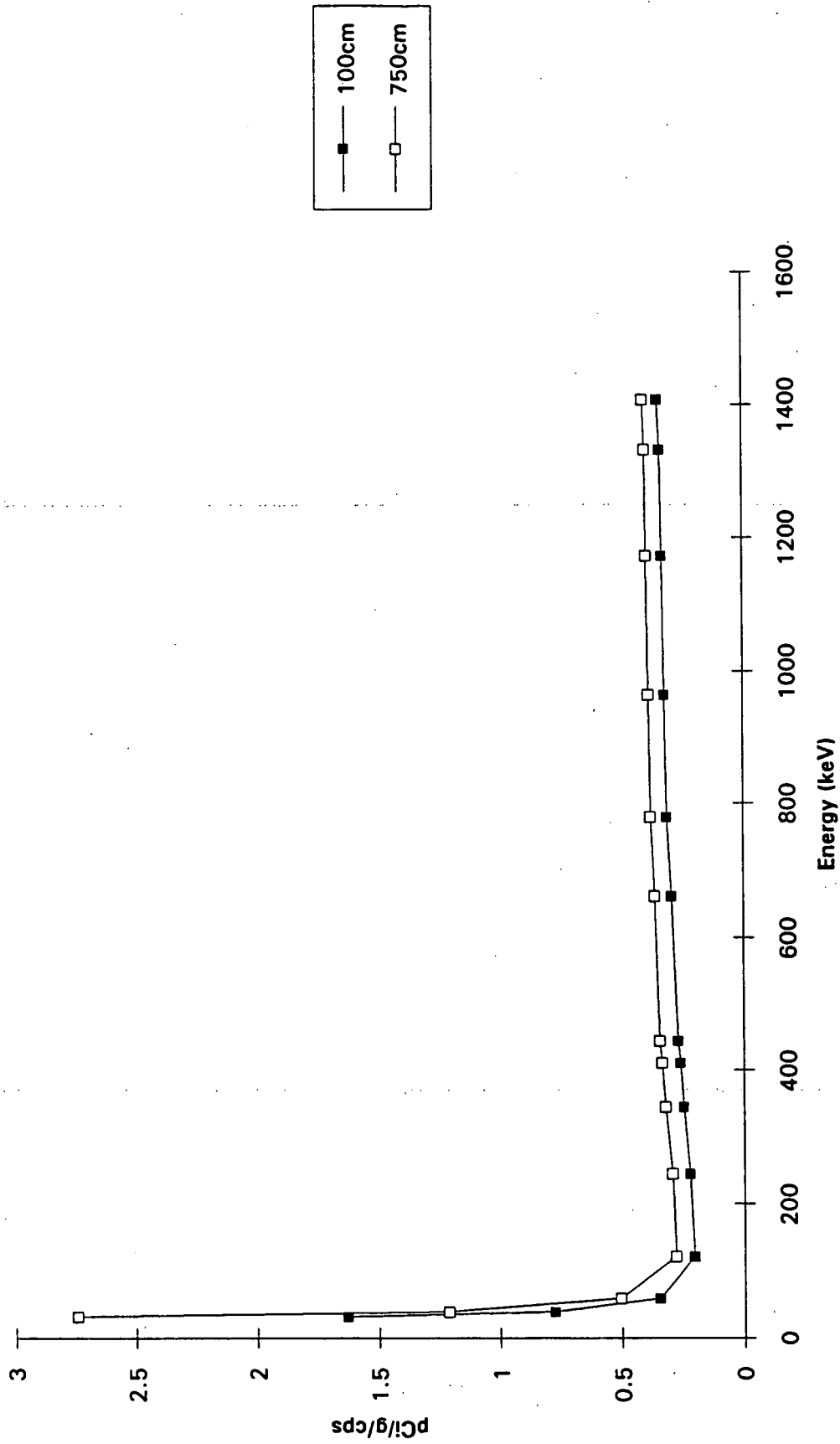


Figure 12. Detector #40227, Conversion Factors as a Function of Energy at Detector Height of 100cm and 750cm.

Detector #40279

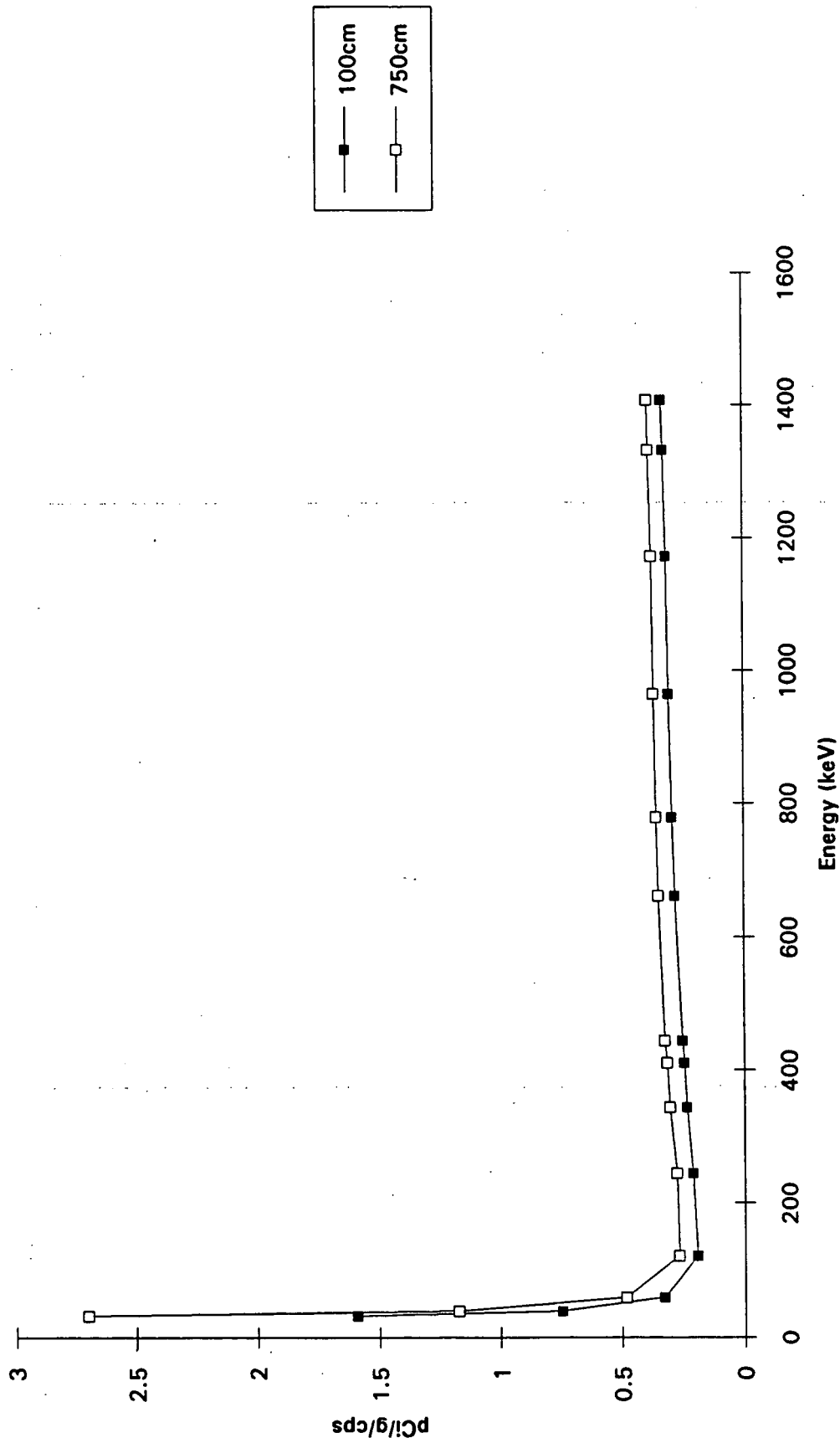


Figure 23. Detector #40279 Conversion Factors vs Energy at 100cm and 750cm Detector Height.

Detector #40293

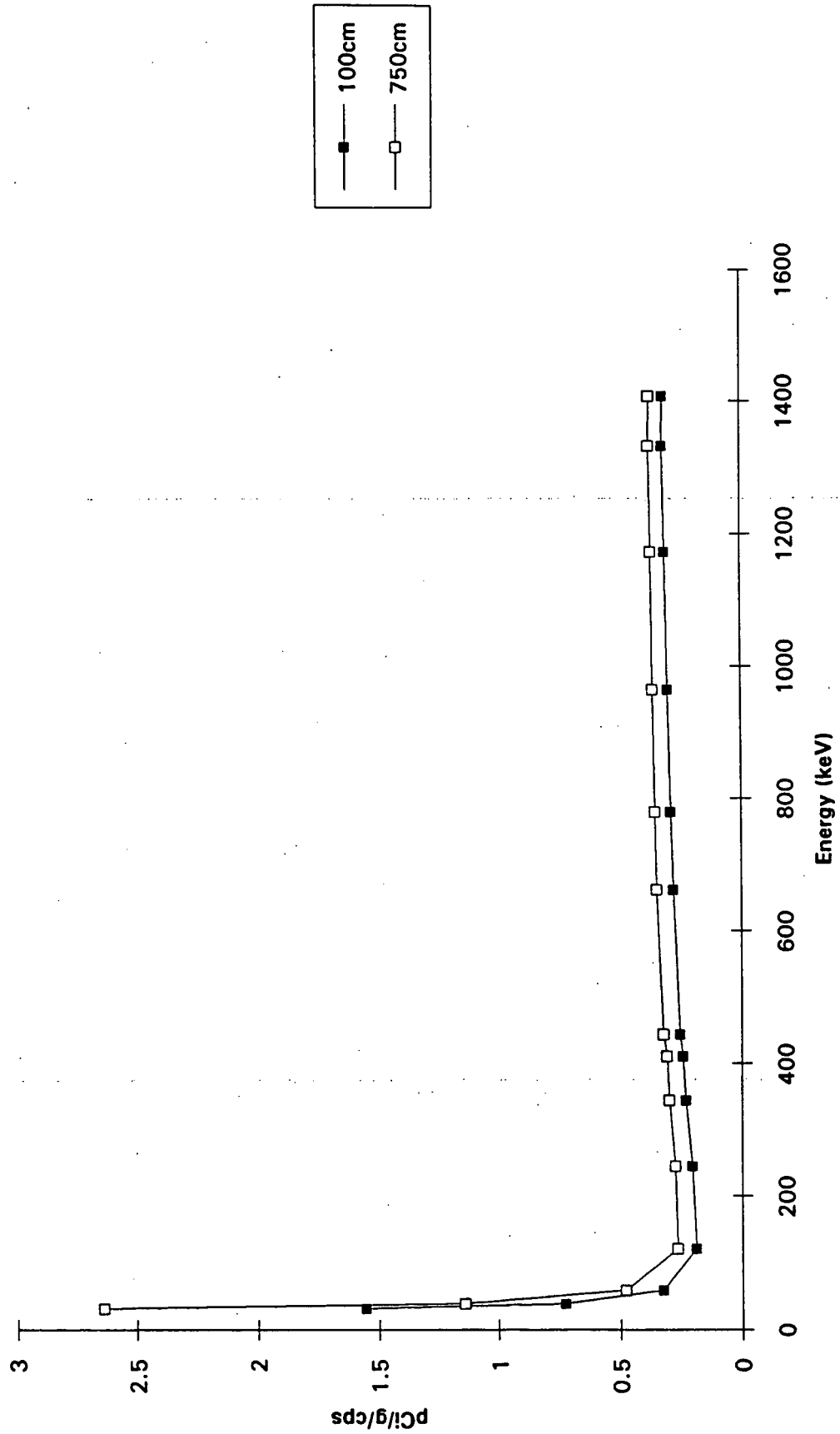


Figure 24. Detector #40293 Conversion Factors as a Function of Energy at Detector Height of 100cm and 750cm.

From the sensitivity calculations the detector 'field of view' can be determined. It should be noted that when an in situ measurement is made the model shows that the detector measures an infinite plane. The detector 'field of view' is defined as that circle on the plane where 90% of the gammas originate that contribute to the photopeak counts. The 'field of view' is a function of gamma-ray energy, vertical distribution, and detector height. 'Field of view' curves for the 1A6 detector package are presented in Figure 25.

The Theory of In-situ Measurement

The unscattered flux of gamma-rays of energy E at a height above a smooth air-ground interface due to an emitter distributed in the soil is given by (see Figure 26):

$$\Phi = \int_0^\infty \int_0^\infty (S_v / 4\pi r^2) \exp[-(\mu/\rho)_a \rho_a r_a] \exp[-(\mu/\rho)_s \rho_s r_s] 2\pi x \, dx \, dz \quad (3)$$

where:

S_v = the activity per unit volume in units of (g/s)/cm³

$r = r_a + r_s$ in units of cm

$(\mu/\rho)_a$ = air attenuation coefficient in units of cm²/g

$(\mu/\rho)_s$ = soil attenuation coefficient in units of cm²/g

ρ_a = air density in units of g/cm³

ρ_s = soil density in units of g/cm³

This expression assumes a source distribution which varies only with depth. For fallout activity the distribution after a period of time can be reasonably approximated by an exponential distribution given by:

$$S_v = S_v^0 e^{-\alpha z} \quad (4)$$

where:

S_v^0 = the activity per unit volume at the surface and

α = the reciprocal of the relaxation length in units of cm⁻¹.

Rewriting Equation (3) in terms of q and z , combining with Equation (4) and integrating over z leads to:

$$\Phi = S_v^0 \int_0^{\pi/2} \frac{\tan \theta \exp[-(\mu/\rho)_a \rho_a h \sec \theta]}{[\alpha + (\mu/\rho)_s \rho_s \sec \theta]} d\theta \quad (5)$$

Vehicle System 'Field of View' for Detector 1A6 and 59.5 keV Gamma-rays

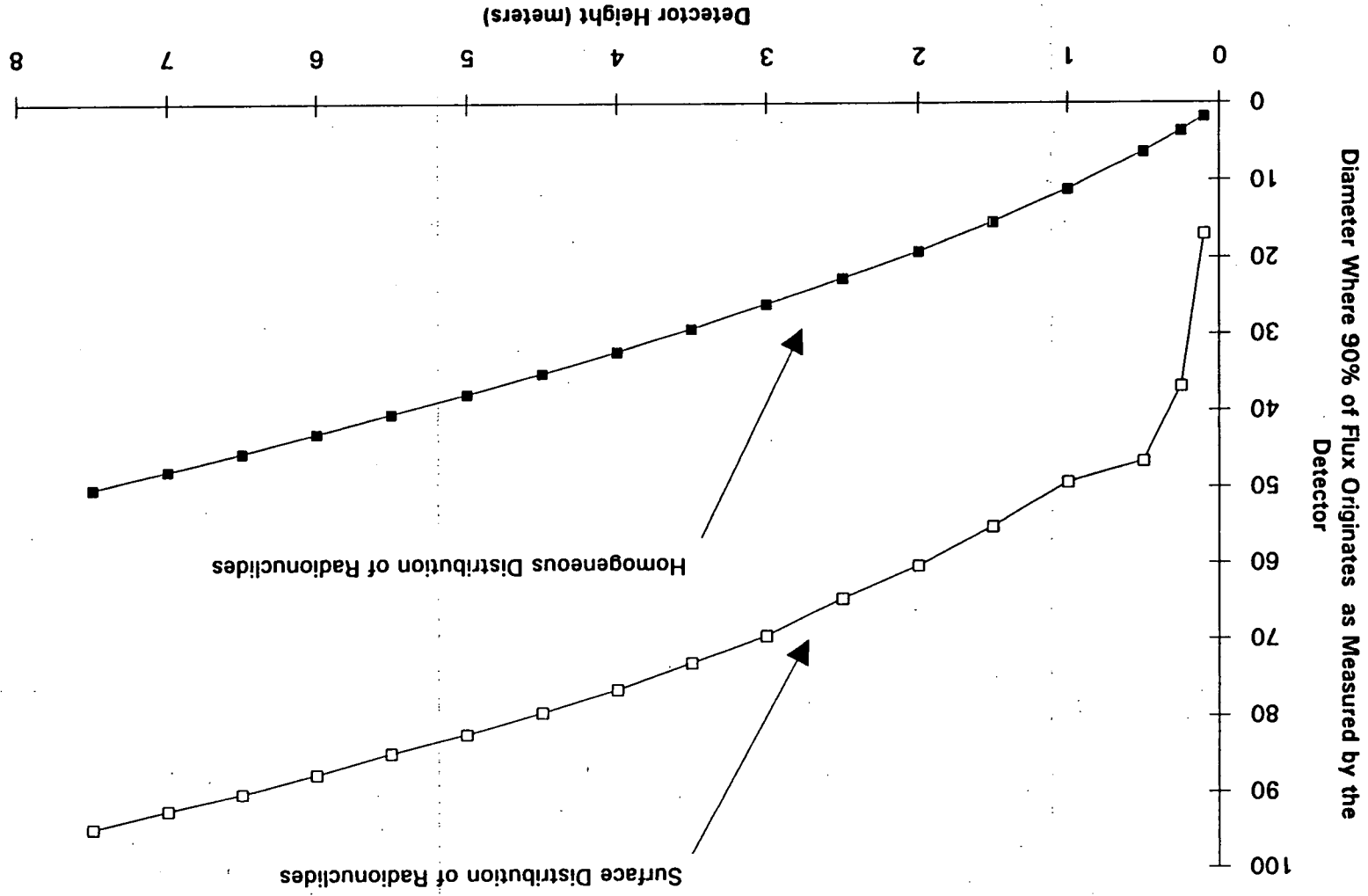


Figure 2.5. 'Field of View' vs Detector Height for 59.5keV

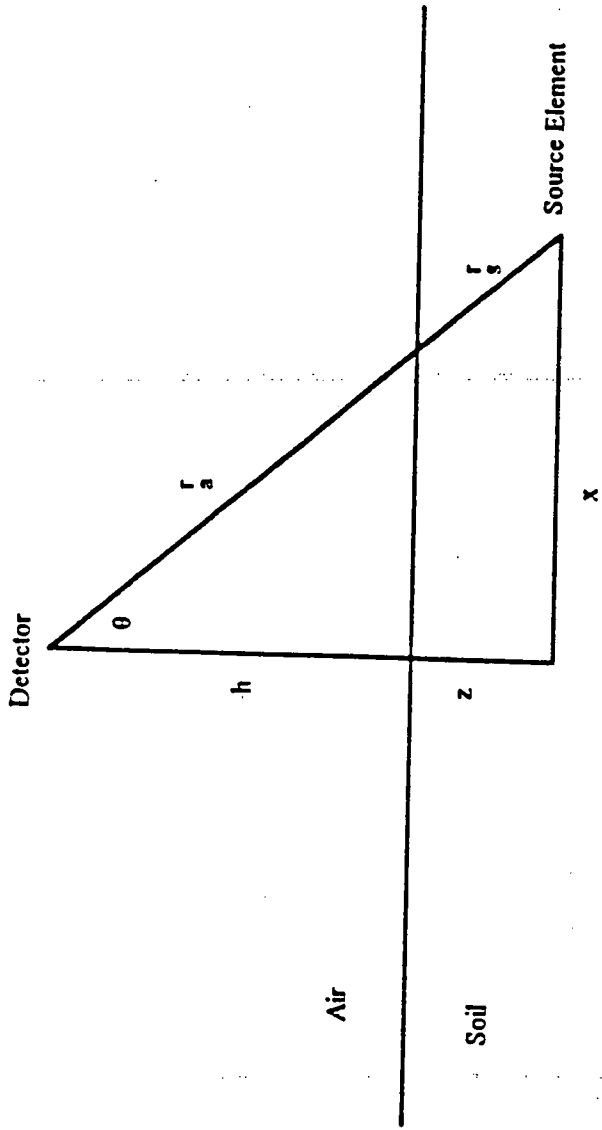


Figure 26. Geometry used in the derivation of conversion factors relating *in situ* photoppeak count rate data to isotope concentration in the ground.

Conversion Factors From Point Sources

The detector response to a given flux of gamma-rays (Φ) of energy E incident at an angle θ can be given in terms of an effective detector area, A, defined by:

$$A = N_p / \Phi \quad (6)$$

where:

N_p = the net photopeak count rate in units of cps.

The effective area, as stated above, for a given energy, varies as a function of the gamma-ray angle of incidence and is normally written as:

$$A = A_0 R(\theta) \quad (2)$$

Both A_0 and $R(\theta)$ can be determined experimentally with point gamma-ray sources.

Combining Equations (6) and (2) with Equation (5) leads to an expression which relates the measured photopeak count rate to source activity in the soil. This is given by:

$$N_p / S_v^0 = [A_0 / 2_0] \int_{\pi/2}^{\theta} \{ R(\theta) \tan \theta \exp[-(\mu/\rho)_s \rho_s h \sec \theta] \} / [\alpha + (\mu/\rho)_s \rho_s \sec \theta] d\theta \quad (7)$$

The conversion factor N_p / S_v^0 given by Equation (7) is in units of cps/(γ/cm^3s).

For a specific isotope the conversion factor is normally changed to units of cps/(pCi/cm³). Multiplying the expression in the brackets in Equation (7) by the soil density (g/cm³) leads to the conversion factor

$N_p^0 / (S_v / \rho)$ normally given in units of cps/(pCi/g).

In general, the average concentration in the top z cm, S_v^z , for a source distributed exponentially with depth is given by:

$$S_v^z = 1/z \int_0^z S_v^0 e^{-\alpha z} dz = [S_v^0 / (\alpha z)] (1 - e^{-\alpha z}) \quad (8)$$

Combining Equations (7) and (8) leads to:

$$S_v^z / \rho / N_p = [(1 - e^{-\alpha z}) / (\alpha z)] B \{ (A_0 \rho_s) / 2_0 \int_{\pi/2}^{\theta} \{ R(\theta) \tan \theta \exp[-(\mu/\rho)_s \rho_s h \sec \theta] \} / [\alpha + (\mu/\rho)_s \rho_s \sec \theta] d\theta \}^{-1} \quad (9)$$

in units of (pCi/g)/cps, where B converts γ/s to pCi for a specific isotope.

This conversion factor has utility when comparing in-situ results with soil sample results where

the soil sample is taken from 0 to z units deep and is finite.

Measurements

Simply stated, as shown by the theory, the measurement takes place with the sensor positioned over the area of interest and a gamma-ray energy spectrum is collected over a period of time. If there is material between the area to be characterized and the detector such as water/snow (see Figure 27), gravel, pavement, concrete, or even clean soil then the measurement becomes more complex. Any material between the sensor and the area of interest will reduce the amount of unscattered flux effectively shielding a potential source term.

The model (Figure 26) assumes an infinite flat plane. In practice, at Rocky Flats, one rarely has a flat horizontal plane to measure. There hillsides, valleys, and other elevations that require characterization. Hillsides can be approximated by tipping the horizontal plane model. This geometry does not affect the characterization results.

When a measurement is taken in a valley the computed activity is normally greater than the actual. This relationship holds true for both point and distributed sources. The area to be characterized is effectively brought closer to the sensor. This reduces the distance and attenuation affects increasing the gamma flux at the detector.

When a measurement is made with the detector on the top of a knoll the computed activity is lower than the actual activity. This is true for both distributed sources and point sources. The area to be characterized has effectively been moved away from the sensor. It is true that the field of view has been effectively increased such that the total volume is greater, but the model has been violated and the assumptions used to compute conversion factors are no longer valid.

The actual geometry for a measurement could be any combination of the above in varying degrees. The area characterization would be affected accordingly. Ideally, sampling strategies would be developed to minimize topographic effects.

Included as Enclosure II are the Lecture Notes from In Situ Gamma-Ray Spectrometry given by Kevin M. Miller and Peter Shebell. These notes are included with permission from Kevin M. Miller. In any event, in situ gamma-ray spectroscopy is another tool available to assist in radiological site characterization.

Effect of Standing Water on The Flux From a Plane Source at 1 Meter

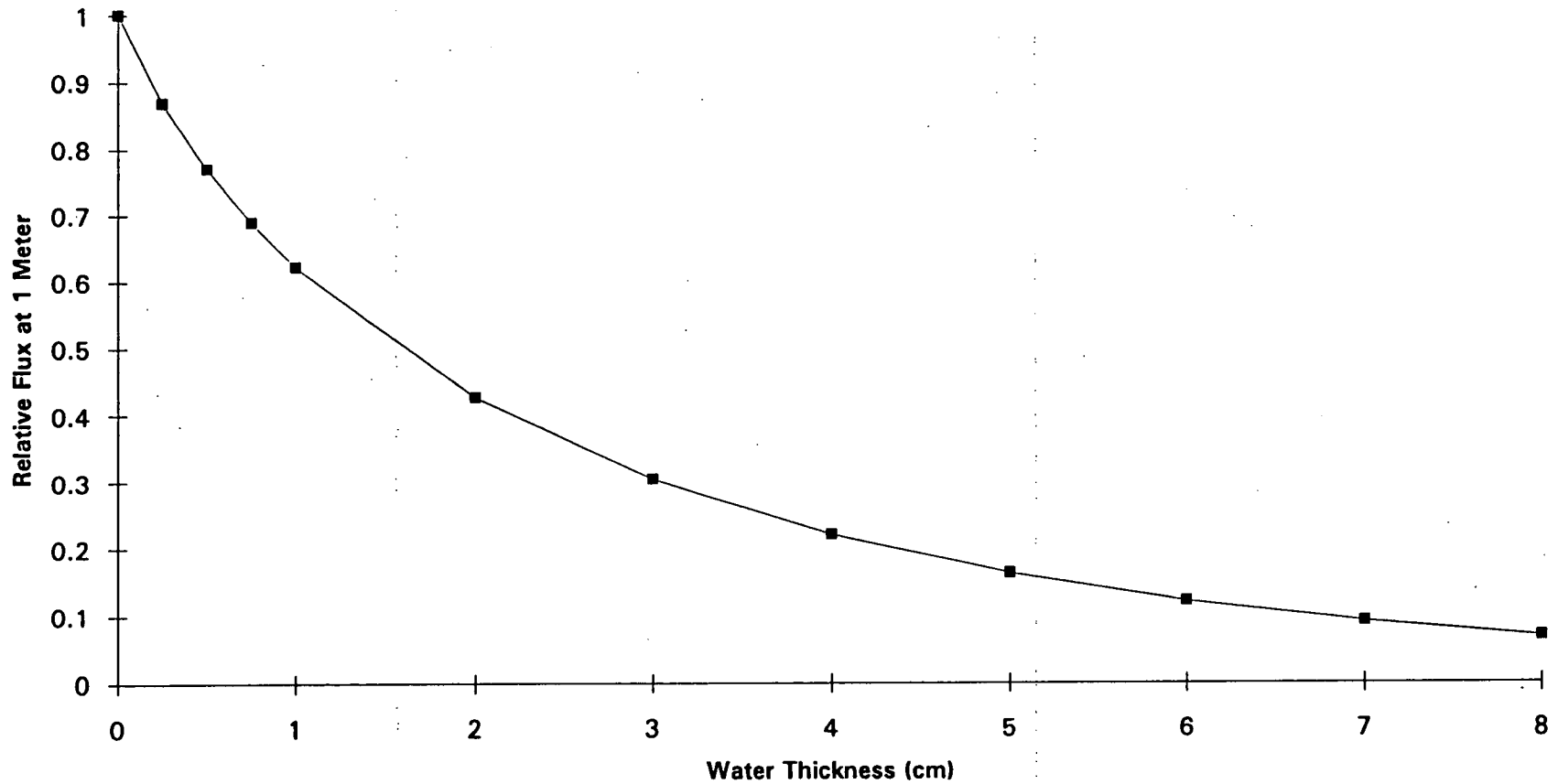


Figure 27. Effect of Water on Gamma-ray Flux

References

EG&G; 1991 Reference Handbook—Nuclear Criticality

EG&G; 1991 Reference Handbook—Basic Radiation Safety

EG&G; 1991 Reference Handbook—Radiation Instrumentation

Keenan, Wood & Klienfiler 1976, General College Chemistry, 5th Edition
Harper & Row, New York, New York.

Knoll, Glenn F.; 1989 Radiation Detection and Measurement, 2nd Edition
John Wiley and Sons.

Knoll, Glenn F.; 1991 Radiation Detection and Measurement, short course notes, University of
Michigan

R. T. Rami

health and safety laboratory

IN SITU Ge(Li) AND NaI(Tl) GAMMA-RAY SPECTROMETRY

H. L. Beck, J. DeCampo and C. Gogolak

September 1972

Inclosure I

IN SITU Ge(Li) AND NaI(Tl) GAMMA-RAY SPECTROMETRY

Harold L. Beck
Joseph DeCampo
Carl Gogolak

September 1972

Health and Safety Laboratory
U. S. Atomic Energy Commission
New York, New York 10014

N O T I C E

This report was prepared as an account of work sponsored by the United States Government. Neither the United States nor the United States Atomic Energy Commission, nor any of their employees, nor any of their contractors, subcontractors, or their employees, makes any warranty, express or implied, or assumes any legal liability or responsibility for the accuracy, completeness or usefulness of any information, apparatus, product or process disclosed, or represents that its use would not infringe privately-owned rights.

Printed in the United States of America
Available from

National Technical Information Service
U. S. Department of Commerce
Springfield, Virginia 22151
Price: Printed Copy \$3.00; Microfiche \$0.65

ABSTRACT

The use of large NaI(Tl) crystals and large Ge(Li) diodes to make in situ measurements of γ -rays from sources in the soil and air is described. Methods for inferring source concentrations and contributions to the total exposure rate from individual emitters are discussed and tables of photon flux to source activity and flux to exposure rate conversion factors are presented. Descriptions are given of the calibration of 4 in. by 4 in. NaI(Tl) detectors, and 25 cm³ and 60 cm³ Ge(Li) diodes. A number of applications of field spectrometry are discussed.

TABLE OF CONTENTS

TEXT	<u>Page</u>
I. Introduction	1
II. Experimental Equipment; Field Procedures.	2
III. The Analysis of <u>In Situ</u> Spectra	4
IV. Calculations of Flux and Exposure Rate	6
Gamma-Ray Flux from Monoenergetic Sources in the Soil.	6
Calculated Fluxes	9
Dependence of Flux on Soil Density	9
Angular Distribution of Flux	10
Dependence of Flux on Soil Composition and Moisture Content.	10
Dependence of Flux on Source Depth Distribution	11
Exposure Rates for Monoenergetic Sources in the Soil	12
Dependence of Exposure Rate on Soil Density	12
Dependence of Exposure Rate on Soil Composition and Moisture Content	13
Exposure Rates for Natural and Fallout Emitters	13
Dependence of Exposure Rates on Radioactive Equilibrium of the ^{238}U and ^{232}Th Series - Radon Emanation	14
Calculations of ϕ/I	16
Importance of Detector Height Above the Interface	17
Sources Outside the Soil Half-Space	18
V. Calibration of Detectors and Analysis of Spectra	19
Detector Response to Known Flux (N_0/ϕ)	19
Calibration Sources	19
Determination of Total Absorption Peak Areas	20
Measured Values of N_0/ϕ	22
Angular Response Correction Factor (N_f/N_0).	23
Final Calibration Factors	24

TABLE OF CONTENTS (Cont'd)

	<u>Page</u>
Corrections for Interfering Peaks.	24
Energy Band Calibration	25
Total Spectrum Energy Calibration.	25
Summary of Calibrations and Analyses.	28
 VI. Applications of Field Spectrometry.	 29
Typical Field Spectra.	29
Examples of Field Spectrometric Results.	29
Determining Source Radioactive Equilibrium.	30
Nuclear Facilities Studies	30
¹⁶ N from BWR Turbines.	31
Radioactive Construction Materials	31
²³⁹ Pu in the Environment.	31
Estimates of Soil ⁹⁰ Sr and ¹³⁷ Cs Levels.	32
Relative Advantages of NaI(Tl) and Ge(Li) Systems	32
 VII. Estimates of Errors in the Determination of Flux, Exposure Rate and Soil Activity.	 33
 VIII. Summary	 35
 Acknowledgments.	 37
 References	 38

TABLES

Table 1. ϕ + Unscattered Flux at One Meter Above Ground for Exponentially Distributed Sources in the Soil	42
Table 2. Mass Attenuation Coefficients in Soils of Varying Moisture Content and Composition of Soil Used in Transport Calculations.	43

TABLE OF CONTENTS (Cont'd)

	<u>Page</u>
Table 3. ϕ - Unscattered Flux per mCi/km ² at One Meter Above Ground for Typical Fallout Isotopes in the Soil.	45
Table 4. ϕ - Unscattered Flux per pCi/g at One Meter Above Ground for Uniformly Distributed ²²⁶ Ra and ²³² Th Sources in the Soil.	46
Table 5. ²³⁸ U, ⁴⁰ K, and ²³² Th Decay Chains	47
Table 6. Percent of Unscattered Flux Entering Detector at Angles Less Than θ for h = 1 Meter.	48
Table 7. Exposure Rate (μ R/hr) at One Meter Above Ground for Exponentially Distributed Monoenergetic Sources in the Soil	49
Table 8. Total Exposure Rate at One Meter Above Ground for Natural Emitters Uniformly Distributed in the Soil.	50
Table 9. Total Exposure Rate (μ R/h) at One Meter Above Ground for Selected Fallout Isotopes in the Soil.	51
Table 10. Error in One Meter Exposure Rates for Infinite Half-Space Geometry Due to Neglecting Air-Soil Differences	52
Table 11. ϕ/I - (One Meter) for Fallout Emitters in the Soil.	53
Table 12. ϕ/I - Ratio of Gamma-Ray Flux Density to Exposure Rate from Natural Emitters in the Soil.	54

TABLE OF CONTENTS (Cont'd)

	<u>Page</u>
Table 13. Physical Characteristics of HASL γ -Ray Detectors	55
Table 14. N_0/ϕ - Total Absorption Peak Counts - 4" x 4" NaI(Tl) Detector	56
Table 15. N_0/ϕ - Total Absorption Peak Counts per Unit Incident Flux - Ge(Li) Detectors	57
Table 16. Angular Correction Factors (N_f/N_0)	58
Table 17. Peak Area Per Unit Exposure Rate (N_f/I) and Peak Area per Unit Activity (N_f/A) for 4"x4" NaI(Tl) Detectors	59
Table 18. Peak Area per Unit Exposure Rate (N_f/I) and Peak Area per Unit Activity (N_f/A) for Ge(Li) Detectors - Natural Emitters	60
Table 19. Peak Area per Unit Exposure Rate (N_f/I) for 60 cc Ge(Li) Detector Fallout	61
Table 20. "Energy" Band Equations for NaI(Tl) Detectors	62
Table 21. Examples of Field Spectrometric Measurements Made with Ge(Li) Detectors and NaI(Tl) Detectors.	63
Table 22. Rough Comparisons of Field Spectrometric Estimates of ^{137}Cs Soil Activity with Nearby ^{90}Sr Soil Sample Measurements	64
Table 23. Conversion Factors and Other Data Useful for Field Spectrometry.	65

TABLE OF CONTENTS (Cont'd)

	<u>Page</u>
ILLUSTRATIONS	
Figure 1. Diagram of field spectrometers and ionization chamber	66
Figure 2. Field equipment showing, left to right, ionization chamber, Ge(Li) detector and NaI(Tl) detector.	67
Figure 3. Electronic equipment in rack in standard station wagon.	68
Figure 4. ϕ , ϕ/I , and I at one meter above the ground vs α/ρ source depth distribution	69
Figure 5. NaI field spectrum	70
Figure 6. <u>In situ</u> spectrum, northeastern U.S.A. location, taken in 1971 with 10 cm by 10 cm NaI(Tl) crystal, 20 minute counting time.	71
Figure 7. <u>In situ</u> spectrum, taken with that in Figure 4 with 60 cm ³ Ge(Li) detector, 40 minute counting time	72
Figure 8. <u>In situ</u> Ge(Li) spectra at fenceline of boiling water reactor	73
Figure 9. <u>In situ</u> 25 cm ³ Ge(Li) spectrum on river bank near fuel reprocessing plant, 72 minute counting time	74
Figure 10. <u>In situ</u> NaI(Tl) spectrum 650 feet from turbine of a 1600 - MWT _{Th} BWR	75

I. INTRODUCTION

The Health and Safety Laboratory (HASL) pioneered the development of in situ gamma-ray spectrometric techniques, first utilizing large NaI(Tl) crystals^(1,2) and later Ge(Li) diodes⁽³⁾. These spectra are used to provide information on the identity of radionuclides in the soil and air, their concentrations in the soil and their individual exposure rate contributions^(4,5).

In situ measurements of soil activity are more sensitive and provide more representative data than data obtained by sample collection and subsequent laboratory analysis. An unshielded detector placed about one meter above the ground detects gamma rays from an area within about a 10 meter radius, representing a large volume of soil compared to the typical soil sample, and comparable counting statistics can be obtained in only a small fraction of the time required for the laboratory analysis. For example, a field spectral analysis for the natural emitters, ^{40}K , ^{238}U and ^{232}Th , can be carried out in approximately 15 minutes with a 4 in. by 4 in. NaI(Tl) detector. A comparable analysis in the laboratory, excluding transportation and sample preparation time, would require several hours. Furthermore, a single soil sample from a site may not be representative of the mean soil activity, so a number of samples or composite samples are required. A single field analysis averages out small local inhomogeneties in the sample.

The most important disadvantage of in situ spectrometry is that the accuracy of the analysis depends on a separate knowledge of the radioactivity distribution with soil depth, and to a lesser extent a knowledge of the soil density, moisture content and chemical composition. We will show, however, that exposure rate estimates are much less sensitive to variations in radionuclide distribution and soil characteristics than are concentration estimates and that very accurate estimates of individual nuclide contributions to the total external exposure rate can be made from the field spectra.

Our NaI(Tl) analysis techniques have been discussed extensively in prior publications⁽¹⁻⁵⁾, and similar work has since been reported by other investigators⁽⁶⁻⁸⁾. The specific application of our analysis to large lithium drifted germanium diodes [Ge(Li)] has only qualitatively been discussed⁽³⁾. In addition, since our last detailed report on spectrometric methods⁽⁶⁾, improved calculations of gamma-ray flux and exposure rate in air as a function of soil concentration have been made, and new and more precise information on the gamma-ray emissions of ^{226}Ra and ^{232}Th daughters has become available. These new data have allowed us to improve the flux to dose conversions used in our spectral analysis.

II. EXPERIMENTAL EQUIPMENT; FIELD PROCEDURES

Figure 1 is a block diagram of our field equipment arrangement. Each detector is placed on a tripod, facing downward toward the soil halfspace, at a distance of 1 meter above the ground (Figure 2). The site is usually chosen to be a flat relatively undisturbed area whose soil is typical of the surrounding environs. We have found that this measurement technique smooths out much of the effect of ground roughness. Extreme roughness will result in anomalies since the soil surface area close to the detector is increased, while the surface contribution from large distances is reduced.

The NaI detectors are usually covered (in addition to the manufacturers standard thin aluminum or stainless steel window) by a 1/4 in. bakelite shield to reduce the beta-ray contribution to the Compton continuum as well as to moderate thermal stresses.

The NaI detectors (usually 4 in. by 4 in. cylindrical crystals attached to 3 in. matched photomultiplier tubes) are coupled through an emitter-follower preamplifier and a 100 ft. coaxial cable to a multichannel analyzer in our field vehicle. The output of the Ge(Li) diode goes to an uncooled preamplifier directly attached to the cryostat, then through a specially designed low noise 100 ft. cable carrying the

preamplifier power and transmitting the signal to a high resolution amplifier and 4000 channel analyzer in the vehicle. The 5 liter dewar attached to the diode-cryostat requires filling every four days and for long trips an extra 30 liter dewar of liquid nitrogen is carried along. The electronic equipment is shockmounted in a rack mounted in a station wagon (Figure 3). Power for operating all the equipment for up to eight hours is supplied by three 95 ampere-hour storage batteries coupled to a solid-state 12 V DC-AC converter. The primary output device is a magnetic tape recorder, however, a parallel printer is also available. The particular analyzer we use was chosen for its low power requirements (~200 watts), its compact size, weight and acceptable temperature stability characteristics.

The Ge(Li) and NaI(Tl) detectors, when not in use, are transported in rugged styrofoam cushioned boxes designed to minimize both mechanical and thermal shock. Portable lead shielding also allows us to use the detectors for counting samples in a fixed geometry in the field.

NaI(Tl) spectra are usually accumulated in from 10 - 20 minutes while Ge(Li) spectra usually require from 30 to 90 minutes counting time depending on the soil activity and active volume of the diode. Although the resolution obtainable in the field is not usually as good as that in the laboratory, we rarely encounter significant deterioration in resolution from gain or zero drift even during very warm or cold days because of the relatively short counting intervals. We use no special gain stabilization equipment. The detector characteristics are discussed more fully in Section V of this report.

Our standard practice at each measurement site is to first monitor the entire area with hand-held, NaI scintillation meters to assure that the radioactivity level is relatively uniform. A high pressure ionization chamber⁽¹⁰⁾ is used to measure the total exposure rate at the site.

III. THE ANALYSIS OF IN SITU SPECTRA

The total absorption peaks in a spectrum are a measure of the gamma-ray flux of a particular energy incident on the detector. By calibrating the detector in the laboratory with standard point sources we have determined the detector response in terms of total absorption peak counts for a given flux as a function of gamma-ray energy and angle of incidence. The area of a total absorption peak in a field spectrum is thus a measure of the actual flux incident on the detector in the field situation. We have also calculated the expected flux at the detector per unit activity of each nuclide in the soil for various source depth distributions and soil properties and obtained theoretical flux to concentration ratios. We extended the method to exposure rate estimates by calculating the total exposure rate expected at various heights above the ground per unit activity of a particular nuclide in the soil, obtaining theoretical flux to exposure rate ratios. Multiplying the absorption peak area response of the detector per unit incident flux by the calculated flux to exposure rate and flux to activity ratios we obtain calibration factors in terms of total absorption peak counts per $\mu\text{R/hr}$ or per pCi/gm for each nuclide of interest.

We can describe the analysis symbolically in the following manner. Let

(N_0/ϕ) = an estimate of the counts per minute obtained under a particular spectrum total absorption peak due to a unit flux of gamma rays of energy E incident on the detector parallel to the axis of symmetry of the detector.

(N_f/N_0) = the angular correction factor applied to (N_0/ϕ) to account for the fact that gamma rays in the field situation are not incident parallel to the detector axis of symmetry. If the detector has a uniform response over the solid angle from which gamma rays enter the detector in the field, then $N_f/N_0 = 1.0$. If not, the measured angular response of the detector

must be integrated over the actual distribution. This latter quantity is a function of energy, source distribution, soil density, and soil composition.

(ϕ) = total flux at the detector per unit soil concentration [(pCi/g) or (mCi/km²)] of a particular nuclide as a function of energy, source distribution, and soil properties.

(I) = exposure rate in $\mu\text{R/hr}$ at one meter above the ground from all gamma rays originating from a particular nuclide and the secondaries produced in the soil and air.

(ϕ/I) = the ratio of the flux at the detector due to gamma rays of energy E emitted as a result of the decay of a particular nuclide and any daughters to the corresponding exposure rate for that nuclide and its daughters in equilibrium, if specified.

Then, the absorption peak counting rate is related to the exposure rate in air above the ground or to radionuclide concentration in the ground by

$$(N_f/I) = (N_f/N_o) (N_o/\phi) (\phi/I) = \text{peak area counts per } \mu\text{R/hr,}$$

$$(N_f/A) = (N_f/N_o) (N_o/\phi) (\phi/A) = \text{peak area counts per minute per pCi/g or mCi/km}^2.$$

This analysis is equally applicable to NaI(Tl) and Ge(Li) detectors, though the estimation of absorption peak areas for the two types of detectors are quite different. The very great resolution of Ge(Li) detectors allows one to measure absorption peak areas due to a given gamma-ray transition with very little interference from neighboring peaks. Often, the areas of several peaks resulting from the same nuclide may be measured. The efficiency of Ge(Li) diodes is still much lower than NaI(Tl) and thus longer counting times are required to obtain comparable statistical precision. The poorer resolution of the NaI(Tl) data often makes difficult the estimation of absorption peak area due to interference from nearby peaks.

Though our calibration data on N_o/ϕ and N_f/N_o are strictly valid only for our particular detectors, except for nominal differences in volume, our NaI(Tl) data should be applicable to other 4 in. by 4 in. detectors and our Ge(Li) data should be instructive in illustrating the differences in NaI and Ge(Li) sensitivity.

The calculations of ϕ , ϕ/A , ϕ/I , and I given in the next section, however, are generally useful for any detector calibration.

IV. CALCULATIONS OF FLUX AND EXPOSURE RATE

Gamma-Ray Flux from Monoenergetic Sources in the Soil

The total flux of gamma rays of energy E at height h cm above a flat air-ground interface due to an emitter distributed in the soil exponentially with depth is given by

$$\phi(r, \theta) = 2\pi \int_0^{\pi/2} \int_{h/w}^{\infty} \frac{S_o}{4\pi r^2} \exp[-(\alpha/\rho)\rho z] r^2 \sin \theta \exp[-\mu_s(r-h/w)] \cdot \exp[-\mu_a(h/w)] dr d\theta, \quad (1)$$

where

r = the distance from each element of differential volume to the detector position,

$w = \cos \theta$,

Z = the depth beneath the surface in cm,

S_o = the surface activity, photons/sec-cm²,

α = the reciprocal of the relaxation length of the assumed exponentially-distributed source activity with depth, cm⁻¹,

ρ = soil bulk density, g/cm³, and

μ_a, μ_s = the air and soil total gamma-ray attenuation coefficients, cm⁻¹.

The dependence of ϕ on the photon angle of incidence with respect to the perpendicular to the earth-air interface, θ , is obtained by integration over r , hence

$$\phi(\omega) = \frac{S_0/\rho}{2} \left[\frac{1}{(\alpha/\rho)\omega + (\mu_s/\rho)} \right] \exp(-t/\omega) \quad (2)$$

where

S_0/ρ is the surface activity per unit mass of soil and the activity at depth ρz g/cm² is given by

$$S/\rho = S_0/\rho \exp(-\alpha/\rho \cdot \rho z), \text{ and}$$

μ_s/ρ is the mass attenuation coefficient for soil and t is the height of the detector above the interface in units of mean free paths of air, i.e.

$$t = (\mu_a/\rho_a) (h\rho_a).$$

Since

$$S_A = \int_0^{\infty} \rho \frac{S_0}{\rho} \exp(-\alpha/\rho \rho z) dz = S_0/\alpha$$

is the total activity in an infinitely deep column of soil of unit cross-sectional area, then equation (2) can be rewritten

$$\phi(\omega) = \frac{\alpha S_A}{2\rho} \exp(-t/\omega) \left[\frac{1}{(\alpha/\rho)\omega + (\mu_s/\rho)} \right] \quad (3)$$

Equations (1-3) give the flux in air at any height t for a source distributed exponentially in the soil as long as we

are dealing with infinite half-space geometry, i.e. as long as variations occur only in the z direction. Any depth distribution can be represented by a superposition of plane sources buried at various depths and equations (1-3) merely represent particular superpositions. For most real situations the actual distribution of activity can be represented by equations (2) and (3). Natural emitters are usually distributed reasonably uniformly in the soil; for this case $\alpha/\rho = 0$ and equation (2) becomes

$$\varphi(\omega) = [(S_0/\rho)/2(\mu_S/\rho)] \exp(-t/\omega) \quad (4)$$

and the total flux,

$$\varphi = \int_0^1 \varphi(\omega) d\omega. \quad (5)$$

Equation (5) generally cannot be evaluated directly but can be solved numerically with the aid of a large computer.

For a plane source on the soil surface, representative of fresh weapons fallout, $\alpha/\rho = \infty$ and from equation (3) we obtain

$$\varphi(\omega) = \frac{S_A}{2\omega} \exp(-t/\omega) \quad (6)$$

and the total flux,

$$\varphi = \int_0^1 \varphi(\omega) d\omega = \frac{S_A E_1(t)}{2}, \quad (7)$$

where $E_1(t)$ is the exponential integral, sometimes also written $-E_i(-t)$. The values of $E_1(t)$ have been tabulated in many mathematical handbooks.

Fallout deposited on the ground tends to approach a distribution which can be reasonably approximated by an

exponential distribution after some time⁽¹¹⁾. The value of α/ρ best describing the distribution will depend on the type of soil, soil density and moisture content. Values of α/ρ ranging from 0.05 to 0.5 have been found to describe realistic fallout distributions adequately, the more aged fallout, of course, being represented by the smaller values⁽¹¹⁾.

Calculated Fluxes

Using equations (2) and (3) we have calculated the unscattered photon flux at one meter above the interface for values of α/ρ ranging from 0 to ∞ . These results are given in Table 1 for various monoenergetic source energies, for a source strength of $S_A = 1.0$ photons/cm²-s except for the case of $\alpha/\rho = 0$ (uniform) where the results are for $S/\rho = 1.0$ photons/s per gram of soil. We used the soil composition given in Table 2.

The choice of doing the $\alpha/\rho \neq 0$ calculations for a fixed total source activity and a varying source depth distribution rather than for a fixed value of surface activity ($S_0/\rho = \alpha S_A/\rho$) results in the $\alpha/\rho = 0$ data not being directly comparable to the $\alpha/\rho \neq 0$ data as tabulated. The effect of source depth distribution is more apparent from this type of normalization, however. The results could be re-normalized by letting $S_0/\rho = 1.0$ photon/g-s for all cases.

In Table 3 we give the fluxes at 1 meter for some typical fallout radionuclides obtained by interpolating the data in Table 1 and multiplying by the given photons/dis. In Table 4 we give similar results for the major ²³⁸U and ²³²Th transitions. The ²³⁸U and ²³²Th decay chains are listed in Table 5.

Dependence of Flux on Soil Density

Although soil densities may vary considerably from site to site, it can be seen from equations (3) and (4) that the soil density enters only in the terms α/ρ and μ_s/ρ . One can obtain the flux for any soil density from the flux vs. (α/ρ) in Table 1 since the quantity μ_s/ρ is independent of density

and depends only on isotopic composition. Although we typically assume a soil density of 1.6 g/cm^3 , the values in Table 1 for any values of ρ and α are equally valid for other values of ρ as long as $\alpha/\rho = \text{constant}$, i.e. the values given for $\alpha = 0.5 \text{ cm}^{-1}$ and $\rho = 1.6$ correspond to the values for $\alpha = 1.0 \text{ cm}^{-1}$ and $\rho = 3.2$. The values given for $\alpha/\rho = 0$ depend only on the source activity per gram of soil material and not the actual soil density.

Angular Distribution of Flux

In Table 6 we give integral angular flux distributions obtained by integrating equation (1) from 0° to θ . From these data it is seen that most of the unscattered gamma rays incident on a detector at one meter above the ground arrive at angles of roughly from $50^\circ - 80^\circ$ from the vertical, i.e. are originating from an area bounded by radii of about 1 to 5 meters. Also for an energy of 662 keV and a relaxation length of 3 cm ($\alpha/\rho = 0.021$) 85% of this flux comes from an area of about 10 meters in diameter. The area "seen" by the detector depends on the height of the detector, of course, as well as on the depth distribution (α/ρ) and to a much lesser extent on the gamma energy of the source.

Dependence of Flux on Soil Composition and Moisture Content

The unscattered flux is not completely independent of μ_s/ρ , the total mass attenuation coefficient of the soil. This quantity depends on the soil composition which itself depends on the soil moisture content. For a fairly wide range of soil contents, however, μ_s/ρ varies over a narrow range, as shown in Table 2. Since for the worst case, a uniformly distributed source as shown in equation 4, the flux varies only as $1/(\mu_s/\rho)$ and since μ_s/ρ changes by at most about 6 - 7% between aluminum and soil with 25% moisture content (Table 2), clearly a knowledge of the exact soil composition is not critical for the calculation of flux. A soil with a significant high Z material content could result in somewhat lower fluxes than are given in Tables 1, 3 and 4, however.

Dependence of Flux on Source Depth Distribution

It can be seen from Table 1 that the flux is strongly dependent on depth distribution, changing for example by almost an order of magnitude at 662 keV (see Table 1) as the source distribution changes from a plane source to a deeply distributed source. Increased soil moisture effectively results in a more deeply distributed source since increased soil moisture increases the density and thus reduces α/ρ .

Clearly, the relation of an in situ flux measurement to total soil concentration requires a fairly good knowledge of the effective depth distribution. Several possible ways come to mind for inferring the depth distribution from measurements of flux. One might infer the depth parameter, α/ρ , from measurements of flux at some energy at several heights above the soil. Unfortunately, the variation of flux with detector height is very insensitive to α/ρ over the first few meters above the interface⁽¹²⁾. For example, the ratio of 662 keV flux at 10 m to that at 1 m for $\alpha/\rho = 0.0625$ is 0.74, while for $\alpha/\rho = 0.1875$ it is 0.70⁽¹²⁾.

An alternative might be to observe the photon flux at two different energies from the same source, e.g. 587 keV and 1596 keV from ^{140}La , or to assume the same depth distribution for say ^{141}Ce and ^{106}Ru (134 keV and 619 keV) which have similar half-lives. From Table 1 we see, however, that the ratio of the 150 keV flux to the 662 keV flux for $\alpha/\rho = 0.21$ is 0.68, while for $\alpha/\rho = 0.063$ it is 0.61, only about a 10% difference in α/ρ for very different photon energies. It is, in fact, very difficult to use measurements of total flux alone to determine α/ρ except perhaps in a very gross manner. This, of course, limits the ability of the field spectrometric method with respect to determining cumulative fallout soil activities unless one has some independent knowledge of the depth distribution. From Table 6, however, we note that the angular flux distributions are somewhat more sensitive to α/ρ and perhaps measurements of this quantity with collimated detectors could be used to infer approximate values of α/ρ .

Exposure Rates for Monoenergetic Sources in the Soil

The total exposure rates at 1 meter per unit concentration of source activity in the soil for monoenergetic sources as a function of source energy are given in Table 7. These data include the contributions from gamma rays scattered in both the soil and air and were determined utilizing a polynomial solution to the gamma-ray transport equation⁽¹²⁾ for the soil composition given in Table 2 and a moisture content of 10% by weight.

Dependence of Exposure Rate on Soil Density

Like the flux the exposure rate is dependent on soil density and composition. The exposure rate due to a source of strength $S_0/\rho \exp(-\alpha/\rho \rho z)$ buried at a depth between z and $z + dz$ centimeters beneath the surface depends only on the number of mean free paths (MFP) to the interface, i.e.

$$I(h) \propto \int_0^{\infty} S_0 F(\mu/\rho, \rho z, h) dz \quad (8)$$

where I is the exposure rate at h meters above the interface and F is a quantity which relates the exposure at h to a plane source at depth z . F depends only on the number of gamma mean free paths (μ/ρ) (ρz) between the height h and the depth z since the exposure rate from a buried plane source can be shown to be only a function of $\mu z = (\mu/\rho) (\rho z)$ ⁽¹²⁾. Equation (8) can be rewritten

$$I(h) \propto \int_0^{\infty} \frac{S_0/\rho}{\mu_s/\rho} F(\text{MFP}) d[(\rho z) (\mu/\rho)] = \int_0^{\infty} \frac{\alpha/\rho S_A}{\mu_s/\rho} F(\text{MFP}) d(\text{MFP}). \quad (9)$$

As was the case for flux the exposure rate for a given S_A varies as α/ρ and one can obtain the value for any soil density by utilizing the Table 7 values with an appropriate value of α/ρ .

Dependence of Exposure Rate on Soil Composition and Moisture Content

The soil density at a given location may vary with time due to changes in soil moisture and ρ may remain constant or vary extremely slowly. Since μ_s/ρ increases only slightly with increasing water content (Table 2), the effect is to reduce the flux and exposure rate somewhat, since in effect each source element is further away from the detector in terms of mean free paths. For $\alpha/\rho = 0$, a uniformly distributed source, an increased moisture content reduces the source per gram of soil (or per MFP) and the exposure rate and flux are both reduced proportionately.

The above discussion assumed a uniform change in soil moisture content over the first several inches of soil, which may not be a realistic assumption for actual soils. In any case, both the flux and exposure rate should change about the same amount for most situations.

Since μ_s/ρ is not completely invariant small changes in the values of calculated exposure rates would result from the actual soil composition being different from that given in Table 2. However, our calculations indicate that these differences for most plausible soils are almost always less than 5% which is the same order as the error in the calculations⁽¹²⁾. Again, however, a soil rich in high Z material would not be represented as well by the exposure rate data in Table 6.

Exposure Rates for Natural and Fallout Emitters

The exposure rates at 1 meter for naturally-occurring radionuclides found in the soil are given in Table 8 while those for fallout emitters are given in Table 9. These data were calculated by folding together interpolated values from Table 7 with the best available data for the number of photons emitted per disintegration at each energy. The data for the fallout nuclides were taken from the Nuclear Data Tables⁽¹³⁾ while those for the ^{238}U and ^{232}Th series are based primarily on recent measurements by Gunnink et al.⁽¹⁴⁾,

Lingeman⁽¹⁶⁾, Mowatt⁽¹⁶⁾, and Maria et al.⁽¹⁷⁾ as well as our own measurements with a Ge(Li) diode⁽¹⁸⁾. Our estimate of the best available gamma emission data for the major lines of the ^{238}U and ^{232}Th series are given in Table 4. These data differ considerably both from the data we used in the past^(1,12) and that given by Hultquist in his early work⁽¹⁹⁾ and the calculated exposure rate to concentration factors for ^{238}U and ^{232}Th , therefore, differ somewhat from those in our previous publications^(1,2,4,5) (see Table 8). In addition, our earlier work⁽¹⁾ was based on a buildup factor calculation of the exposure rate which neglected differences between gamma-ray transport in air and soil. The approximate error resulting from the latter treatment can be seen in Table 10 for the case of a uniformly distributed source when we compare exposure rates calculated from transport theory with those calculated using the simple single medium buildup factor approach. As can be seen, the differences are only about 10% except for very low energies.

Although our new exposure rate per unit soil activity conversion factors for both ^{238}U and ^{232}Th are smaller than those used previously, implying that the exposure rates calculated at one meter from measured soil activity are somewhat less than previously thought, the total change in the ^{238}U series factor is only about 20% and in the ^{232}Th factor about 15%. Since our values for ϕ and N_0/ϕ have also been revised, our earlier estimates of exposure rates based on in situ spectral measurements are probably in error by less than these amounts.

Dependence of Exposure Rates on Radioactive Equilibrium of the ^{238}U and ^{232}Th Series - Radon Emanation

In using these conversion factors one should remember that they refer to concentrations in in situ soil and not in the dry sieved soil which is usually measured in the laboratory. Soil moisture content by weight of 10 - 20% seems to be fairly typical in the Eastern United States with wide variations from soil to soil.

The calculations also assumed that all daughters are in radioactive equilibrium with their parents. Actually, some fraction of the radon and thoron produced (see Table 5)

emanates from the soil matrix, diffuses through the soil air to the interface and then disperses throughout the atmosphere. The escape of ^{222}Rn is much more likely than that of ^{220}Rn because of its much longer half-life. The fraction of radon which escapes in situ soil, or emanation coefficient, varies considerably from soil to soil, typical values being about 20 - 30% although values as high as 50% are not uncommon^(20,21). Since most of the exposure rate from the ^{238}U series is from radon daughters (see Table 4), we can, to a good approximation, assume that the fraction of radon escaping into the soil air and then to the atmosphere will result in an equivalent reduction in gamma exposure rate at 1 meter. Under a steady-state condition, there will be some small contribution from this fraction whose source distribution can be represented by two exponential distributions, one in the atmosphere and one in the soil. For normal atmospheric diffusion and typical surface level radon air concentrations, we estimate this contribution to be only a few tenths of a $\mu\text{R/hr}$. During an inversion, however, the exposure rate would, of course, be somewhat increased since the radon would remain closer to the interface.

Errors would result when using a field measurement of the ^{214}Bi or ^{214}Po photon fluxes to estimate ^{238}U soil concentration or a laboratory measurement of equilibrium ^{232}U soil concentration to evaluate the one meter exposure rate. In these cases one would need to know both the emanation fraction and the approximate exposure rate contributions from radon in the soil air and atmosphere. The field spectrometric determination of exposure rate utilizes the ratio of flux to exposure rate and since both quantities contain a contribution from the emanated radon, the exposure rate estimate obtained by using a slightly incorrect value for ϕ/I would not be expected to be greatly in error. Indeed, as the radon builds up in the soil or near the ground due to increased soil moisture, frozen ground, or an atmospheric temperature inversion, the actual ratio of ϕ/I will approach the value used routinely (the equilibrium infinite half-space value) and the error in determining the exposure rate will be even smaller.

Disequilibrium in the ^{238}U series and ^{232}Th series can be investigated using field Ge(Li) spectra. For the ^{238}U

series one can obtain flux estimates from the 186 keV ^{226}Ra line as well as from lines of radon daughters and thus obtain rough estimates of the emanation fraction. Similarly, any disequilibrium in the ^{232}Th series can be investigated by obtaining flux estimates from several spectral lines characteristic of the different important gamma emitting nuclides in the series. We have not yet exploited the possibilities in this area.

Calculations of ϕ/I

The ratio of flux to exposure rate is the most important quantity needed for determining exposure rates from in situ field spectra. Fortunately some of the problems mentioned in connection with the measurement of source activity for varying depth distributions are not as troublesome when determining exposure rate.

In Table 11 we give values for ϕ/I for energies of prominent gamma-ray peaks corresponding to the major fallout emitters in the soil. The total exposure rate values were taken from Table 9.

In Figure 4 are plots of ϕ vs α/ρ , I vs α/ρ , and ϕ/I vs α/ρ , for 662 keV. The first two quantities vary over a range of almost a factor of 10 between a plane source and a deeply distributed source, but the ratio varies only by 25 - 30%. Thus, even if we have a poor knowledge of the actual depth distribution, our error in field spectrometric estimates of exposure rate is reasonably limited. This is particularly true for deeply distributed radionuclides, i.e. slight deviations of the natural emitters from a completely uniform distribution will not materially effect ϕ/I . In addition, since the density (water content) enters into both the flux and exposure rate calculations in almost the same manner (see equations 1 - 8), the ratio ϕ/I is fairly insensitive to the actual density and is almost completely invariant for the uniformly-distributed natural emitters. Similarly, ϕ/I is also insensitive to the exact soil composition. The values for ϕ/I are thus of more universal utility when used for interpreting field spectra.

The values of ϕ/I for the important gamma rays from ^{238}U , and ^{232}Th and ^{40}K are given in Table 12. It should be noted that the values for ϕ/I given here for the 1.76 MeV ^{214}Bi line or the 2.62 MeV ^{232}Th line differ from the values used in our previous work⁽⁶⁾ since both our values for I and for the unscattered flux have been revised. The 1.76 MeV value is only about 10% lower than our previous value and the ^{40}K value changes by only about 5%, although the ^{232}Th value is 20% lower.

The values of ϕ/I given here may not, of course, be the final ones because uncertainties in some of the photons per disintegration values are still known only to $\pm 10\%$. The data in Table 1 - 7, however, allow the reader to revise the tabulated values of ϕ/I based on any new data or to calculate values for energies and radionuclides not given. Any errors due to differing soil composition and uneven moisture content, even though they may result in quite large errors in the individual values of flux and exposure rate, should not materially affect the ratio.

Importance of Detector Height Above the Interface

All of the quantities above have been calculated for a distance of one meter above the interface in air at 20°C and 760 mm of Hg. It was previously shown that for almost all depth distributions except those approaching a plane source on the surface, the exposure rate and flux vary slowly with height above the interface⁽¹²⁾. Thus one need not correct for changes in air mass due to changing environmental conditions nor is it important that the detector distance be exactly one meter. For example, the flux and exposure rate at one meter due to a ^{137}Cs (662 keV) source distributed in the soil with $\alpha/\rho = 0.63$ are only reduced by 10% and 7%, respectively, from the values at the interface itself. For more uniform source distributions, the decrease with height is even less and the ratios of ϕ/I are relatively insensitive to the exact detector height.

In real life, the earth-air interface is not a flat plane. This fact manifests itself most significantly when the amplitude of the earth surface undulations become significant

with respect to the detector height. The calculated exposure rates and fluxes then vary from the measured values since in effect the detector "sees" a different amount of source than in the calculational model. Again, the ratio ϕ/I should be the quantity least affected. Ground roughness may, however, effectively make a surface source appear to be distributed in depth and in fact many investigators simulate ground roughness by a buried plane source. In a real situation, therefore, the detector height could be important if a measurement of flux or total exposure rate alone is being attempted. Our experience indicates that the ratio of ϕ/I is sufficiently invariant with respect to ground roughness that good results can be obtained for natural emitter exposure rates inferred from flux measurements even over quite poor half-spaces.

Sources Outside the Soil Half-Space

All of the preceding discussion has been for sources in the soil half-space. Field spectrometry is, of course, useful for measuring the gamma rays from other sources, such as noble gases in airborne effluents from nuclear facilities, ^{16}N gamma rays from nuclear power plant turbines employing primary steam from the reactor, other sources of direct radiation from nuclear facilities, and locally contaminated areas. In each case a knowledge of the source geometry is required in order to use the measured flux to infer either source concentration or exposure rate.

These situations are usually difficult to model, as for example the plume of noble gases from a nuclear facility, however, field spectra are useful for identifying the contributors to flux and exposure rate. By utilizing the field spectra to calculate natural and fallout exposure rates and then subtracting these contributions from an ionization chamber measurement of total exposure rate, one can obtain the exposure rate due to the other sources identified in the field spectra.

V. CALIBRATION OF DETECTORS AND ANALYSIS OF SPECTRA

Detector Response to Known Flux (N_0/ϕ)

The first important requirement for measuring gamma-ray flux is a detector which is accurately calibrated, both as a function of energy (N_0/ϕ) and as a function of angular incidence (N_f/N_0). Each of the detectors described in Table 13 was calibrated in the laboratory by exposure to known fluxes from standard point sources placed at distances ranging from about 1 - 6 meters from the face of the detector. It is important to place the source as far from the detector as possible in order to simulate a plane beam of incident photons. Corrections must be made for attenuation in the air between the source and the detector and for self-absorption in the source if any. When calibrating the NaI(Tl) detectors, the sources used were chosen to simulate the peaks routinely analyzed in field spectra. For the Ge(Li) detectors, a much more extensive calibration was desired since the increased resolution means one can utilize photopeaks at almost every energy.

Calibration Sources

Many of the standard sources used were obtained from the International Atomic Energy Agency or National Bureau of Standards although a number were standardized here at HASL using beta-gamma coincidence counting. In all cases the beta emission rate of the standards was known to a few percent. For a few sources, uncertainties in gamma emission rate or half-life resulted in uncertainties in the measured N_0/ϕ greater than $\pm 5\%$. The use of a large number of sources, and the subsequent fitting of a smooth curve to the data, resulted in what we believe are values of N_0/ϕ for the Ge(Li) detectors whose accuracy is better than 5% at all energies and better than 2% at energies above 200 keV. The N_0/ϕ values determined for the NaI(Tl) detectors are somewhat less accurate ($\sim 5\%$) because of the problem of measuring the peak area for a given incident flux.

Determination of Total Absorption Peak Areas

In the case of the Ge(Li) detector calibration, the total absorption peak area obtained due to a given incident flux is determined by fitting the continuum under the peak by an exponential function and then ascribing all the counts above this baseline to the total absorption of incident flux. The calibrations are all carried out by superimposing the source response on top of laboratory background in order to simulate the field situation as closely as possible.

In reality the continuum dominated primarily by Compton scattered gamma rays is not a true exponential. Some investigators fit the peak by assuming it to have a Gaussian shape with a skewed low energy tail. Others fit the continuum by a straight line. We have found by comparing several methods with our method for estimating peak areas, we can determine the actual number of total absorption events within about 2% for our 60 cm³ Ge(Li) detector and that the more sophisticated techniques do not seem to result in significantly better analyses. For field spectra the statistical counting error for even the strongest peaks is about 5 - 10% for a 30 minute counting interval, and this uncertainty has a greater effect on both the fit to the continuum and the estimate of peak area than the particular method used to fit the continuum.

All of our analyses of Ge(Li) peak areas are done semi-automatically by displaying a portion of the spectrum on a cathode ray screen, instructing a small computer to fit an exponential between two channels indicated by the operator, strip the continuum away and estimate the peak area. The operator can have the computer smooth the data if necessary in order to aid him in determining the end channels for fitting.

The NaI(Tl) peak areas are also estimated by fitting the Compton continuum with an exponential curve as shown in Figure 5. Because of the poorer resolution only very prominent peaks can be resolved, however. As can be seen in the figure which shows a typical field spectrum with fallout present, the 1.46 MeV ⁴⁰K, 1765 KeV ²¹⁴Pb and 2.62 MeV ²⁰⁸Tl

peaks are quite prominent and their areas can be estimated readily. The fallout peaks are less prominent and the estimates of their areas are considerably less precise.

The calibration of the NaI(Tl) detector for N_0/ϕ is more difficult than for the Ge(Li) detector since the determination of peak area does not usually account for all the totally absorbed gamma rays (i.e. the exponential fit over the large number of channels encompassed by the typical peak is not an optimum fit). Comparisons of peak areas obtained by subtracting background for monoenergetic calibration source exposures indicate that this method of estimating the continuum results in approximately 20% of the total absorption peak area being missed. However, we found that this percentage is relatively constant among field spectra, because the shape of the NaI continua are relatively constant. This is because the Compton scattered gamma rays from the natural emitters in the soil dominate the NaI(Tl) spectrum and the spectrum is relatively invariant to the amount of K, Th, and U in the soil or to the size of the individual total absorption peaks on the continuum. Thus, if we calibrate the detector in a situation similar to that in the field (i.e. use laboratory background) the absorption peak count fraction we obtain for the calibration is approximately the same as the fraction we obtain in the field for the same incident flux. We can thus obtain a good measure of the in situ flux.

Since this fraction varies somewhat with source energy⁽¹⁾, however, it is mandatory to calibrate for the energies one wishes to measure. The most important criterion here is to be consistent, i.e. to determine peak areas for field spectra in a manner identical to that used for calibration. We were able to do this for all energies except for ^{40}K (1.46 MeV), which is not available as a standard. Here we originally had to rely on calibration measurements using ^{24}Na (1.38 MeV) or ^{42}K (1.58 MeV)^(1,5). A later comparison in the field of the Ge(Li) and NaI(Tl) spectrometers, which will be discussed later, indicated we were able to obtain a reasonably good estimate of N_0/ϕ for 1.46 MeV.

Another method would be to simulate a source of ^{40}K using KCl or K_2CO_3 , measure the flux using the $\text{Ge}(\text{Li})$ detector, and then use the measured flux to calibrate the NaI detectors.

Measured Values of N_0/ϕ

The values obtained for N_0/ϕ for two 4 in. by 4 in. $\text{NaI}(\text{Tl})$ detectors, for the original HASL 25 cm^3 $\text{Ge}(\text{Li})$ diode and our present 60 cm^3 diode are given in Tables 14 and 15 along with a description of the calibration sources used. The values for N_0/ϕ for the large $\text{Ge}(\text{Li})$ detector can be represented to within a few percent by the function $\ln(N_0/\phi) = 4.48 - 1.03 \ln E(\text{MeV})$ over the range 180 keV to 3.0 MeV. Since for the $\text{Ge}(\text{Li})$ detector N_0/ϕ is actually a measure of the total absorption probability, we are justified in drawing a smooth curve and interpolating between energies. This is not justified for $\text{NaI}(\text{Tl})$ spectrometry because the N_0/ϕ values are dependent on the experimenter's method of estimating the continuum.

Table 13 gives pertinent data regarding the construction, efficiency and resolution of each of the detectors calibrated. In all cases the flux referred to is the flux incident on the actual detector at the point of interaction. Note that as long as the source to detector calibration distance is long compared to the distance between the actual point of interaction in the detector and the face of the housing, no significant error results from measuring distances with respect to the housing faces. We determined, by placing sources at various distances from 50 cm to 2 meters from the face of the detector, that the median distance of effective interactions in our 60 cm^3 diode was about 1.6 cm from the housing face. Gamma-ray absorption in the housing is included as part of the detector response.

Note that the values of N_0/ϕ in Table 14 for the two $\text{NaI}(\text{Tl})$ detectors differ by only a few percent from each other, but by about 15% from the values reported for our original 4 in. by 4 in. detectors⁽⁵⁾. This discrepancy indicates that one can be wrong in assuming that two $\text{NaI}(\text{Tl})$ detectors of the same nominal size procured at different times, even from the same supplier, will have the same size. The reduction in N_0/ϕ seemed to be the same for all energies

measured in the present calibration which were not as extensive as that carried out previously, so we merely reduced the N_0/ϕ data in HASL-170⁽⁶⁾ by the appropriate fraction when determining N_0/ϕ for energies not used in the recalibration.

Angular Response Correction Factor (N_f/N_0)

A complete flux response calibration of the detectors requires a correction factor to account for the fact that the gamma rays incident on the detector in the field situation are not (as shown in Table 6) incident along the axis of symmetry. If $N(\theta)/N_0$ is the ratio of the response to gamma rays of energy E at angle θ with respect to the response at $\theta = 0^\circ$, then

$$N_f/N_0 = \frac{1}{\phi} \left[\int_0^{\pi/2} \phi(\theta) \frac{N(\theta)}{N_0} d\theta \right]. \quad (10)$$

Fortunately, $N(\theta)$ is nearly unity over all θ for both detectors for all except very low energy gamma rays. This results in values of N_f/N_0 (see Table 16) for the NaI(Tl) peaks of interest most of which are less than 1.1 and in 60 cm³ Ge(Li) values almost all equal to 1.0 for gamma rays from the soil half space. The angular response of our original 25 cm³ Ge(Li) detector was more skewed, resulting in larger values of N_f/N_0 . The N_f/N_0 ratios were calculated by numerically integrating Equation (10) using a smooth fit to the experimental angular response data to interpolate over $N(\theta)/N_0$. Because the final correction factor is small, errors involved in this interpolation is small. $\phi(\theta)$ is given by equation (4) in section III.

The angular response of our Ge(Li) detectors is somewhat asymmetrical in the azimuthal direction because of the mounting arrangement, cold finger connection and electrode connections. These deviations from symmetry, however, are quite small except at very low energies (< 100 keV), and involve only a small portion of the total solid angle.

Final Calibration Factors

The final sensitivities of each detector in terms of total absorption peak counts per unit soil activity $N_f = (N_0/\varphi)$ $(N_f/N_0)\varphi$ and peak counts per unit exposure rate $N_f = (N_0/\varphi)$ $(N_f/N_0)(\varphi/I)$ are given in Tables 17 and 18. Note that the 60 cm³ Ge(Li) detector has an effective sensitivity at lower energies which is greater than its volume ratio to the 25 cm³ detector would indicate, due to its flatter angular response as well as relatively greater sensitivity at higher energies than at lower energies.

Note also that the final conversion factors for exposure rate vs. source depth distribution vary over a much smaller range than the corresponding factors for soil activity.

Corrections for Interfering Peaks

The values for N_f and N_f/I in Table 18 for certain weak lines such as the 768 keV of ²¹⁴Bi, the 665 keV ²¹⁴Bi line, and the 300 keV ²¹²Pb line should not be used as the primary means for determining the flux or exposure rate from the nuclide in question. They do allow a rough estimate of the interference fraction due to a strong peak of the same or very nearly same energy corresponding to a second nuclide. For example, the 766 keV ⁹⁵Nb peak must be corrected for the 768 keV ²¹⁴Bi peak, the 662 keV ¹³⁷Cs for the 665 keV ²¹⁴Bi peak, etc. We have attempted to include values for all the radium and thorium lines which interfere with important fallout nuclides or with other stronger radium and thorium lines. However, when sources other than those listed are present the investigator should determine any other possible interferences and calculate correction factors based on the data in the Tables in this report.

For the NaI(Tl) detector, the values for the 583 keV ²⁰⁸Tl line and 609 keV ²¹⁴Bi line are given primarily to allow an estimate of the interference in the broad peak centered approximately around 662 keV when significant amounts of ¹³⁷Cs are present. A correction factor to the 514 keV ¹⁰⁶Ru line is not given since besides the 510 keV

^{206}Tl line there is also a significant contribution from annihilation photons from both cosmic rays and from the pair productions of the higher energy gamma rays in the soil, air and detector housing. Thus, only very large amounts of ^{106}Ru can be readily quantitated with the NaI spectra.

Energy Band Calibration

We have showed that, where only low-energy fallout emitters are present, one could simplify the analyses of NaI(Tl) field spectra for the natural emitters^(1,2,5). A so-called energy band analysis, which is well suited to computer data processing, involves the calculation of the spectrum "energy" (total counts per channel multiplied by the energy represented by that channel) in bands of channels centered on the 1.46 MeV ^{40}K peak, the 1.76 MeV ^{214}Bi peak and the 2.62 MeV ^{208}Tl peak and applies a set of simultaneous equations to calculate these exposure rate contributions. The three equations relating U, Th and K exposure rates to the three band energies were determined by carrying out a regression analysis on a large number of field spectra for which the individual exposure rate values were determined from the peak method. As long as the "energy" in the three chosen bands was due entirely to one or more of the three isotopes and the geometry and source depth distribution were constant, this method worked and proved to give more precise results than the peak method. Because we lacked sufficient field data with our NaI(Tl) detectors to carry out a similar regression analysis, we simply revised the equations given in HASL-170 based on the observed differences in efficiency and our new values for $\phi/I^{(5)}$. The primes on E in the new equations, shown in Table 20, indicate that the energy in each band due to cosmic rays (which is a function of altitude) must be subtracted before applying the equations. The appropriate cosmic-ray correction factors, based on revising the data in HASL-170 for reduced efficiency, are also given in Table 20. The new equations, for the field data obtained so far with the new detectors, give comparable results to the peak method.

Total Spectrum Energy Calibration

The exposure rate in air,

$$I \propto \int_0^{\infty} \phi(E) \mu_e/\rho E dE,$$

where $\phi(E)$ is the flux of gamma rays of energy E and μ_e/ρ is the mass energy absorption coefficient in air. For energies between a few hundred keV and several MeV μ_e/ρ is fairly constant with energy. Also, for low energies the probability of an incident photon being totally absorbed by a large NaI(Tl) detector is fairly large (on the order of 50 - 100% from 100 keV to ~1 MeV). Most of the exposure rate in air, about 75%, due to emitters in the soil is due to gamma rays between 100 keV and 1.5 MeV⁽¹²⁾. Couple this with the fact that the spectrum of gamma rays from natural emitters is quite invariant to the actual proportions of U, Th and K in the soil⁽¹²⁾ and one can see why the total "spectrum energy" is a reasonable measure of free air exposure from natural radioactivity in the soil. In essence the large crystal measures the flux to a fairly high degree of accuracy and, even though it measures a slightly smaller proportion of the flux as the energy increases and some of the secondary scattered energy escapes the detector, this decrease is compensated by correspondingly smaller values of μ_e/ρ at energies above 1 MeV relative to values below 1 MeV.

Unlike many NaI(Tl) instruments, which are based on the assumption that the counting rate above some bias level is proportional to the exposure rate, thus implying that the spectral shape of the gamma-ray field is invariant, this total energy technique requires only that the counts in a channel be proportional to $\phi(E) (\mu_e/\rho)$ for that energy, and is, therefore, less sensitive to spectral changes. For example, a counter using a large NaI(Tl) detector would record the exposure rate from a unit flux of 60 keV photons as being almost equal to the exposure rate from a unit flux of 1464 keV photons since, even at 1.46 MeV, a pulse would be recorded due to the high probability of a Compton collision in the detector even though many of the secondaries would escape the crystal. In the total energy technique, the higher energy counts are weighted by the energy deposited to reflect more correctly their relative contribution to the exposure rate. The slightly larger total absorption at 60

keV reflects the larger value of (μ_e/ρ) relative to 1500 keV gamma rays.

The total energy technique was tested between 150 keV and 3.4 MeV by comparing the exposure rates determined from our large NaI(Tl) crystals with high pressure ionization chamber measurements for a variety of gamma ray fields. The total energy method results were proportional to exposure rate for various radiation fields varying from low-energy fallout radiation to a predominantly ^{40}K dominated field.

Another advantage in using the NaI detector as a dosimeter is its relative small response to cosmic-ray secondaries over the range of 150 keV to 3.4 MeV. This has allowed us to check independently the cosmic-ray calibrations of our high pressure ionization chambers⁽⁵⁾.

We determined the "spectrum energy" calibration factors for our present 4 in. by 4 in. detectors in two ways. First, we exposed the detectors to a known exposure rate from a point ^{226}Ra source in the laboratory as determined by an ionization chamber measurement. This measurement was corrected to account for the fact that the gamma rays in the laboratory were incident along the detector axis. The angular correction factor (1.11) was estimated by folding in our previous calculations of the angular exposure rate distribution for a field situation⁽¹²⁾ with the measured response of "spectrum energy" as a function of the angle of incidence.

The second method of determining the proportionality factor was to compare measurements of "spectrum energy" for actual field spectra with simultaneous ionization chamber measurements over a range of fields. The two methods gave essentially the same calibration factors. We noted again that these factors were about 85% of the values obtained for our previous 4 in. by 4 in. detectors. These total "energy" to exposure rate conversion factors are given in Table 20, along with the appropriate cosmic-ray correction factors.

One further point regarding the use of "spectrum energy" technique is that although at $h = 1$ meter about 40% of the

gamma ray flux is below 150 keV this flux (about half of which is due to skyshine) accounts for less than 10% of the exposure rate^(12,22). Thus, integrating from 150 keV up does not introduce serious error into exposure rate estimates, however, a count rate meter biased below 150 keV will be sensitive to changes in low energy flux and, because of the large fraction of "skyshine", will be quite angularly dependent.

Summary of Calibrations and Analyses

Because of the length and complexity of the preceding discussion it may be valuable to summarize the use of field spectrometry to determine source activity or exposure rates from particular nuclides in the soil:

1. Determine the response of the detector to a known flux of gamma rays of energy E , incident along the detector axis, where E is the energy of a prominent gamma-ray transition characteristic of the source. (N_0/ϕ - Tables 14, 15).
2. Using equations (3) or (4) for the angular incidence of gamma rays on the detector for given source depth distributions, determine the correction to be made to N_0/ϕ . (N_f/N_0 - Table 16).
3. If the source is one for which we have already calculated the flux ϕ , for the gamma-ray energy of interest (Table 3 or 4), and the exposure I (Table 8 or 9), multiply each of these values by N_0/ϕ and N_f/N_0 to obtain the required calibration factor.
4. If the nuclide and source distribution is one for which we have not determined ϕ and I , use the data in Table 1 or interpolations thereof and appropriate values of photons per disintegration to determine ϕ . Using the data in Table 7, or interpolations thereof, sum over all the gamma-ray transitions for a given nuclide to determine I for that source for a depth distribution of interest.
5. Finally, to determine the source activity or exposure rate from a specific radionuclide, estimate the peak area in the field spectrum in a manner identical to that used

during the calibration, subtract any counts in the peak due to the same energy transitions from other nuclides (see "Corrections for Interfering Peaks", page 24), and then divide by the appropriate calibration factor to obtain the desired activity or the exposure rate.

VI. APPLICATIONS OF FIELD SPECTROMETRY

Typical Field Spectra

Figure 6 shows a NaI(Tl) field spectrum obtained at a location in the Northeastern United States. Figure 7 shows the Ge(Li) spectrum obtained with the 60 cm³ Ge(Li) detector simultaneously at the same site. The Ge(Li) spectrum represents a 30 - 40 minute measurement and the NaI(Tl) spectrum, 20 minutes. The former spectrum conveys far more information even though the efficiency of the detector is lower. For example, one can measure fluxes at several dozen energies, including that due to ¹⁴⁴Ce (134 keV) and ¹²⁵Sb (428 keV) which are not identifiable in the NaI(Tl) spectrum. In addition, the important ¹³⁷Cs peak is completely resolved instead of being partially combined with an array of Th and U peaks.

Examples of Field Spectrometric Results

Table 21 gives some individual nuclide exposure rates calculated from spectra for a variety of environmental radiation fields and compared with independent ionization chamber measurements. Even the NaI(Tl) spectrometer is a powerful tool, as is shown, for example by the data obtained at Bikini Atoll for a pure fallout field. Comparing exposure rates at a number of the sites illustrates that both methods give comparable exposure rate results for the natural emitters and major fallout nuclides, and as expected the Ge(Li) detector is more useful for analyzing more complex fields. The relative accuracy of the spectrometric analysis methods described earlier is indicated in the table by the degree to which the

sum of the individual nuclide exposure rates add up to the total (ionization chamber) measured exposure rate over a wide range of radiation fields.

Determining Source Radioactive Equilibrium

The statistical precision of the flux measured from a single major peak is less precise for a Ge(Li) than for a NaI(Tl) spectrum. We can, however, measure the flux from several lines for say the ^{238}U or ^{232}Th series and obtain a more precise measurement of the exposure rate from the whole series. In the case of the ^{232}Th series, one can ascertain the degree of equilibrium among various nuclides in the series (particularly the degree of equilibrium between MsTh_2 and its daughters since ^{224}Ra may be leached out of some soils and between ^{228}Ra (186 keV) and radon daughters).

Nuclear Facilities Studies

In addition to measuring exposure rates and concentrations of natural emitters and deposited fallout emitters, field spectrometry is also quite valuable for investigating the radiation field around nuclear facilities. Even when a nuclear facility is operating, the natural background and fallout exposure rate levels can be unambiguously distinguished by Ge(Li) field spectrometry from the exposure rate contributions from other sources, such as effluent noble gases and direct radiation from waste storage and steam turbines.

Figure 8 shows Ge(Li) spectra obtained at a site near a boiling water reactor (BWR) nuclear plant with the wind blowing from the BWR stack toward the detector and in the opposite direction. The peaks due to the noble gases can be clearly identified and the fluxes of these gamma rays at the detector estimated. For accurate measurements, however, we need to know the geometry of the plume in order to relate fluxes at the indicated energies to exposure rates from the individual nuclides. We can, however, test models of plume geometry by using the ratios of fluxes at the detector due to different gamma-ray energy lines from the same nuclide, for example the 403 keV to 2556 keV ^{87}Kr lines or the 196 to 2196 keV ^{88}Kr lines. The total plume exposure rate can, of course,

be easily obtained by subtracting the spectrometrically determined natural and fallout components from the total exposure rate determined with the ionization chamber.

The Ge(Li) spectrum can be used to quantitate the exposure rates or concentrations of any nuclides deposited on the ground, such as ^{131}I or ^{134}Cs , using the usual techniques. An example of a situation which could be analyzed semi-quantitatively is shown in Figure 9, a Ge(Li) spectrum obtained along a river bank near a nuclear fuel reprocessing plant. Here the clay apparently filtered and concentrated certain nuclides present in the water (particularly cesium), resulting in a substantial increase in local environmental radiation levels.

^{16}N from BWR Turbines

Another application of field spectrometry is the measurement of the flux and exposure rate in the environment due to the high energy gamma rays from ^{16}N in the steam passing through the turbines of large BWR plants (Figure 10). Here the high sensitivity of NaI(Tl) even at these higher gamma-ray energies provided a sensitive indication of the presence of higher energy gamma rays; particularly since there are no natural or fallout emitted gamma rays above 3.0 MeV. Using the measured flux and the total spectrum energy above 3 MeV Lower⁽²³⁾ has shown that quite accurate estimates of ^{16}N environmental exposure rates can be made.

Radioactive Construction Materials

We have also used in situ spectrometry to qualitatively identify the presence of low energy gamma rays from radium present in uranium tailings used for building construction and to identify the source of elevated exposure rate levels in structures built using high phosphate material or certain types of uranium bearing shale.

^{239}Pu in the Environment

Field spectrometry can also be used to monitor special radiation contamination situations such as deposited ^{239}Pu

in the soil surface. Here, large area, thin NaI(Tl) detectors are used to monitor the 60 keV ^{241}Am gamma rays which accompany ^{239}Pu . Our laboratory studies of the response of our large 60 cm³ Ge(Li) at 60 keV indicate that one could identify elevated levels of ^{239}Pu in the environment. Though systematic studies have not been made, one notes that a large fraction of the low energy flux contributing to the Compton continuum in the 60 keV energy region is due to "skyshine" and, therefore, the "background" in this region can probably be dramatically reduced by judicious shielding and the ability to measure the 60 keV line enhanced.

Estimates of Soil ^{90}Sr and ^{137}Cs Levels

Finally, field spectrometry is useful for rapid determinations of the variation of fallout within some geographical area. Here, as mentioned previously, we need to know the depth distribution of radioactivity fairly accurately to arrive at a very accurate concentration measurement, though one can still obtain a picture of the gross variation with location. For example, Table 22 shows estimates of ^{137}Cs activity in soil in the mid 1960's made by measuring the 662 keV flux at 1 meter above the ground, assuming that a 3 cm relaxation length represents the mean depth distribution ($\alpha/\rho = 0.21$, at that time was a reasonable value based on the few available measurements) and the empirically accepted fact that the $^{90}\text{Sr}/^{137}\text{Cs}$ activity is about 1.5⁽²⁴⁾. Estimates from field spectrometry can be seen to compare well with the soil sample results of Hardy and Alexander⁽²⁴⁾. The fact that one can estimate the gross activity of ^{137}Cs or ^{90}Sr at a site to even an accuracy of a factor of two (if the assumed depth distribution was wrong) seems significant in the light of the speed with which the spectral measurements can be made.

Relative Advantages of NaI(Tl) and Ge(Li) Systems

Although Ge(Li) spectra clearly give much more information than the NaI(Tl) spectra, to gather and utilize this information requires a large capacity multichannel analyzer having 1000 or more channels, a separate amplifier, liquid nitrogen supply and readout equipment to store the large amount of data. One also obtains much more data for analysis than may

be needed for a particular problem. Conversely the NaI(Tl) detector requires only a 200 - 400 channel analyzer and a parallel printer. Power requirements can be met with only one 12 V storage battery and a small rotary inverter. One can operate the equipment required for a NaI(Tl) field spectrum out of the trunk of a standard auto. For most "natural background" measurements, it is clear from the data in the preceding tables that the NaI analysis is completely adequate.

Though the cost of the Ge(Li) system is quite high, its utility is obvious for investigating complex radiation fields. The proper mounting in a station wagon or panel truck allows the spectrometer to be easily transported and allows maximum utilization both as a field spectrometer and as a standard laboratory counting system.

VII. ESTIMATES OF ERRORS IN THE DETERMINATION OF FLUX, EXPOSURE RATE AND SOIL ACTIVITY

We have tried to indicate at each step the necessary approximations and possible sources of error. It is clear that the final assessment of the accuracy of the method must rely on (1) cross-calibrations by other techniques of analysis and (2) the degree by which the sum of the individual exposure rates agrees with independently measured total exposure rates over a wide range of K, Th, U and fallout combinations.

We previously showed that the use of NaI(Tl) spectrometry to measure the soil activity of U, T and K was quite accurate having tested the assumptions of half-space geometry, uniformly distributed sources, insensitivity to soil density, etc. by comparing field spectrometric estimates of in situ soil activity with laboratory analyses of soil samples taken at a large number of sites⁽¹⁾. For both K and Th our estimates of concentration correlated very closely with the laboratory estimates, although the field estimates were in general about 10% lower than the laboratory results. This was expected, however, since the latter were concentrations in dry soil and

an average increase of 10% in soil density due to in situ moisture content appeared reasonable. Individual comparisons in some cases showed poorer agreement and this probably reflected more the problem of obtaining a representative soil sample at a site than an error in the field spectral analysis. The U series comparison was, of course, very poor reflecting primarily the different radon emanation fractions at the various sites; since most of the soils were counted in the laboratory after being allowed to reach equilibrium. A few samples which were counted in the lab after drying and before being allowed to reach equilibrium indicated losses of from 30% to 50% of the radium equivalent gamma activity.

In the previous section we compared our field spectrometric estimates of ^{137}Cs and ^{90}Sr measurements on laboratory samples, indicating in general very good agreement.

Table 21 indicated the degree to which the individual exposure rate estimates sum to the total ionization chamber value of exposure rate. These data are in general accord with our experience at most reasonably flat "half space" sites and are the best indication of the validity of our individual exposure rate estimates.

In general, the largest percentage error in exposure rate is obtained for the ^{238}U series, primarily because of the emanation of radon and its subsequent movement within the atmosphere. Besides resulting in a somewhat altered source distribution with respect to our model, the decreased flux results in poorer quality counting data. For example, it is frequently quite difficult to accurately estimate the small flux of 1.76 MeV gamma rays present from NaI(Tl) spectral data. Combining the accuracy of flux estimation ($\pm 20\%$) with the uncertainty in radon contribution we estimate our ^{238}U series exposure rate values are correct to about 25%. Because of the ability to resolve the 295, 350, and 609 keV U peaks with the Ge(Li) detector we are able to obtain much better measurements of flux ($\sim \pm 5\%$ s.d.) and we estimate our Ge(Li) ^{238}U exposure rate measurements to have an accuracy of ± 10 to 15%. In terms of the error in total exposure rate this percentage is small since generally ^{238}U contributes only

about 20% to the total gamma exposure rate. The ^{40}K estimates are the most accurate and we feel our measurements of flux are good to better than 5% and our estimates of exposure rate to about 5 - 10%. Thorium-232 exposure rates are also believed to be correct to about 5 - 10%.

The error in estimating fallout soil activities has already been shown to be dominated by the accuracy of the assumed depth distribution. We estimate we can infer ^{137}Cs exposure rates to $\pm 15\%$ with the NaI(Tl) detector and $\pm 10\%$ with the Ge(Li) under most circumstances.

These are accuracy estimates and include systematic errors such as uncertainties in branching ratios. The precision of a single measurement depends on the statistical significance of the counting rate data under the photopeaks of interest. For prominent peaks such as the 1464 keV ^{40}K peak the precision can be better than the accuracy, i.e. we can reproduce the measurement to better than a few percent although the actual error in our estimate of exposure rate may be much greater. Thus, it is quite feasible to use the spectrometric technique to study small time variations in background due to changes in soil moisture, radon emanation, and "natural fallout".

VIII. SUMMARY

We have attempted in this report to summarize all of our work to date on in situ field spectrometry, presenting in detail the theoretical basis for interpreting field spectra to determine soil concentrations and exposure rates as well as illustrating the laboratory calibration of our particular detectors. In doing so we have tried to indicate the "detector independence" of the method, pointing out that the detector can be any instrument which measures the gamma-ray fluxes at particular energies.

We have pointed out the use of particular field spectrometric systems for investigating various environmental radiation fields, both natural and man-made. Field spectrometry is a powerful tool for studying external environmental radioactivity. It allows one to obtain quantitative data over large areas in a short time, a task that is clearly impractical by conventional sample gathering and subsequent laboratory analysis. It also allows one to pick and choose sites for further or for more intensive study, provides at the very least qualitative information on the sources contributing to the gamma-ray exposure at a site and at its best a complete quantitative picture of the gamma-ray field.

We have attempted to include in this report the theoretical data necessary to infer soil activity and free air exposure rate for any source whose depth distribution in the soil can be represented by a superposition of exponentials and whose energy lies between 50 keV and 3 MeV. Thus, it would be an easy matter for instance for any investigator to use the tables in this report to estimate the flux at 1 meter above the ground due for example to a quasi-plane source of ^{134}Cs or ^{60}Co or any other similarly unlikely contamination situations.

All of the data in this report refer to measurements to be made at or near the earth-air interface. Clearly there are similar possibilities for field spectrometry from aircraft. We previously discussed the variation of exposure rate and flux with altitude⁽¹²⁾ and these data can be used to infer appropriate values of ϕ/I above the ground. The theoretical results are being modified as necessary to reflect the more accurate data for photons per disintegration in the ^{238}U and ^{232}Th series, as well as to provide energy and angular distributions for photon flux as well as for exposure rate as a function of altitude.

ACKNOWLEDGMENTS

The authors wish to acknowledge the considerable contributions to this work by several of our HASL colleagues, in particular, Peter Raft, Wayne Lowder, Burton Bennett, and James E. McLaughlin. We wish to particularly thank the HASL Instrumentation group for their help in the design, procurement, and construction of the instrument systems described in this report.

REFERENCES

1. Beck, H. L., Condon, W. J., and Lowder, W. M.
Spectrometric Techniques for Measuring Environmental Gamma Radiation
USAEC Report HASL-150, October (1964)
2. Lowder, W. M., Condon, W. J., and Beck, H. L.
Field Spectrometric Investigations of Environmental Radiation in the U.S.A.
The Natural Radiation Environment, Ch. 35 (Adams, J.A.S., Lowder, W. M., Editors)
Univ. of Chicago Press, Chicago (1964)
3. Beck, H. L., Lowder, W. M., and McLaughlin, J. E.
In Situ External Environmental Gamma-Ray Measurements Utilizing Ge(Li) and NaI(Tl) Spectrometry and Pressurized Ionization Chambers
Proc. of Symposium on Rapid Methods for Measuring Radioactivity in the Environment
IAEA-SM-148/2, Vienna (1971)
4. Lowder, W. M., Beck, H. L., and Condon, W. J.
Spectrometric Determination of Dose Rates from Natural and Fallout Gamma-Radiation in the United States, 1962 - 1963
Nature, 202, 745-749 (1964)
5. Beck, H. L., Lowder, W. M., Bennett, B. G., and Condon, W. J.
Further Studies of External Environmental Radiation
USAEC Report HASL-170, March (1966)
6. Moriuchi, S., and Miyanaga, I.
A Spectrometric Method for Measurement of Low-Level Gamma Exposure Dose
Health Physics, 12, 541 (1966)

7. Pensko, J.
Dosimetry of Environmental Gamma Radiation in Poland by
Means of Gamma-Ray Spectra in the Field
Central Laboratory for Radiological Protection Report
CLOR-48/D, Warsaw (1966)
8. Cardinale, A., and Frittelli, L.
Improved Methods for the Measurement of Gamma Exposure
Rate in the Natural Radiation Environment
Comitato Nazionale Energia Nucleare Report RT/FI(68)54,
Rome (1968)
9. Phelps, P. L., Anspaugh, L. R., Koranda, J. J., and
Huckabay, G. W.
A Portable Ge(Li) Detector for Field Measurement of
Radionuclides in the Environment
IEEE Transactions on Nuclear Science 1972 (in press)
10. DeCampo, J., Beck, H. L., and Raft, P., High
Pressure Ionization Chambers for the Measurement of
Environmental Exposure Rates
USAEC Report HASL-260 (1972)
11. Beck, H. L.
Environmental Gamma Radiation from Deposited Fission
Products, 1960 - 1964
Health Physics, 12, 313-322 (1966)
12. Beck, H. L., and De Planque, G.
The Radiation Field in Air Due to Distributed Gamma-Ray
Sources in the Ground
USAEC Report HASL-195, May (1968)
13. Martin, M. J., and Blichert-Toft, P. H.
Radioactive Atoms
Nuclear Data Tables, Section A, Vol. 8, Nos. 1-2,
October (1970)
14. Gunnink, R., Niday, J. B., Anderson, R. P., and Meyer,
R. A.
Gamma-Ray Energies and Intensities
LRL Report UC10-15439 (1969)

15. Lingeman, E. W. A., Konijn, J., Polak, P., and Wapstra, A. H.
The Decay of ^{214}Pb and other ^{226}Ra Daughters
Nuclear Physics, A 133, 630-647 (1969)
16. Mowatt, R. S.
 ^{152}Eu and ^{226}Ra Relative γ -Ray Intensities for Rapid
Efficiency Calibrations of Ge(Li) Detectors
Canadian Journal of Physics, 48, 2606-2608 (1970)
17. Maria, H., Ythier, C., Ardison, G., Dalmasso, J., and Forest, H., Compt. Rend., Ser. B., Vol. 265, pp. 1138-40 (1967);
Vol. 267, pp. 1109-1112; (1968); Vol. 269, pp. 785-788,
(1969); Vol. 269, pp. 1003-1006 (1969); Vol. 272,
pp. 905-908 (1971).
18. Beck, H. L.
The Absolute Intensities of Gamma Rays from the Decay of
 ^{238}U and ^{232}Th (to be published)
19. Hultquist, B.
Studies of Naturally Occurring Ionizing Radiations, with
Special Reference to Radiation Doses in Swedish Houses
of Various Types
Kungl. Svenska Vetenskapsakad. Handl. 6 Ser. 4, No. 3,
p. 125 (1956)
20. Baranov, V. L., as quoted in Grammkov, A. B.
Field Emanation Method, Radiometric Methods in the
Prospecting of Uranium Ores, Moscow: State Scientific-
Technical Publishers of Literature of Geology and
Mineral Resources Conservation (1957) [In English
Transl. USAEC Report AEC-tr-3738 (1959)]
21. Vinogradov, A. P.
The Geochemistry of Rare and Dispersed Chemical Elements
in Soils, Ch. 16, 2nd ed., p. 212 (1959) [Translated
from Russian: New York: Consultants Bureau, p. 212 (1959)]

22. Beck, H. L.
The Physics of Environmental Radiation Fields
Proceedings of the 2nd International Symposium on the
Natural Radiation Environment, Houston, Texas (1972)
[in press]
23. Lowder, W. M., Raft, P. D., and Gogolak, C. V.
Environmental Gamma Radiation from N-16 in Reactor
Turbines
Transactions of the American Nuclear Society, 15, June
(1972)
24. Hardy, E., Private Communication (1971)

TABLE 1

ϕ - UNSCATTERED FLUX AT ONE METER ABOVE GROUND FOR EXPONENTIALLY DISTRIBUTED SOURCES IN THE SOIL*

Source Energy (keV)	$(\alpha/\rho) - \text{cm}^2/\text{g}$						
	0 (Uniform)	0.0625	0.206	0.312	0.625	6.25	∞ (Plane)
50	1.4403	0.0816	0.2245	0.3049	0.4748	1.147	1.577
100	2.7744	0.1458	0.3627	0.4708	0.6786	1.359	1.710
150	3.3264	0.1702	0.4103	0.5261	0.7438	1.427	1.775
200	3.9056	0.1843	0.4550	0.5770	0.8018	1.483	1.804
250	4.0640	0.2008	0.4697	0.5910	0.8185	1.506	1.863
364	4.7184	0.2268	0.5158	0.6429	0.8775	1.578	1.933
500	5.3904	0.2519	0.5595	0.6918	0.9334	1.650	1.995
662	6.1456	0.2788	0.6041	0.7412	0.9889	1.719	2.054
750	6.5312	0.2919	0.6257	0.7649	1.015	1.752	2.084
1000	7.5280	0.3245	0.6769	0.8209	1.077	1.830	2.151
1173	8.1472	0.3437	0.7067	0.8531	1.113	1.874	2.189
1250	8.4384	0.3523	0.7198	0.8675	1.129	1.895	2.205
1333	8.7504	0.3617	0.7336	0.8826	1.145	1.914	2.224
1460	9.1472	0.3731	0.7511	0.9011	1.166	1.941	2.247
1765	10.091	0.3997	0.7897	0.9428	1.211	1.997	2.294
2004	10.818	0.4188	0.8173	0.9725	1.243	2.036	2.334
2250	11.397	0.4357	0.8414	0.9982	1.271	2.071	2.358
2500	12.173	0.4536	0.8667	1.025	1.300	2.105	2.385

*The activity at depth Z cm or ρZ g/cm² is S (gammas emitted per gram soil per sec) = $\alpha/\rho S_A e^{-(\alpha/\rho)(\rho Z)}$ where $S_A = 1.0$ gamma/cm²-s is the total number of gammas emitted in a column of area 1 cm² and infinite depth (see equation 3). For $\alpha/\rho = 0$, $S_0/\rho = 1.0$ gammas emitted per gram of soil for all Z .

TABLE 2

MASS ATTENUATION COEFFICIENTS IN SOILS OF VARYING MOISTURE
CONTENT AND COMPOSITION OF SOIL USED
IN TRANSPORT CALCULATIONS

E (keV)	$(\mu/\rho) - \text{cm}^2/\text{g}$				
	Soil 0% H ₂ O	Soil 10% H ₂ O	Soil 25% H ₂ O	Alum.	Air
20	3.01	2.78	2.05	3.22	0.683
25	2.34	1.52	1.13	1.76	-
30	1.00	0.938	0.838	1.03	0.315
35	0.656	0.644	0.566	0.669	-
40	0.470	0.471	0.433	0.492	0.225
45	0.380	0.381	0.338	0.386	-
50	0.327	0.314	0.298	0.319	0.193
55	0.282	0.277	0.265	0.277	-
60	0.254	0.248	0.239	0.246	0.177
65	0.233	0.230	0.221	0.219	-
70	0.218	0.214	0.206	0.205	-
75	0.204	0.202	0.194	0.193	-
80	0.192	0.190	0.189	0.185	0.161
85	0.189	0.185	0.181	0.177	-
90	0.179	0.178	0.175	0.171	-
95	0.173	0.173	0.170	0.166	-
100	0.166	0.167	0.167	0.160	0.151
150	0.138	0.139	0.141	0.134	0.134
200	0.124	0.125	0.127	0.120	0.123
250	0.114	0.115	0.118	0.111	-
300	0.106	0.108	0.109	0.103	0.106
350	0.100	0.101	0.105	0.098	-
400	0.0950	0.0963	0.0975	0.0925	0.0953
450	0.0906	0.0919	0.0931	0.0875	-
500	0.0869	0.0875	0.0894	0.0844	0.0868
550	0.0831	0.0844	0.0856	0.0806	-
600	0.0800	0.0813	0.0825	0.0775	0.0804
650	0.0769	0.0788	0.0800	0.0756	-
700	0.0744	0.0756	0.0775	0.0731	-
750	0.0725	0.0731	0.0750	0.0706	-

TABLE 2 (Cont'd)

E (keV)	$(\mu/\rho) - \text{cm}^2/\text{g}$				
	Soil 0% H ₂ O	Soil 10% H ₂ O	Soil 25% H ₂ O	Alum.	Air
750	0.0725	0.0731	0.0750	0.0706	-
800	0.0706	0.0713	0.0725	0.0681	0.0706
850	0.0681	0.0694	0.0706	0.0669	-
900	0.0669	0.0675	0.0688	0.0644	-
950	0.0656	0.0650	0.0669	0.0631	-
1000	0.0638	0.0638	0.0650	0.0614	0.0635
1500	0.0515	0.0521	0.0530	0.0500	0.0517
2000	0.0444	0.0449	0.0456	0.0432	0.0444
2500	0.0398	0.0401	0.0413	0.0388	-
3000	0.0362	0.0364	0.0371	0.0353	0.0358

Composition by weight of soil used in transport calculations:

Al₂O₃ - 13.5%

Fe₂O₃ - 4.5%

SiO₂ - 67.5%

CO₂ - 4.5%

H₂O - 10%

TABLE 3

ϕ - UNSCATTERED FLUX PER mCi/cm² AT ONE METER ABOVE GROUND FOR
TYPICAL FALLOUT ISOTOPES IN THE SOIL

Isotope	E _γ (keV)	γ's/dis.	(α/ρ) - cm ² /g					
			0.0625	0.206	0.312	0.625	6.25	∞ (Plane)
¹⁴⁴ Ce	134	.108	6.51(-5)	1.59(-4)	2.04(-4)	2.90(-4)	5.63(-4)	6.99(-4)
¹⁴¹ Ce	145	.490	3.03(-4)	7.43(-4)	9.43(-4)	1.34(-3)	2.57(-3)	3.21(-3)
¹³¹ I	364	.824	6.92(-4)	1.58(-3)	1.96(-3)	2.67(-3)	4.82(-3)	5.88(-3)
¹²⁵ Sb	428	.296	2.63(-4)	5.89(-4)	7.39(-4)	9.88(-4)	1.75(-3)	2.15(-3)
¹⁴⁰ La	487	.45	4.13(-4)	9.19(-4)	1.14(-3)	1.54(-3)	2.71(-3)	3.30(-3)
¹⁰³ Ru	497	.89	8.20(-4)	1.84(-3)	2.27(-3)	3.08(-3)	5.43(-3)	6.59(-3)
¹⁰⁶ Ru	512	.206	1.94(-4)	4.34(-4)	5.33(-4)	7.16(-4)	1.27(-3)	1.53(-3)
¹⁴⁰ Ba	537	.238	2.29(-4)	5.11(-4)	6.25(-4)	8.37(-4)	1.47(-3)	1.78(-3)
¹²⁵ Sb	601	.184	1.84(-4)	4.02(-4)	4.90(-4)	6.57(-4)	1.14(-3)	1.38(-3)
¹⁰³ Ru	610	.054	5.33(-5)	1.18(-4)	1.44(-4)	1.93(-4)	3.40(-4)	4.06(-4)
¹⁰⁶ Ru	622	.10	1.00(-4)	2.19(-4)	2.68(-4)	3.59(-4)	6.29(-4)	7.55(-4)
¹³⁷ Cs	662	.846	8.73(-4)	1.89(-3)	2.32(-3)	3.08(-3)	5.38(-3)	6.42(-3)
⁹⁵ Zr	724	.435	4.67(-4)	9.98(-4)	1.22(-3)	1.61(-3)	2.82(-3)	3.33(-3)
⁹⁵ Zr	757	.543	5.91(-4)	1.27(-3)	1.54(-3)	2.07(-3)	3.54(-3)	4.22(-3)
⁹⁵ Nb	766	.998	1.09(-3)	2.35(-3)	2.85(-3)	3.85(-3)	6.59(-3)	7.77(-3)
¹⁴⁰ La	816	.231	2.58(-4)	5.47(-4)	6.67(-4)	8.97(-4)	1.54(-3)	1.81(-3)
⁵⁴ Mn	835	1.0	1.13(-3)	2.39(-3)	2.89(-3)	3.89(-3)	6.66(-3)	7.84(-3)
¹⁴⁰ La	1597	.956	1.38(-3)	2.71(-3)	3.26(-3)	4.21(-3)	6.93(-3)	8.03(-3)
⁶⁰ Co	1173	1.0	1.27(-3)	2.62(-3)	3.16(-3)	4.12(-3)	6.93(-3)	8.10(-3)
⁶⁰ Co	1333	1.0	1.34(-3)	2.72(-3)	3.27(-3)	4.24(-3)	7.08(-3)	8.23(-3)

TABLE 4

φ - UNSCATTERED FLUX PER pCi/g AT ONE METER ABOVE GROUND FOR UNIFORMLY DISTRIBUTED ²²⁶Ra AND ²³²Th SOURCES IN THE SOIL

Decaying Isotope	E (keV)	γ's/dis.*	Flux (γ's/cm ² -s)	Decaying Isotope	E (keV)	γ's/dis.*	Flux (γ's/cm ² -s)
²²⁶ Ra	186	0.034	4.58(-3)	²¹² Pb	239	0.490	7.25(-2)
²¹⁴ Pb	242	0.070	1.04(-2)	²²⁴ Ra	241		
	295	0.179	2.91(-2)	²⁰⁸ Ac	270	0.065	1.02(-2)
	352	0.350	6.01(-2)	²⁰⁸ Tl	277		
²¹⁴ Bi	609	0.430	9.42(-2)	²⁰⁸ Ac	282		
	666	0.015	3.39(-3)	²¹² Pb	301	0.034	5.53(-3)
	768	0.048	1.17(-2)	²⁰⁸ Ac	338	0.129	2.18(-2)
	934	0.031	8.10(-3)	Mixed	328-340	0.172	2.90(-2)
	1120	0.145	4.21(-2)	²⁰⁸ Ac	463	0.047	9.20(-3)
	1238	0.056	1.72(-2)	²⁰⁸ Tl	510	0.096	1.93(-2)
	1378	0.046	1.49(-2)	²⁰⁸ Tl	583	0.300	6.39(-2)
	1401-08	0.038	1.25(-2)	²¹² Bi, ²⁰⁸ Ac	727	0.079	1.86(-2)
	1510	0.021	7.12(-3)	²²⁶ Ac	755	0.011	2.70(-3)
	1730	0.028	1.02(-2)		772	0.017	4.10(-3)
	1765	0.147	5.39(-2)		795	0.049	1.20(-2)
	1848	0.021	7.91(-3)		830+35+40	0.038	9.40(-3)
	2205	0.047	1.95(-2)	²⁰⁸ Tl	860	0.047	1.18(-2)
	2448	0.015	6.66(-3)	²⁰⁸ Ac	911	0.290	7.55(-2)
²²⁸ Ac	129	0.025	2.90(-3)		965+69	0.230	6.13(-2)
	210	0.041	5.80(-3)		1588	0.046	1.23(-2)
				²⁰⁸ Tl	2615	0.360	0.167

*Transitions for which γ's/dis. <.02 are not listed except where they are required to correct measurements of the flux from some other natural or fallout emitter. Series equilibrium is assumed.

TABLE 5

 ^{235}U , ^{40}K , AND ^{232}Th DECAY CHAINS

Isotope	Decay Mode	$T_{1/2}$	Isotope	Decay Mode	$T_{1/2}$	
^{232}Th	α	1.40(10)y	$^{232}\text{U}(\text{UI})$	α	4.5(9)y	
↓			↓			
$^{228}\text{Ra}(\text{MsI})$	β^-	6.7 y	$^{228}\text{Th}(\text{UXI})$	β^-	24.1 d	
↓			↓			
$^{228}\text{Ac}(\text{MsII})$	β^-	6.13 h	$^{228}\text{Pa}(\text{UXII})$	β^-	1.18 m	
↓			↓			
^{228}Th	α	1.91 y	$^{228}\text{U}(\text{UII})$	α	2.5(5)y	
↓			↓			
$^{224}\text{Ra}(\text{ThX})$	α	3.64 d	$^{224}\text{Th}(\text{Io})$	α	8(4)y	
↓			↓			
$^{220}\text{Rn}(\text{thoron})$	α	54.5 s	^{220}Ra	α	1622 y	
↓			↓			
$^{216}\text{Po}(\text{Th-A})$	α	0.16 s	$^{222}\text{Rn}(\text{radon})$	α	3.83 d	
↓			↓			
$^{212}\text{Pb}(\text{Th-B})$	β^-	10.64 h	$^{218}\text{Po}(\text{RaA})$	$\alpha(99.97\%)$	3.05 m	
↓			↓			
$^{212}\text{Bi}(\text{Th-C})$	$\alpha(36\%)$ $\beta^-(64\%)$	60.5 m	$^{214}\text{Pb}(\text{RaB})$	β^-	26.8 m	
↓			↓			
$^{212}\text{Po}(\text{Th-C}')$	α	3(-7)s	$^{214}\text{Bi}(\text{RaC})$	$\beta^-(99\%)$	19.7 m	
↓			↓			
$^{208}\text{Tl}(\text{Th-C}')$	β^-	3.1 m	$^{214}\text{Po}(\text{RaC}')$	α	1.6(-4)s	
↓			↓			
^{208}Pb	Stable		$^{210}\text{Tl}(\text{RaC}')$	β^-	1.5 m	
			↓			
			$^{210}\text{Pb}(\text{RaD})$	β^-	22 y	
			↓			
^{40}K	β^-	1.28(9)y	$^{210}\text{Bi}(\text{RaE})$	β^-	5.02 d	
↓			↓			
^{40}A			Stable	↓		
^{40}Ca			Stable	^{210}Po	α	1383 d
			↓			
			^{206}Pb	Stable		

TABLE 6

PERCENT OF UNSCATTERED FLUX ENTERING DETECTOR AT ANGLES LESS
THAN θ FOR $h = 1$ METER

θ (deg.)	Tan $\theta=R$ (meters)	145 keV			662 keV			1460 keV		
		$\alpha/\rho=0,$	$=0.21,$	$=\infty$	$\alpha/\rho=0,$	$=0.21,$	$=\infty$	$\alpha/\rho=0,$	$=0.21,$	$=\infty$
90	-	100	100	100	100	100	100	100	100	100
84	9.95	93	89	62	92	85	53	92	83	51
79	4.90	84	76	45	82	70	39	82	67	36
73	3.18	73	64	34	72	58	30	72	54	27
66	2.29	63	52	26	62	46	23	61	43	21
60	1.73	53	42	20	52	37	17	52	33	16
53	1.33	43	32	15	41	28	13	41	25	11
46	1.02	32	23	10	31	20	9	31	18	8
37	0.75	21	15	6	21	13	6	21	11	5
26	0.48	11	7	3	10	6	3	10	5	2

Note: θ is measured with respect to the normal to the interface, i.e.,
 $\theta = 90^\circ$ is parallel to the interface.

TABLE 7

EXPOSURE RATE ($\mu\text{R/hr}$) AT ONE METER ABOVE GROUND FOR EXPONENTIALLY DISTRIBUTED MONOENERGETIC SOURCES IN THE SOIL*

Source Energy (keV)	$(\alpha/\rho) - \text{cm}^2/\text{g}$						
	0 (Uniform)	0.0625	0.206	0.312	0.625	6.25	∞ (Plane)
50	0.88	-	-	-	-	-	-
100	2.05	~0.095	0.185	0.215	0.270	0.400	0.438
150	3.39	0.140	0.285	0.335	0.418	0.620	0.700
200	4.88	0.200	0.390	0.460	0.570	0.845	0.960
250	6.37	0.256	0.491	0.583	0.731	1.08	1.25
364	10.2	0.404	0.771	0.896	1.11	1.63	1.91
500	14.4	0.558	1.03	1.23	1.52	2.27	2.60
662	19.6	0.738	1.37	1.60	1.97	2.95	3.39
750	22.6	0.837	1.54	1.80	2.21	3.32	3.80
1000	30.4	1.10	2.00	2.32	2.85	4.28	4.86
1173	36.2	1.28	2.31	2.63	3.27	4.87	5.52
1250	38.4	1.33	2.41	2.79	3.42	5.14	5.86
1333	41.8	1.42	2.56	2.95	3.62	5.35	6.16
1460	45.1	1.54	2.75	3.18	3.88	5.73	6.56
1765	54.6	1.78	3.25	3.75	4.40	6.45	7.78
2004	62.2	2.07	3.60	4.13	5.00	7.15	8.20
2250	69.5	-	-	-	-	-	-
2500	77.2	-	-	-	-	-	-
2750	85.0	-	-	-	-	-	-

*The activity at depth Z cm or ρZ g/cm² is S (gammas emitted per gram soil per sec) = $\alpha/\rho S_A e^{-(\alpha/\rho)(\rho Z)}$ where $S_A = 1.0$ gamma/cm²-s is the total number of gammas emitted in a column of area 1 cm² and infinite depth (see equation 3). For $\alpha/\rho = 0$, $S_0/\rho = 1.0$ gammas emitted per gram of soil for all Z .

TABLE 8

TOTAL EXPOSURE RATE AT ONE METER ABOVE GROUND FOR NATURAL EMITTERS UNIFORMLY DISTRIBUTED IN THE SOIL

Isotope	$\mu\text{R/h}$	$\mu\text{R/h}$
	pCi/g	unit concentration
^{40}K	0.179	1.49 per % K
^{226}Ra +daughters	1.80	0.61 per 0.358×10^{-6} ppm Ra
^{214}Pb	0.20	0.07 " " "
^{214}Bi	1.60	0.54 " " "
^{238}U +daughters	1.82	0.62 per ppm ^{238}U
^{232}Th +daughters	2.82	0.31 per ppm ^{232}Th
^{228}Ac	1.18	0.13 " "
^{208}Tl	1.36	0.15 " "
^{212}Bi	0.09	0.01 " "
^{212}Pb	0.09	0.01 " "
Other	0.09	0.01 " "

Note: Values quoted in reference 1 based on old decay scheme data and buildup factor calculations were:

$$^{238}\text{U} - 0.76 (\mu\text{R/h})/\text{ppm}$$

$$^{232}\text{Th} - 0.36 (\mu\text{R/h})/\text{ppm}$$

$$^{40}\text{K} - 1.71 (\mu\text{R/h})/\% \text{ K}$$

TABLE 9

TOTAL EXPOSURE RATE ($\mu\text{R/h}$) AT ONE METER ABOVE GROUND FOR SELECTED
FALLOUT ISOTOPES IN THE SOIL

Isotope	Source Activity (mCi/km^2)	$(\alpha/\rho) - \text{cm}^2/\text{g}$					
		0.0625	0.206	0.312	0.625	6.25	= (Plane)
^{144}Ce	1.0	6.25(-5)	1.34(-4)	1.56(-4)	1.96(-4)	2.86(-4)	3.27(-4)
$^{144}\text{Ce}+^{144}\text{Pr}^*$	2.0	1.85(-4)	3.51(-4)	4.05(-4)	5.03(-4)	7.22(-4)	8.34(-4)
^{141}Ce	1.0	2.60(-4)	5.23(-4)	6.21(-4)	7.68(-4)	1.15(-3)	1.31(-3)
^{131}I	1.0	1.56(-3)	2.92(-3)	3.35(-3)	4.20(-3)	6.91(-3)	7.28(-3)
^{136}Sb	1.0	1.77(-3)	3.33(-3)	3.82(-3)	4.86(-3)	7.14(-3)	8.29(-3)
^{140}Ba	1.0	7.74(-4)	1.45(-3)	1.69(-3)	2.09(-3)	3.16(-3)	3.66(-3)
^{140}La	1.0	8.98(-3)	1.63(-2)	1.88(-2)	2.40(-2)	3.56(-2)	3.96(-2)
$^{140}\text{Ba}+^{140}\text{La}^*$	2.15	1.11(-2)	2.02(-2)	2.33(-2)	2.97(-2)	4.40(-2)	4.92(-2)
^{103}Ru	1.0	1.97(-3)	3.66(-3)	4.30(-3)	5.37(-3)	7.90(-3)	9.22(-3)
$^{106}\text{Ru}+^{106}\text{Rh}^*$	2.0	7.74(-4)	1.43(-3)	1.67(-3)	2.11(-3)	3.17(-3)	3.65(-3)
^{137}Cs	1.0	2.31(-3)	4.29(-3)	4.99(-3)	6.17(-3)	9.24(-3)	1.06(-2)
^{95}Zr	1.0	3.02(-3)	5.51(-3)	6.36(-3)	7.81(-3)	1.17(-2)	1.35(-2)
^{95}Nb	1.0	3.15(-3)	5.74(-3)	6.66(-3)	8.14(-3)	1.24(-2)	1.41(-2)
$^{95}\text{Zr}-^{95}\text{Nb}$	3.155	9.91(-3)	1.79(-2)	2.07(-2)	2.54(-2)	3.84(-2)	4.39(-2)
^{54}Mn	1.0	3.40(-3)	6.29(-3)	7.22(-3)	8.88(-3)	1.34(-2)	1.54(-2)
^{60}Co	1.0	9.99(-3)	1.80(-2)	2.06(-2)	2.55(-2)	3.78(-2)	4.32(-2)

*Assuming daughter is in equilibrium with parent-exposure rate is for 1 mCi/km^2 of parent activity.

TABLE 10

ERROR IN 1 METER EXPOSURE RATES FOR INFINITE HALF-SPACE GEOMETRY DUE TO NEGLECTING AIR-SOIL DIFFERENCES (BUILD-UP FACTOR APPROACH)

E (keV)	Soil-Air/Soil-Soil
250	0.79
364	0.87
500	0.90
1000	0.94
1500	0.95
2000	0.96
2500	0.95

TABLE 11

ϕ/I -(ONE METER) FOR FALLOUT EMITTERS IN THE SOIL -
 $(\gamma' s/cm^2-s) / (\mu R/h)$

Isotope	E γ (key)	$(\alpha/\rho) - cm^2/g$					
		0.0625	0.206	0.312	0.625	6.25	∞ Plane
¹⁴⁴ Ce	134	1.04	1.19	1.31	1.48	1.97	2.14
¹⁴⁴ Ce- ¹⁴⁴ Pr	134	0.352	0.453	0.504	0.577	0.780	0.838
¹⁴¹ Ce	145	1.17	1.42	1.52	1.74	2.23	2.45
¹³¹ I	364	0.444	0.541	0.585	0.636	0.702	0.808
¹²⁵ Sb	428	0.149	0.177	0.193	0.203	0.245	0.259
¹⁴⁰ La	487	0.046	0.056	0.061	0.064	0.076	0.083
¹⁴⁰ Ba- ¹⁴⁰ La	487	0.037	0.045	0.049	0.052	0.062	0.067
¹⁰³ Ru	497	0.416	0.503	0.528	0.574	0.687	0.715
¹⁰⁶ Ru- ¹⁰⁶ Rh	512	0.251	0.303	0.319	0.339	0.401	0.419
¹⁴⁰ Ba	537	0.296	0.352	0.370	0.400	0.465	0.486
¹⁴⁰ Ba- ¹⁴⁰ La	537	0.0206	0.0253	0.0268	0.0282	0.0334	0.0362
¹²⁵ Sb	601	0.104	0.121	0.128	0.135	0.160	0.166
¹⁰³ Ru	610	0.0271	0.0322	0.0335	0.0359	0.0430	0.0440
¹⁰⁶ Ru	622	0.129	0.153	0.160	0.170	0.198	0.207
¹³⁷ Cs	662	0.377	0.440	0.465	0.499	0.582	0.606
⁹⁵ Zr	724	0.155	0.181	0.192	0.206	0.241	0.247
⁹⁵ Zr- ⁹⁵ Nb	724	0.0476	0.0557	0.0589	0.0634	0.0734	0.0758
⁹⁵ Zr	757	0.196	0.230	0.242	0.265	0.303	0.313
⁹⁵ Zr- ⁹⁵ Nb	757	0.0602	0.0709	0.0744	0.0815	0.0922	0.0961
⁹⁵ Nb	766	0.346	0.409	0.428	0.473	0.531	0.551
⁹⁵ Zr- ⁹⁵ Nb	766	0.239	0.282	0.297	0.328	0.371	0.381
¹⁴⁰ La	816	0.0287	0.0336	0.355	0.0374	0.0433	0.0457
¹⁴⁰ Ba- ¹⁴⁰ La	816	0.0232	0.0270	0.0286	0.0302	0.0350	0.0368
⁵⁴ Mn	835	0.332	0.380	0.400	0.438	0.497	0.509
¹⁴⁰ La	1597	0.154	0.166	0.173	0.175	0.195	0.203
¹⁴⁰ Ba- ¹⁴⁰ La	1597	0.124	0.134	0.140	0.142	0.158	0.163
⁶⁰ Co	1173	0.127	0.146	0.153	0.162	0.183	0.188
⁶⁰ Co	1333	0.134	0.151	0.159	0.168	0.187	0.191

TABLE 12

ϕ/I -RATIO OF GAMMA-RAY FLUX DENSITY TO EXPOSURE RATE FROM
NATURAL EMITTERS IN THE SOIL

Parent Isotope	E_γ (keV)	ϕ/I ($\frac{\gamma' s/cm^2-s}{\mu R/h}$)	Parent Isotope	E_γ (keV)	ϕ/I ($\frac{\gamma' s/cm^2-s}{\mu R/h}$)
Uranium Series, I = $1.82 \frac{\mu R/h}{pCi/g}$			Thorium Series, I = $2.82 \frac{\mu R/h}{pCi/g}$		
²²⁶ Ra	186	2.52 (-3)	²²⁸ Ac	129	1.03 (-3)
²¹⁴ Pb	242	5.71 (-3)		210	2.06 (-3)
	295	1.60 (-2)	²¹² Pb	239	2.57 (-2)
	352	3.30 (-2)	²²⁴ Ru	241	
²¹⁴ Bi	609	5.18 (-2)	²²⁸ Ac	270	3.62 (-3)
	666	1.86 (-3)	²⁰⁸ Tl	277	
	768	6.43 (-3)	²²⁸ Ac	282	
	934	4.45 (-3)	²¹² Pb	301	2.96 (-3)
	1120	2.31 (-2)	²²⁸ Ac	338	7.73 (-3)
	1238	9.45 (-3)	Mixed	328-340	2.03 (-2)
	1378	8.19 (-3)	²²⁸ Ac	463	3.26 (-3)
	1401-08	6.87 (-3)	²⁰⁸ Tl	510	6.84 (-3)
	1510	3.91 (-3)	²²⁸ Tl	583	2.27 (-2)
	1730	5.60 (-3)	²¹² Bi, ²²⁸ Ac	727	6.60 (-3)
1765	2.96 (-2)	²²⁸ Ac	755	9.57 (-4)	
1845	4.35 (-3)		772	2.45 (-3)	
2205	1.07 (-2)		795	4.25 (-3)	
2448	3.66 (-3)		830+835+840	3.23 (-3)	
Potassium, I = $0.179 \frac{\mu R/h}{pCi/g}$			²⁰⁸ Tl	860	4.18 (-3)
⁴⁰ K	1464	0.203	²²⁸ Ac	911	2.68 (-2)
				965-969	2.17 (-2)
				1588	4.36 (-3)
			²⁰⁸ Tl	2615	5.92 (-2)

TABLE 13

PHYSICAL CHARACTERISTICS OF HASL γ -RAY DETECTORS

Detector No.	514	484	730	785
Type	Closed Coaxial Cylindrical Ge(Li)	Closed Coaxial Cylindrical Ge(Li)	Harshaw Integral Line NaI(Tl)	Harshaw Integral Line NaI(Tl)
Size	4.3 cm x 4.4 cm (L)	-	~4" x 4"	~4" x 4"
Efficiency*	2.17	0.82	37	36
Resolution†	2.3 keV	2.3 keV	52 keV	54 keV
Peak/Compton Ratio‡	30/1	24/1	-	-
Active Volume	~60 cm ³	~25 cm ³	~820 cm ³	~820 cm ³
Drift Depth	~1.7 cm	-	-	-
Bias Voltage	2200 V	2200 V	900 V	900 V

*Counts per unit incident flux at 662 keV.

†FWHM at 662 keV.

‡Evaluated at 1.33 MeV.

TABLE 14

N_0/ϕ - TOTAL ABSORPTION PEAK COUNTS -
4" x 4" NaI(Tl) DETECTOR^a

Calibration Source	Energy (keV)	N_0/ϕ $\frac{\text{cpm}}{\gamma/\text{cm}^2-\text{s}}$		
		Detector #ED-730	Detector #EA-785	Old 4"x4" Detectors
⁸⁶ Sr	514	2690	2525	3250
¹³⁷ Cs	662	2333	2238	2238
⁵⁴ Mn	835	2075	2060	2400
²⁴ Na	1370	1635 ^B	168 ^B	1900
²²⁶ Ra	1765	980 ^C	970 ^C	1150
²⁰⁸ Tl	2615	892	970	1140 ^D

^a With $\frac{1}{4}$ " bakelite shield.

^B Inferred from ratio of previous readings to HASL-170 data.

^C Based on branching ratios in Table 4.

^D Inferred from 2.73 MeV ²⁴Na line.

TABLE 15

N_0/ϕ - TOTAL ABSORPTION PEAK COUNTS PER UNIT INCIDENT FLUX -
Ge(Li) DETECTORS

Calibration Source	E(keV)	γ 's/dis.	Standardized By	N_0/ϕ $\frac{\text{cpm}}{\gamma/\text{cm}^2\text{-s}}$	
				25 cc Ge(Li)	60 cc ^a Ge(Li)
²⁴¹ Am	59.5	0.353	IAEA	276±5	287±7
¹⁷⁰ Tm	84	0.033	HASL	-	438±25
¹⁴⁴ Ce	133.5	0.108	HASL	-	596±12
¹⁴¹ Ce	145.5	0.490	HASL	-	585±10
¹³⁹ Ce	165	0.80	HASL	-	594±15
⁵⁷ Co	122.1	0.856	IAEA	423±8	565±12
¹⁹⁸ Au	411.8	0.955	HASL	89.0±4.0	224±3
²² Na	511.0	1.81	IAEA	-	171±4
"	1274.5	1.00	IAEA	20.6±1.0	67.0±2.0
⁸⁵ Sr	514.0	0.993	HASL	66.0±3.0	171±4
¹³⁷ Cs	661.6	0.846	HASL-IAEA	49.0±2.0	130±3
⁵⁴ Mn	834.8	1.00	"	33.0±1.0	100±2
⁸⁸ Y	898.0	0.934	HASL	30.0±1.0	97.0±3.0
"	1836.1	0.994	"	13.2±0.5	47.5±1.0
⁶⁵ Zn	1115.5	0.506	"	-	82.0±2.0
⁶⁰ Co	1173.2	0.999	HASL-IAEA	-	74.4±1.0
"	1332.5	1.00	"	-	65.6±1.0
²⁴ Na	1368.5	1.0	-	-	63.8 ^B
"	2754.1	0.999	-	-	30.4±0.6
²²⁸ Th	2615	0.36	NBS	-	33.1±1.0

^a These data fit the following function from 200 keV to 3 MeV with a maximum deviation of ~3%: $\ln N_0/\phi = 4.48 - 1.03 \ln E$, where E is in MeV.

^B Normalized

TABLE 16

ANGULAR CORRECTION FACTORS (N_f/N_0)

E (keV)	$(\alpha/\rho) - \text{cm}^2/\text{g}$			
	0	0.206	0.625	∞ Plane
<u>$N_f/N_0 - 60 \text{ cm}^3 \text{ Ge(Li)}$</u>				
60	0.69	0.68	0.66	0.65
122	0.94	0.93	0.92	0.90
145	1.00	1.00	0.99	0.97
>155	1.0	1.0	1.0	1.0
<u>$N_f/N_0 - 25 \text{ cm}^3 \text{ Ge(Li)}$</u>				
134	0.70	-	-	-
352	0.79	-	-	-
609	0.84	-	-	-
1120	0.91	-	-	-
1765	0.98	-	-	-
<u>$N_f/N_0 - 4" \times 4" \text{ NaI(Tl)}$</u>				
511	1.14	1.14	1.14	1.14
583	1.12	1.12	1.12	1.12
662	1.11	1.11	1.11	1.11
750	1.10	1.10	1.10	1.10
1464	1.07	-	-	-
1765	1.04	-	-	-
2615	1.02	-	-	-
Total "Energy" - 4" x 4" NaI, $N_f/N_0 = 1.11$				

TABLE 17

PEAK AREA PER UNIT EXPOSURE RATE (N_f/I) AND PEAK AREA PER UNIT ACTIVITY (N_f/A) FOR 4"x4" NaI(Tl) DETECTORS^a

Isotope	E (keV)	α/ρ	No. 730		No. 785		Old Detectors Ref. 5	
			N_f/I^B	N_f/A^C	N_f/I^B	N_f/A^C	N_f/I^B	N_f/A^C
²³⁸ U	609+665	0	151	275	142	259	150	335
	1765	0	36	66	35	64	45	100
²³² Th	583	0	64	180	61	171	65	213
	2615	0	59	166	58	165	58	190
⁴⁰ K	1464	0	352	63	344	62	390	80
¹³⁷ Cs	662	0.0625	967	2.24	928	2.15	-	-
		0.206	1129	4.85	1083	4.65	1375	-
		0.312	1193	5.95	1145	5.71	-	-
		0.625	1281	7.90	1228	7.58	-	-
		6.25	1494	13.8	1433	13.2	-	-
		∞	1555	16.5	1492	15.8	-	-
⁹⁵ Zr-Nb ^b	<750>	0.0625	820	7.81	793	7.53	-	-
		0.206	964	17.33	930	16.72	1150	-
		0.312	1018	21.03	980	20.28	-	-
		0.625	1115	28.30	1078	27.30	-	-
		6.25	1266	48.58	1221	46.87	-	-
		∞	1406	57.40	1258	55.37	-	-

^a With $\frac{1}{4}$ " bakelite shield.

^B cpm/ ($\mu R/h$)

^C cpm per pCi/g of in situ soil material including moisture ($\alpha/\rho=0$) or per mCi/km² ($\alpha/\rho \neq 0$).

^b Equilibrium assumed.

TABLE 18

PEAK AREA PER UNIT EXPOSURE RATE (N_f/I) AND PEAK AREA PER UNIT ACTIVITY
(N_f/A) FOR Ge(Li) DETECTORS - NATURAL EMITTERS

Isotope	E (keV)	60 cc Ge(Li)				25 cc Ge(Li)	60 cc Ge(Li)
		N_0/ϕ	N_f/N_0	c/I	N_f/I^*	N_f/A^{**}	N_f/A^{**}
^{40}K	1464	59.8	1.0	0.203	12.1	3.37	2.17
^{238}U Series	186	510	1.0	2.52(-3)	1.29	0.44	2.35
	242	388		5.71(-3)	2.22	0.73	4.04
	295	315		1.60(-2)	5.04	1.58	9.17
	352	255		3.30(-2)	8.42	2.78	15.3
	609	143		5.18(-2)	7.41	2.25	13.5
	666	132		1.86(-3)	0.25	-	0.45
	768	114		6.43(-3)	0.73	0.21	1.33
	934	94.2		4.45(-3)	0.42	-	0.76
	1120	78.0		2.31(-2)	1.80	0.49	3.28
	1238	70.0		9.45(-3)	0.66	-	1.20
	1378	63.3		8.19(-3)	0.52	-	0.94
	1730	50.0		5.60(-3)	0.28	-	0.51
	1765	49.0		2.96(-2)	1.45	0.40	2.64
	2204	39.5		1.07(-2)	0.42	-	0.77
^{232}Th	129	580	1.0	1.03(-3)	0.60	-	1.68
	210	442		2.06(-3)	0.91	-	2.57
	239-41	388		2.57(-2)	9.97	3.28	18.1
	270-82	335		3.62(-3)	1.21	-	3.42
	301	305		1.96(-3)	0.60	-	1.69
	338	260		7.73(-3)	2.01	0.68	5.67
	328-40	265		1.03(-2)	2.73	-	7.70
	463	195		3.26(-3)	0.64	-	1.79
	510	176		6.84(-3)	1.20	-	3.39
	583	154		2.27(-2)	3.50	1.1	9.86
	727	122		6.60(-3)	0.81	-	2.27
	755	118		9.57(-4)	0.11	-	0.32
	772	115		1.45(-3)	0.17	-	0.47
	795	112		4.25(-3)	0.48	-	1.34
	830-40	108		3.33(-3)	0.36	-	1.01
	860	103		4.18(-3)	0.43	-	1.21
	911	97.0		2.68(-2)	2.60	0.71	7.33
	965+69	91.0		2.17(-2)	1.97	0.53	5.57
	1588	54.7		4.36(-3)	0.24	0.063	0.67
2615	32.8		5.92(-2)	1.94	-	5.48	

*cpm/ ($\mu\text{R/h}$)

**cpm/ (pCi/g)

TABLE 19

PEAK AREA PER UNIT EXPOSURE RATE (N_f/I) * FOR 60 cc Ge(Li) DETECTOR-FALLOUT

Isotope	E (keV)	N_0/ϕ	$(\alpha/p) - \text{cm}^2/\text{g}$					
			0.0625	0.206	0.312	0.625	6.25	∞ Plane
$^{144}\text{Ce-Pr}^{**}$	134	596	208	267	294	337	451	479
^{141}Ce	145	585	678	831	880	998	1278	1390
^{131}I	364	250	111	135	146	159	201	202
^{125}Sb	428	210	31.3	37.2	40.5	42.6	51.5	54.4
	601	145	15.1	17.5	18.6	19.6	23.2	24.1
^{140}Ba	537	162	48.0	57.0	59.9	64.8	75.3	78.7
^{140}La	487	180	8.28	10.1	11.0	11.5	13.7	14.9
	1597	55	8.47	9.13	9.52	9.63	10.7	11.2
^{103}Ru	497	180	74.9	90.5	95.0	103	124	129
$^{106}\text{Ru-}$ ^{106}Rh	512	175	32.3	53.0	55.8	59.3	70.2	73.3
	622	140	18.1	21.4	22.4	23.8	27.7	29.0
^{137}Cs	662	130	49.0	57.2	60.5	64.9	75.7	78.8
^{95}Zr	724	122	18.9	22.1	23.4	25.1	29.4	30.1
	757	117	22.9	26.9	28.3	31.0	35.5	36.6
^{95}Nb	766	114	39.4	46.6	48.8	53.9	60.5	62.8
^{54}Mn	835	106	20.1	40.3	42.4	46.4	52.7	54.0

*cpm/ ($\mu\text{R/h}$); for N_f/A multiply values by I from Table 9.

**Equilibrium assumed.

Table 20

"ENERGY" BAND EQUATIONS FOR NaI(Tl) DETECTORS"Energy" Bands

ΔE_1	1.32 MeV to 1.60 MeV
ΔE_2	1.62 MeV to 1.90 MeV
ΔE_3	2.48 MeV to 2.75 MeV
ΔE_{Total}	0.15 MeV to 3.4 MeV

Exposure Rate Equations

<u>Detector #730</u>		<u>Detector #785</u>	
$K = .085 E_1' - .060 E_2' - .024 E_3'$		$K = .087 E_1' - .061 E_2' - .024 E_3'$	
$U = .421 E_2' - .224 E_3'$		$U = .433 E_2' - .230 E_3'$	
$T = .292 E_3'$		$T = .297 E_3'$	
$I = E_T' / 37.9$		$I = E_T' / 36.5$	

where K, U, T, are the exposure rates in $\mu R/h$ for ^{40}K , the ^{238}U series, the ^{232}Th series, respectively, and I is the total exposure rate. E_1' , E_2' , E_3' , E_T' are respectively the total "energy" in BeV/20 min. in ΔE_1 , ΔE_2 , ΔE_3 , ΔE_{Total} (see text) corrected for cosmic ray exposure.

Cosmic Ray Response - BeV/20 min.

<u>Altitude</u>	<u>E_1</u>	<u>E_2</u>	<u>E_3</u>	<u>E_{Total}</u>
0'	0.40	0.35	0.30	7.7
1000'	0.42	0.37	0.32	8.2
2000'	0.46	0.40	0.34	8.9
3000'	0.52	0.45	0.36	9.8
4000'	0.60	0.53	0.38	11.0
5000'	0.70	0.63	0.41	12.8
8000'	1.28	1.10	0.94	24.7

TABLE 21

EXAMPLES OF FIELD SPECTROMETRIC MEASUREMENTS MADE WITH Ge(Li) DETECTORS
AND NaI(Tl) DETECTORS

Location	Detector Type	$\mu\text{R/h}$						Sum	Ion Chamber
		K	U	T	Cs	Zr-Nb	Other		
Joliet, Ill. 1971	Ge(Li)	2.8	1.2	2.5	0.2	0.3	0.1	7.1	7.8
	NaI(Tl)	2.7	1.1	2.4	0.3	0.2	-	6.7	
Channahan, Ill. 1971	Ge(Li)	2.6	1.0	1.9	0.2	0.3	0.1	6.1	5.9
	NaI(Tl)	2.4	1.1	1.8	0.2	0.2	-	5.7	
Morris, Ill. 1971	Ge(Li)	2.2	1.4	1.7	0.1	0.3	<0.1	5.7	-
	NaI(Tl)	2.2	1.2	1.8	0.1	0.2	-	5.5	
Waterford, Conn. 1971	Ge(Li)	1.7	1.7	3.0	0.6	0.2	-	7.2	7.6
	NaI(Tl)	1.7	1.4	3.4	0.4	0.1	-	7.0	
Waterford, Conn. 1971	Ge(Li)	2.4	1.6	2.9	0.7	0.2	-	7.8	8.0
	NaI(Tl)	2.4	2.1	3.1	0.4	0.1	-	8.1	
Forked River, N. J. 1971	Ge(Li)	0.2	0.8	0.9	0.6	0.2	-	2.7	2.6
	NaI(Tl)	0.2	0.9	0.8	0.7	0.2	-	2.8	
Forked River, N. J. 1971	Ge(Li)	0.3	0.5	0.6	0.8	0.1	-	2.3	2.1
	NaI(Tl)	0.3	0.5	0.5	0.8	0.1	-	2.2	
Denver, Colo. 1955	NaI(Tl)	3.4	2.4	7.4	0.3	-	0.2	13.7	13.8
Bikini, Atoll 1967	NaI(Tl)	0	0	0	19.0	-	5.8	24.8	24.0

TABLE 22

ROUGH COMPARISONS OF FIELD SPECTROMETRIC ESTIMATES OF ^{137}Cs SOIL
ACTIVITY WITH NEARBY ^{90}Sr SOIL SAMPLE MEASUREMENTS

Site	Soil Sampling Date	Field Measurement Date	mCi/cm ²		Notes
			Inferred from Soil Sample	Field Spectrum	
Fort Collins, Colo.	4/65	9/65	80	50	A, B, C
Salt Lake City, Utah	9/65	8/65	157	58	A, B, C
Derby, Colo.	9/65	8/65	93	77	A, B, C
Rapid City, S.D.	9/65	8/65	147	127	A, B, C
New Orleans, La.	3/66	9/65	76	62	A, B, C
Beltsville, Md.	11/65	11/65	95±15	109	B

Notes:

- A The ^{137}Cs soil activity was inferred from a radiochemical determination of ^{90}Sr by multiplying by 1.5.
- B The field spectral analysis assumed $\alpha/p = 0.206$ for all sites, which may be too large since all the field spectrometric values are lower than the values referred from the samples.
- C Except for Fort Collins the soil sampling and field spectrometric sites are not identical but are in the nearby vicinity of each other.
- D Using measured depth distribution - actual ^{137}Cs soil analysis.

TABLE 23
 CONVERSION FACTORS AND OTHER DATA USEFUL
 FOR FIELD SPECTROMETRY

$$1 \mu\text{R/h} = 65.9 \text{ MeV/g-s}$$

$$1 \text{ mrad/y} = 0.130 \mu\text{R/h}$$

$$1 \mu\text{R/h} = 7.65 \text{ mrad/y}$$

$$1 \text{ mCi/km}^2 = 0.386 \text{ mCi/mi}^2$$

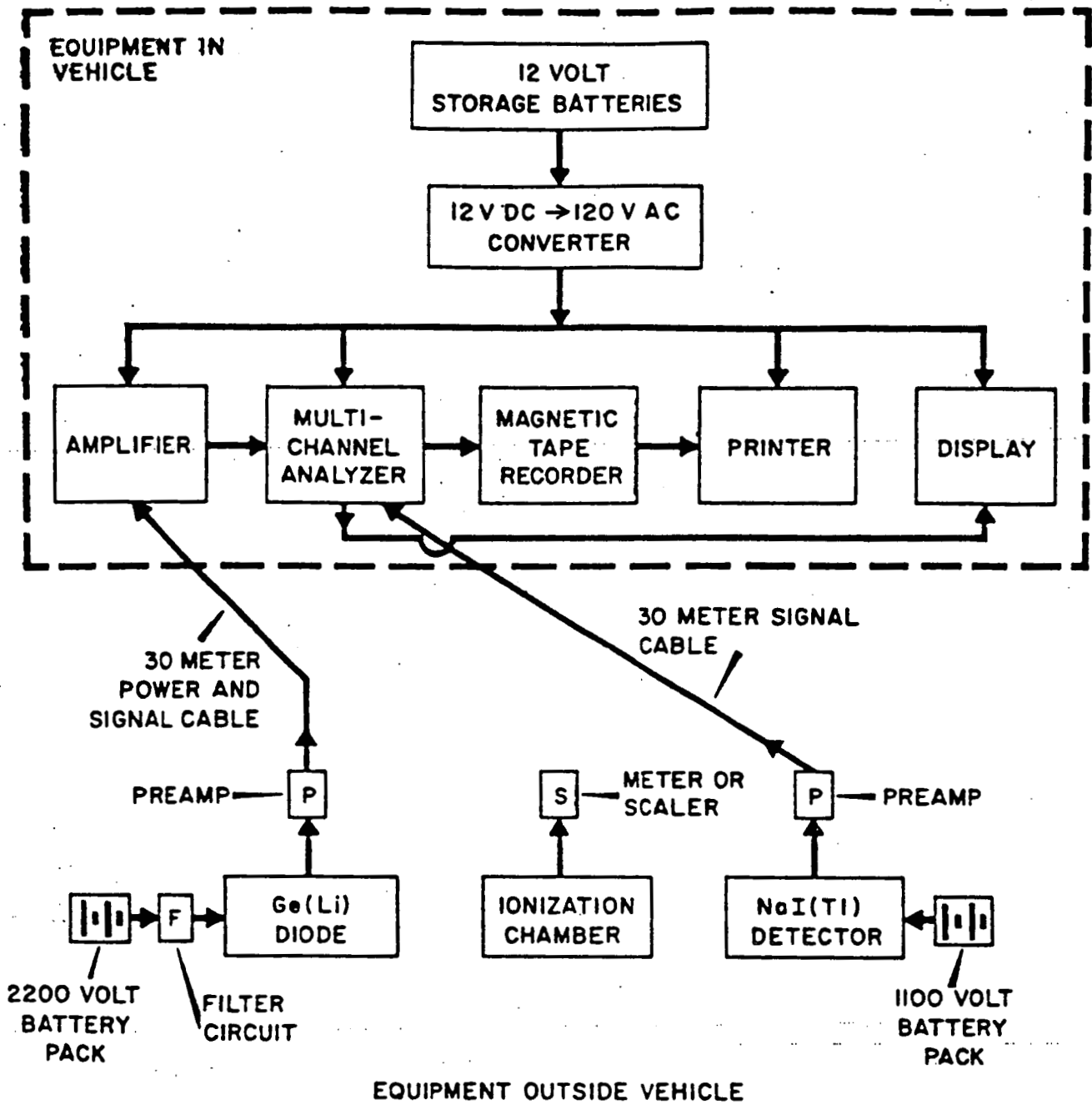
$$3.361 \times 10^{-7} \text{ curies/g } ^{238}\text{U}$$

$$1.09 \times 10^{-7} \text{ curies/g } ^{232}\text{Th}$$

$$0.988 \text{ curies/g } ^{226}\text{Ra}$$

$$3.30 \text{ gammas/s(1.46 MeV) } ^{40}\text{K} \text{ Potassium}$$

$$1 \text{ pCi} = 0.45 \text{ dpm}$$



HASL FIELD SPECTROMETRIC SYSTEMS

Figure 1. Diagram of field spectrometers and ionization chamber.

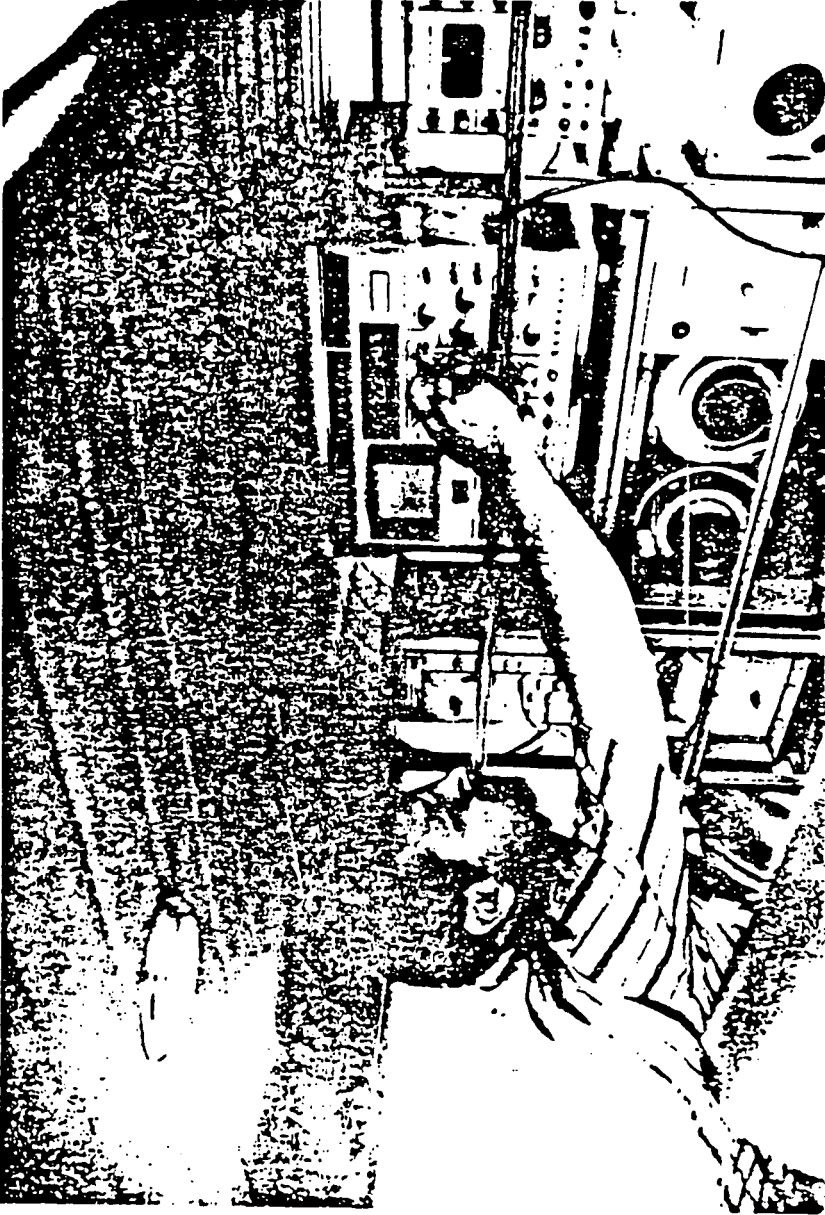


Figure 3. Electronic equipment in rack in standard station wagon.

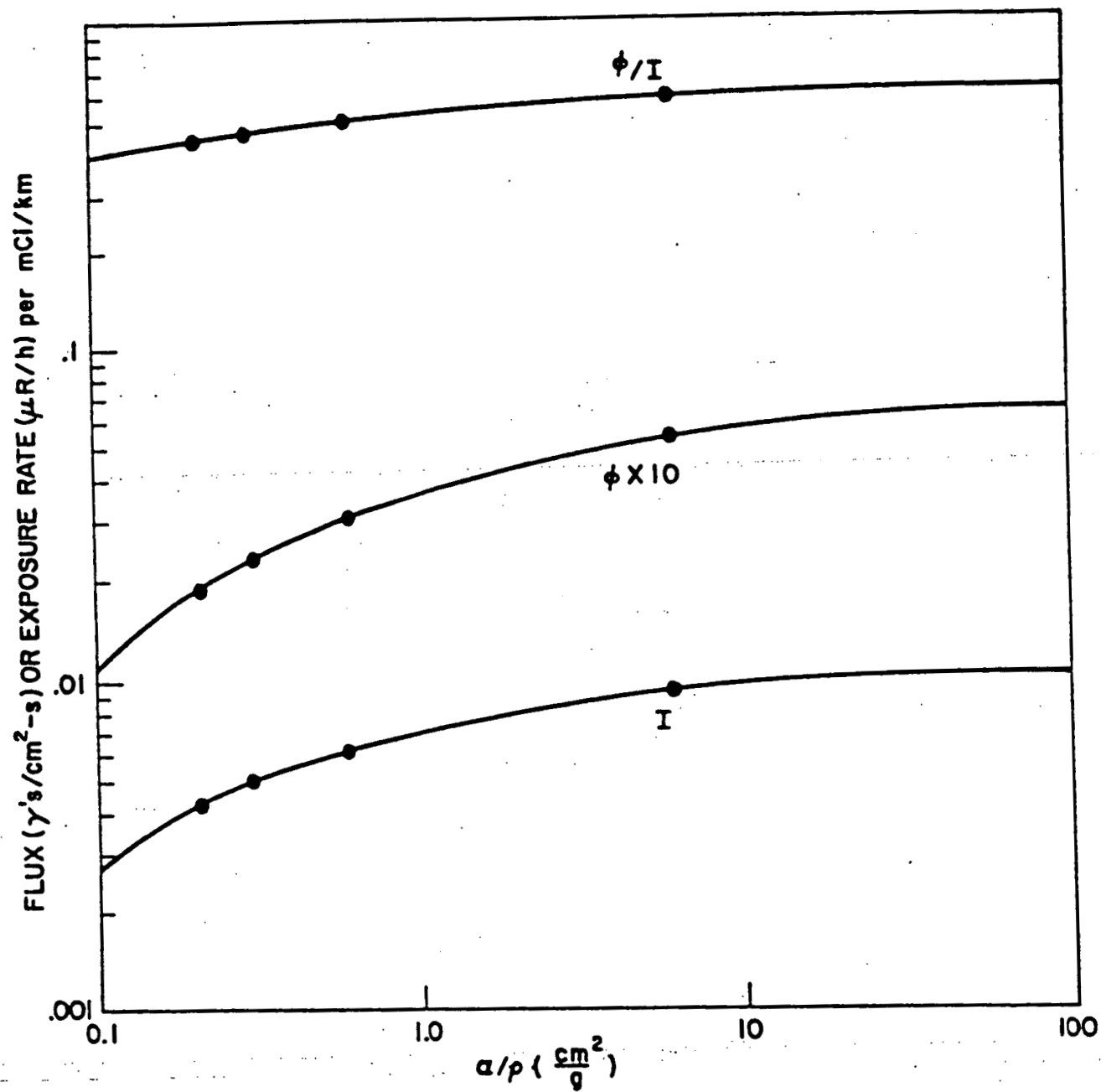


Figure 4. ϕ , ϕ/I , and I at one meter above the ground vs a/ρ source depth distribution.

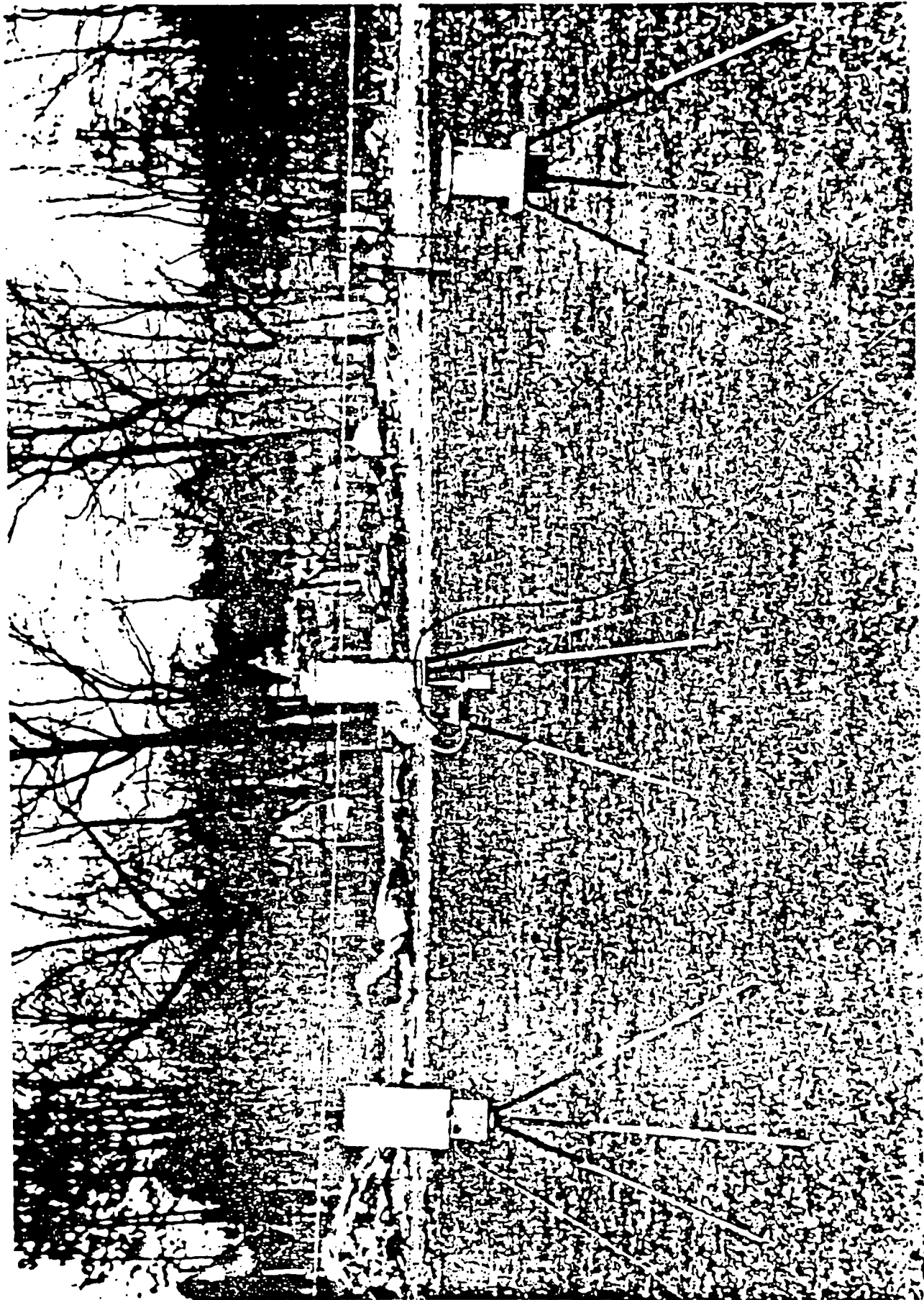


Figure 2. Field equipment showing, left to right, ionization chamber, Gc (J.i.) detector and NaI (Tl) detector

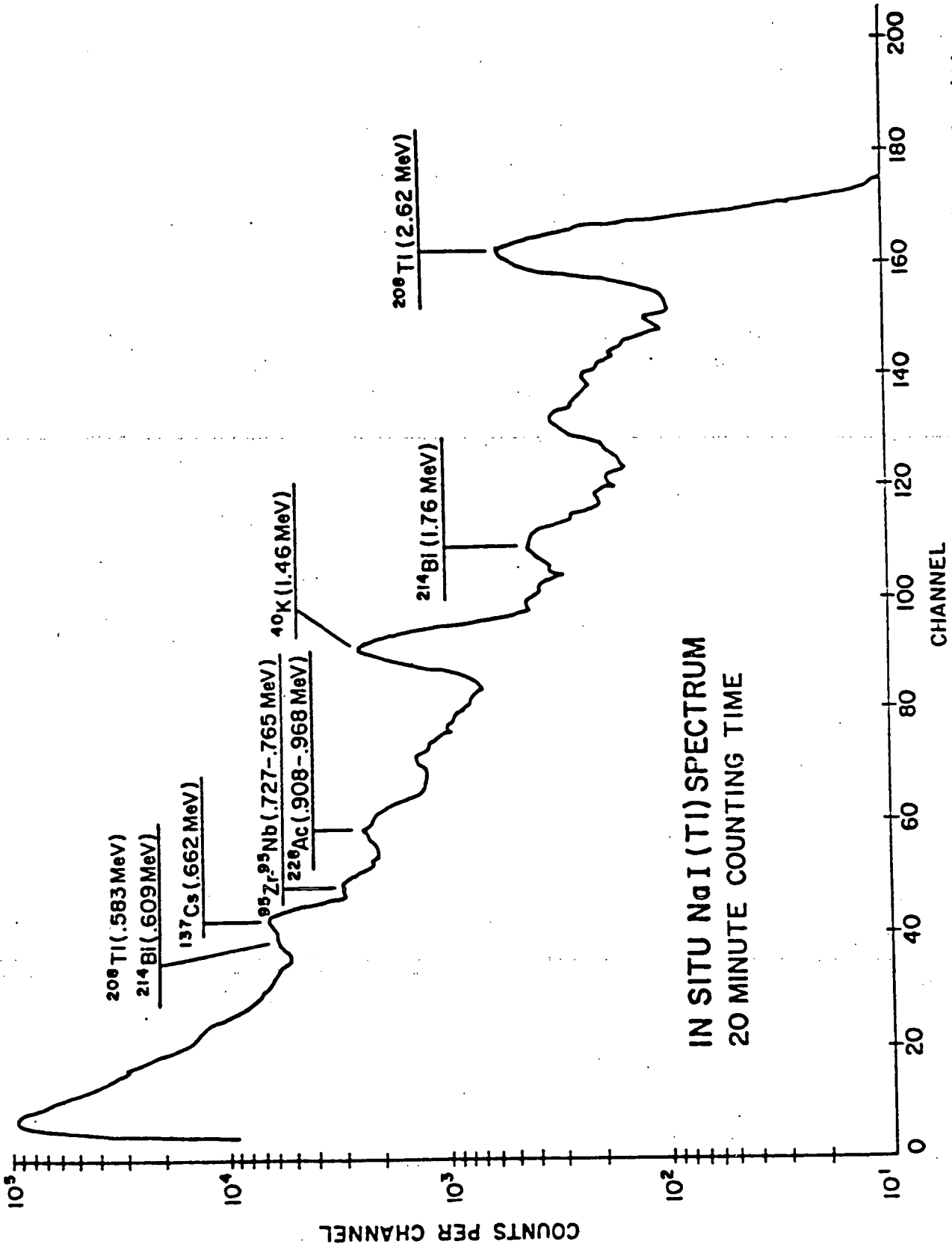


Figure 6. In situ spectrum, northeastern U.S.A. location, taken in 1971 with 10 cm by 10 cm NaI(Tl) crystal, 20 minute counting time.

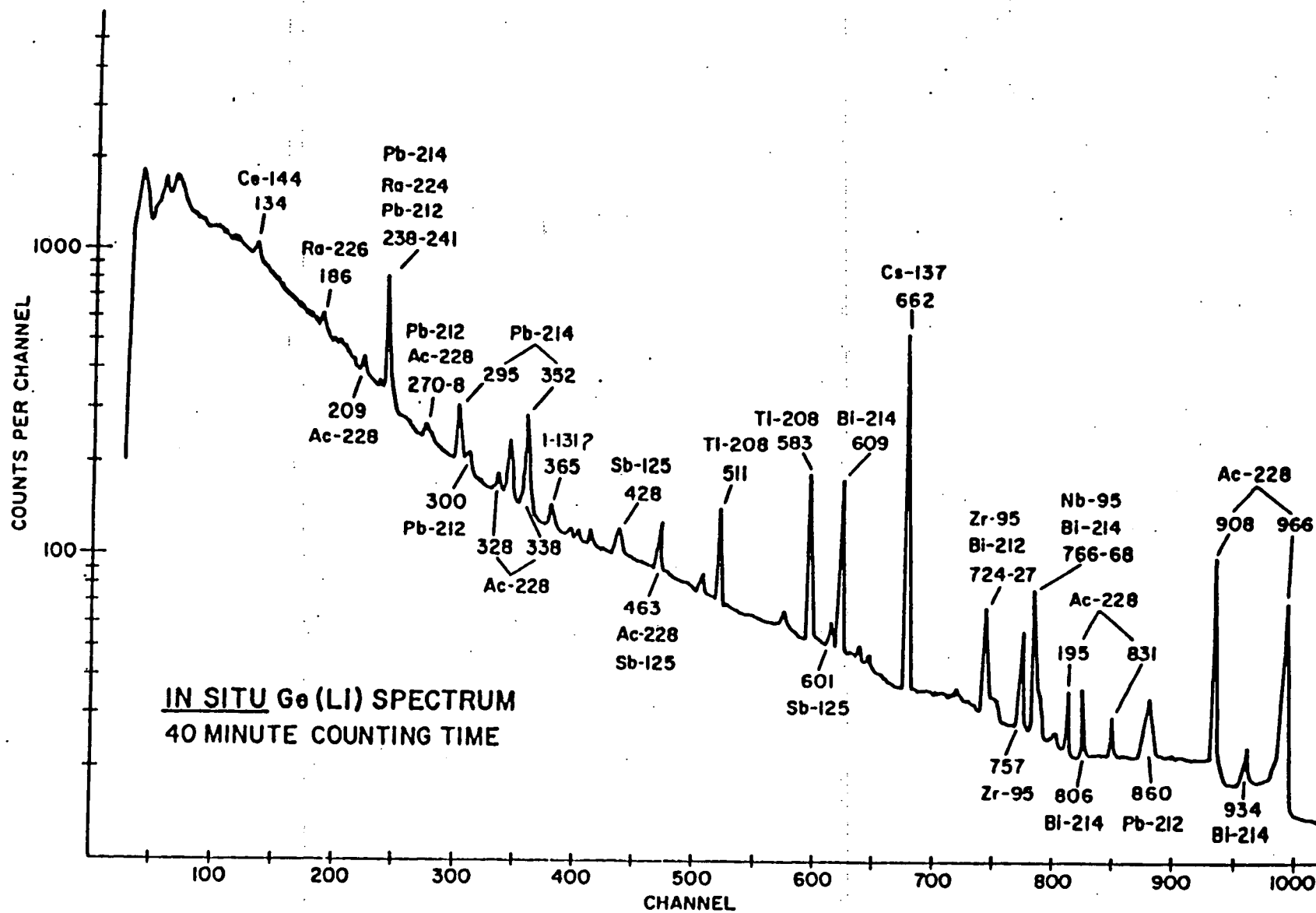


Figure 7. In situ spectrum, taken with that in Figure 6 with 60 cm³ Ge(Li) detector, 40 minute counting time. Photon energies in keV.

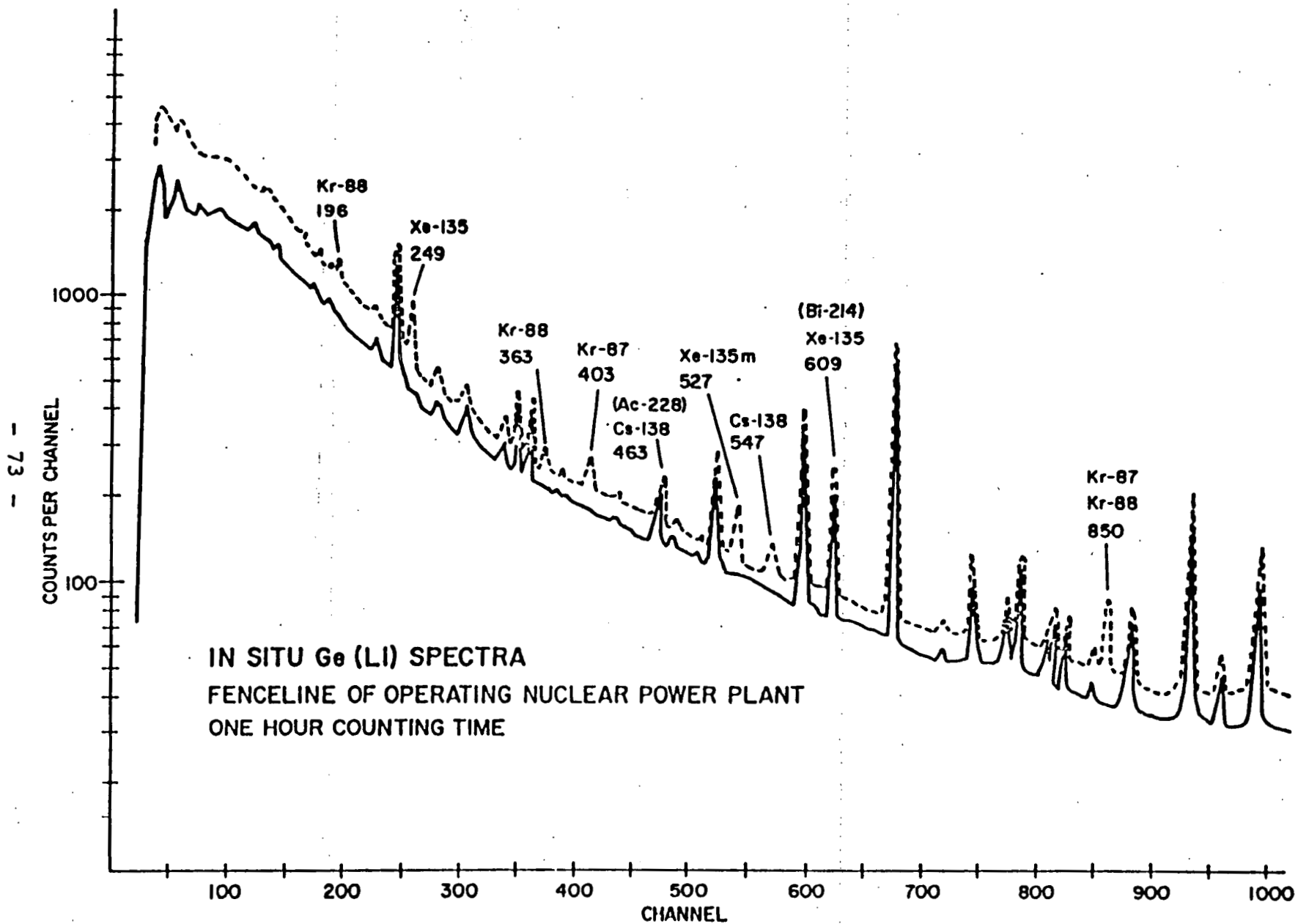


Figure 8. In situ Ge(Li) spectra at fence line of boiling water reactor. Upper spectrum with gaseous plume overhead; bottom spectrum with wind blowing away from detector.

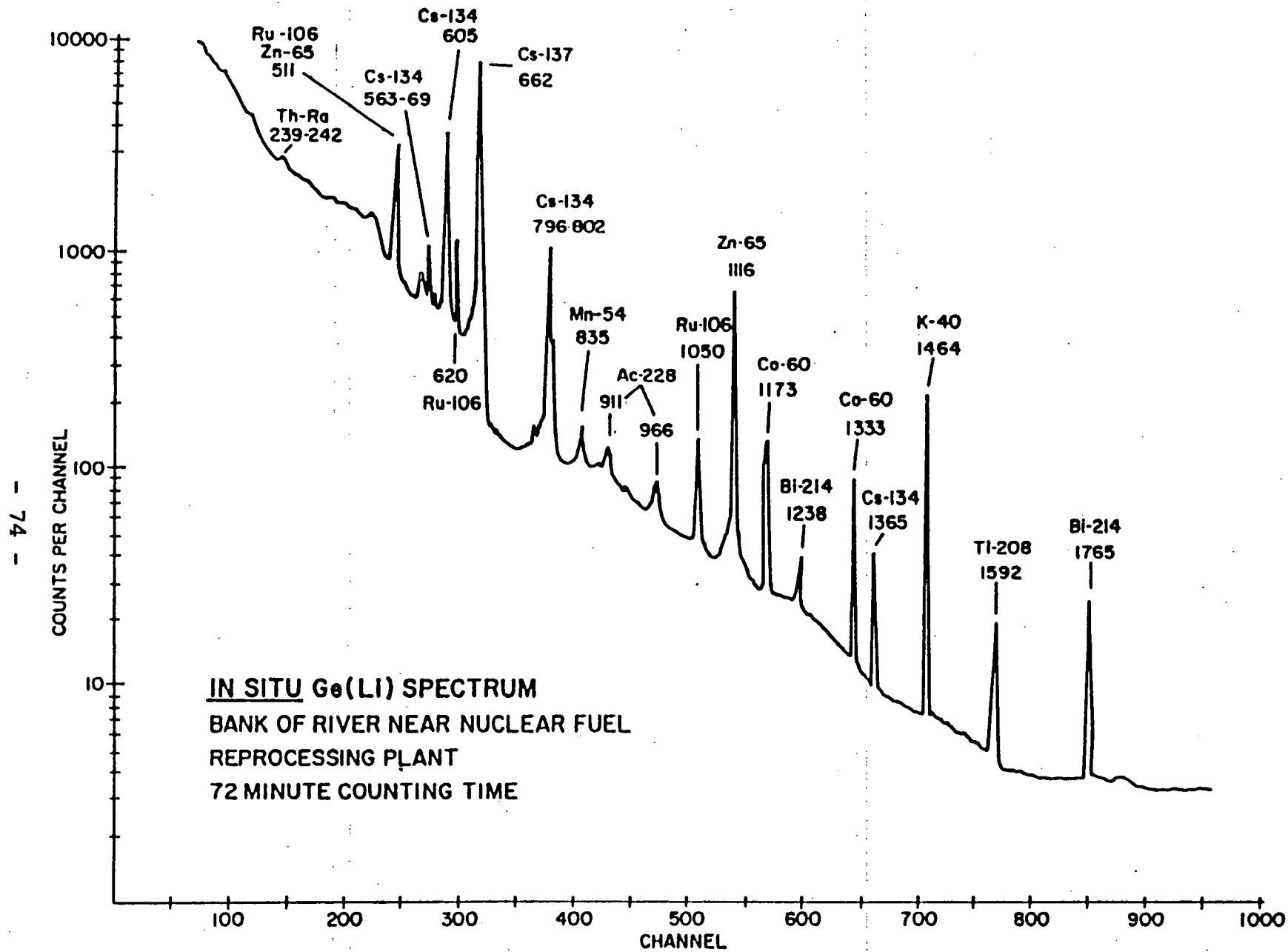


Figure 9. In situ 25 cm³ Ge(Li) spectrum on river bank near fuel reprocessing plant, 72 minute counting time.

ENVIRONMENTAL GAMMA RADIATION SPECTRUM 650-FT FROM TURBINE OF 1600 MWt BWR

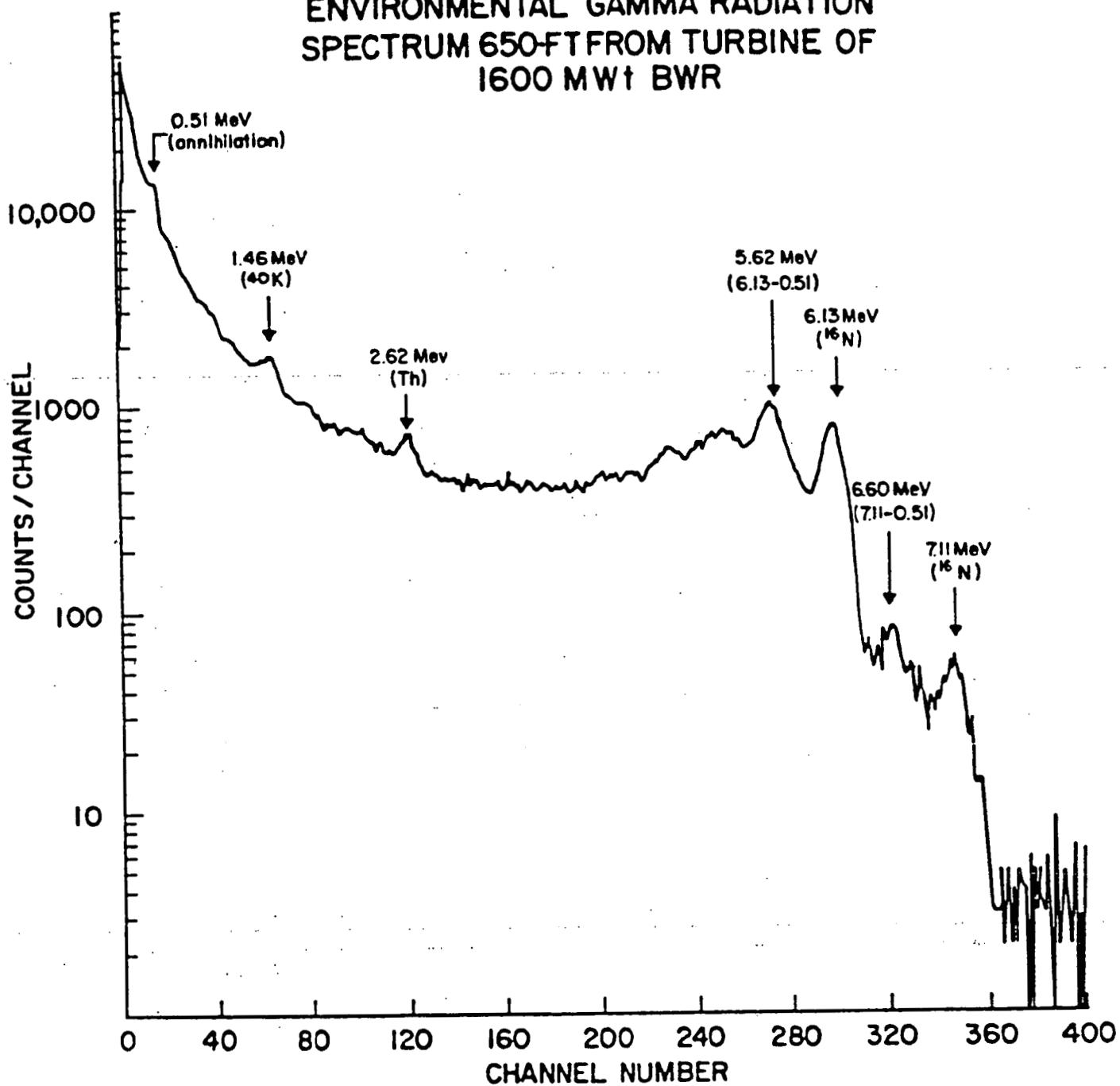


Figure 10. In situ NaI(Tl) spectrum 650 feet from turbine of a 1600 - MW_{Th} BWR.

IN SITU
GAMMA-RAY SPECTROMETRY

***A SHORT COURSE
FOR
ENVIRONMENTAL RADIATION RESEARCHERS***

Lecture Notes

by

Kevin M. Miller

and

Peter Shebell

United States Department of Energy
Environmental Measurements Laboratory

Enclosure II

NOTICE

This set of notes is not a formal publication of the Environmental Measurements Laboratory. They should not be referenced without permission of the authors and if such permission is granted they should be referenced as a private communication and not as a report.

FOREWORD

Most of us who deal with aspects of ionizing radiation in the environment are familiar with basic dose rate measurements using survey instruments. Perhaps we can recall instances when we have walked about a site with a meter in our hand and measured external radiation levels. This constitutes an *in situ* measurement in its most basic form, one which deals with a single parameter such as the exposure rate. For more information on the radiation field at the site, one can take a soil sample and return it to the lab for analysis. Gamma-ray counting on a Ge detector might then be employed to determine the specific radionuclides present in the sample. This could be done for strictly qualitative purposes or it could be extended quantitatively to include the measurement of the concentrations of radionuclides in the samples. Consider, however, the concept of bringing the spectrometer to the sample, rather than the other way around. By using a high resolution Ge detector placed over the ground one is essentially measuring an oversized soil sample. The detector thus functions as a sophisticated survey instrument. Like the laboratory-based analysis of soil samples, one can identify radionuclides present in a qualitative manner by simply looking for the presence of peaks at characteristic energies. Taking the technique to a higher level, one can convert the measured peak count rate into some meaningful quantity such as the concentration of these nuclides in the soil or, in the case of deposited fallout, the activity per unit area. It is also possible to infer the contribution of each individual nuclide to the dose rate in air. This course will introduce you to these techniques, known as "*in situ* gamma-ray spectrometry". A generalized approach is taken so that the individual will be able to adapt the technique to unique situations. To this end, a basic grounding in the theory is given, however short-cut methods are also presented for those who may employ the technique for approximate measurements. Example calculations are given to clarify the presentation. It is hoped that this material, though serving as an introductory course, is sufficient to allow newcomers in the field to confidently apply *in situ* techniques in their field investigations of environmental radiation and radioactivity. For those who wish to pursue aspects of this subject in greater detail, appropriate references are given.

ACKNOWLEDGEMENTS

The authors acknowledge the work of past and present EML colleagues who have contributed much over the years to the field of environmental radiation research and the application of *in situ* spectrometry. In particular, we note the accomplishments of Wayne Lowder, Harold Beck and Carl Gogolak in the field. We also call attention to the adoption of the techniques described herein and the developments that have been made by many other laboratories in the U.S. and around the world.

Some of the material presented here is taken from a draft that has been prepared by one of us (Miller) as a report committee member for the International Commission on Radiation Units and Measurements (ICRU). This material, together with additional contributions from other authors, is due to be published as a formal ICRU report on *in situ* gamma-ray spectrometry. In addition, many of the figures and tables appearing in these course notes have been taken from other EML publications in the subject area.

TABLE OF CONTENTS

FOREWARD		ii
ACKNOWLEDGEMENTS		iii
INTRODUCTION		1
CHAPTER 1	INSTRUMENTATION	3
	Detectors, Pulse Height Analyzers, Field Setup	
CHAPTER 2	THEORY	7
	Basic Calibration Parameters, Source Distributions Photon Flux Calculation, Dependence of the Flux on the Parameters α/ρ and μ_g/ρ , Dependence of the Flux on the Source Geometry, Other Factors Affecting Flux	
CHAPTER 3	DETECTOR CALIBRATION	16
	Response at Normal Incidence, Angular Response, Generic Conversion Factors	
CHAPTER 4	INFERRED QUANTITIES	23
	Concentrations in Soil, Deposition/Inventory, Dose Rate in Air	
CHAPTER 5	RADIATION SOURCES IN THE ENVIRONMENT	27
	Natural Emitters, Fallout Emitters, Cosmic Radiation	
CHAPTER 6	QUALITY ASSURANCE	31
	Error Estimates, Sources Depth Profile Determinations, Comparisons to Soil Samples, Comparisons to Total Ionization	
USEFUL CONVERSION FACTORS		35
SUGGESTED READINGS		36

CHAPTER 1

INSTRUMENTATION

Detectors

Although measurements can be conducted with NaI scintillation detectors, as they were in the 1960's, the energy resolution of Ge solid state detectors and the fact that they are available with efficiencies as great as that of a 3x3 inch NaI make them the detectors of choice. As with any counting system, the size of the detector that is needed is related to the source strength, the counting time, and the desired statistical counting error. For typical environmental radiation fields, a detector with a quoted 25% efficiency would be large enough to give $\pm 5\%$ (1σ) counting error for natural emitters using a one hour count time. A quick 10 minute count would be sufficient to provide lower limits of detection on the order of 100 Bq m^{-2} for many common fission products residing at the surface of the soil. Higher sensitivity and/or reduced counting times can be achieved with larger detectors. Depending upon the application, a smaller detector might actually be a better choice in order to reduce counting dead time when when making measurements in highly contaminated areas.

Another consideration is the choice between a P type and an N type Ge crystal. For applications that involve the measurement of low energy gamma rays, such as from ^{241}Am (59.5 keV), the N type has better sensitivity. Figure 1.1 shows a comparison in the efficiency between two typical detectors.

Older lithium drifted Ge detectors can function perfectly well, however, the fact that intrinsic or high-purity Ge can warm up without damage makes them the best for field work.

Quality Ge detectors can be expected to have energy resolutions of 2 keV or better at 1332 keV. Better energy resolution allows a greater separation of two

peaks that are close in energy. Also, each individual peak is narrower and therefore lower statistical counting errors are achieved since there is less continuum counts under the peak.

Modern Ge detectors are equipped with built-in pre-amplifiers. For field work where battery power is used, it is important to specify a low-power pre-amp when ordering a detector. This will extend the operational time in the field since the pre-amp is a principal draw on power.

Although measurements in the field can be performed with a Ge detector in almost any type cryostat-dewar configuration, performance and ease of handling is best achieved with a small dewar (1 to 2 liters) that can be tripod mounted with the detector facing down. For convenience, a 24 hour liquid nitrogen holding time is desirable as this then requires filling only once a day, although it may be safer to maintain a twice a day schedule. Ge detectors can also be cooled with electrically powered apparatus, however, this may not be as convenient for field use with battery powered equipment. To maintain a ready-to-use capability, it is possible to mate small dewars to automatic filling apparatus in the laboratory or to larger gravity-feed storage dewars. As for orientation, a detector facing sideways (the axis of symmetry parallel to the ground) should be avoided because it introduces complicated angular corrections. A detector facing down will provide the maximum count rate, although one facing up (with the dewar underneath) can be used as well.

Pulse Height Analyzers

A Ge detector can be connected to a full laboratory instrumentation package that is carried in a van and powered with a motor generator or battery bank. This was the norm in the early days of field spectrometry. Today, it is far more convenient to make use of portable battery-powered analyzers which are specifically designed for field work. These units not only serve as multichannel pulse height analyzers but also provide pre-amp power and high voltage to the detector. This

type of analyzer with the Ge detector and a set of connecting cables is all that is needed for a complete spectrometry system. Also available now are portable laptop computer-based systems which have the capability to run more sophisticated analysis programs. An overnight recharge is generally sufficient to provide 8 hours of operational time in the field for either the full-function analyzer or the computer based system. In the latter case, the computer can be shut off to conserve its own limited battery supply, while a spectrum continues to collect in the memory of the analyzer base unit.

One additional component needed for practical application of *in situ* spectrometry is a method of spectrum storage since it is likely that many spectra will be collected during the course of a site investigation. Some portable analyzers have built-in mini-cassette data storage capability while others rely on an external portable audio cassette recorder. The PC based systems have the advantage of being able to store numerous spectra directly on the internal disk drive.

Field Setup

The ideal site for collecting a spectrum would be a large (20 meter diameter or more) flat, open area with little or no natural or man-made obstructions. The area to be measured can be scanned first with a suitably sensitive survey meter to insure that there is rough uniformity in background dose rate. It is also possible to move the Ge detector about and obtain quick (1 to 5 minute spectra), observing that a full absorption peak count rate does not change substantially for a nuclide under study. For measuring fallout that was deposited in the past, the land should not have been disturbed by plowing or by wind or water erosion. For standard measurements, the detector (Ge crystal) should be at a height of 1 meter above the ground, although a variation of as much as 50 cm in either direction will not introduce a large error. While collecting a spectrum, personnel should stand away from the detector. Since the operator may wish to examine the spectrum during collection, it is best to position the analyzer away from the detector using cable lengths of a few meters.

As with any gamma-ray spectrometer system, the amplifier gain and analyzer conversion rate must be adjusted to provide a spectrum in the energy region of interest. For environmental gamma radiation, this would be from about 50 keV out to 2.615 MeV, normally the highest energy line seen. For a 4000 channel analyzer, a conversion rate of 1keV per channel will suffice in most cases although 0.5 keV per channel may be desirable for certain *in situ* applications to take advantage of the higher energy resolution of the detector at low energies.

CHAPTER 2

THEORY

Basic Calibration Parameters

For sample analysis in the laboratory, calibrations are generally performed with solutions in the same counting geometry or spiked matrices such as soil and vegetation. In principle, one could calibrate a Ge detector for field use with very large (approaching an infinite half-space) calibrated areas as well. In practice, a far more convenient and flexible approach is to calculate the flux distribution on the detector for a given source geometry, determine the detector response with calibrated point sources and then perform an integration.

The fundamental quantities used for *in situ* spectrometry include full absorption peak count rate (N), fluence rate (ϕ), and source activity (A). In practice, one would like a single factor to convert from the measured peak count rate in a spectrum to the source activity level in the soil or the dose rate in air. This factor can be calculated from three separately determined terms as follows:

$$\frac{N_f}{A} = \frac{N_f}{N_o} \cdot \frac{N_o}{\phi} \cdot \frac{\phi}{A} \quad (2.1)$$

where N_f/A is the full absorption peak count rate at some energy, E , from a gamma transition for a particular isotope per unit activity of that isotope in the soil, N_o/ϕ is the full absorption peak count rate per unit fluence rate for a plane parallel beam of photons at energy, E , that is normal to the detector face, N_f/N_o is the correction factor for the detector response at energy, E , to account for the fact that the fluence from an extended source in the environment will not be normal to the detector face but rather distributed across some range in angles and ϕ/A is the fluence rate at energy, E , from photons arriving at the detector unscattered due to a gamma transition for a particular isotope per unit activity of that isotope in the soil.

The term N_0/ϕ is purely detector dependent while the term N_f/N_0 is dependent on both the detector characteristics and the source geometry. These two terms will be covered in the following chapter on detector calibration. The term ϕ/A is not dependent on the detector characteristics but rather on the source distribution in the soil and will be dealt with in the following sections.

Unscattered Flux

The theoretical model for an *in situ* measurement is illustrated in Figure 2.1. A gamma detector is located above a source that is distributed in, or deposited on a volume of soil. Let r_D be the vector which designates the position of the detector relative to the origin O. Moreover, let r designate the position of a differential volume of soil, and let r_i designate the location of the air-ground interface. For a gamma source of energy E, the total unscattered flux is given by

$$\phi = \int_V \frac{f(r)}{4\pi(r_D-r)^2} \exp\left[-\frac{\mu_s}{\rho} \rho(r_i-r) - \frac{\mu_a}{\rho_a} \rho_a(r_D-r_i)\right] dV \quad (2.2)$$

where $f(r)$ is the source strength at r , μ_s/ρ is the mass attenuation coefficient for soil (cm^2/g) and μ_a/ρ is the mass attenuation coefficient for air.

Source Distributions

The most common natural sources of gamma radiation in the environment are the gamma emitters in the ^{238}U and ^{232}Th series and ^{40}K . Anthropogenic sources include depositon from weapons testing and reactor effluent in the form of fallout. It is generally assumed that activities of fallout in the soil vary only with depth, while the natural radionuclides would be distributed uniformly.

The distribution of naturally occurring gamma emitters can then be expressed as

$$f(z) = S_V \quad (2.3)$$

where S_V is the soil activity per unit volume (photons/cm³-s). In the case of fallout that has not been driven into the soil, such as fresh fallout from weapons testing, a plane source would seem most plausible. We have

$$f(z) = S_A \delta(z-z') \quad (2.4)$$

where S_A is the surface activity (photons/cm²-s), and z' is the distance from the detector to the air-ground interface. Aged fallout is reasonably approximated by an exponential distribution of the form

$$f(z) = S_0 \exp\left(\frac{-\alpha}{\rho} \rho z\right) \quad (2.5)$$

where $(1/\alpha)$ is known as the relaxation length (cm), ρ is the soil density (g/cm³), and S_0 is the surface activity (photon/cm²-s).

In general, one relaxation length is that thickness of shield that will attenuate the flux to 1/e of its original intensity. Since we are dealing with a source term, the source depth parameter, α/ρ , indicates the degree of self-absorption that will occur due to the penetration of the fallout into the soil matrix. For example, assuming a soil density of 1.6 g/cm³ and a relaxation length of 1mm will yield a source depth parameter of 6.25 cm²/g. The relaxation length in this case indicates that the fallout has penetrated the soil to the extent that 63% of the activity is contained within the first millimeter of soil. This is considered to be a very shallow distribution. Alternatively, a relaxation length of 10 cm will yield a source depth

parameter of $.0625 \text{ (cm}^2/\text{g)}$, and this is considered to be a deep distribution. We note that the product ρz is the mass depth and is more fundamentally related to flux than linear depth z because the number of atoms per unit length of soil is dependent upon the soil density. For the remainder of this chapter we will always assume a soil density of 1.6 g/cm^3 .

It is convenient to think of the uniform and plane distributions as special cases of the exponential distribution. The plane distribution is obtained in the limit $\alpha \rightarrow \infty$, and the uniform distribution is the case where $\alpha = 0$. It must be pointed out that in terms of evaluating equation 2.2 for the flux, each case must be treated separately. The flux for a uniform distribution, for example, cannot be obtained in the limit $\alpha \rightarrow 0$. In the case of a uniform distribution we are specifically referring to the natural emitters whose concentration is independent of depth, while in the case of fallout deposition, the flux from a uniform distribution obtained in the limit $\alpha \rightarrow 0$ must, as we shall see later, vanish.

In general any distribution which varies in the z direction can be approximated by a superposition of plane sources buried at various depths

$$f(z) = \sum_i S_i \delta(z - z_i) \quad (2.6)$$

This distribution is useful for the case where there is markedly different soil strata of varying nuclide concentration.

The arrangement suggested in Figure 2.1 can be simplified by assuming a flat air-ground interface and infinite volume of soil. This particular geometry is referred to as an infinite half-space. Our specific model used to evaluate this case is illustrated in Figure 2.2. The detector is positioned at the origin, with the air-ground interface located a distance h below the detector. Hence, the ideal set-up for an *in situ* measurement would be a large, flat open field with little or no surface features and no obstructions that could substantially reduce the photon flux.

Photon Flux Calculation

Assuming an exponential distribution, equation 2.2 can now be written as

$$\phi = 2\pi \int_h^\infty \int_0^\infty \frac{S_0}{4\pi\omega^2} \exp\left(\frac{-\alpha}{\rho} \rho z\right) \exp\left[-\frac{\mu_s}{\rho} \rho(z-h)\omega - \frac{\mu_a}{\rho_a} \rho_a h\omega\right] d\omega dz \quad (2.7)$$

where $\omega = \sec \theta$, $\rho(z-h)$ is the mass depth of soil, and $\rho_a h$ is the mass depth of air.

The exact solution to (2.7) is

$$\frac{\phi}{S_0} = \frac{1}{2} \left[E_1\left(\frac{\mu_a}{\rho_a} \rho_a h\right) - \exp\left(-\frac{\alpha}{\rho} \frac{\rho}{\mu_s} \frac{\mu_a}{\rho_a} \rho_a h\right) E_1\left[\left(1+\frac{\alpha}{\rho} \frac{\rho}{\mu_s}\right) \frac{\mu_a}{\rho_a} \rho_a h\right] \right] \quad (2.8)$$

The function $E_1(x)$ is known as the exponential integral and is defined as

$$E_1(x) = \int_x^\infty \frac{e^{-t}}{t} dt \quad (2.9)$$

Figure 2.3 is a plot of $E_1(x)$. It is important to note how rapidly $E_1(x)$ falls off with x .

For a uniform distribution we have

$$\phi = 2\pi \int_h^\infty \int_1^\infty \frac{S_V}{4\pi\omega} \exp\left(-\frac{\mu_s}{\rho} \rho(z-h)\omega - \frac{\mu_a}{\rho_a} \rho_a h\omega\right) d\omega dz \quad (2.10)$$

where S_V is the soil activity per unit volume (photons/cm³-s). The exact solution to (2.10) is

$$\frac{\phi}{S_V/\rho} = \frac{1}{2} \frac{\mu_a}{\rho_a} \frac{\rho}{\mu_s} \rho h \left\{ \frac{\exp[(\mu_a/\rho_a)\rho_a h]}{(\mu_a/\rho_a)\rho_a h} - E_1\left(\frac{\mu_a}{\rho_a} \rho_a h\right) \right\} \quad (2.11)$$

The flux from a plane source distribution can be obtained from equation 2.8 in the limit $\alpha/\rho \rightarrow \infty$

For a plane source distribution we have

$$\frac{\phi}{S_0} = \frac{1}{2} E_1\left(\frac{\mu_a}{\rho_a} \rho_a h\right) \quad (2.12)$$

Flux computations can be performed on a case by case basis, however, it is convenient and generally sufficiently accurate to use the results of (Beck et al, 1972) which were performed for a standard height of 1 meter for a soil with a representative mix of elements. The total fluence is tabulated in Table 1 of that report for various values of α/ρ at different energies. The distribution with respect to the angle θ can be found in Table 6 of the same report.

Dependence of the Flux on the Parameters α/ρ and μ_s/ρ

We see in equation 2.8 that the flux from an exponentially distributed source depends the product $(\alpha/\rho)(\rho/\mu_s)$. This term can be expressed as $(1/\mu_s)/(1/\alpha)$, which is just the mean-free-path (MFP) for a photon of energy E in soil per unit relaxation length. If $(1/\mu_s)/(1/\alpha) \geq 1$, then a minimum of 63 % of the fallout is within one MFP of the air-ground interface. So for the case of a very shallow distribution $(1/\mu_s)/(1/\alpha)$ can be quite large. Since the term $E_1[\mu_a/\rho_a(1+(\alpha/\rho)(\rho/\mu_s)(\rho_a h))]$ goes to zero faster than the exponential diverges, the flux from a shallow distribution approaches the

flux from a plane source distribution in the limit $\alpha/\rho \rightarrow \infty$. This fact is reflected in figure 2.4. Here we have a plot of ϕ/S_0 as a function of α/ρ for several different energies. Note the flatness of the graphs for $\alpha/\rho > 100$. We note, however, that since typical values for α/ρ obtained from soil samples rarely exceed $6.25 \text{ cm}^2/\text{g}$, and since the source geometry for this model assumes a perfectly smooth interface, the case of a plane source distribution is unrealistic for most *in situ* measurements.

For the case of a very deeply distributed source $(1/\mu_g)/(1/\alpha)$ is nearly zero. It follows from equation 2.8, that in the limit $\alpha/\rho \rightarrow 0$, the flux vanishes. That is, the flux from a deeply distributed source has diluted its concentration to the point that no photons are able to reach the detector without interacting with the soil. This too is reflected in figure 2.4. Note that the flux approaches zero as $\alpha/\rho \rightarrow 0$.

Figure 2.5 is a plot of the flux a function of energy for a uniform depth profile. It must be emphasized that this situation is not to be confused with the deeply distributed source described previously. The uniform source distribution arises primarily with the natural emitters and not from fallout.

Dependence of the Flux on the Source Geometry

Figures 2.6 and 2.7 show the fraction of the total flux as a function of the horizontal distance from the detector for several energies. Figure 2.6 is for a deep distribution, while Figure 2.7 is for a shallow one. The essential point is the relationship between the source distribution and the contribution to the total flux from various horizontal distances. For $\alpha/\rho = 6.25 \text{ cm}^2/\text{g}$, roughly 40 to 50 % of the flux comes from horizontal distances greater than 10 meters, while for $\alpha/\rho = 0.0625 \text{ (cm}^2/\text{g)}$, only about 10 to 20% of the flux comes from distances greater than 10 meters. The immediate implication of this fact is that for the accurate measurement of recent fallout deposition, corrections for a limited halfspace may be necessary if the site to be measured has obstructions within a 100 meters radius.

Figures 2.8 and 2.9 show the fraction of the total flux as a function of the linear depth beneath the air-ground interface for several energies. Figure 2.8 is for a deep distribution, while Figure 2.9 is for a shallow one. Here, the essential point is that even for a relatively deep distribution ($\alpha/\rho=0.0625 \text{ cm}^2/\text{g}$), over 90% of the total flux comes from the first 10 cm of soil. The situation is even more extreme in the case of a shallow distribution. In Figure 2.9 we can see that that roughly 75% of the total flux comes from the first 1mm of soil. It must be pointed out that in the case of $\alpha/\rho=6.25 \text{ cm}^2/\text{g}$, 63% of the total concentration lies within that first millimeter of soil.

Other Factors Affecting Flux

Excessive ground roughness effectively provides additional self-absorption and therefore makes the source appear more deeply distributed.

Variations in soil density are effectively factored out of the relationship because the concentration of radionuclides in the soil is given per unit mass. Thus, a soil with twice the normal density will have half the concentration and therefore provide half the flux.

The precise soil composition is generally not needed. A typical soil composition might consist of 68% silicon dioxide, 14% aluminium oxide, 5% iron oxide, 5% carbon dioxide, and 10% water. Varying the soil composition will effect the flux through the mass attenuation coefficients. The variation in soil composition will, in the very extreme cases, result in a few percent error in the flux for medium and high energy photons. Figure 2.10 shows the relative error in the flux for a 1% deviation from the assumed mass attenuation coefficient of soil as a function of the source depth parameter. As one would expect, the more deeply distribution source is more sensitive to the specific soil composition. Clearly, a low energy, deeply distributed source requires the specific mass attenuation coefficient to ultimately determine an accurate source activity.

Since, at a height of 1 meter, the mass depth of air is typically one-tenth the mass depth of soil, uncertainty in the flux due to a deviation from the assumed mass attenuation coefficient of air is regarded as negligible. However variations in the density of air could produce as much as a 5 to 7% error in the flux for a very shallow distribution. For purposes of *in situ* spectrometry, variations in the air density occur only with altitude. Figure 2.11 shows the relative error in the flux as a function of height for several different energies and two different source distributions. We have assumed that the density of air decreases exponentially with the height above sea level and a scaling height of 7 km. This figure demonstrates the necessity to correct for air density for fresh fallout at high altitudes.

CHAPTER 3

DETECTOR CALIBRATION

Response at Normal Incidence

The response of the detector to photons at normal incidence is represented by the term N_0/ϕ which was introduced in equation 2.1 in the previous chapter. In general, the response of a detector to incident photon fluence is a complex function of a number of factors such as crystal size, shape, mounting, housing, and inactive volume regions. Estimates of these parameters can be provided by the manufacturer and then used as input to computer codes for determining the detector efficiency as a function of energy. More commonly, experimental determinations of detector response are performed using certified calibration sources. One standard measure of a Ge detector performance is the efficiency at 1332 keV relative to a 3x3 inch NaI crystal. This measurement is performed with a ^{60}Co point source positioned 25 cm from the detector face at normal incidence. For purposes of *in situ* gamma-ray spectrometry, a more meaningful measurement is to determine the full absorption peak count rate per unit incident fluence rate at a given energy for plane parallel radiation which requires a larger source to detector distance. In the case of long Ge crystals, the standard measurement distance of 25 cm underestimates the efficiency that would be achieved for *in situ* spectrometry since the distance to the effective crystal center is larger. True plane parallel incidence would be accomplished for a point source at infinite distance. For practical applications, however, a source distance of 1 to 2 meters can suffice considering that the dimensions of a Ge crystal are on the order of a few cm or less.

The full absorption peak count rate N , sometimes referred to as the peak area, is computed as the sum of the counts across those channels that represent a peak in the spectrum minus the counts in the underlying continuum, sometimes referred to as the baseline or background. All modern full-function analyzers and software analysis packages allow the user to set up a region of interest (representing the

peak) and the peak area is automatically calculated. Generally, on the order of three to five channels on both the low and high energy side of the peak are used as a basis to infer the continuum counts.

The fluence rate, $\phi(E)$, at the detector is given by the expression

$$\phi(E) = \frac{R(E)}{4\pi x^2} \quad (3.1)$$

where $R(E)$ is the gamma ray emission rate at that energy and x is the source to detector distance. The attenuation effect of the source encapsulation should be taken into account along with that of the air between the source and detector, particularly for low energy gamma rays and large values of r .

The determination of the ratio of N_0 to $\phi(E)$ must be done at several different energies over the effective operating energy range of the instrument. For environmental gamma radiation, this would be up to 2.615 MeV, a principal gamma ray emitted by ^{208}Tl in the naturally occurring ^{232}Th series (although there may be applications for studying N-16 near operating reactors in which case, 7 MeV). The effective low end point will depend upon the type of detector which would be about 60 keV for P-type Ge and down to 10 keV for N-type.

Although almost any certified gamma source can be used to measure the detector efficiency at a particular energy, the use of longer-lived isotopes is recommended so that measurements can be repeated throughout the lifetime of the same detector. In addition, the use of the same set of sources for two different detectors will reduce systematic differences in their responses. It is also effective to use multiple gamma emitters such as ^{152}Eu and ^{154}Eu since they can provide many data points across a wide energy range. While these isotopes generally introduce some difficulty in the interpretation of the detector response for close-in geometries due to the effects of cascade coincidence summing, the effect is negligible at source distances of a meter or more. Also, ^{241}Am (59.5 keV), ^{137}Cs (661.6 keV),

and ^{60}Co (1173.2 keV and 1332.5 keV) are common isotopes that can provide data points at low, medium, and high energies, respectively. Although it has a relatively short half-life of 1.9 years, ^{228}Th provides a crucial high energy point at 2.615 from its progeny, ^{208}Tl . Mixed gamma-ray point sources specifically made for calibrating Ge detectors are regularly available from the National Institute of Standards and Technology (NIST).

A precise determination of $N_0/\phi(E)$ should take into account that the calculation of the fluence rate at the detector will depend upon the distance from the point source to average point of interaction within the crystal and the window to crystal distance. At low energies (< 100 keV), the penetration of the photons into the crystal is minimal and the distance to the front surface can be taken to be the value of r plus the manufacturer's estimated window to crystal distance. For high energies (> 1 MeV), the value of r can be measured to the geometric midpoint of the crystal since the penetration is high and the interactions are spread throughout. For medium energies, the mean penetration into the crystal can be estimated from the photon cross section data for Ge or can be experimentally determined by plotting the inverse of the square root of the peak count rate versus the source to window distance for two or more distances. This would be done for a few different energies. The intercept on the plots for a specific energy then represents the effective penetration into the crystal at that energy plus the window to crystal distance. An example of the results of this experimental determination are shown in Figure 3.1.

The precise value of r becomes less important as the source to detector distance increases relative to the crystal dimensions. For a crystal that is 6 cm long, the difference in the fluence rate at 1 meter is close to 6% for front surface as opposed to crystal midpoint distances. At 2 meters the difference is reduced to 3%.

Once the value of $N_0/\phi(E)$ has been determined at several different energies, a polynomial fit can be applied across the energy range. Alternatively, a simple straight line fit on a log-log plot is adequate between 300 and 2000 keV. It can be

expected that this simplest of approaches would fit the data to within $\pm 3\%$. Since each source has some uncertainty in the quoted activity, a best fit straight line is perhaps a more realistic choice over a forced fit curve with many points of inflection. If suitable calibration sources are not available outside this energy range, extrapolations of the straight line fit down to 200 keV and up to 3 MeV would generally not introduce significantly larger errors. For comparison, Figure 3.2 shows examples of calibration fits for eight different detectors of various sizes, as measured by the manufacturer's quoted relative efficiency at 1332 keV.

Angular Response

Although the response of a detector to photon flux at normal incidence provides a general measure of the sensitivity for *in situ* measurements, the actual full calibration of the detector for most applications involves the response at other angles of incidence because one is generally measuring extended sources in the environment and not aiming the detector towards a point source. In these circumstances, photons will be incident on the detector through the side wall and even possibly at angles corresponding to a photon path through the dewar. For this reason, some consideration must be given to the crystal shape, dewar size and detector orientation in the field.

Due to the cylindrical shape of the Ge crystal, it can be assumed that there is a uniform response about its axis of rotation. This can be checked experimentally for a detector to insure that the mounting structure has not introduced any substantial asymmetrical response characteristics. For typical applications in the field, the orientation of the detector should be with the axis of rotation perpendicular to the ground thus eliminating any dependence on angle of photon incidence about the azimuth.

The response in the plane perpendicular to the detector face is generally not uniform. For the measurement of a source in a half-space geometry where the

detector is faced toward the ground, the range of angles would be 0 degrees (normal incidence to the detector face) to 90 degrees (sidewall incidence). This would be the ideal orientation for measuring ground sources, i.e., facing down with the dewar overhead. Although it may seem unconventional, it is still possible to perform measurements over soil with the detector facing up and the dewar underneath. In this case the range in the photon angles of incidence would be 90 to 180 degrees, relative to the detector face. In either case, the detector response about the angles of photon incidence must be determined. This is accomplished by counting point sources at a fixed distance at least 1 meter at several angles. The peak count rates at a given energy can be normalized to 0 degree incidence and fitted to a smooth curve on a plot. Figures 3.3 and 3.4 show examples for two different detectors across the full range in angles, 0 to 180 degrees, where 0 degrees represents normal incidence on the detector face. The data in Figure 3.3 are for a detector with a small 1.2 liter cryostat while the data in Figure 3.4 are for a detector with a dipstick cryostat in a 17 liter dewar. In practice, this later detector would be situated facing up in the field and the flux would be incident in the range of 90 to 180 degrees.

Whereas the total volume of the Ge crystal is closely related to the quoted efficiency, the shape of the crystal is the fundamental controlling factor for the variation in response at other than normal incidence. Based on theoretical considerations, and as found in experimental studies on detectors (Helfer and Miller, 1988), a cylindrical crystal with a length (L) greater than the diameter (D) will tend to have a higher response at angles off normal incidence. The response for a detector where L is less than D would tend to be opposite to this since less surface area is presented to the fluence at sidewall incidence. The variation in response would be least for crystals where $L = D$. In general, response variations with angle would be most pronounced at lower energies where the efficiency would be related to the effective area that intercepts the photon fluence. At higher energies, the angular response characteristics are less sensitive to the crystal shape since primary and secondary absorption occurs throughout the volume of the Ge crystal. To illustrate these characteristics, the responses (relative to normal incidence) for three different crystal shapes (as measured by the L/D ratio) are presented for three

separate energies in Figures 3.5, 3.6, and 3.7. These data are indicative of the general behavior that would be found for Ge detectors, although the exact angular response would be expected to vary among detectors with the same L/D ratio because of different sizes and variations in attenuation properties associated with mounting and housing. At very low energies (< 100 keV), the effects of attenuation by the detector mounting and housing material can substantially reduce the efficiency for flux incident on the detector sidewall and no general behavior can be predicted.

The angular correction factor is computed as a weighted average of the normalized detector response as a function of angle, $N(\theta)/N_0$, over the flux angular distribution,

$$\frac{N_f}{N_0} = \frac{1}{\phi} \int_{\theta_1}^{\theta_2} \phi(\theta) \frac{N(\theta)}{N_0} d\theta \quad (3.2)$$

For a detector positioned in a half space source geometry, the limits of integration in the above equation would be 0 to $\pi/2$. The sensitivity in the case of measurements over a soil half space is maximized with the detector facing downward, in which case 0 degrees is the perpendicular to the ground plane and normal incidence at the detector face.

Equation 3.2 can be evaluated numerically using the experimental data for $N(\theta)/N_0$ and calculated values of $\phi(\theta)$ for different source energies and geometries.

Figure 3.8 shows the results for three different shape detectors for two different source geometries, a plane source atop the ground and a uniformly distributed source with depth. As explained previously, when the crystal length/diameter ratio is close to 1, a more uniform angular response can be expected and this is also reflected in the behavior of the function N_f/N_0 . Also, as expected, the angular response tends to flatten out at high energies, but can be vary quite a bit at low energies. Although the value of N_f/N_0 can be seen to vary considerably for different

detectors and as a function of energy for a given detector, it is important to note that there are only minor differences for different source depth distributions. This results from the fact that, at a given energy, the angular distribution of the fluence does not change dramatically with the source depth profile. This is fortunate in that a large error will not result in the measurement of fluence rate if the source depth profile is not known.

The situation of a detector facing upward with the dewar underneath will result in a lower efficiency for the measurement of radionuclides in soil. The dewar itself will substantially attenuate the photon fluence from the ground underneath and, in general, the detector mounting will result in a lower response at incident angles at the back end of the crystal. However, since the angular distribution of the fluence is peaked toward the horizontal direction, the overall effect is not substantial. The data of Helfer and Miller (1988) indicate that the value of N_f/N_0 would only be reduced by a few percent for surface source distributions for detector facing up as compared to facing down. For a uniform source distribution in the soil, the reduction would be typically 10 to 20 percent.

Generic Conversion Factors

In lieu of developing a full calibration for a detector, generic calibration factors can be applied if a high degree of accuracy is not required. These factors were developed on the basis of experimental findings on the response characteristics of a number of different Ge detectors of various sizes and shapes and have been published in (Helfer and Miller, 1988). The only parameters needed are the manufacturer's quoted efficiency at 1332 keV, the crystal L/D ratio, and the detector orientation in the field (facing up or down). These generic factors are estimated to have an uncertainty of $\pm 10\%$ at energies above 500 keV and $\pm 15\%$ between 200 and 500 keV. Due to the sensitivity of the response at low energies to individual detector characteristics, they cannot be used below 200 keV.

CHAPTER 4

INFERRED QUANTITIES

Concentration in Soil

Having determined the three separate quantities, N_o/ϕ , N_f/N_o , and ϕ/A , their product yields the desired conversion factor, N_f/A . For radionuclides uniformly distributed with depth in the soil ($\alpha/\rho = 0$), the term A is in units of activity per unit mass. As such, there is no need to determine the soil density.

Although the assumption of a uniform profile in the soil for natural emitters is generally safe, unusual situations where there is markedly different soil strata of varying nuclide concentration may produce anomalous results. This situation could arise if landscaping has been performed where topsoil from a different area has been used. Also, evaluations of the ^{238}U series must be done with the awareness that ^{222}Rn escapes from the soil and that the important gamma emitting progeny, ^{214}Pb and ^{214}Bi , may not be in equilibrium with ^{226}Ra in the soil. In fact, there may be a measurable contribution to the fluence rate at one meter above the soil from the progeny in the air, particularly under atmospheric inversion conditions. Disequilibrium is also possible for the ^{232}Th series due to the exhalation of ^{220}Rn (thoron), although this is less likely to be as severe due to its relatively short half life.

Another effect that may interfere with the interpretation of a spectrum is that of radon progeny scavenging during precipitation. In this situation the ^{214}Pb and ^{214}Bi assume a surface source distribution that can considerably alter the flux and dose rate. For this reason (and to keep people and equipment dry!) it is best to avoid measurements during and for about 2 to 3 hours following rain.

It is possible to consider a fallout product as having a uniform profile if it is deeply distributed or has been mixed through soil cultivation. Depending upon the

source gamma energy, plowing to depths of 15 to 30 cm essentially accomplishes this. Although the distribution does not extend to infinity in a situation such as this, in terms of the total gamma flux seen above ground, it is effectively infinite in depth. For *in situ* applications such as this, the concentration that is measured can be considered as representative of the surface soil.

Deposition/Inventory

For radionuclides that are exponentially distributed with depth ($\alpha/\rho > 0$), the term A is in units of activity per unit area. Although the results of analyses of environmental samples are frequently reported in terms of concentration, the fundamental quantity that is of most use for assessing fallout products is the deposition (sometimes referred to deposition density or inventory). Whereas the deposition remains a constant, the concentration of a fallout product will vary depending upon the depth distribution. To illustrate this point, consider a radionuclide such as ^{137}Cs that was deposited in an area 30 years ago from atmospheric nuclear weapons testing. Where the surface soil has retained it, a sample down to 5 cm will yield some concentration, x. On an adjacent strip of land that was plowed deeply, the same sampling protocol will yield a concentration of perhaps only 0.2x. Obviously, this would be a flawed scheme for investigating a potential local source of contamination. Instead, consider a soil core that was taken down to 30 cm. The measured concentration of an aliquot of this sample should be multiplied by the entire sample mass to give the total activity in the core and then divided by the sample area to give activity per unit area. This would yield the same result for both sites. The only precaution is to sample to a great enough depth to collect essentially all of the deposited activity.

In order to make an accurate assessment of deposited activity with *in situ* spectrometry, an estimate or actual measurement of α/ρ must be made. As such, the time of deposition must be taken into account and assurances that no erosional processes or human activities such as plowing have disturbed the site. For fresh

fallout that is dry deposited, the assumption of a surface source ($\alpha/\rho = \infty$) is generally not justified due to the effects of soil surface roughness which effectively buries the source and lowers the fluence at the detector. Wet deposition processes will also tend to distribute the fallout within the surface soil layer such that the assumption of a surface source would not be correct. Experience has shown that a more realistic assumption of α/ρ would be on the order of 1 to 10 $\text{cm}^2 \text{g}^{-1}$. Depending upon the degree of uncertainty that is acceptable, experimental determination of the profile may be required via soil sampling. For deposition that occurred in the past, soil sampling is generally required to obtain an accurate value of α/ρ . This will be discussed in Chapter 6.

In making measurements of deposition, one must be aware of the sensitivity of the inferred inventory to the value of α/ρ . Figure 4.1 shows an example of the results of a calibration for a 22% efficient Ge detector. The conversion factor, N_f/A , is plotted as a function of the source depth constant, α/ρ , for the commonly encountered fission product ^{137}Cs . The conversion factor is seen to change relatively little for values of $\alpha/\rho > 1 \text{ cm}^2 \text{g}^{-1}$ (shallow source depth distribution) as compared to values of $\alpha/\rho < 1 \text{ cm}^2 \text{g}^{-1}$ (deep source depth distribution). In effect, the error made in inferring the source activity will not be large for a fresh deposition event even if the profile is not precisely known. Conversely, if a measurement of aged fallout is made, accurate results will only be obtained if the profile is determined by some independent means, i.e., soil sampling.

Dose Rate in Air

One of the most useful quantities that can be determined with *in situ* gamma-ray spectrometry is the dose rate in air (or the exposure rate) for the individual radionuclides present at a site. To do this, the results of transport calculations are used for the infinite half space geometry and the exponential source distribution. The conversion factors, I/A , exposure rate per unit activity in the soil, can be found

in (Beck et al, 1972) and (Beck, 1980). One can incorporate these factors directly in to the detector calibration using the relationship

$$\frac{N_f}{I} = \frac{N_f/A}{I/A} \quad (4.1)$$

where N_f/I is the full absorption peak count rate per unit exposure rate for that nuclide.

The factor I/A takes into account all of the gamma rays emitted in the decay of that nuclide. Therefore, one does not have to analyze every peak for that nuclide. In practice, however, it is best analyze more than just one peak, especially if they are well separated in energy, to check agreement.

What is not obvious in this analysis is the fact that the derived quantity, N_f/I , is less sensitive to α/ρ than is N_f/A . This results from the fact that as the source distribution in the soil gets deeper, the primary flux decreases relatively rapidly compared to the scattered component. However, this scattered component still contributes to the dose rate. To illustrate this, Figure 4.2 compares these two calibration factors N_f/I and N_f/A as a function of the relaxation depth, α^{-1} , where the soil density = 1.6 g cm^{-3} . This range in depth profiles extends from that of a fresh deposit to one that is perhaps 30 years old. It can be seen that the exposure rate factor varies by only 50% or so whereas the inventory factor varies by about a factor of 7. Thus, only a rough estimate of the depth profile is needed to predict the dose rate. At the same time, substantial errors can be made in the inventory estimate if the wrong depth profile is used.

CHAPTER 5

RADIATION SOURCES IN THE ENVIRONMENT

Natural Emitters

Virtually any spectrum collected over soil will reveal the presence of the three primordial natural radionuclides, ^{238}U , ^{232}Th , and ^{40}K . In the case of ^{238}U , detection is made through the analysis of its progeny, principally, ^{214}Pb and ^{214}Bi . For ^{232}Th , the progeny ^{228}Ac and ^{208}Tl are commonly used. As mentioned previously, these radionuclides are generally distributed uniformly with depth in the soil. As such, the the appropriate quantity to report is the concentration, i.e., the specific activity (pCi/g, Bq/kg, etc.). Since these natural radionuclides are likely to contribute substantially to the total gamma flux, the exposure rate rate or dose rate in air is a useful quantity to report as well. As explained in the following section, the summation of all contributions to the dose rate should be made and compared to a reading from an instrument such as a PIC.

Table 5.1 lists some of the more prominent peaks that are seen in a spectrum and which are the best to analyze. As a standard practice, the conversion factors N_f/A and/or N_f/I should be computed for these lines as they will almost always be used.

One characteristic of an *in situ* spectrum is that the continuum rises substantially at low energies due to the absorption of scattered radiation in the air by the Ge crystal. This makes it difficult to detect and analyze peaks below about 200 keV. For instance, the rather weak 186 keV peak from ^{226}Ra superimposed on this large continuum does not usually give highly precise results due to the counting error.

One cosmogenically produced isotope that can sometimes be seen is ^7Be (478 keV, 53 day half-life). Since it is produced in the atmosphere and deposited on the earth's surface, it can be expected to have an exponential profile like that of a typical fission fallout product. Due to its short half-life, it can also be expected to lie close to the soil surface and thus have a high value of α/ρ .

Fallout Emitters

Due to nuclear weapons testing in the atmosphere, measurable amounts of the fission product ^{137}Cs can be seen in surface soils around the world. Also, many areas, especially in Europe, show the activation product, ^{134}Cs , along with additional amounts of ^{137}Cs from Chernobyl fallout. Other, less intense, and shorter lived isotopes from Chernobyl such as ^{125}Sb and ^{106}Ru can be sometimes seen as well.

For common fallout products such as these and for other isotopes which one expects to encounter, it is useful to determine the conversion factor N_d/A and plot it for several different values of α/ρ . A smooth curve can be drawn through the points or a fit can be applied such as show in the previous chapter (Figure 4.1).

For *in situ* applications where there is potential for inhomogeneity in the horizontal distribution of deposited activity due to sparse ground cover, accurate measurements can still be performed providing that the scale of these inhomogeneities is small in comparison to the field of view of the detector. As an example, fallout in semi-arid regions may tend to clump under scattered plants from the effects of wind blown soil. If the depth distribution of the radionuclides is approximately the same for bare ground as well as under the plants, no correction is needed as the application of the appropriate conversion factor for that depth distribution will yield the the average inventory for that site. However, it is possible that there may two or more distinct depth profiles associated with the various ground covers in which case separate determinations must be made. The

infinite half space in this circumstance can be considered a collection of sub-spaces, each with its own characteristic radionuclide inventory and depth profile. The conversion factor for field spectrometry is then computed as an average, weighted by the fraction of the total deposited activity associated with each ground cover. An estimate of this can be made through selected soil sampling to determine the inventory and by measuring the fraction of the half space for each ground cover. In a strict sense, the *in situ* spectrum in this situation does not provide an independent measure of the deposited activity in that there is a reliance on the data provided by the soil samples. However, the average conversion factor is bounded by the range in respective values for each type of ground cover. This range may be small compared to the variation in inventory so that the *in situ* spectrum provides a reasonably accurate average without resorting to far more extensive soil sampling. For more details on this subject, the reader is referred to (Miller and Helfer, 1985).

Cosmic Radiation

A portion of the continuum seen in a Ge spectrum is due to the interaction of cosmic-ray secondary radiation in the crystal. The degree of this contribution can be estimated from the count rate above the 2.615 MeV line from ^{208}Tl . Generally, it is a small fraction of the count rate due to terrestrial gamma radiation. The overall effect is to increase somewhat the error associated with the analysis of a peak in the spectrum in that the continuum under that peak is slightly higher.

It is important to realize, however, that a measurement of the external dose rate will include a contribution from the cosmic component. Many survey instruments have some response to cosmic radiation. If a comparison is made between a survey instrument reading and the sum of the dose rates inferred from peak analysis with a Ge detector, it must be remembered that the latter provides only the terrestrial gamma component.

In general, the dose rate from cosmic radiation increases towards the earth's poles and decreases toward the equator. For mid-latitudes, Figure 5.1 provides a useful conversion from altitude/pressure to cosmic ray dose rate. In practice, a reading with a pressure meter would be the preferred method with which to infer the cosmic ray component. In place of this, a geological survey map can be used to find one's altitude. In using this chart, a limitation on its accuracy must be recognized. There are variations of a few percent with the 11 year solar cycle and somewhat smaller variations with season. During periods of maximum solar activity (as measured by sunspots for instance), the cosmic component tends to be lower while during periods of a "quiet" sun it is higher. The overall uncertainty given both these spatial and temporal variations is estimated to be on the order of ten percent.

CHAPTER 6

QUALITY ASSURANCE

Error Estimates

Sources of random and systematic uncertainties for *in situ* spectrometry include deviations in the assumed source geometry parameters, soil density and mass attenuation coefficients, detector parameters, and counting statistics. For the case of a fresh deposition event, the source geometry and soil parameters are not crucial. It is unlikely that errors greater than 10% would result since the source is near the soil surface. For more deeply distributed radionuclides, errors relating to departures from the assumed source geometry and soil medium attenuation are not readily predictable. For this reason, it is important to corroborate estimates of inventory with independent methods such as soil sampling (see below).

Systematic error relating to detector calibration can be estimated based on the quoted uncertainties of the calibration sources used. These would tend to be around 3% or less. Calibration source uncertainty is not a factor for the angular response determination since the measurements are normalized. There is, however, a few percent uncertainty in the application of a value of N_f/N_0 due to variations in the angular distribution of the flux with source depth profile and any experimental error in the measurement of angles during the calibration.

One source of error that should be reported and which is easy to estimate is the statistical counting error (sometimes referred to as $\pm 1\sigma$) for each peak analyzed. Software peak analysis routines generally calculate such an error. If not, a basic estimate is given by the square root of the sum of the peak (net) counts and the gross counts in the region of interest. The relative error would simply be this quantity divided by the peak counts.

As a general quality control practice, the detector calibration should be checked on a regular basis. To do this, the value of N/ϕ can be measured at two energies, one high and the other low, and for two angles, normal incidence and sidewall incidence. The detector performance over time should be evaluated as any deterioration in the energy resolution could point to loss in efficiency as well. If the detector is repaired by the manufacturer, a complete recalibration may be necessary, particularly if the crystal has been reworked.

Source Depth Profile Determinations

In certain *in situ* applications, and particularly for deposited radionuclides that have weathered into the soil, one would like to ascertain the source depth distribution. This can be done by taking soil samples from different depths. One of the easiest ways in which to do this is to hammer a corer (sometimes referred to as a cookie cutter) into the ground and remove a soil section. If the soil bore hole does not collapse, one can continue the procedure to greater depths with longer corers, taking care not to spill topsoil into the hole. Alternatively, once the corer is in the ground, the area is defined and various depth layers can be carefully spooned out. It is best to take several cores in this manner, and composite the samples. More complete information on soil sampling can be found in the EML Procedures Manual.

Useful depth increments for the determination of α/ρ are 0 - 2.5 cm, 2.5 - 5 cm, (or a combined 0-5 cm), 5 - 10 cm, 10 - 15 cm, and 15 - 30 cm (or a combined 10 - 30 cm). Uniformity of the natural emitters with depth can be checked by counting these samples in a laboratory based shielded detector. Moreover, a plot of the concentration with depth for man-made activity can yield the depth penetration factor α/ρ . A convenient method is to compute the total activity in the core (assuming it was of great enough depth to contain all of the deposited activity) and then plot the fraction of the total below a given depth versus that depth. The depth should be in terms of mass per unit area (g/cm^2), which is simply the original wet

mass divided by the area of the corer. A straight line fit to the data points provides a slope which is just the value of α/ρ (cm^2/g). Figures 6.1 and 6.2 show several examples of depth profiles that were determined in this manner.

In the case of a radionuclide that has two or more prominent gamma lines well separated in energy, it is possible to infer the depth profile by comparing the ratio of measured fluxes for the two lines to the calculated ratio as a function of the depth parameter α/ρ . Although this technique does not require the collection and analysis of soil samples, sufficient sensitivity can only be achieved with a strong source since the statistical counting error must be low. It is most effective if the measurement can be made for a very low energy and a very high energy peak as the variation in flux ratio will be greatest in this case.

Comparison to Soil Samples

The simplest comparison to make between *in situ* spectrometry and soil sample analysis is a comparison of concentrations for the natural emitters. Some caution is needed here for the ^{238}U - ^{226}Ra series, however, since the emanation of ^{222}Rn from either the soil in the field or from the sample complicates matters. Typically, disequilibrium on the order of 10 to 20% can result if the the soil is open to the free air. This would be the case for for surface soil. For a sample that has been sealed in a container (not porous to radon and with no air space at the top where radon could collect and the progeny plate out) equilibrium would be achieved in several half-lives, about 3 weeks.

Another factor to consider in the ^{238}U series is ^{210}Pb (22 year half-life). Since this nuclide follows ^{222}Rn in the decay chain, it cannot be expected to be in equilibrium for surface soils. In wet regions, it is likely to have a higher concentration than ^{226}Ra and in dry regions, a lower concentration.

An important consideration in making a comparison with soil samples is soil moisture content. Generally, samples are dried before counting. In order to make a valid comparison to *in situ* measurements, it is necessary to weigh the sample wet and correct the dry concentration to wet concentration. This might typically be a 10 to 25 % correction.

Comparisons of fallout activity are generally best made in terms of activity per unit area as pointed out before. Due to the potential inhomogeneity in the horizontal distribution of fallout activity, a representative soil sample would generally have to measure several hundred cm^2 and be comprised of several cores from different spots.

Comparisons to Total Ionization

One of the best techniques to employ for quality assurance purposes is to make a dose rate comparison between results obtained with the Ge detector and those of another instrument. For instance, the total dose rate in air from penetrating radiation (gamma and cosmic) in the environment can be made fairly accurately with a properly calibrated pressurized ionization chamber. This can be compared with the sum of the dose rates for each nuclide from spectrometric determinations with the cosmic component added in. Agreement to within $\pm 5\%$ is a sign that the detector calibration is good and that the assumed source geometry is correct. Disagreement by more than 10% points to a calibration problem or a radical departure from the assumed source geometry.

USEFUL CONVERSION FACTORS

Basic Units

$$1 \text{ R} = 2.58 \times 10^{-4} \text{ C/kg}$$

$$1 \text{ mCi/km}^2 = 37 \text{ Bq/m}^2$$

$$1 \text{ mCi/km}^2 = 1 \text{ nCi/m}^2$$

$$1 \text{ mCi/km}^2 = 0.1 \text{ pCi/cm}^2$$

$$1 \text{ pCi/g} = 2.22 \text{ dpm/g}$$

$$1 \text{ pCi/g} = 37 \text{ Bq/kg}$$

Other Factors

$$1 \mu\text{R/h} \rightarrow 8.7 \text{ nGy/h}$$

for a soil half-space:

$$1 \text{ pCi/g of } ^{238}\text{U} + \text{progeny} \rightarrow 1.90 \mu\text{R/h}$$

$$1 \text{ Bq/kg of } ^{238}\text{U} + \text{progeny} \rightarrow 0.45 \text{ nGy/h}$$

$$1 \text{ pCi/g of } ^{232}\text{Th} + \text{progeny} \rightarrow 2.82 \mu\text{R/h}$$

$$1 \text{ Bq/kg of } ^{232}\text{Th} + \text{progeny} \rightarrow 0.66 \text{ nGy/h}$$

$$1 \text{ pCi/g of } ^{40}\text{K} \rightarrow 0.179 \mu\text{R/h}$$

$$1 \text{ Bq/kg of } ^{40}\text{K} \rightarrow 0.042 \text{ nGy/h}$$

SUGGESTED READINGS

Publications of EML (HASL)

Beck, H. L., J. DeCampo, and C. Gogolak

"In situ Ge(Li) and NaI(Tl) gamma-ray spectrometry"

USDOE Report HASL-258 (1972)

The "Bible" of in situ gamma spectrometry. A complete description of theory and application with data tables. As useful today as when it was first published.

Beck, H. L.

"The Physics of Environmental Gamma Radiation Fields"

J. A. S. Adams, W. M. Lowder, and T. F. Gesell (Editors)

In: The Natural Radiation Environment II, CONF-720805-P1, pp. 101-134 (1972)

A fundamental review of the properties of gamma radiation fields in the environment. Basic flux, exposure rate, and angular distribution data.

Beck, H.L.

Exposure Rate Conversion Factors for Radionuclides Deposited on the Ground

USDOE Report EML-378 (1980)

Tables listing the exposure rate per unit deposited activity for over 100 of the most common fission isotopes and over 50 activation products. The conversion factors are given for four different source depth profiles ranging from a recent deposition event to an aged fallout situation.

Chieco, N. A., D. C. Bogen, and E. O. Knutson (eds.)

EML Procedures Manual

USDOE Report HASL-300, 27th edition, Vol. 1, Section 3 (1990)

Information on the instrument systems and techniques employed for environmental radiation measurements with emphasis on calibration procedures. Devices covered include Ge and NaI detectors, pressurized ionization chambers, and thermoluminescence dosimeters.

Helfer, I. K., and K. M. Miller

"Calibration Factors for Ge Detectors Used for Field Spectrometry"

Health Physics 55, 15-29 (1988)

For those who do not have the time or resources to calibrate their detector, this reference contains equations and tables that provide generic factors based on a manufacturer's quoted specifications for the Ge crystal. Above energies of 500 keV, these factors are estimated to be accurate to within 10%.

Miller, K. M., and I. K. Helfer

"In situ Measurements of ^{137}Cs Inventory in Natural Terrain"

in: Environmental Radiation '85, Proceedings of the Eighteenth Midyear Topical Symposium of the Health Physics Society, 243-251 (1985)

The basic approach is described for making measurements at sites with sparse ground cover where fallout was deposited many years ago and where it is likely to have been redistributed by wind and water erosion.

Miller, K. M.

"A Spectral Stripping Method for a Ge Spectrometer used for Indoor Gamma Exposure Rate Measurements"

USDOE Report EML-419 (1984)

A more advanced topic for experienced gamma spectroscopists. This technique involves additional experimental determinations of detector response and the application of an unfolding routine. It yields the incident flux spectrum (both primary and scattered) which can then be converted to exposure rate. No knowledge of the source geometry is needed.

Table 5.1

Energy (keV)	Nuclide	Parent Series	Comments
186	^{226}Ra	^{238}U	low intensity, high continuum, cannot be resolved from ^{235}U peak at 185 keV
239	^{212}Pb	^{232}Th	strong peak, contribution from ^{224}Ra peak at 241 keV, interference from ^{214}Pb peak at 242 keV
295	^{214}Pb	^{238}U	generally clean peak, fairly strong
352	^{214}Pb	^{238}U	generally clean, strong peak
583	^{208}Tl	^{232}Th	generally clean, strong peak
609	^{214}Bi	^{238}U	strong peak, interference from 605 keV peak if ^{134}Cs is present
911	^{228}Ac	^{232}Th	generally clean, strong peak
965+969	^{228}Ac	^{232}Th	doublet, not as strong as 911 peak
1120	^{214}Bi	^{238}U	reasonably strong, continuum relatively low
1461	^{40}K	-	clean, strong, only peak for this nuclide
1765	^{214}Bi	^{238}U	reasonable strong, continuum low
2615	^{208}Tl	^{232}Th	clean, strong, continuum very low

CONTRIBUTION TO TOTAL 662 keV PRIMARY FLUX AT 1 METER ABOVE GROUND FOR TYPICAL ^{137}Cs SOURCE DISTRIBUTION

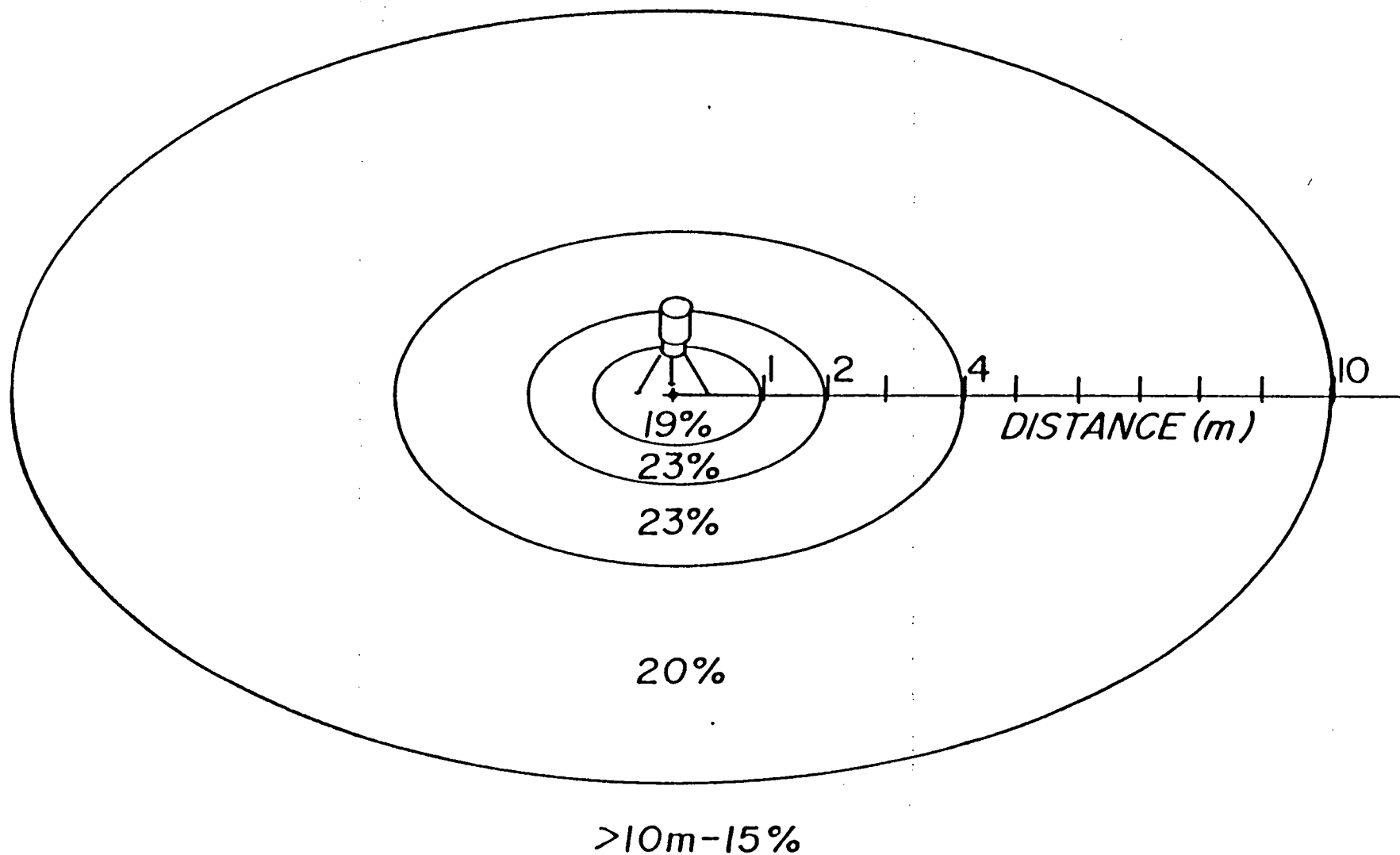


Figure I,1

Ge DETECTOR RESPONSE

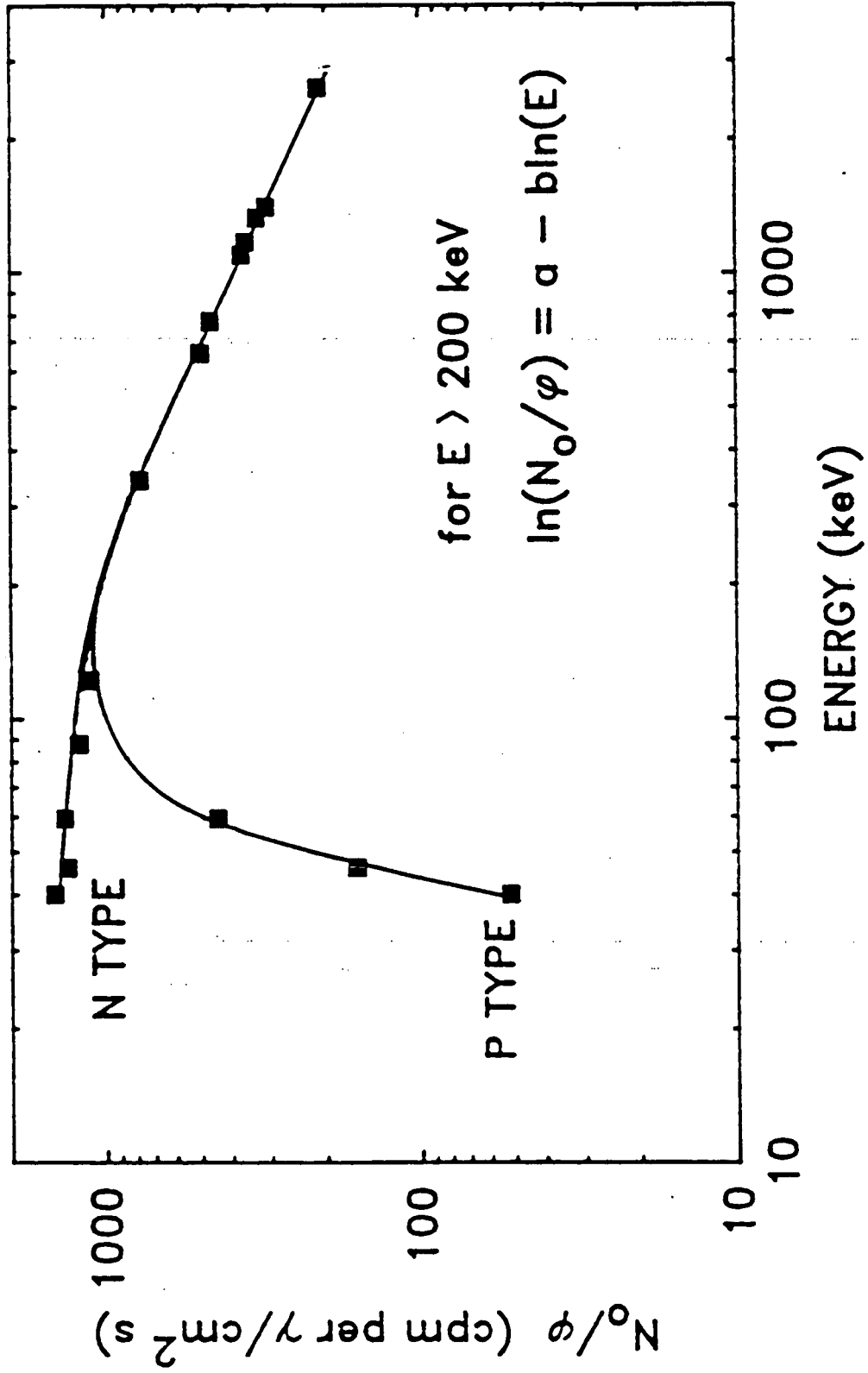


Figure 1.1

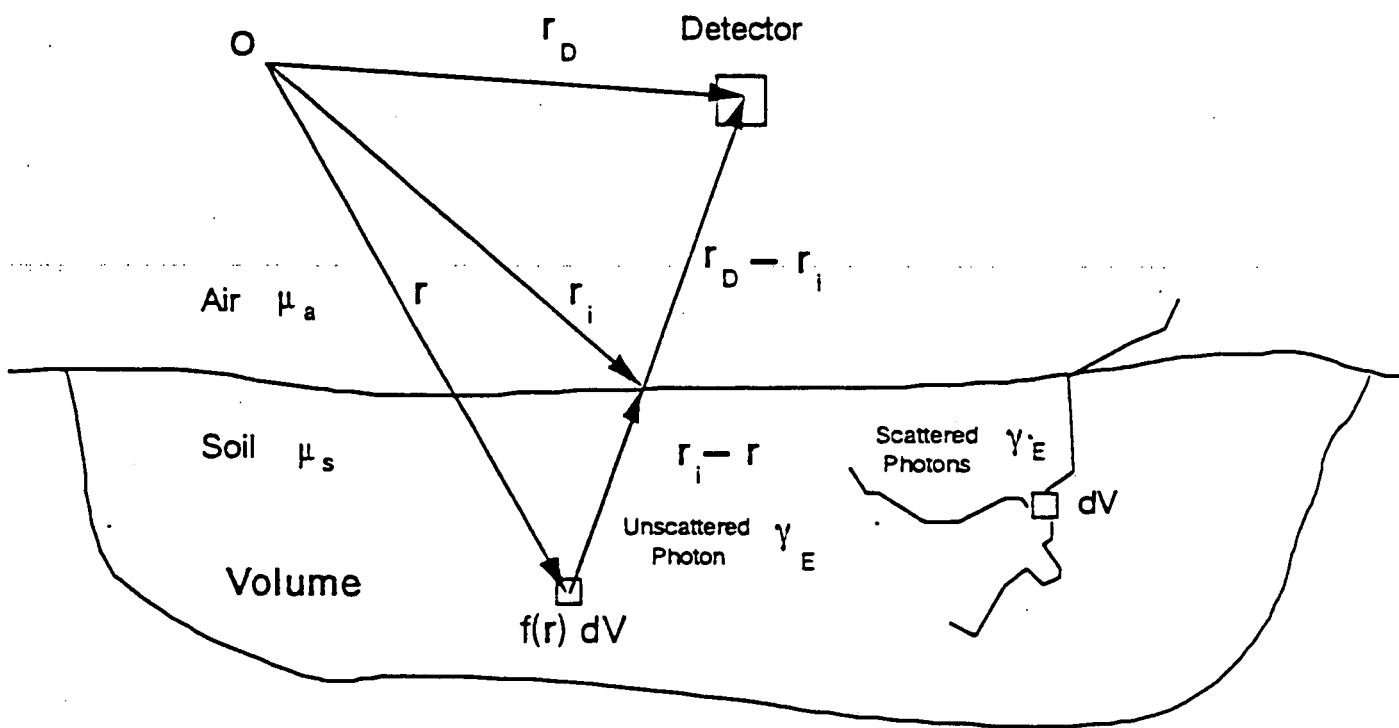


Figure 2.1

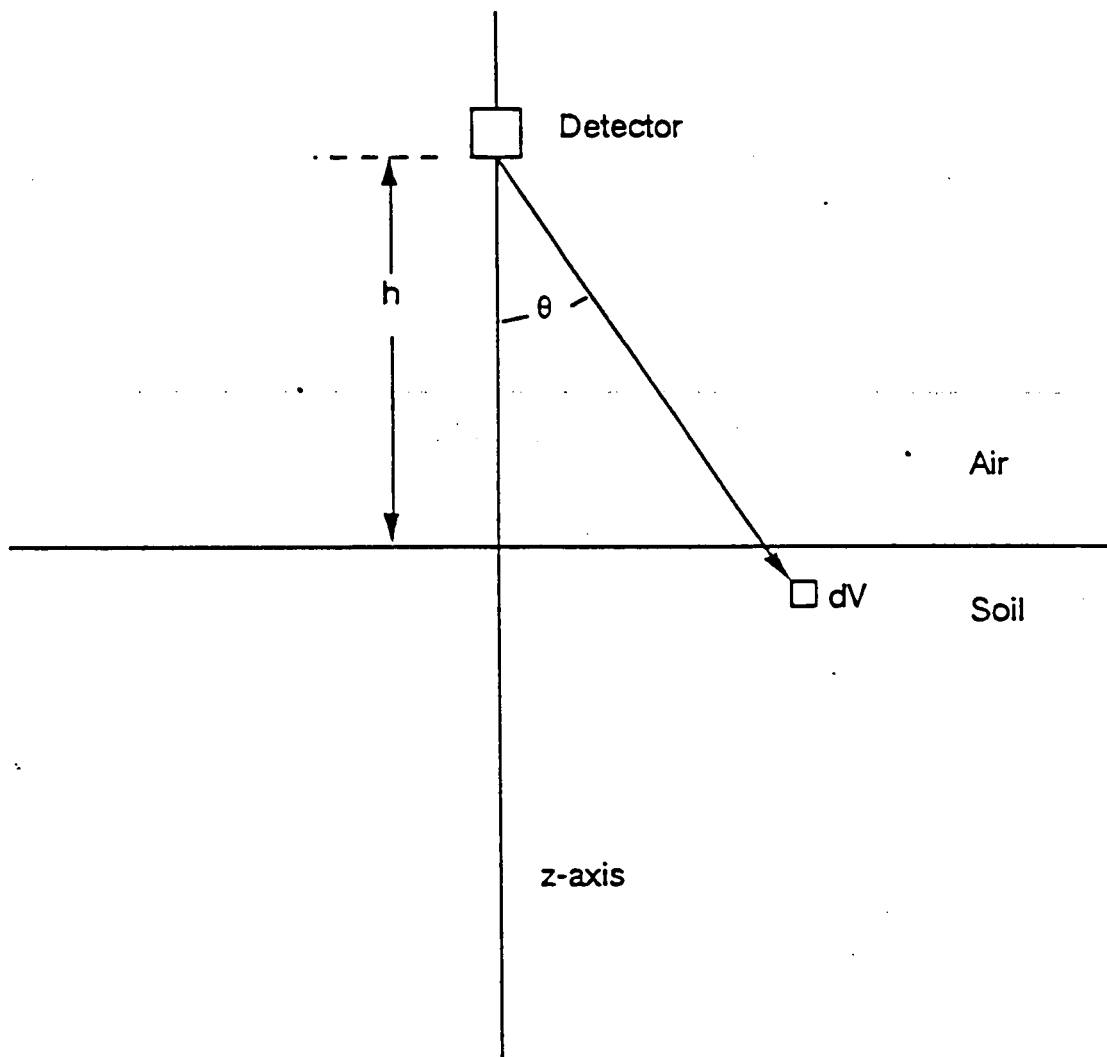


Figure 2.2

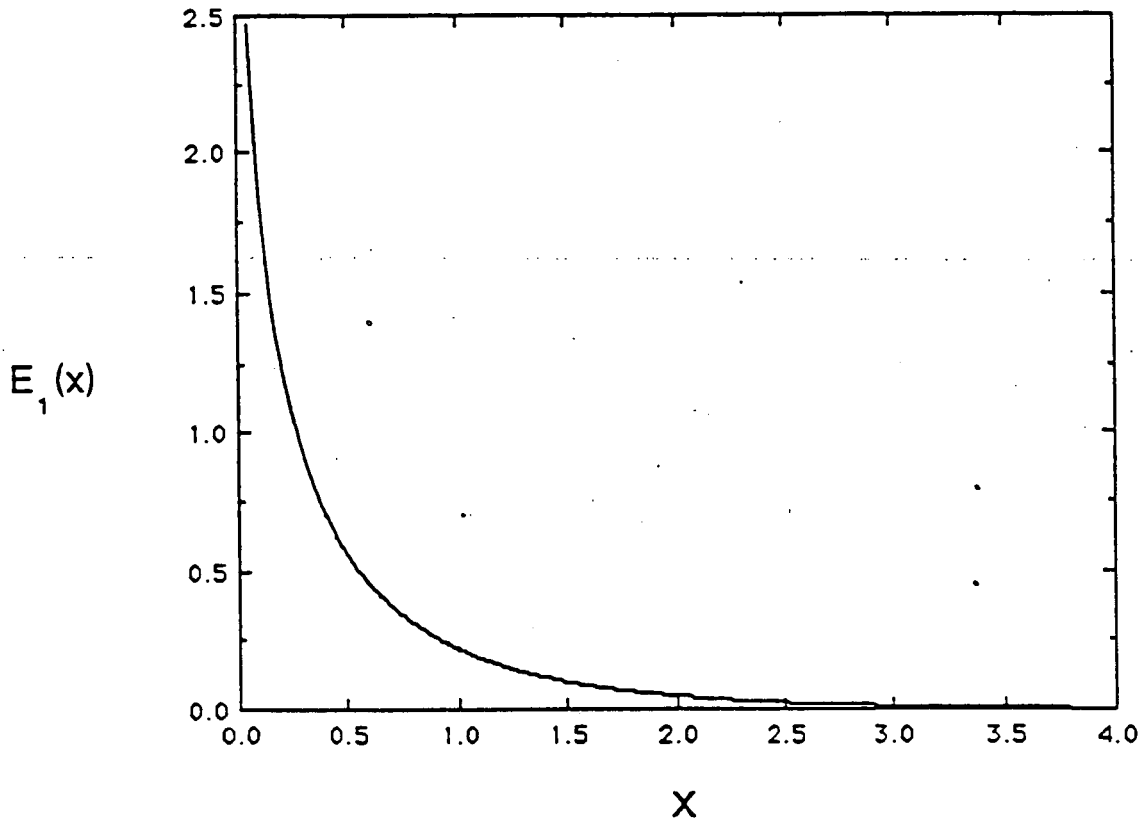


Figure 2.3

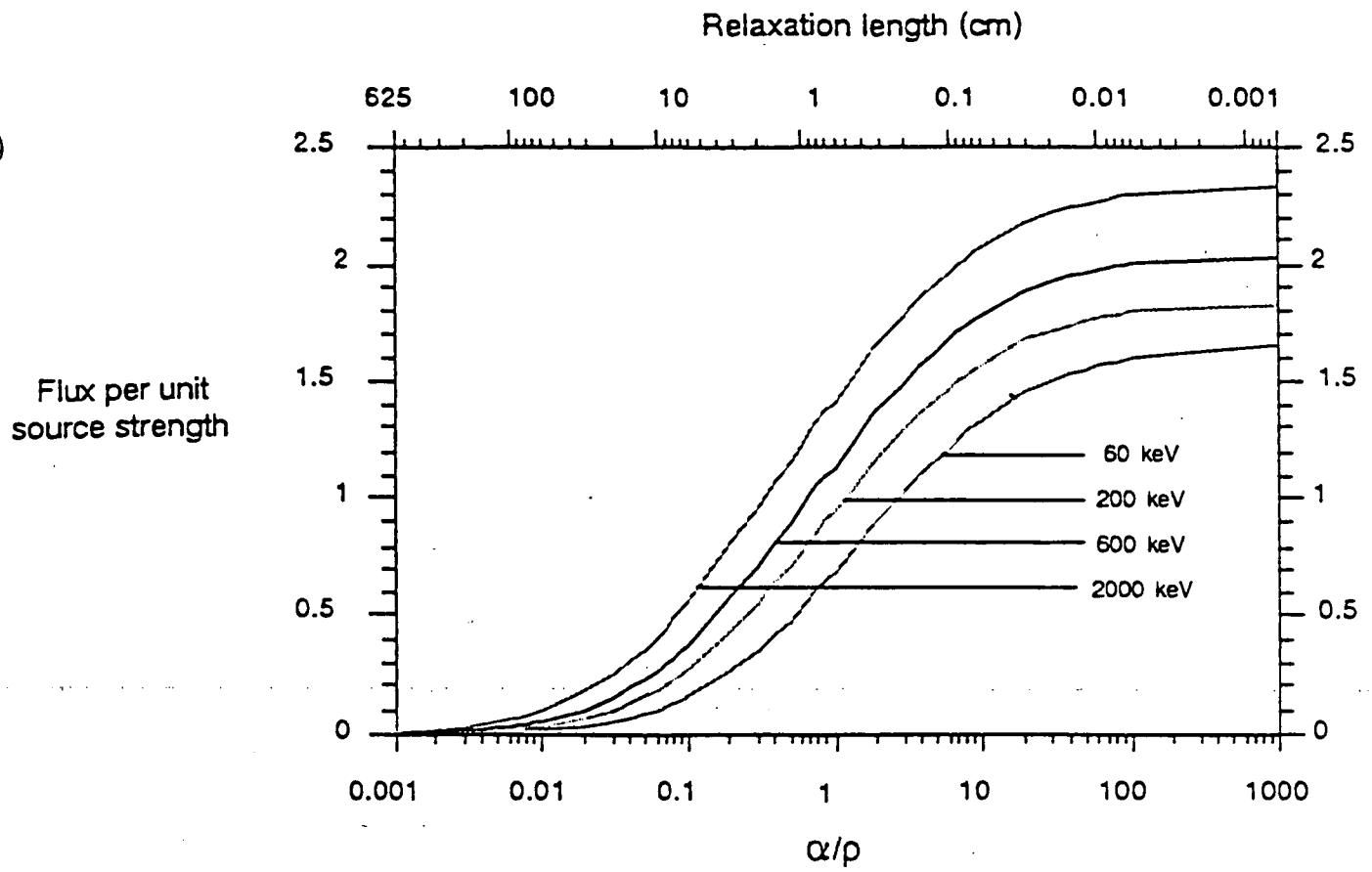


Figure 2.4

Uniform Depth Profile

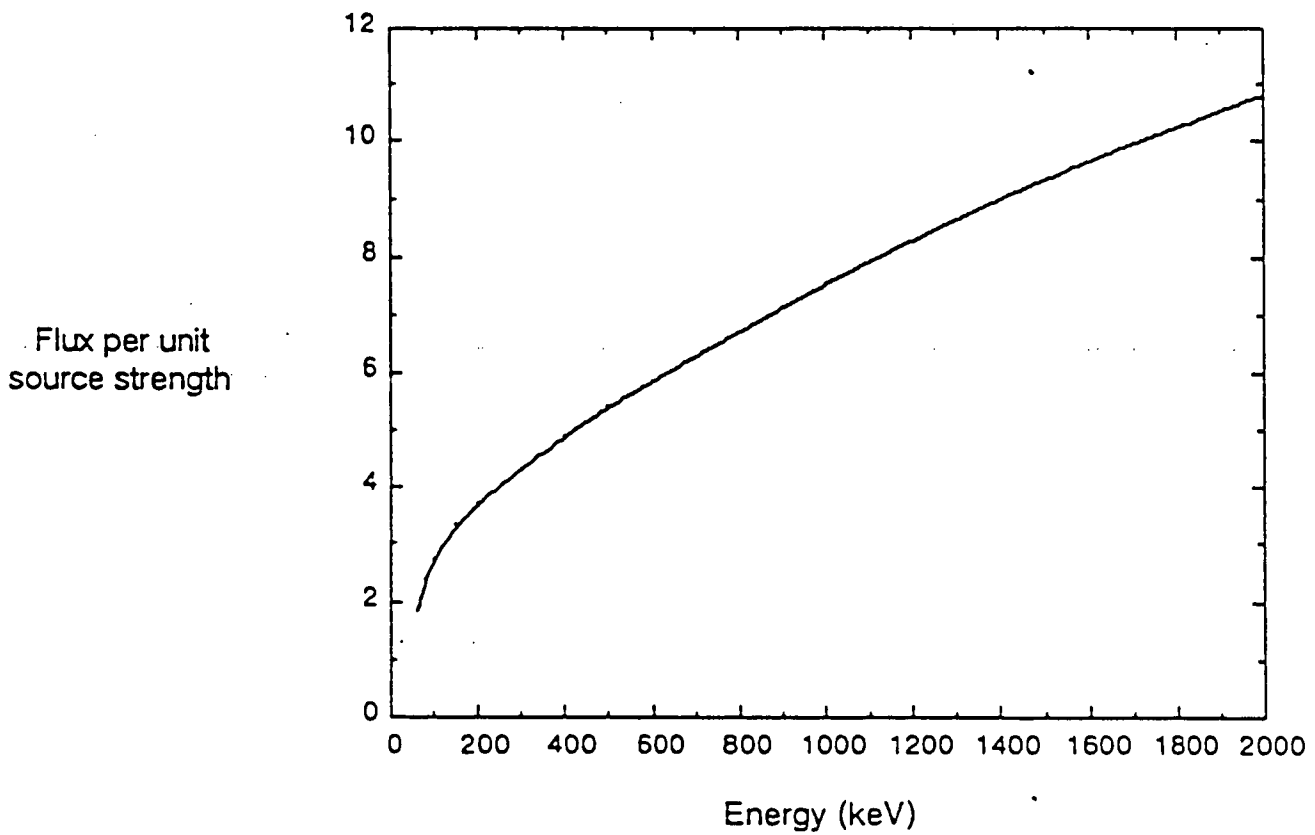


Figure 2.5

Fraction
of total flux

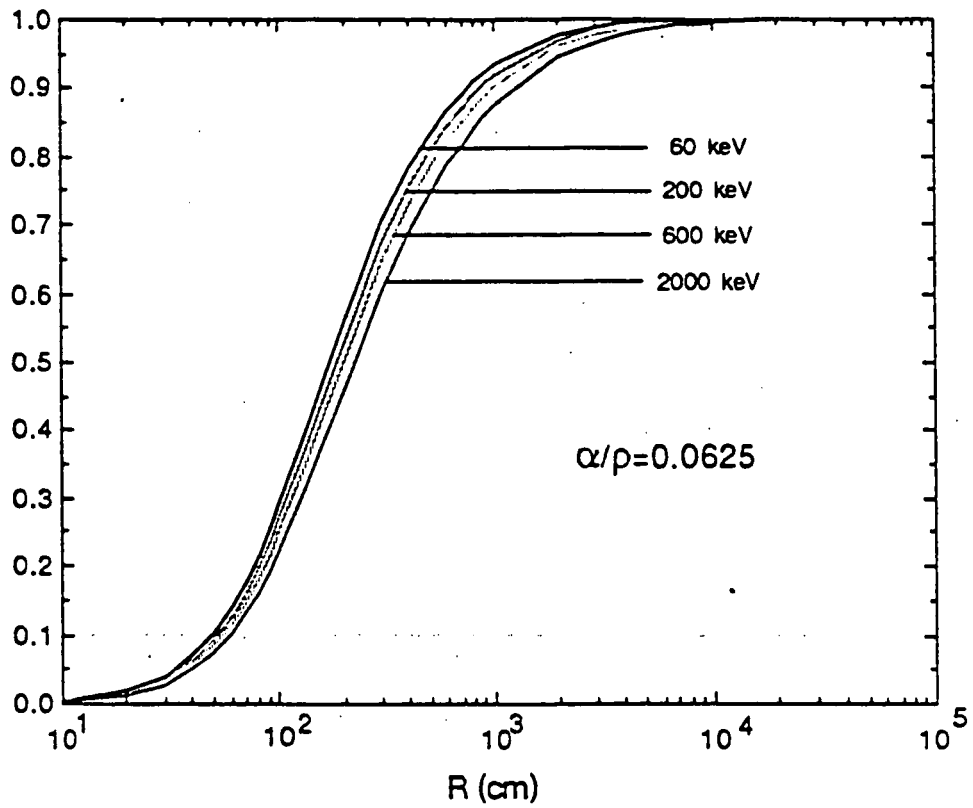


Figure 2.6

Fraction
of total flux

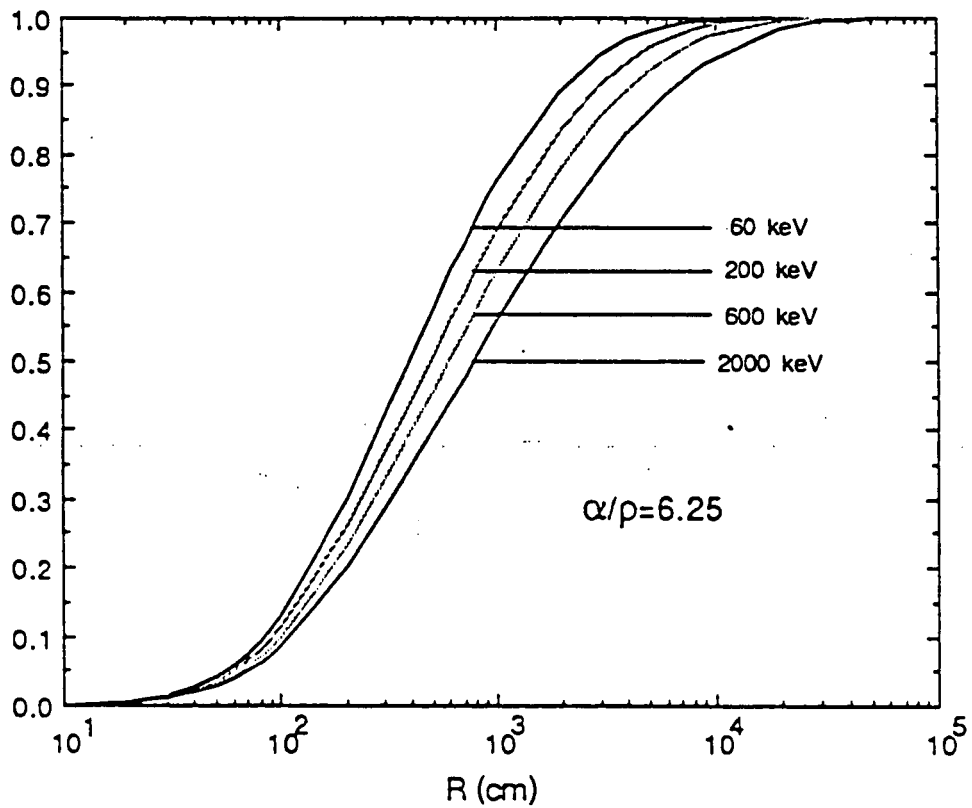


Figure 2.7

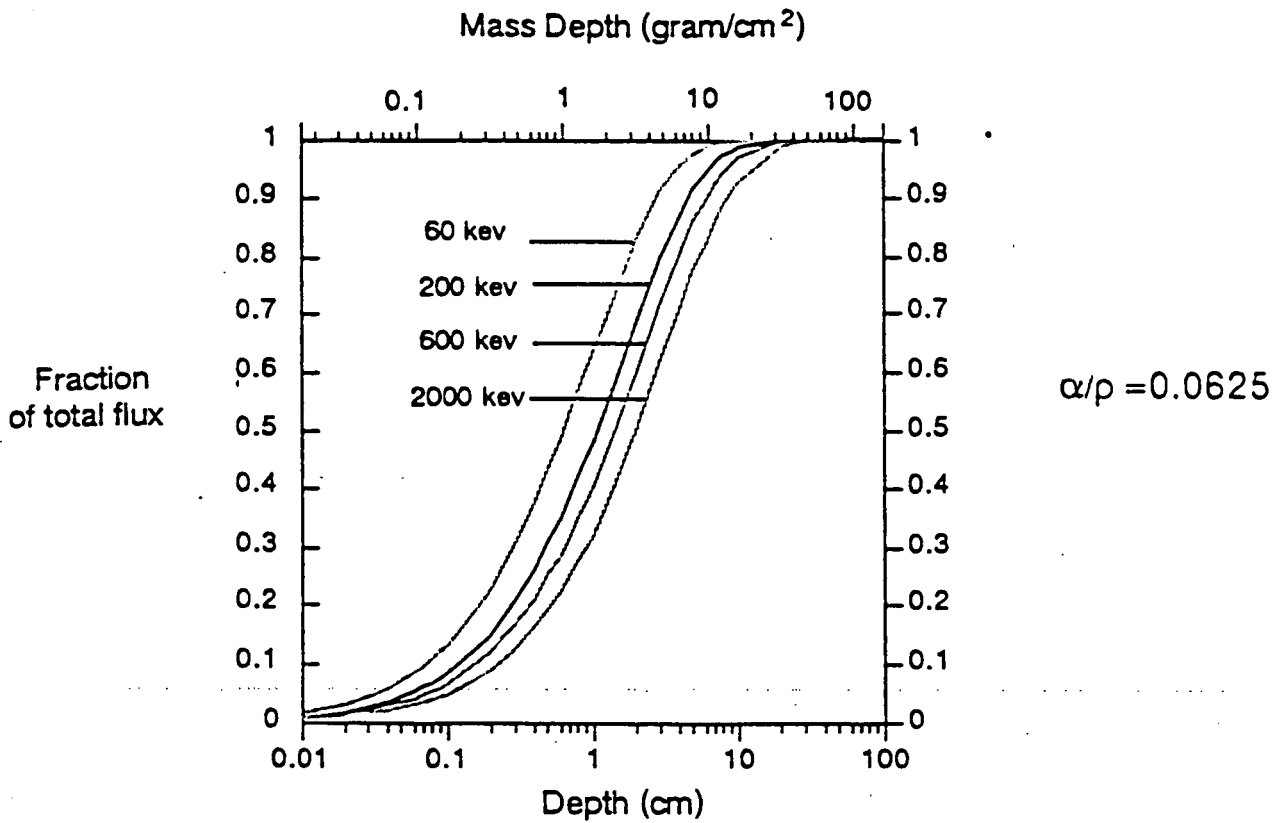


Figure 2.8

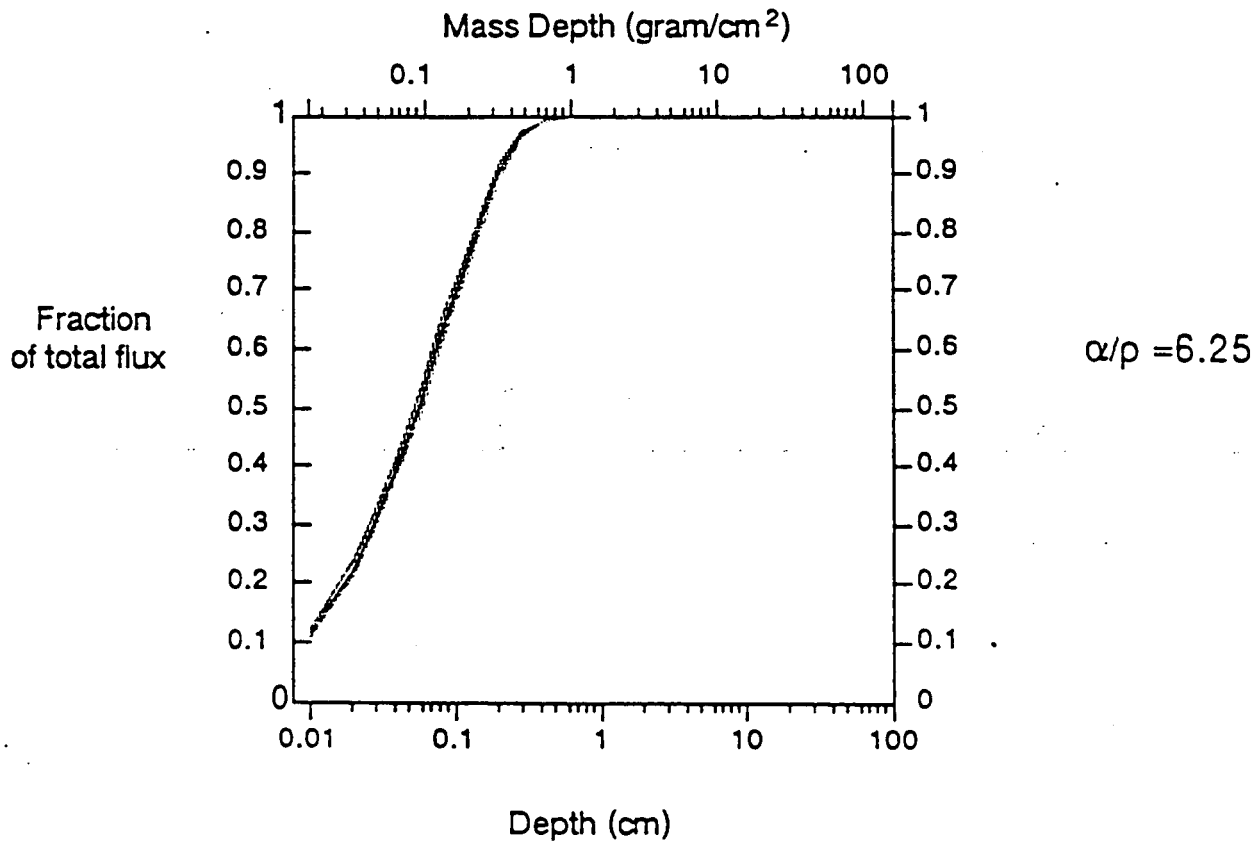
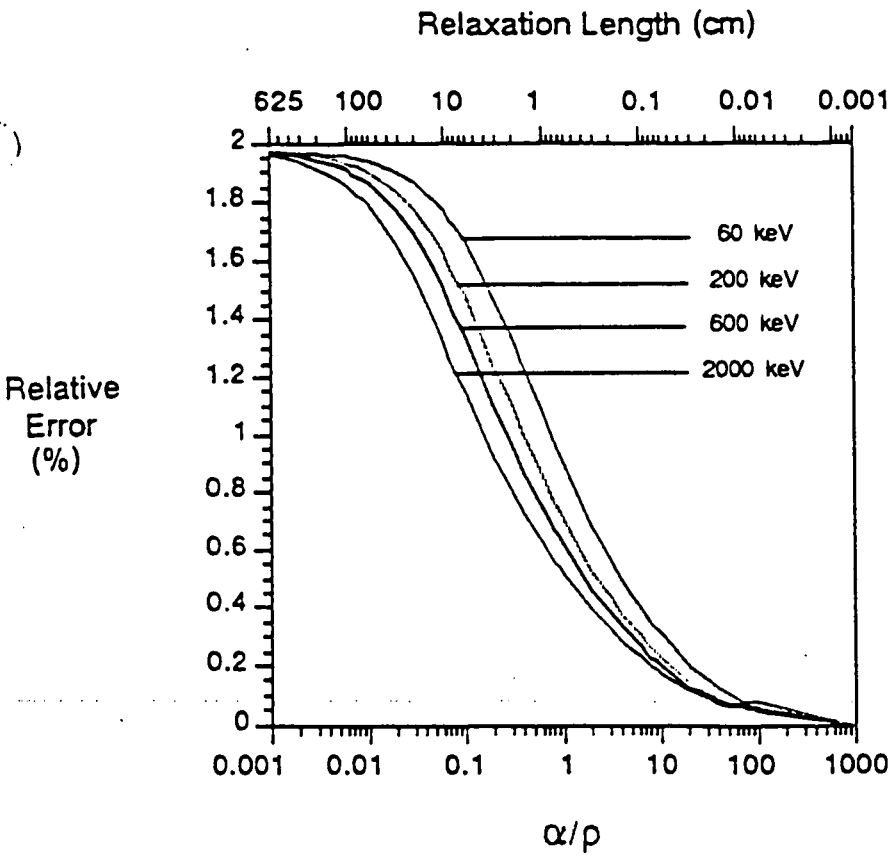


Figure 2.9



Relative error in the flux due to a 1% uncertainty in the mass attenuation coefficient of soil.

Figure 2.10

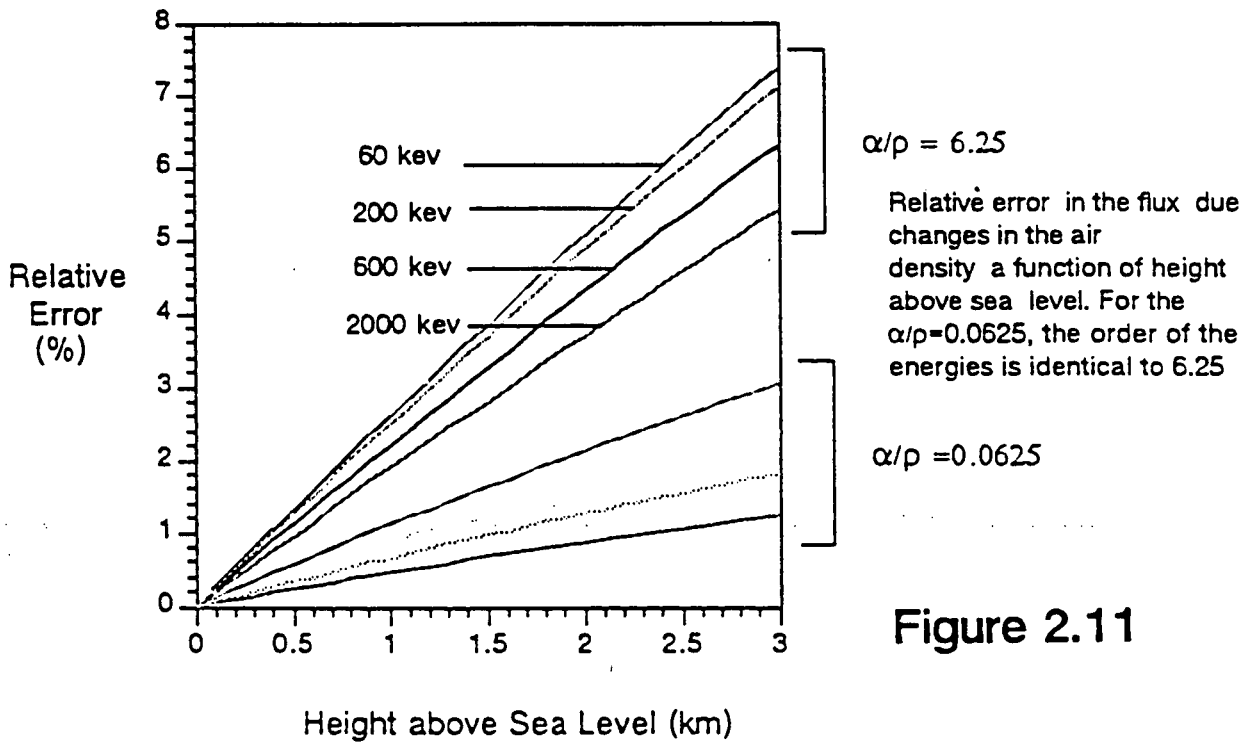


Figure 2.11

Figure 3.1

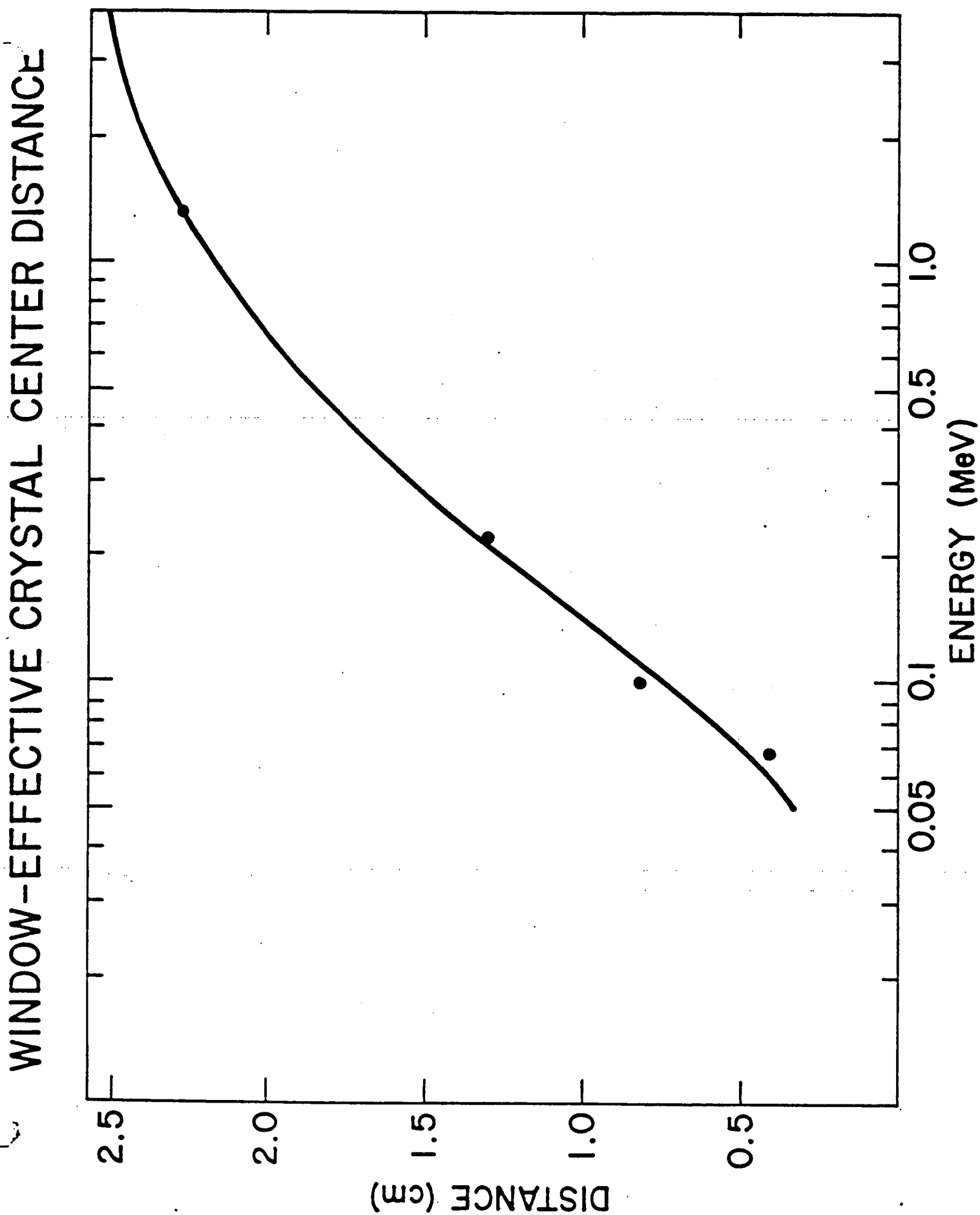
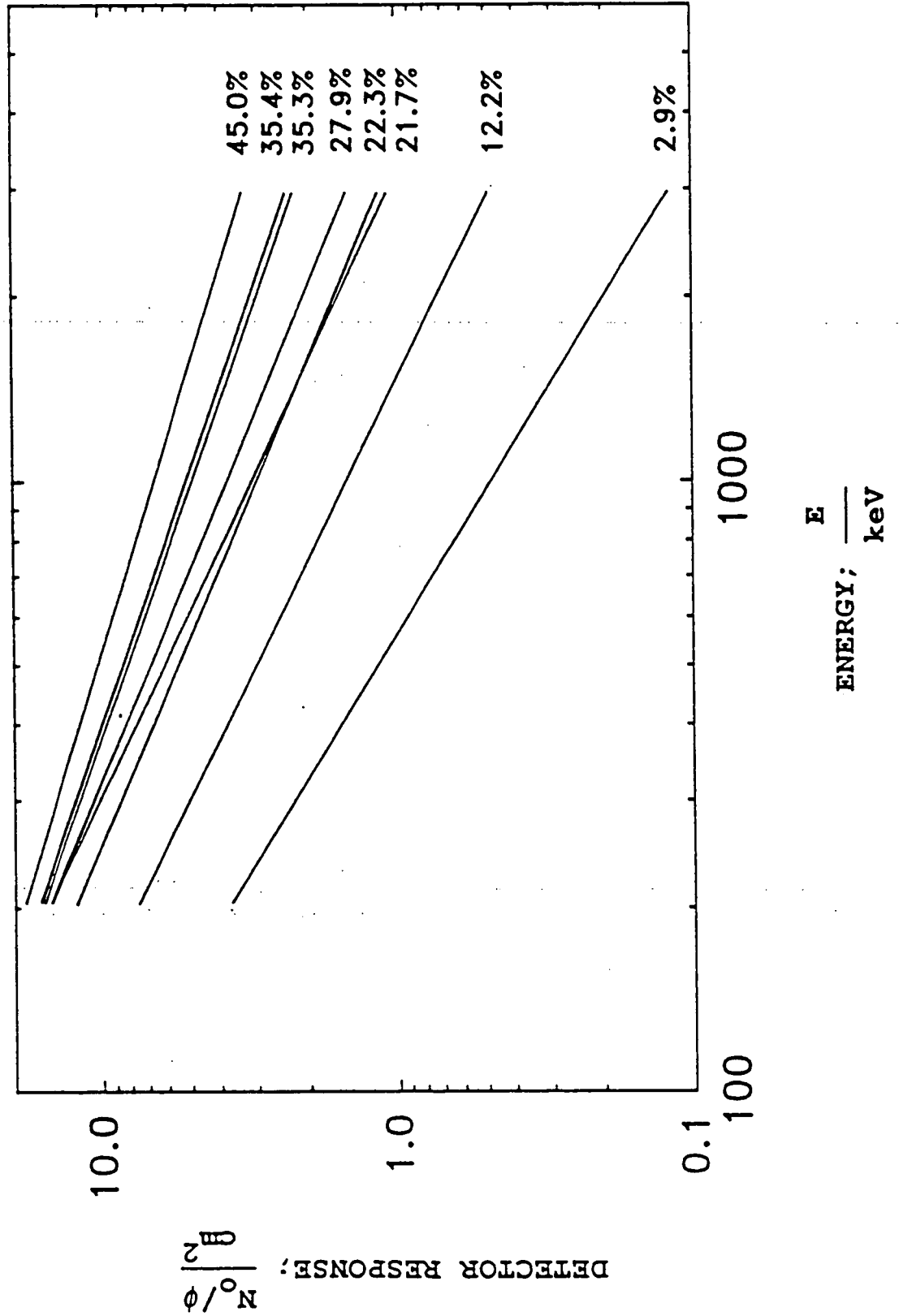


Figure 3.2



Ge DETECTOR #1030 ANGULAR RESPONSE

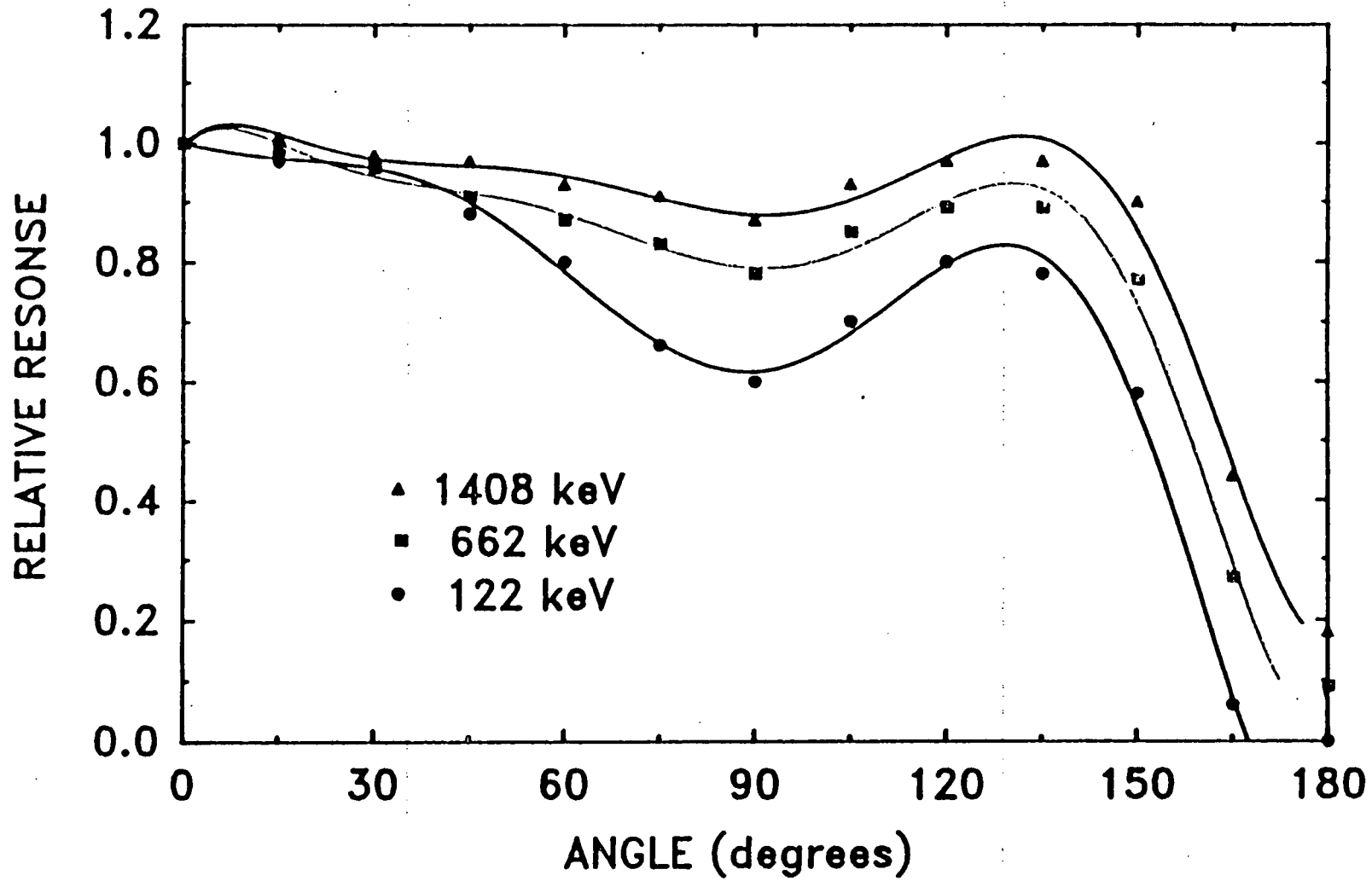


Figure 3.3

Figure 3.4

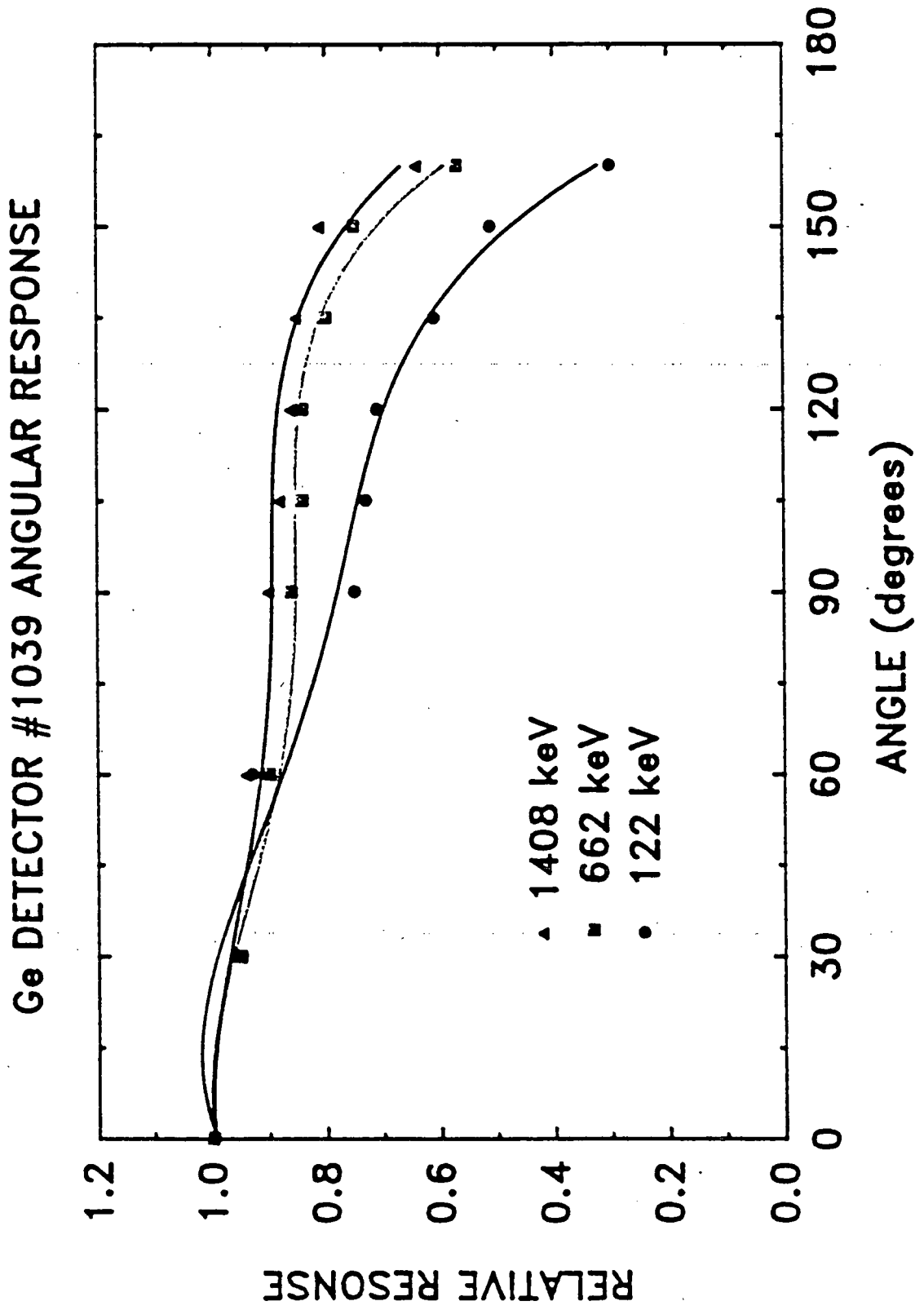
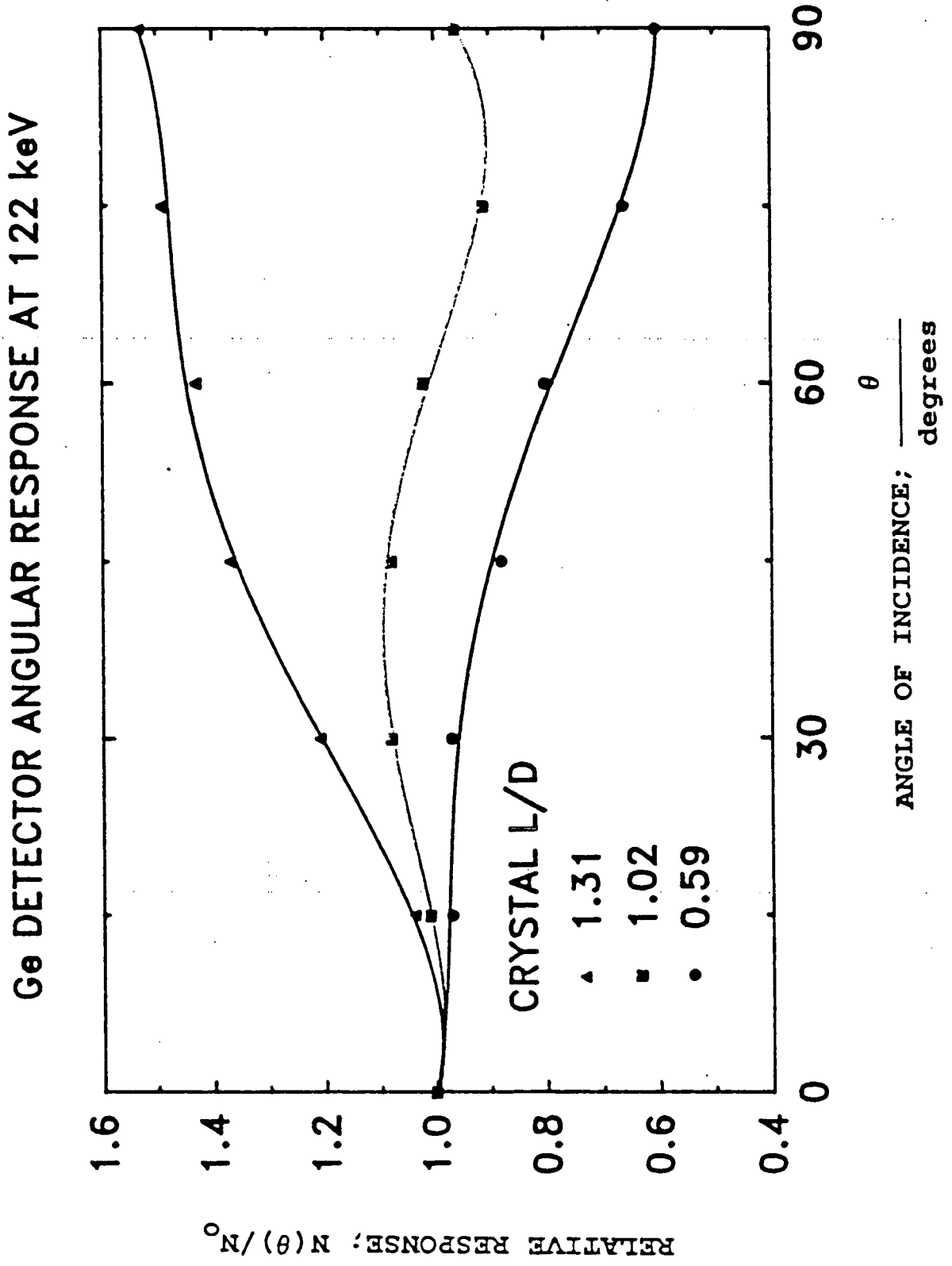


Figure 3.5



Ge DETECTOR ANGULAR RESPONSE AT 662 keV

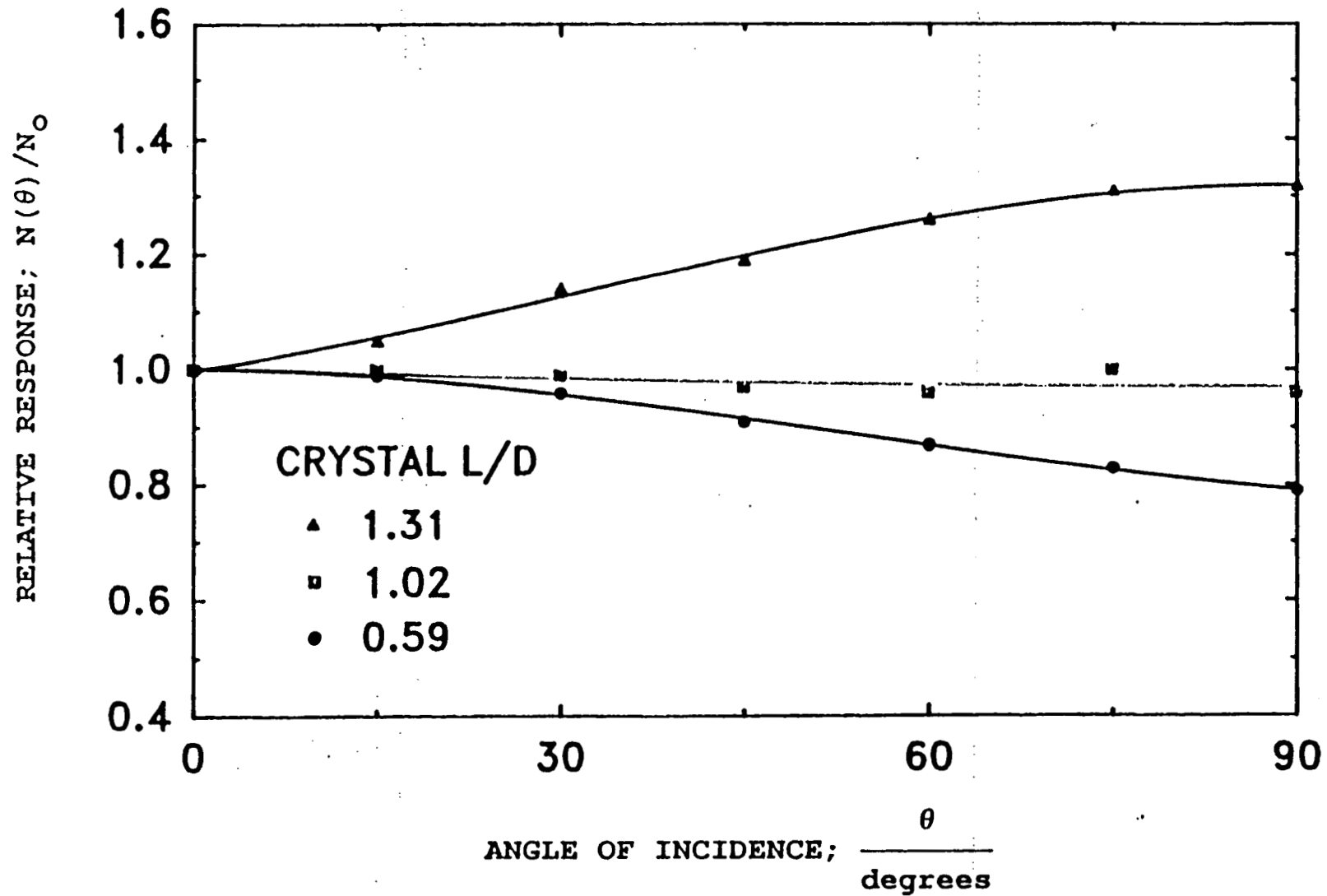


Figure 3.6

Ge DETECTOR ANGULAR RESPONSE AT 1408 keV

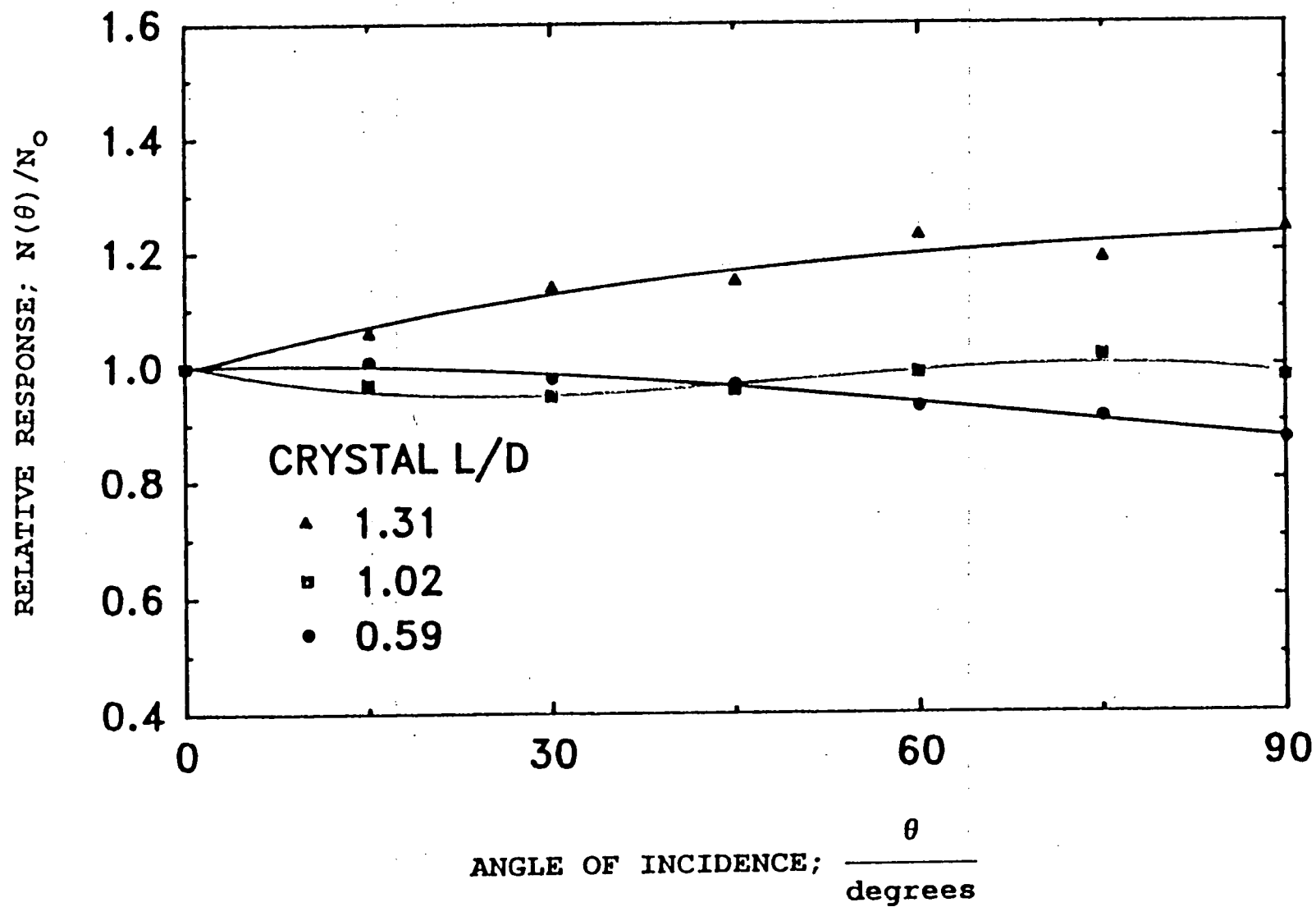


Figure 3.7

Figure 3.8

Ge DETECTOR ANGULAR CORRECTION FACTOR

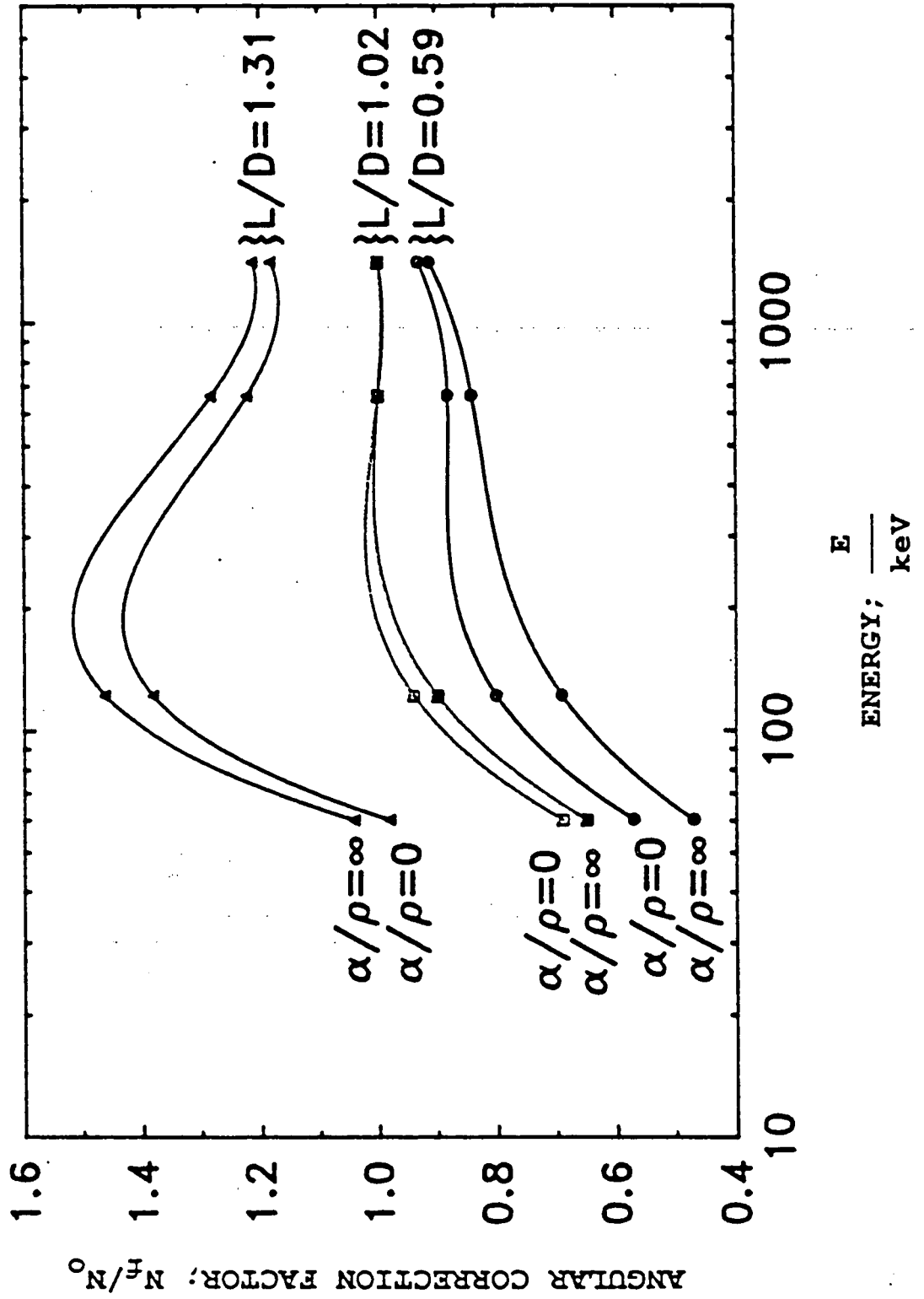


Figure 4.1

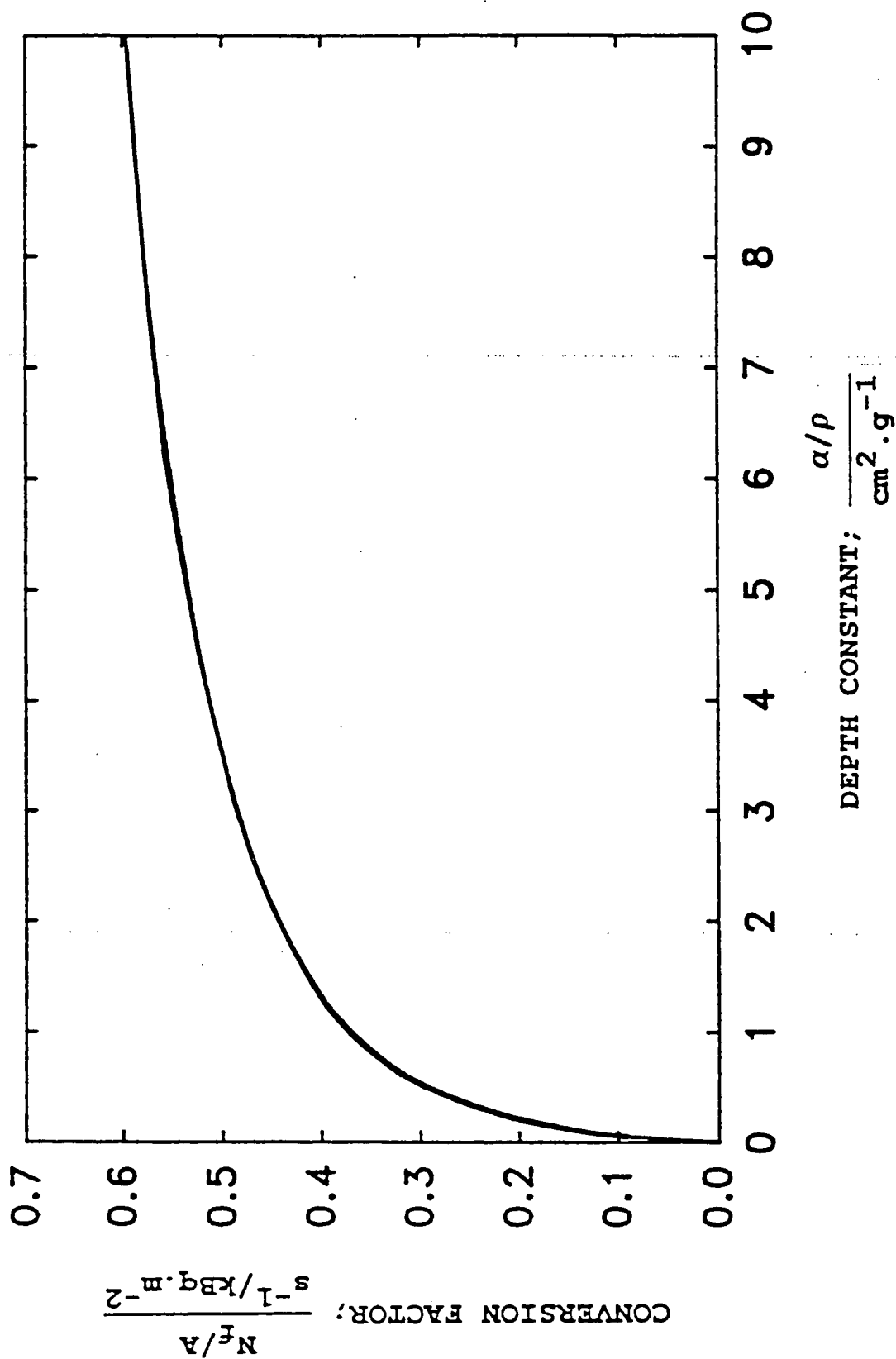
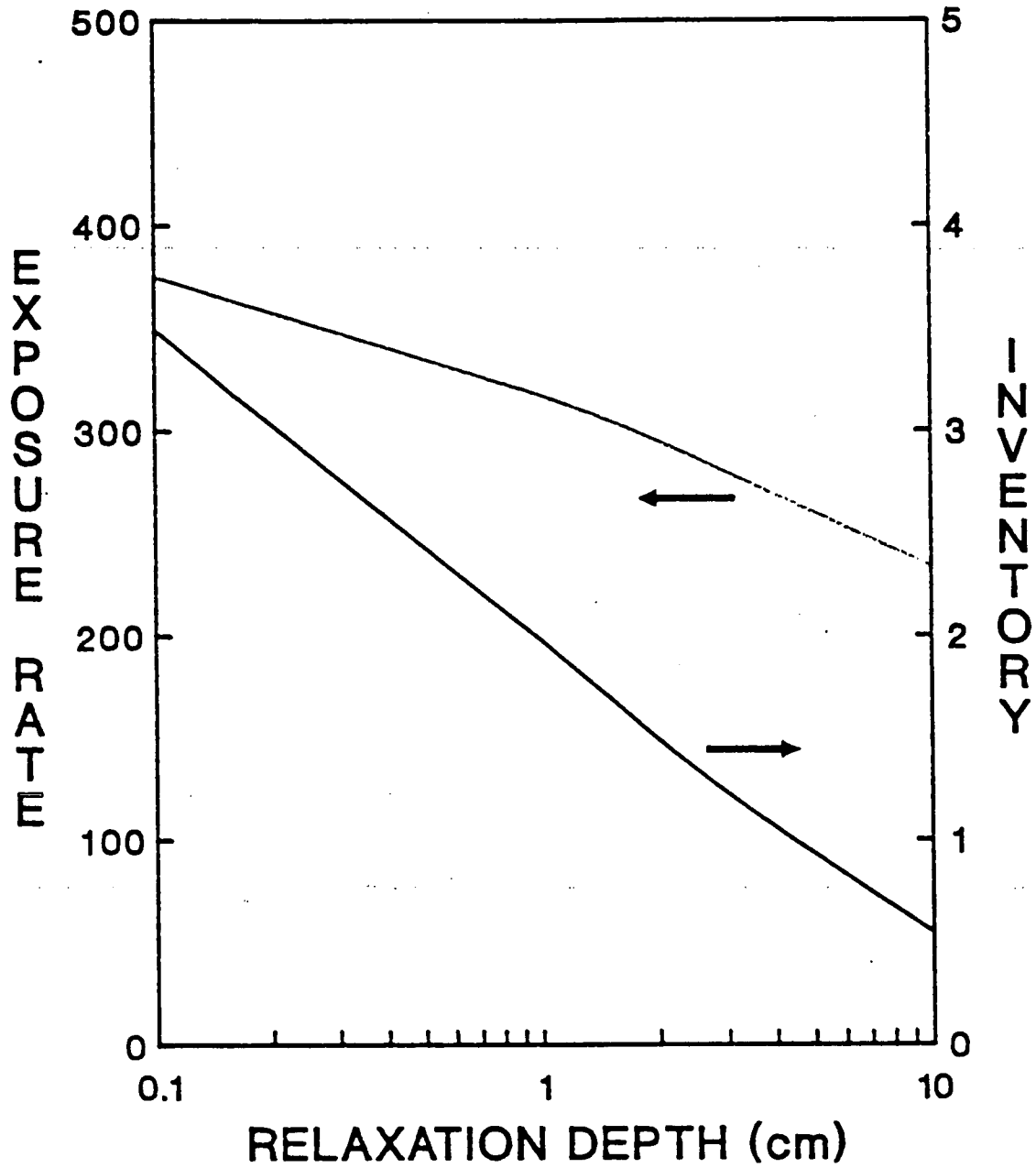


Figure 4.2

CONVERSION FACTORS FOR Cs-137
45% EFFICIENT Ge DETECTOR



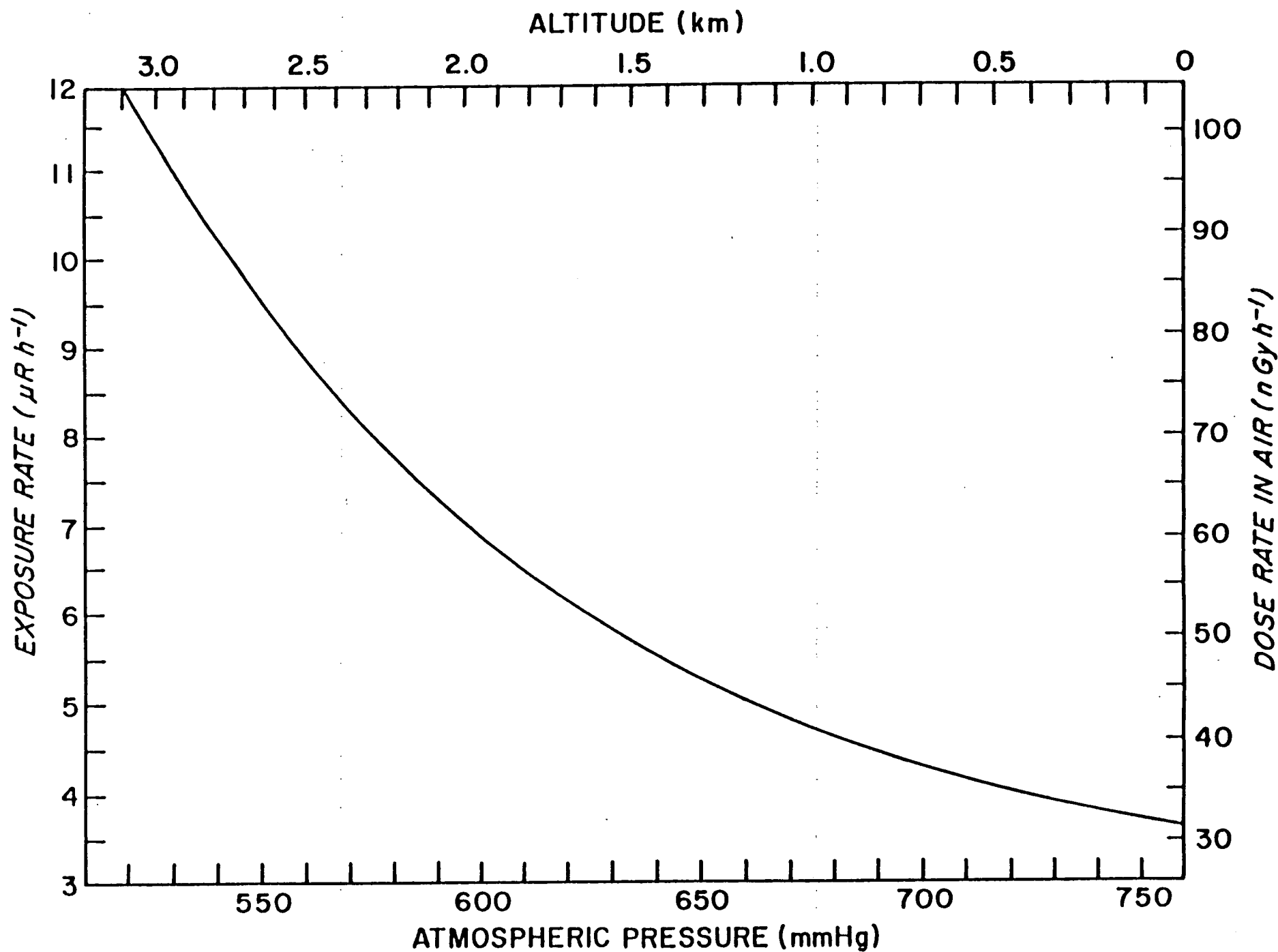


Figure 5.1

Figure 6.1

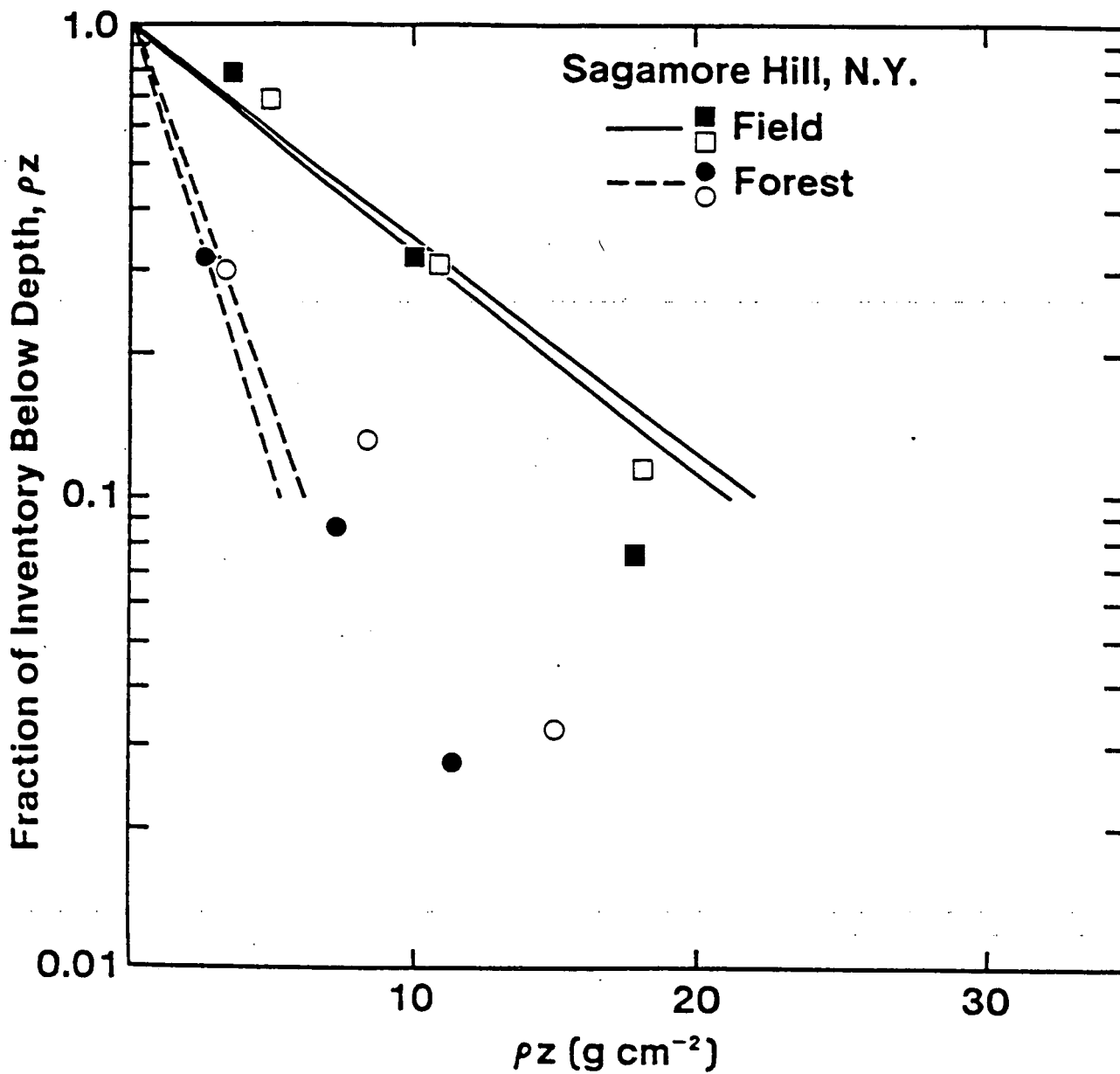


Figure 6.2

